APEX-913

METALLIC FUEL ELEMENT MATERIALS

Comprehensive Technical Report, General Electric
Direct-Air-Cycle, Aircraft Nuclear Propulsion
Program

By
R. C. Lever

June 20, 1962

Flight Propulsion Laboratory Department
General Electric Company
Cincinnati, Ohio

LEGAL NOTICE

DISCLAIMER

DISCLAIMER

Portions of this document may be illegible in electronic image products. Images are produced from the best available original document.

COMPREHENSIVE TECHNICAL REPORT
GENERAL ELECTRIC DIRECT-AIR-CYCLE
AIRCRAFT NUCLEAR PROPULSION PROGRAM

METALLIC FUEL ELEMENT MATERIALS

Author: R. C. LEVER
Contributors: C. O. TARR, R. K. BETTS
Editors: C. P. MALONE
M. L. HALTERMAN

June 20, 1962

GENERAL ELECTRIC COMPANY
NUCLEAR MATERIALS AND PROPULSION OPERATION
(Formerly Aircraft Nuclear Propulsion Department)
FLIGHT PROPULSION LABORATORY DEPARTMENT
Cincinnati 15, Ohio

ABSTRACT

This is one of twenty-one volumes summarizing the General
Electric Company's direct-air-cycle aircraft nuclear propulsion
program. Additional copies are available from the United States
Atomic Energy Commission, Division of Technical Information
Extension, Oak Ridge, Tennessee.

The APEX number and title of each volume in the series is
shown in the following list.

ABSTRACT

This is one of twenty-one volumes summarizing the Air-craft Nuclear Propulsion Program of the General Electric Company. This portion describes work on Metallic Fuel Element Materials. Information on properties, fabrication procedures, test data, and technical developments in high-temperature gas-cooled metallic nuclear fuel element technology are presented. Nuclear fuel element materials suitable for gas-cooled reactors with gas exit temperatures of from 1200°F to somewhat higher than 2000°F are discussed and test results summarized.

The general objective of the fuel element materials development program was to provide materials for the design of reactors for militarily useful aircraft power plants. Service lives from a few hours to a thousand hours were considered, depending upon the mission contemplated.

The report includes discussions and data on nuclear fuel elements containing dispersed uranium dioxide with a matrix and cladding of stainless steel, nickel-chromium alloy, iron-chromium-yttrium alloy, iron-chromium-aluminum alloy, niobium alloy, or chromium alloys.

ACKNOWLEDGMENT
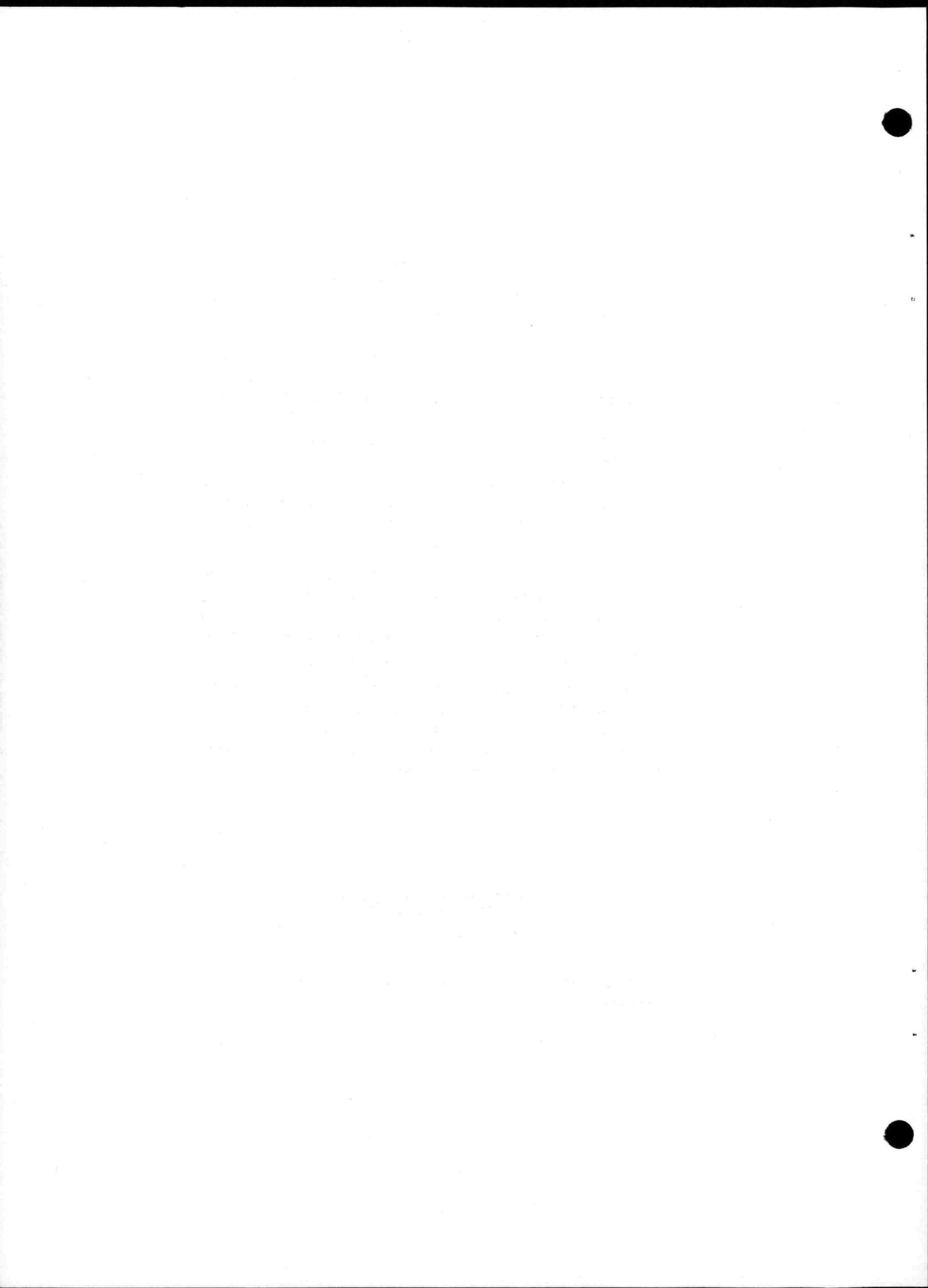
PREFACE

In mid-1951, the General Electric Company, under contract to the United States Atomic Energy Commission and the United States Air Force, undertook the early development of a militarily useful nuclear propulsion system for aircraft of unlimited range. This research and development challenge to meet the stringent requirements of aircraft applications was unique. New reactor and power-plant designs, new materials, and new fabrication and testing techniques were required in fields of technology that were, and still are, advancing very rapidly. The scope of the program encompassed simultaneous advancement in reactor, shield, controls, turbomachinery, remote handling, and related nuclear and high-temperature technologies.

The power-plant design concept selected for development by the General Electric Company was the direct air cycle turbojet. Air is the only working fluid in this type of system. The reactor receives air from the jet engine compressor, heats it directly, and delivers it to the turbine. The high-temperature air then generates the forward thrust as it exhausts through the engine nozzle. The direct air cycle concept was selected on the basis of studies indicating that it would provide a relatively simple, dependable, and serviceable power plant with high-performance potential.

The decision to proceed with the nuclear-powered-flight program was based on the 1951 recommendations of the NEPA (Nuclear Energy for the Propulsion of Aircraft) project. Conducted by the Fairchild Engine and Airplane Corporation under contract to the USAF, the five-year NEPA project was a study and research effort culminating in the proposal for active development of nuclear propulsion for manned aircraft.

In the ensuing ten years, General Electric's Aircraft Nuclear Propulsion Department carried on the direct air cycle development until notification by the USAF and USAEC, early in 1961, of the cancellation of the national ANP program. The principal results of the ten-year effort are described in this and other volumes listed inside the front cover of the Comprehensive Technical Report of the General Electric Direct Air Cycle·Aircraft Nuclear Propulsion Program.

Although the GE-ANPD effort was devoted primarily to achieving nuclear aircraft power-plant objectives (described mainly in APEX-902 through APEX-909), substantial contributions were made to all aspects of gas-cooled reactor technology and other promising nuclear propulsion systems (described mainly in APEX-910 through APEX-921). The Program Summary (APEX-901) presents a detailed description of the historical, programmatic, and technical background of the ten years covered by the program. A graphic summary of these events is shown on the next page.

Each portion of the Comprehensive Report, through extensive annotation and referencing of a large body of technical information, now makes accessible significant technical data, analyses, and descriptions generated by GE-ANPD. The references are grouped by subject and the complete reference list is contained in the Program Summary, APEX-901. This listing should facilitate rapid access by a researcher to specific interest areas or
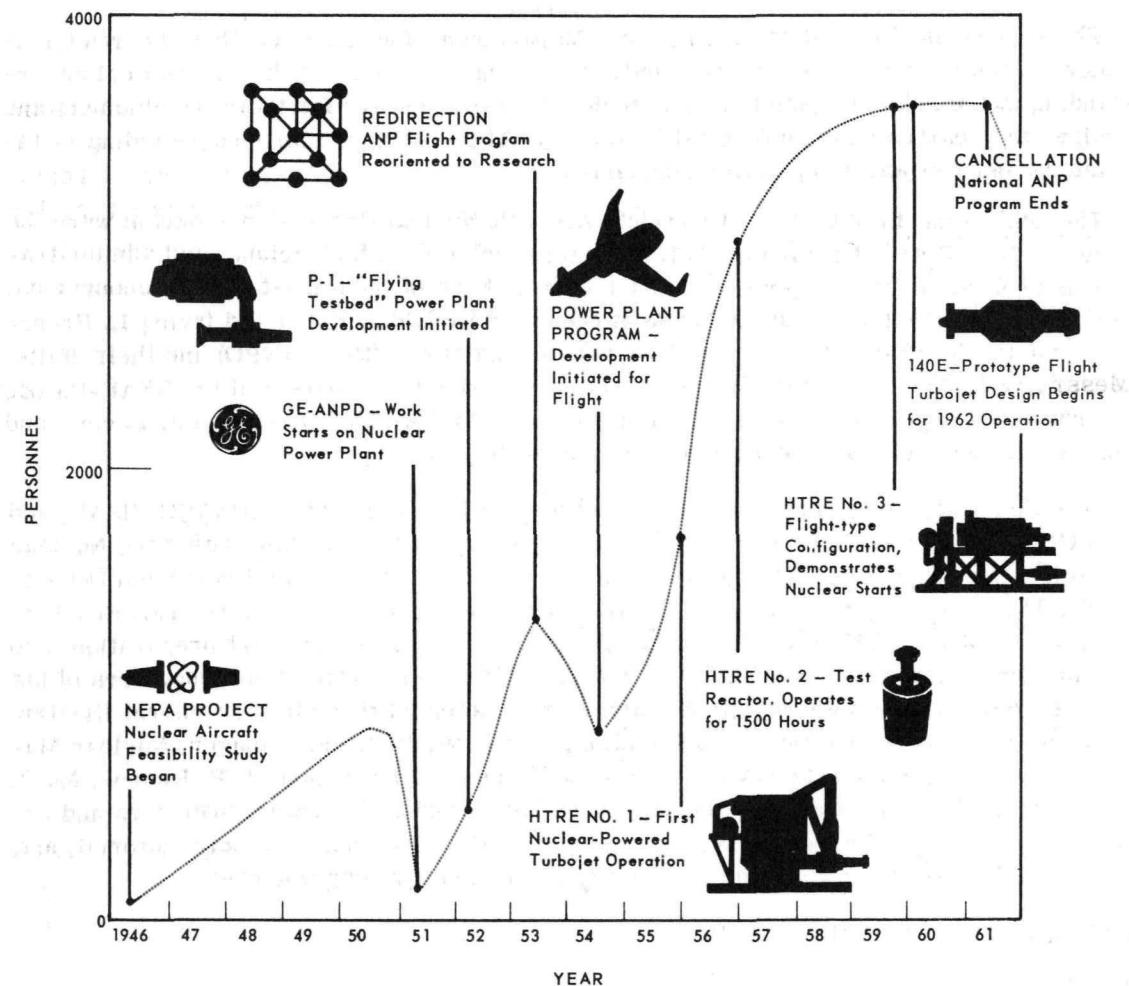
Summary of events — General Electric Aircraft Nuclear Propulsion Program*

6

sources of data. Each portion of the Comprehensive Report discusses an aspect of the Program not covered in other portions. Therefore, details of power plants can be found in the power-plant volumes and details of the technologies used in the power plants can be found in the other volumes. The referenced documents and reports, as well as other GE-ANPD technical information not covered by the Comprehensive Report, are available through the United States Atomic Energy Commission, Division of Technical Information Extension, Oak Ridge, Tennessee.

The Report is directed to Engineering Management and assumes that the reader is generally familiar with basic reactor and turbojet engine principles; has a technical understanding of the related disciplines and technologies necessary for their development and design; and, particularly in APEX-910 through APEX-921, has an understanding of the related computer and computative techniques.

The achievements of General Electric's Aircraft Nuclear Propulsion Program were the result of the efforts of many officers, managers, scientists, technicians, and administrative personnel in both government and industry. Most of them must remain anonymous, but particular mention should be made of Generals Donald J. Keirn and Irving L. Branch of the Joint USAF-USAEC Aircraft Nuclear Propulsion Office (ANPO) and their staffs; Messrs. Edmund M. Velten, Harry H. Gorman, and John L. Wilson of the USAF-USAEC Operations Office and their staffs; and Messrs. D. Roy Shoults, Samuel J. Levine, and David F. Shaw, GE-ANPD Managers and their staffs.

This Comprehensive Technical Report represents the efforts of the USAEC, USAF, and GE-ANPD managers, writers, authors, reviewers, and editors working within the Nuclear Materials and Propulsion Operation (formerly the Aircraft Nuclear Propulsion Department). The local representatives of the AEC-USAF team, the Lockland Aircraft Reactors Operations Office (LAROO), gave valuable guidance during manuscript preparation, and special appreciation is accorded J. L. Wilson, Manager, LAROO, and members of his staff. In addition to the authors listed in each volume, some of those in the General Electric Company who made significant contributions were: W. H. Long, Manager, Nuclear Materials and Propulsion Operation; V. P. Calkins, E. B. Delson, J. P. Kearns, M. C. Leverett, L. Lomen, H. F. Matthiesen, J. D. Selby, and G. Thornton, managers and reviewers; and C. L. Chase, D. W. Patrick, and J. W. Stephenson and their editorial, art, and production staffs. Their time and energy are gratefully acknowledged.

THE EDITORIAL BOARD:

Paul E. Lowe
Arnold J. Rothstein
James I. Trussell

November 8, 1961

CONTENTS

8

FIGURES

11

TABLES

14

1. INTRODUCTION AND SUMMARY

Metallic fuel element work covered approximately a decade (1951 to 1961) of effort from the initial temperature requirement of 1800° F for 100 hours to the final requirement of 2500° F for 1000 hours. In all the programs, particular reactor operating conditions governed the testing and, as such, parametric studies were minimized. Also, as more stringent operating conditions were imposed, a particular fuel system was dropped in favor of another system with greater temperature capabilities. In only one system was there a sustained effort maintained to characterize its operating capabilities. This system employed 80Ni - 20Cr fuel elements, discussed in section 3. In this system as well as the others studied, the fissile material was UO_2 incorporated in the core matrix by the use of powder metallurgy techniques.

In addition to the 80Ni - 20Cr system, various other systems were investigated. These included (1) Type 310 stainless steel-UO_2 core clad with stainless steel, discussed in section 2; (2) niobium-UO_2 core clad with Fe-Cr-Al, discussed in section 4; (3) Cr-Ti-UO_2 core clad with Fe-Cr-Y, discussed in section 5; (4) Fe-Cr-Y-UO_2 core clad with Fe-Cr-Y, discussed in section 6; (5) Cr-Ti-UO_2 core clad with Cr-Y, discussed in section 7; and (6) coated niobium discussed in section 8.

1.1 TYPE 310 STAINLESS STEEL-UO_2 CORE CLAD WITH STAINLESS STEEL

Initial designs and plans for the first power plant, which was designated the P-1 power plant, was started late in 1951. APEX-202 of this Comprehensive Technical Report gives details of the P-1 power plant. Specifications for metallic fuel elements for use in this power plant included a 1650° F average temperature and a maximum temperature of 1800° F with a service life of 100 hours at a stress of 1000 psi. Stainless steel Type 310 (and 309) was investigated as a material for matrix and cladding.

Stainless steel fuel elements were fabricated as sheet with a cladding thickness of about 0.005 inch and cores of the same thickness containing 25 to 30 weight percent UO_2. Most of the initial work on uranium dioxide dispersions in metallic systems was conducted during the development of the completely protected heterogeneously dispersed uranium dioxide in this system.

The fuel elements essentially met the service requirement of 1650° F for 100 hours but were limited to temperatures below 1740° F by insufficient oxidation resistance and strength.

The development of stainless steel fuel elements by GE-ANPD was terminated in 1953 when the reactor performance requirements were increased and 80Ni - 20Cr fuel elements, indicated greater temperature capabilities.

1.2 Ni-Cr FUEL ELEMENTS

The high strength and better oxidation resistance of the 80Ni - 20Cr alloy, as compared to Type 310 stainless steel, and more stringent reactor-performance requirements led to the development of 80Ni - 20Cr fuel elements. Mofification to this alloy resulted in improvements in strength and oxidation resistance.

The fuel element materials finally adopted consisted of enriched UO_2 mixed with 80Ni - 20Cr alloy with 40 to 42 weight percent UO_2 and clad with a niobium-modified 80Ni - 20Cr alloy. Of all the fuel element systems studied by GE-ANPD, the 80Ni - 20Cr system was the most thoroughly developed.

Concentric-ring-type fuel elements were used in Heat Transfer Reactor Experiment No. 1 (HTRE No. 1), No. 2 (HTRE No. 2), and No. 3 (HTRE No. 3). Design and operational details of these reactor experiments may be found in APEX-904, -905, and -906 of this Comprehensive Summary Report, respectively. During the period 1953 to 1959, the technology of 80Ni - 20Cr fuel elements was developed. This fuel system proved stable, reliable, and amenable to fabrication into a variety of shapes and configurations.

1.3 Nb-UO_2 CORE CLAD WITH Fe-Cr-Al

Considerable effort was spent on the utilization of Fe-Cr-Al clad niobium fuel elements for operating temperatures up to about $2300^{\circ}F$. The major problem with this type was interfacial reactions between core and cladding resulting in the formation of a brittle interface and/or diffusion of uranium. Investigation of this system was dropped in favor of others that appeared more promising.

1.4 Cr-Ti-UO_2 CORE CLAD WITH Fe-Cr-Y

An oxidation resistant alloy with a composition of 69Fe - 30Cr - 1Y (weight percent) gave indications of meeting the requirements, in December 1957, for a service life of 100 hours at $2100^{\circ}F$. The addition of 1 weight percent titanium added to the Cr-UO_2 core gave improved strength to that part of the system. The above requirements were met and surpassed. The development program up to June 30, 1961, had achieved a cladding alloy capable of even higher temperature, longer life in the Fe-Cr-Y system. The nominal composition of the alloy was 64Fe - 34.5Cr - 1.5Y. Additions of Al to the Fe-Cr-Y system markedly improved oxidation resistance. Details of the development program including fuel ribbon fabrication, cartridge assembly, clad alloy production, and property data are presented.

1.5 Fe-Cr-Y-UO_2 CORE CLAD WITH Fe-Cr-Y

The ability to improve oxidation resistance with small additions of yttrium was demonstrated in 1957 and resulted in the investigation of the Fe-Cr-Y clad Fe-Cr-Y-UO_2 system early in 1958. A fueled material capable of operation at $2100^{\circ}F$ for 100 hours under a load of 1000 psi with a maximum elongation of 5 percent was desired. Both ribbon and wire fuel geometries were investigated. It was determined that this system would not meet the strength requirement.

1.6 Cr-Ti-UO$_2$ CORE CLAD WITH Cr-Y

Both ribbon and wire configurations of this material were investigated from 1951 to 1959. It was found that a 1 weight percent yttrium addition did much to improve the oxidation resistance of chromium cladding in the 2100° to 2500°F temperature range, and that a 1 weight percent addition of titanium increased core strength. Work on this system was terminated when emphasis shifted to ceramic systems. Details of the program, particularly those relating to alloy development, are presented.

1.7 COATED NIOBIUM

Intensive development of a niobium fuel element was started with the investigation of protective coatings to satisfy service requirements in oxidizing environments up to 2500°F for periods up to 1000 hours. The element, niobium, was attractive because of its favorable nuclear cross section, high strength at elevated temperatures, low thermal expansion, and other desirable properties including workability.

Coatings investigated were based on aluminum, zinc, silver, and tin or combinations of these elements in the main. Additions of Ti and Cr to the Al coatings were found beneficial. The aluminum coatings gave good oxidation resistance at 2500°F but were deficient at intermediate temperatures. The zinc coatings while fairly effective below 1800°F were unsatisfactory at higher temperatures. A complex coating consisting of Ag - 22Sn - 15Al - 0.5Ti - 0.5Cr lasted 1000 hours at 2200°F and 100 hours at 2300°F.

In addition to coating studies on niobium, an alloy development program was carried out to achieve more oxidation resistance in the base system. Alloys investigated included compositions of the niobium-aluminum, niobium-aluminum-titanium, and niobium-aluminum-titanium-chromium systems with other additions in some cases. Some improvement in oxidation resistance was noted in many cases, but no completely satisfactory alloy was developed.
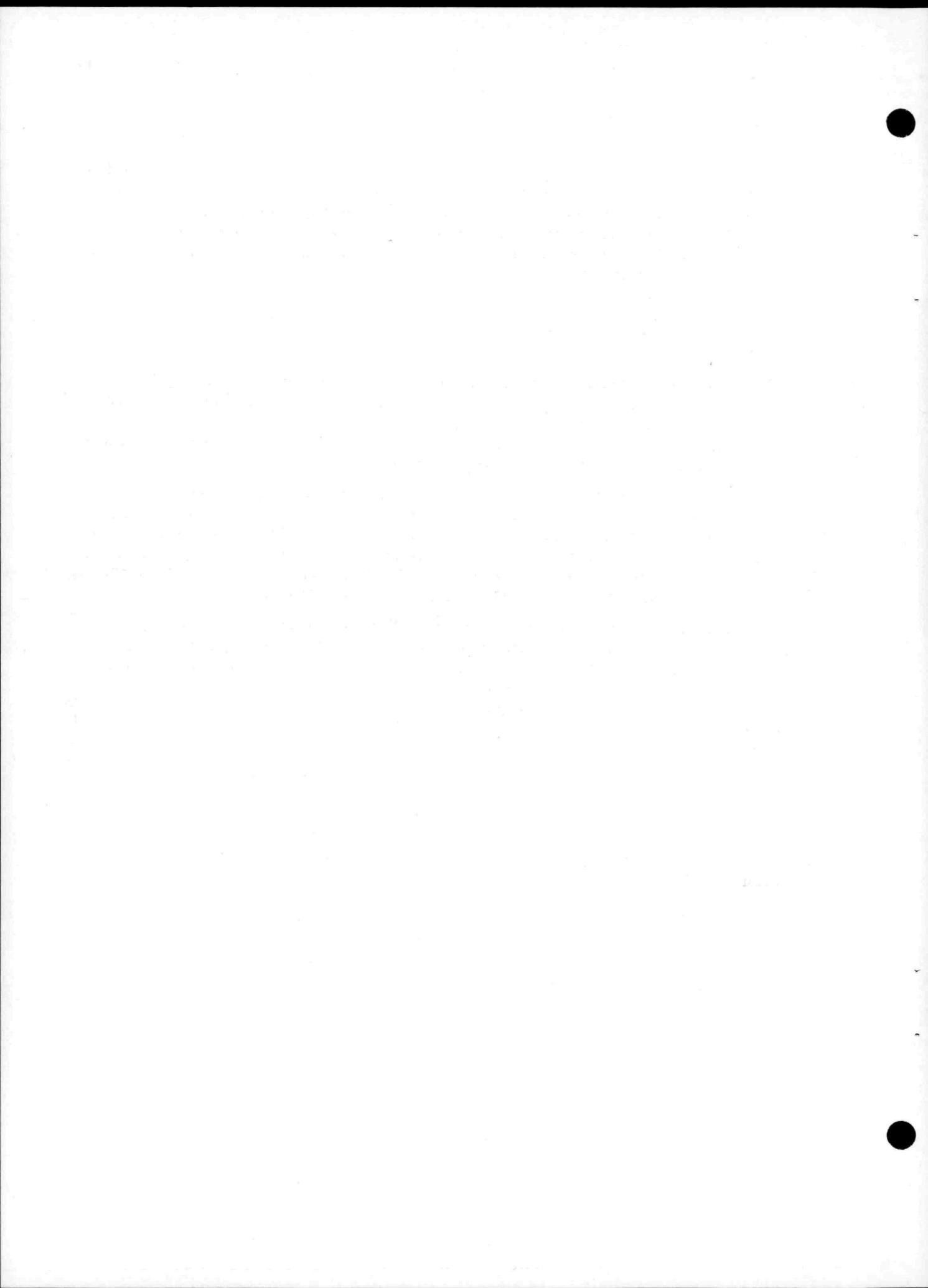
2. TYPE 310 STAINLESS STEEL-UO₂ CORE CLAD WITH Fe-Cr-Al

Although the high temperature requirements for aircraft nuclear power plants led to early interest in ceramic materials, it was apparent that considerable basic work was required to develop satisfactory ceramic fueled materials. The initial objective of a limited flight test permitted a reduced requirement for fueled materials. A maximum temperature of 1800°F for 100 hours was considered adequate.

2.1 MATERIAL SELECTION

Available metals and alloys expected to meet these requirements and not containing elements which would make the fuel investment prohibitively large were surveyed.[1,2] Alloy stainless steel Types 309, 310, 442, and 446 warranted first consideration. Heat transfer area and critical mass required the fuel elements to be about 0.015 inch thick.

For a fuel element approximately 0.015 inch thick, oxidation resistance is an extremely important factor. Types 442 and 446 stainless steel were not investigated further because of their poorer oxidation resistance and low rupture strength. Type 310 stainless steel possesses the most favorable oxidation resistance. But, since Type 309 yields a lower cross section, it was initially chosen for investigation. The lower strength properties of Type 309 resulted in a decision to utilize a modified Type 310 stainless steel as the basic material for fuel element fabrication.

Commercial Type 310 stainless steel is an austenitic, ferrous-base alloy containing nominally 25 percent chromium and 20 percent nickel. To obtain more favorable nuclear properties, the nickel content was modified to 17 percent. This, in turn, necessitated the reduction of the chromium content to maintain a stable austenitic structure. Elements, such as cobalt, boron, and cadmium, with high cross sections were kept as low in quantity as possible. A certain amount of carbon, nitrogen, and manganese was retained to aid in stabilization of austenite and to guard against hot-shortness during rolling.

Uranium dioxide was chosen as a fuel because of its refractory nature, stability, availability, and non-reactivity with Type 310 stainless steel. Information available on fabrication and processing of oxide-dispersion type nuclear fuel elements developed earlier by NEPA at Oak Ridge added to the attractiveness of this type of fuel element.

2.2 FABRICATION AND PROCESS DEVELOPMENT

2.2.1 RIBBON-TYPE FUEL ELEMENTS

Four techniques explored for fabricating fuel sheet included the sandwich technique, frame technique, tube technique, and powder frame technique.[1,2] In most cases the fueled core was first formed by dispersing UO₂ powder in Cr, Ni, and Fe powders and then cold pressing and sintering in dry H₂. Oxide impurities were thus reduced, and the sintered body had a theoretical density of approximately 80 percent.

2.2.1.1 Sandwich

In the sandwich technique, a sintered core was sandwiched between stainless steel cladding plates that overlapped edges by 0.1 inch. The assembly was hot-pressed in a molybdenum-lined graphite die at 2300°F (1260°C) at 3000 psi. The molybdenum liner prevented carburization of the stainless steel. An alumina or beryllia coating on the molybdenum prevented diffusion. The overlapping edges were sealed by heliarc welding. The structure of the compact at this point was weak and required working to develop a strong, continuous stainless steel structure.

2.2.1.2 Frame

The frame technique was a modification of the sandwich technique. Instead of depending on welded edges, a metal frame was placed around the compact before hot pressing to provide a positive core seal and maintain more accurate control over core dimensions. The compact, at 80 percent of theoretical density, had to be thicker initially to obtain a high-density core after hot pressing. In addition, the matching interface surfaces of core, frame, and cladding had to be kept free of oxidation for bonding to take place.

2.2.1.3 Tube

In the tube technique a sintered core was inserted into a flattened tube and the ends sealed by welding. The composite was then reduced directly to fuel sheet. The method had the advantage of being simple, but the disadvantage of less flexibility.

2.2.1.4 Powder Frame

The powder frame technique[4] was similar to the frame technique except that a powder frame was used to eliminate the differences in density. The bonding achieved was improved by this method because surface films initially present in both powder and sheet materials were disrupted. After pressing, the edges were welded as in the sandwich technique. This method offered reproducibility and flexibility.

The powder frame technique was eventually chosen for emphasis. The core and frames were cold pressed separately in rectangular steel dies of appropriate dimensions. The core was then inserted in the frame and the compact sintered for a period of 1 hour at 1900°F in dry hydrogen (dew point -70°F).

In order to establish an initial bond between the cladding and core, the billets were assembled and hot pressed prior to rolling. Hot pressing was performed at a temperature of 2200°F under 3000-psi pressure. A graphite die was used to enclose the billets during the pressing operation. Pressure was applied by a graphite plunger operated from a hydraulic press. An argon atmosphere was maintained within the pressing chamber, and the billets and interior die surfaces were coated with an alumina wash to prevent carbon pickup at die surfaces and welding between adjacent billets. A 40-KVA induction unit was used for heating.

After hot pressing, the billets were rolled to the desired fuel thicknesses by a combination of hot and cold rolling. Hot rolling was carried out at 2050°F with relatively heavy initial reductions to establish the clad-to-core bond. The billets were given a total hot reduction of approximately 90 percent and then cleaned by sand-blasting. After an anneal in hydrogen at 2050°F, the sheets were cold rolled to the desired final thickness.

Depending on the finished length of fuel ribbon desired, the billet or ribbon was cut to a predetermined length after completion of the rolling operation. Any exposed edges were sealed by means of a stainless steel strip or wire brazed in place. The brazed end seals showed greater promise than end seals made by welding since clearer lines of demarcation between fuel and seal were obtained.

2.2.2 WIRE-TYPE FUEL ELEMENTS

Wire-type fuel elements of stainless steel composition were fabricated. The process was similar to that described in the Ni-Cr wire-type fuel element fabrication techniques discussed in section 3.2.2.1.

2.3 ALLOY DEVELOPMENT

2.3.1 BRAZE ALLOYS[3]

Commercial brazing alloys were determined to be unacceptable for oxidation resistance and nuclear reasons. Two braze alloys were developed with the composition and properties listed in Table 2.1. The Ni-Cr-Si braze composition No. 62 had the minor disadvantage of becoming slightly contaminated with small amounts of uranium. This was believed to result from a reaction between UO_2 and silicon during the period the braze was liquid. Consequently attempts were made to substitute germanium for silicon, giving rise to alloy composition No. 72.

TABLE 2.1

BRAZE ALLOY COMPOSITIONS AND PROPERTIES

Property[a]	Alloy No. 62	Alloy No. 72
Composition, weight percent	68.5Ni, 20Cr, 11.5Si	57Ni, 13Cr, 30Ge
Composition, atomic percent	59.5Ni, 19.6Cr, 20.9Si	59.5Ni, 15.3Cr, 25.2Ge
Oxidation resistance	>310 stainless steel	>310 stainless steel
Hardness (R_c)	58	42
Melting point, $^\circ$F	2040 ± 25	1950 ± 5
Brazing temperature, $^\circ$F	2150	2150
Tensile strength at 70°F, psi	40,000	60,000
Reduction in area at 70°F, percent	10	5 to 10
Tensile strength at 1800°F, psi	12,000	not determined
Reduction in area at 1800°F, percent	1	not determined

[a]Mechanical properties based on transverse rupture test.

When No. 62 braze was used, joint strengths in the order of 100,000 psi were obtained with joints of zero clearance. As gap tolerance was increased to 0.002 inch, this strength dropped rapidly to 50,000 psi but fell no further as the gap was increased to 0.006 inch. It was believed that, as the gap is increased beyond 0.001 inch, the effects of diffusion are negligible. With gaps smaller than 0.001 inch, considerable interdiffusion of base metal and braze occurred. Later modifications of alloy No. 62 resulted in the development of No. 81 braze alloy, which is in very wide use commercially.

2.3.2 CLADDING ALLOYS

Constituents such as carbon, silicon, sulfur, and phosphorous may affect the strength properties adversely. Manganese, niobium, and titanium added in proper amounts may have beneficial effects, although experiments incorporating additions of Mn failed to achieve significant improvement in strength properties.

An unknown phase was observed to form in 310 stainless steel when heated to approximately 1900°F. Initial experimentation established this phase to be a nitride, probably of chromium. The precipitate was observed to be both intergranular and transgranular

in a form and amount that could be expected to embrittle. In further experimentation, strips of 310 stainless steel were heated in air so that a temperature gradient of from black heat to 2050°F existed along the specimens. The heating period was 150 hours. After heating, specimens were cooled and examined metallographically. A second phase was not found in those sections of the specimens which experienced temperatures below 1900°F. On the other hand, formation of precipitate was observed in sections heated above 1900°F with large amounts of precipitate forming slightly above this temperature, at 1950° to 2000°F.

To determine the effect of atmosphere on phase formation, a series of specimens was heated for 150 hours at 1900°F in atmospheres consisting of 20 percent O_2 and 80 percent A, 100 percent A, and 100 percent N_2.

The material heated in N_2-free atmospheres remained single-phased, while the material heated in N_2 contained large amounts of second phase.

Improvement of the alloy was also attempted through small additions of Nb to the basic composition, but no significant improvement in oxidation resistance under stress was obtained at 1800°F and 2000°F.

2.4   FUEL

At an early date, a proportional relationship was shown to exist between the volume of stainless steel displaced by UO_2 and the structural strength of fuel sheet up to 45 percent UO_2. Increased fuel concentration beyond 45 percent UO_2 resulted in a sharp decrease of properties. The particle size adapted for use in fabrication was 10 to 44 microns.[3] Presence of a significant number of particles below 10 microns or over 44 microns was found to seriously affect structural integrity at fuel concentrations in the order of 30 percent or more.

A detailed study was made of chemical and mechanical methods for synthesizing and sizing UO_2 particles. The only process that appeared to offer promise was based on high-temperature recrystallization. The UO_2 starting material used for developing the high-temperature recrystallization process was obtained from Mallinkrodt Chemical Company. The material was prepared by hydrogen reduction of U_3O_8 obtained by the thermal decomposition of uranyl nitrate. The as-received UO_2 powder was sieved through a -325 mesh screen to remove large agglomerates. The particles were then heated in a covered molybdenum crucible to between 2800°F and 3100°F and held at temperature for one-half to 2 hours depending on the particle size of the starting material. During this heat treatment, a solid-vapor phase reaction takes place. The result is the sublimation of the fine particles and the growth of large crystals. The large percentage of fines in the starting material causes a partial sintering of the charge into a friable mass that had to be broken up. Although the percentage of fines was less than that found in original material, it was still too large for stainless steel fuel-element application. To further lower the percentage of fines, the charge was reheated in a covered molybdenum crucible to between 3200°F and 3300°F and held at temperature for 10 to 15 minutes. In the absence of a large percentage of fines in the starting material, the granular charge was easily broken up after the second firing and passed through a 325-mesh sieve. Losses were found to be low during heat treatment. There was a 0.6 weight percent loss during the first firing and approximately 0.2 weight percent loss in the second firing. Analytical analysis indicated that the weight changes noted were caused by changes in composition rather than loss in uranium.

2.4.1 OXIDATION RESISTANCE[3,4]

2.4.1.1 Unstressed Conditions

The oxidation resistance of 310 stainless steel fuel sheet under isothermal, unstressed conditions is given in Table 2.2 and Figure 2.1.

Oxidation of fuel sheet proceeds by a mechanism that superimposes intermittent stringer penetration upon a more or less uniform surface attack. Since the uniform surface attack at normal operating temperatures is well below 0.002 inch, the operating limitations were set by the frequency and degree of stringer penetration.

Figure 2.1 shows, in graphic form, the maximum penetration given in Table 2.2. If 0.002 inch is accepted as correct for the thickness of stainless steel required to reduce fission fragment escape to acceptable levels, the data in the figure indicates that under isothermal, unstressed conditions the fuel element cladding will perform satisfactorily at temperatures at least as high as 1800°F. At elevated temperatures, the degree of oxide penetration is dependent upon applied stress. For this reason, when stainless steel fuel elements are to be subjected to appreciable stresses while at elevated temperatures, it is necessary to consider stress-oxidation phenomena.

TABLE 2.2

OXIDATION OF 310 STAINLESS STEEL FUEL SHEET FOR 100 HOURS UNDER ISOTHERMAL, UNSTRESSED CONDITIONS

Temperature, °F	Average Penetration, 10^{-3} inches	Stringers Per Lineal Inch To 0.002 Inch	Stringers Per Lineal Inch Beyond 0.002 Inch	Maximum Penetration, 10^{-3} inches
1500	0.4	25	0	0.5
1650	0.4	50	0	0.8
1800	0.5	100	0	1.2
2000	1.0	350	0	1.7
2100	1.5	450	0	1.9
2200		Completely oxidized		
2400		Completely oxidized		

2.4.1.2 Stressed Conditions

Tensile stress during oxidation increases the depth of stringer penetration into the fuel sheet cladding, as indicated in Figure 2.2, showing the maximum penetration noted after 100 hours at a series of temperatures and stresses. The data suggest that up to the nominal operating temperature of 1650°F, stringer penetration is not sufficiently severe to cause failure in less than 100 hours at stress levels at least as high as 1800 psi at 1650°F and 3500 psi at 1500°F. Premature failure at or below the nominal design temperature is more likely to be caused by rupture than by oxide penetration. If local excursions as high as 1800°F are experienced, the data indicates that oxide penetrations may reach 0.002 inch in depth at stresses as low as 250 psi and will extend completely into the core at stresses as high as 1000 psi. At 1800°F, then, premature failure could take place by excessive oxide penetration, rather than physical rupture of the sheet.

It is evident that for full, 100-hour operation, the maximum temperature had to be held to less than 1800°F if appreciable stresses existed in fuel element configurations.

26
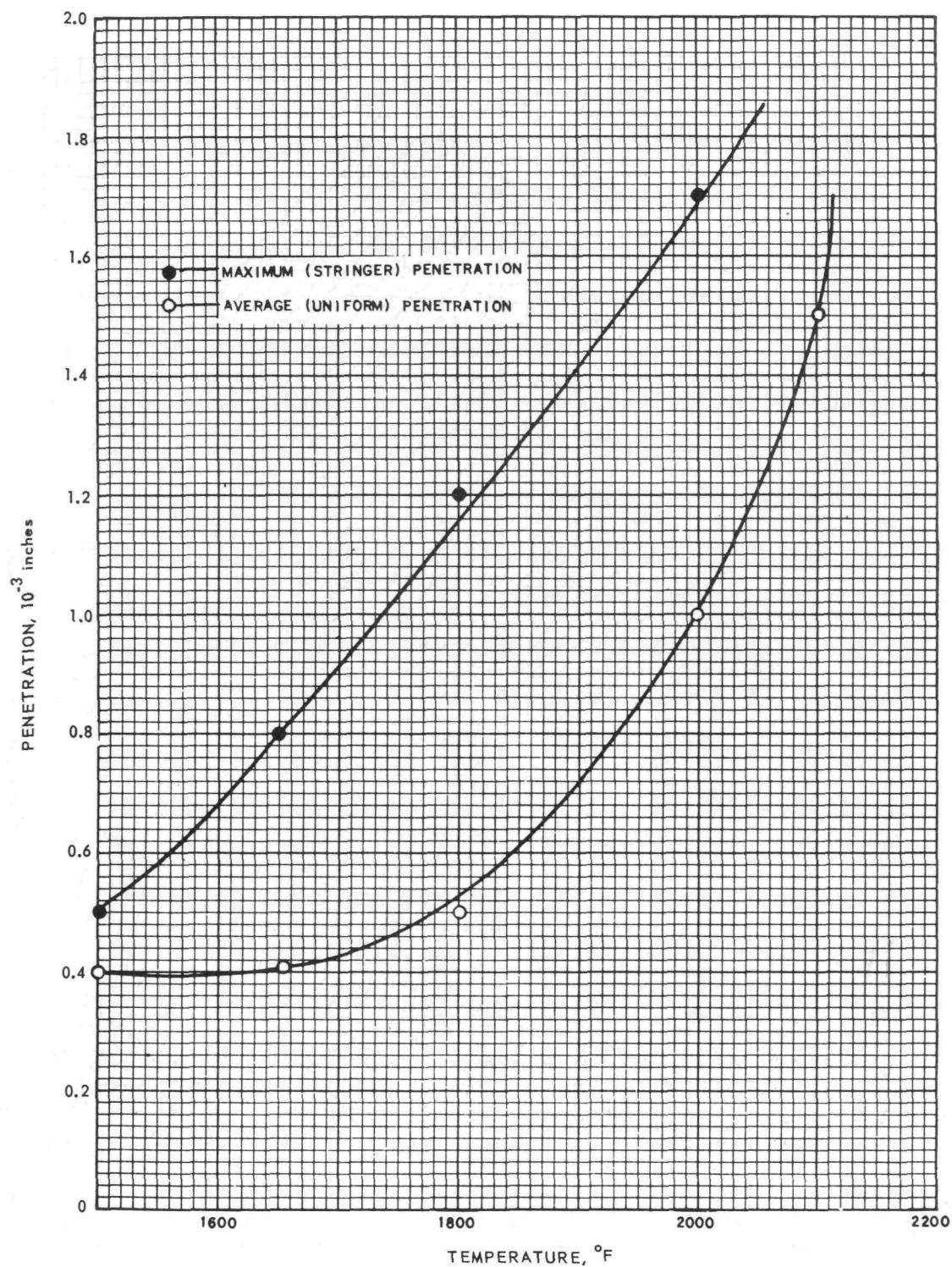
Fig. 2.1 – Oxide penetration of R-1 fuel sheet cladding in 100-hour unstressed isothermal tests
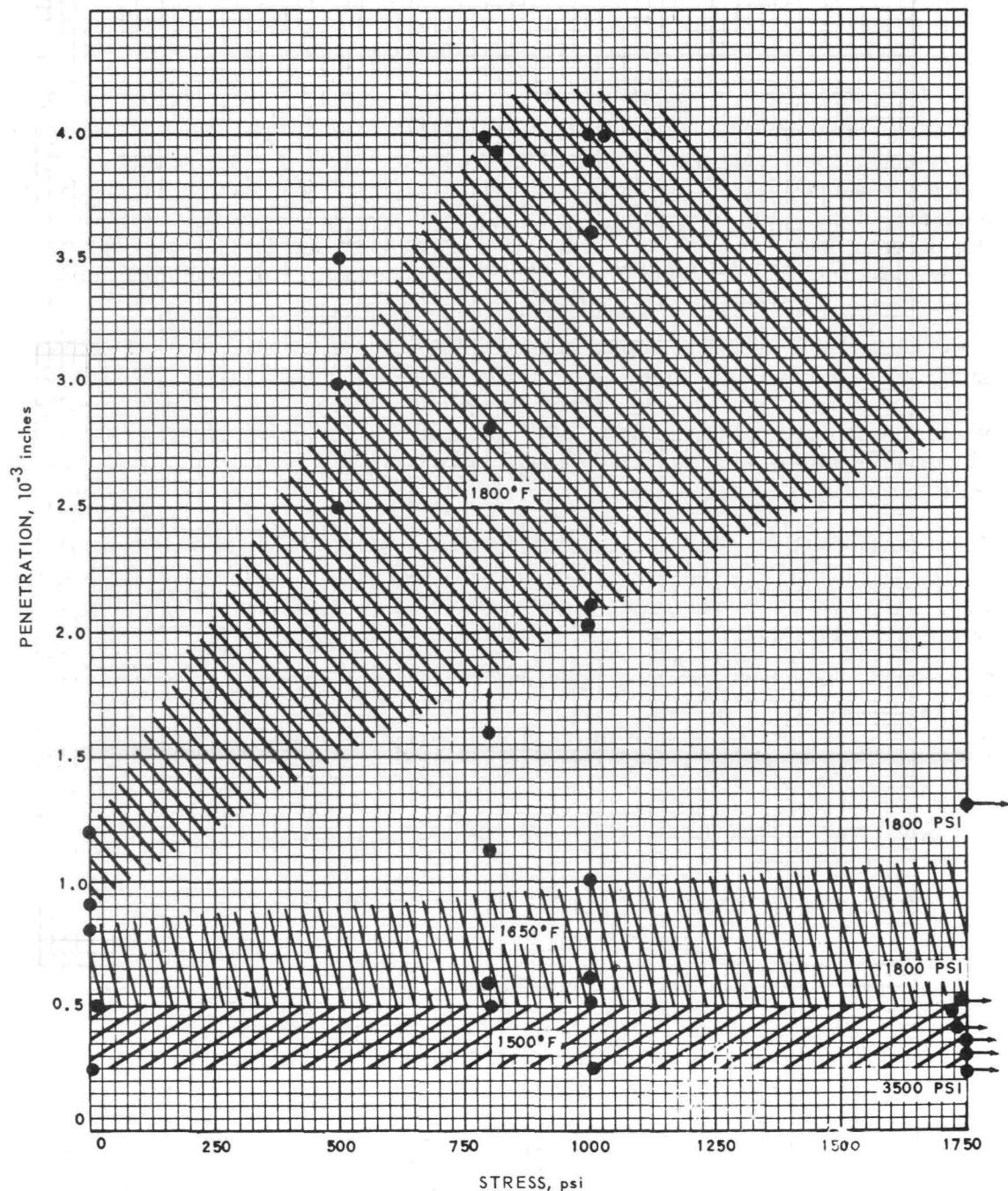
Fig. 2.2 — Effect of tensile stress on maximum oxide penetration of R-1 fuel sheet in 100 hours

If a stress of 1000 psi were assumed, for example, and the maximum permissible penetration were 0.002 inch, the curve illustrates that temperatures should not exceed 1740°F. The conclusion is that these elements can be subjected for only limited periods of time to temperatures of 1800°F or more. If they are subjected to such elevated temperatures, the stresses must be kept very low to prevent failure by stress oxidation.

2.4.2 TEMPERATURE CYCLING EFFECTS[4]

If stainless steel fuel sheet is subjected to a series of thermal cycles in the unstressed condition, the maximum oxide penetration will be of the same order of magnitude as for an isothermal specimen held for the same total time at a temperature equal to the maximum temperature of the cycle. For example, an unstressed specimen subjected to 45,000 cycles between 1800°F and 1300°F over a period of 100 hours was found to have oxide stringers penetrating to a depth of 0.0010 inch. An isothermal test at 1800°F resulted in penetration of 0.0012 inch after 100 hours.

It was not possible to draw a definite picture of the effect of thermal and stress cycles upon the stress-rupture life of the fuel elements. Data from other sources[1] have shown that the accuracy of a prediction of rupture life under cyclic conditions is largely dependent upon the geometry of the cyclic curve. If the true value of applied stress is known, the rupture life will be somewhere between the extreme values found to exist under isothermal conditions at that stress.

The importance of the effect of temperature upon fuel sheet life can be readily seen from data in Table 2.3. In the table, a value of unity was assigned to the 1650°F rupture-stress, creep, and oxide penetration of fuel sheet. That is, if the nominal operating temperature is 1650°F:

1. A 150°F rise in temperature is equivalent to reducing the nominal rupture stress by one-half.
2. A 150°F rise in temperature will result in 8.6 times nominal creep extension.
3. A 150°F rise in temperature will result in 1.5 times nominal oxide penetration if unstressed.
4. A 150°F rise in temperature will result in 4 times nominal oxide penetration if stressed to 1000 psi.

TABLE 2.3

TEMPERATURE FACTORS IN FUEL ELEMENT LIFE

Temperature, °F	Rupture Factor	Creep Factor	Unstressed Oxidation Factor	Stressed Oxidation Factor
1500	2	0.16	0.6	0.5
1650	1[a]	1[b]	1[c]	1[d]
1800	0.5	8.6	1.5	4
2000	0.3	–	2.1	Complete failure

[a]Stress for rupture in 100 hours (2200 psi at 1650°F).
[b]Total extension in 100 hours at 1000 psi (0.28 percent at 1650°F).
[c]Maximum oxide penetration 100 hours (0.8 mil at 1650°F).
[d]Maximum oxide penetration 100 hours (1.0 mil at 1650°F, 1000 psi).

2.4.3 MECHANICAL PROPERTIES

2.4.3.1 Tensile Strength

The elevated-temperature short-term tensile properties of fuel sheet are as illustrated in Figure 2.3. The average tensile strength varies from 23,000 psi ($\pm$4500 psi) at 1500^{O}F to 7000 psi ($\pm$500) at 2000°F. All data on strength properties, unless otherwise noted, are for fuel sheet containing 30 weight percent UO_2 in the core, sheet thickness of 0.012 inch and clad thickness of 0.004 inch. All test pieces were annealed at 1950°F and given a simulated braze cycle at 2150°F prior to testing. In Figure 2.4 the average tensile strength of fuel is compared to the range of values noted for commercial grades of Type 310 stainless steel. It is apparent the short-time tensile strength of 30 percent fuel sheet lies within the normal behavior pattern of Type 310 stainless steel. The fact that values for fuel sheet lie in the lower portion of the normal scatter band can be explained by the presence of 30 percent nonmetallic UO_2 in the core. If it is assumed that the UO_2 particles act as voids within the core and thus reduce the effective load-bearing area, the unit stresses would be increased by about 8 percent. That this assumption is essentially correct is illustrated by Figure 2.5 where the tensile strength of fuel sheet is compared to that of fuel-free cladding stock.

2.4.3.2 Ductility

Figure 2.6 describes the ductility of fuel sheet as measured during short-time tensile test. The figure illustrates the range of values found to exist for specimens taken from a number of fuel billets. Elongations range from a minimum of 10 percent $\pm$ 2 percent at 1650°F to a maximum of 17 percent $\pm$ 3 percent at 2000°F. Average ductility of fuel sheet is compared to the normal scatter band for commercial Type 310 stainless steel. Note that the elongation for fuel sheet lies below the range of values normally encountered for fuel-free Type 310 commercial sheet as shown in Figure 2.6. This is the not-unexpected effect of adding a large volume of nonmetallic UO_2 to the center of the sheet.

2.4.3.3 Stress-Rupture Properties[7]

The stress-rupture properties of fuel sheet are presented in Figure 2.7. The data covers a range of 1200° to 2000°F. At the normal design temperature of 1650°F, the 100-hour rupture-stress is 2300 psi, while at a temperature of 1800°F, the stress for equivalent life is reduced to 1200 psi. A generalized stress-rupture curve is presented in Figure 2.8 in the form of a master rupture curve for fuel sheet. Such a curve finds particular application in prediction of rupture times for stresses or temperatures not embraced in the experimental area recorded in Figure 2.7. Predictions from the master rupture curve are generally within 10 percent of the experimentally determined value for temperatures up to 1800°F. At higher temperatures, the predicted stress-rupture data are less precise, with predicted stresses being on the conservative side. At 2000°F, for example, master rupture data predicts 10-hour life at a stress of 1150 psi, whereas experimentally the stress for 10-hour life is found to be 1500 psi.

At elevated temperatures, fuel element life was measured not only by rupture but also by excessive oxidation. For this reason, a designer must temper the stress-rupture data given above by stress-oxidation data given earlier.

A comparison between the stress-rupture properties of fuel sheet and those of commercial 310 stainless steel is made in Figure 2.9. It will be noted that the 100-hour rupture stress for fuel sheet lies at the lower limit of the scatter band found to exist for commercial grades of Type 310 stainless steel.
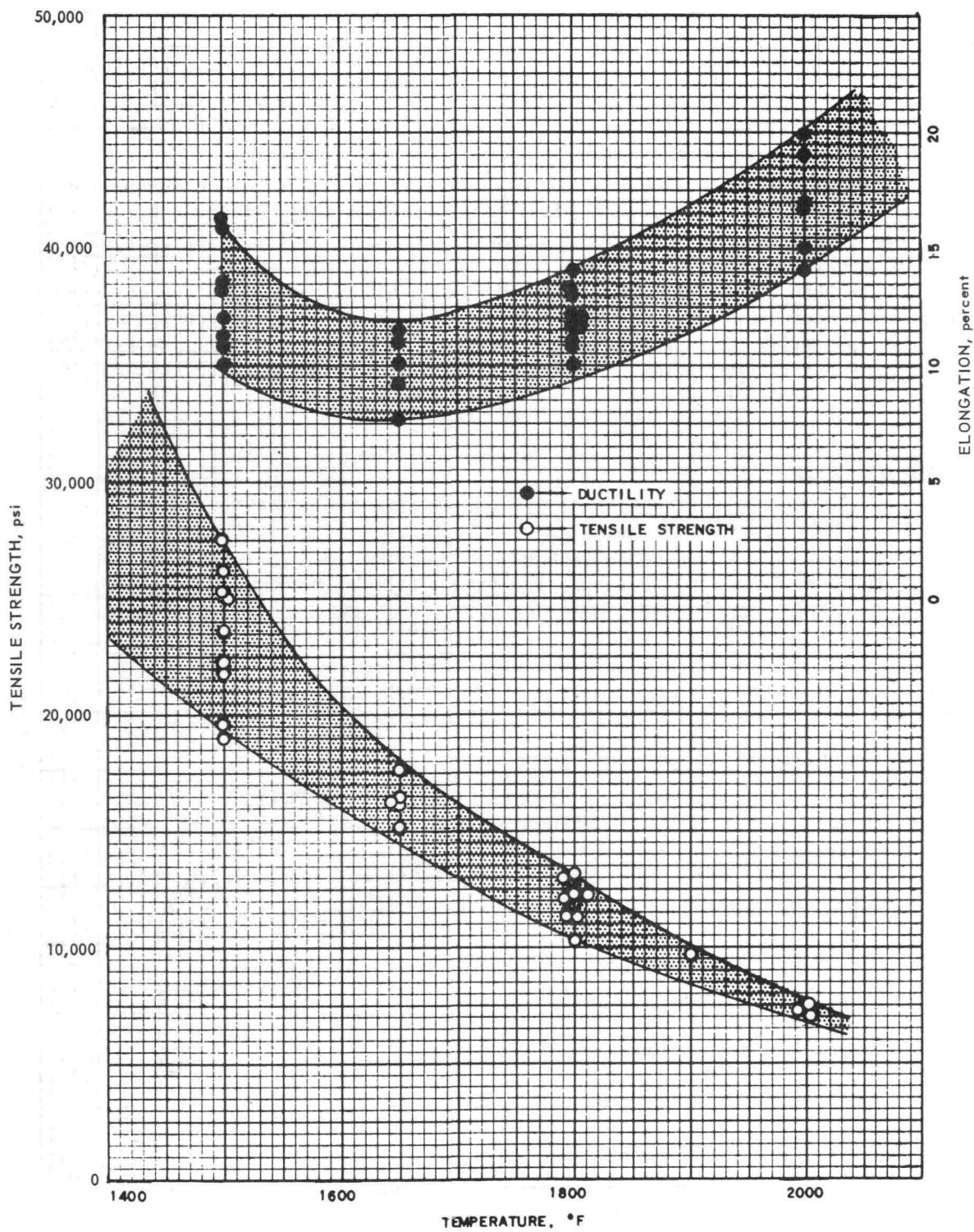
Fig. 2.3 – Tensile strength of Type 310 stainless steel fuel sheet with 30 weight
percent UO_2 core
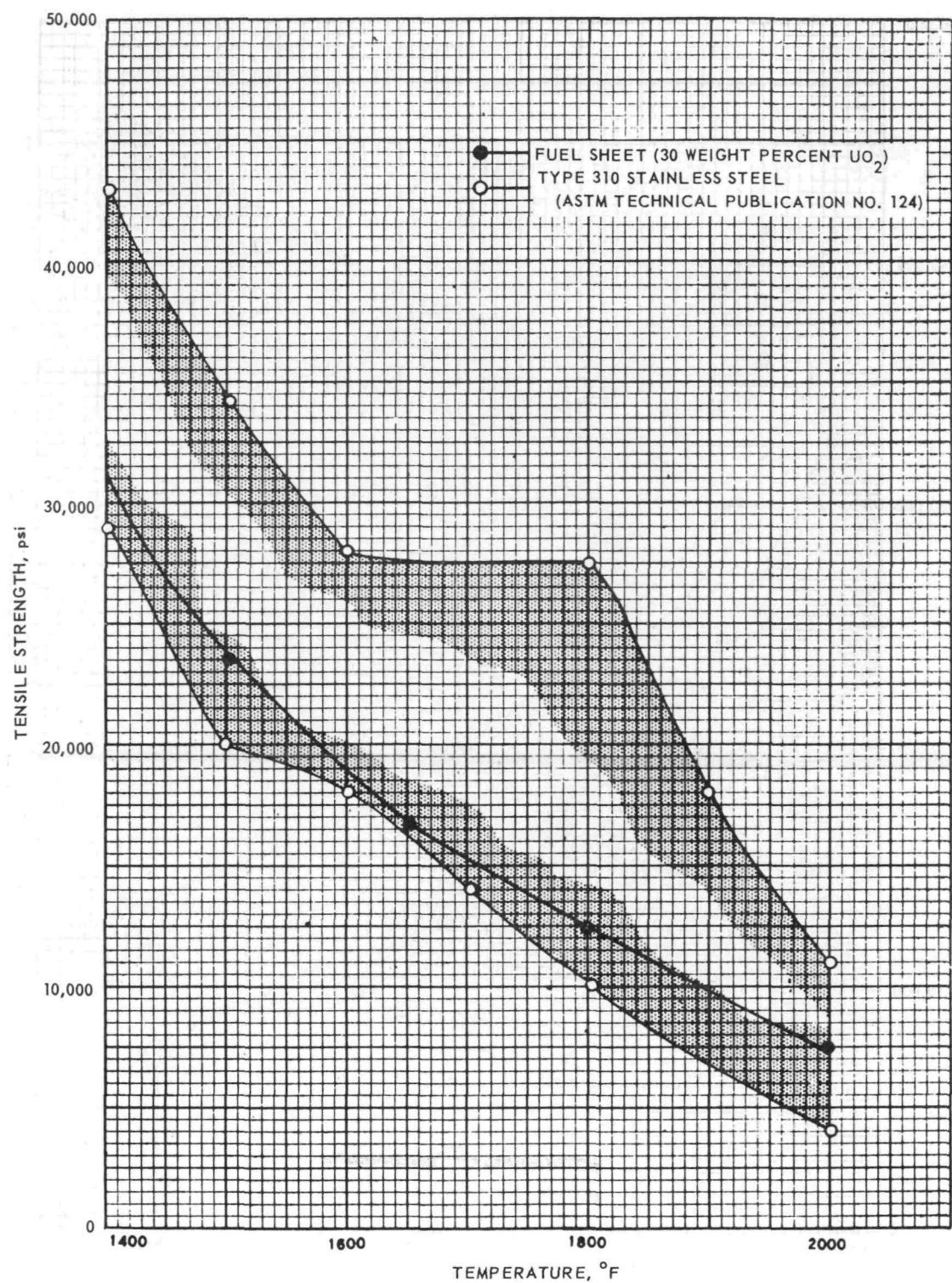
Fig. 2.4 — Tensile strength of R-1 fuel sheet versus commercial Type 310 stainless steel
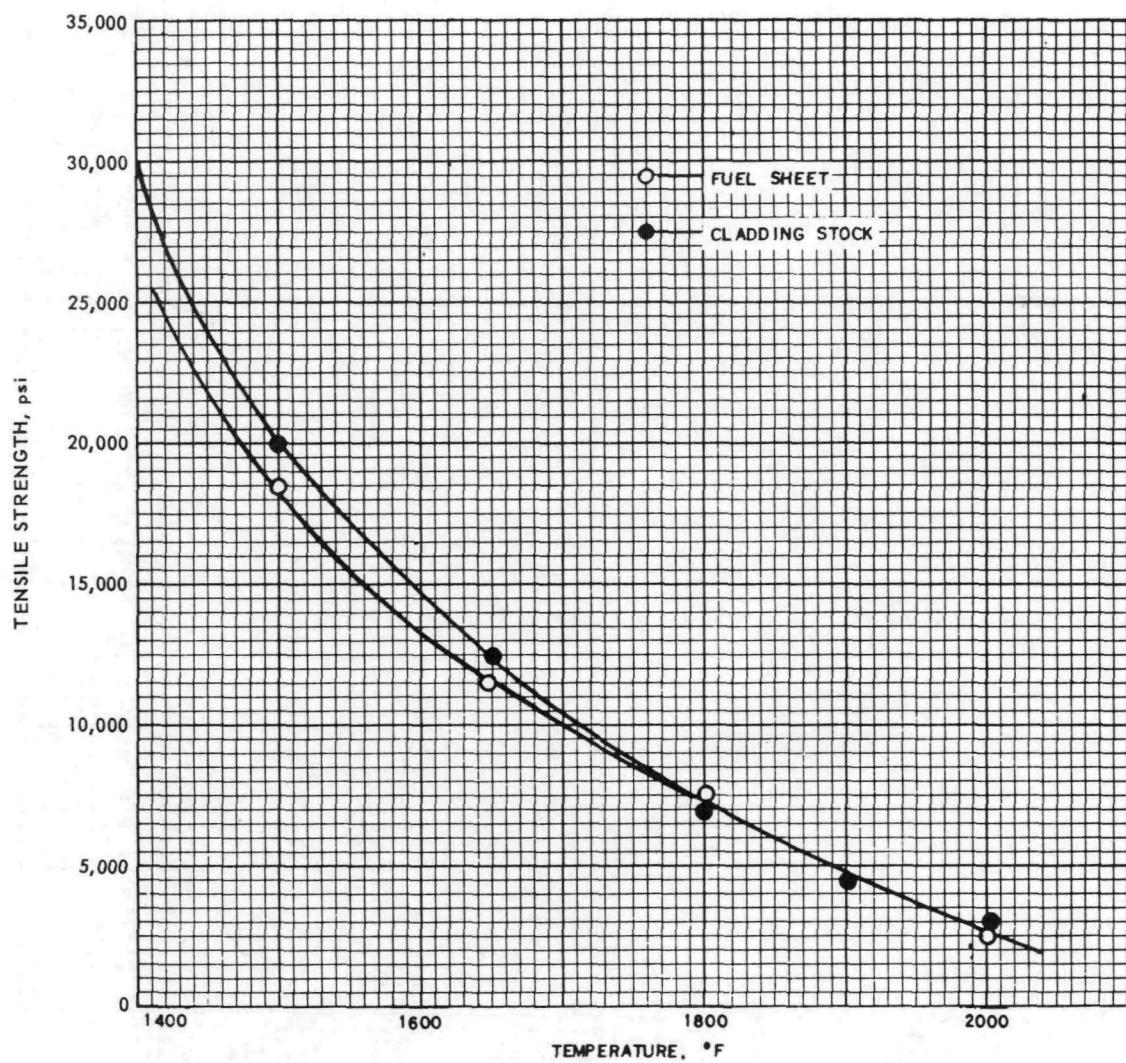
Fig. 2.5 — Tensile strength fuel sheet versus R-1 cladding stock
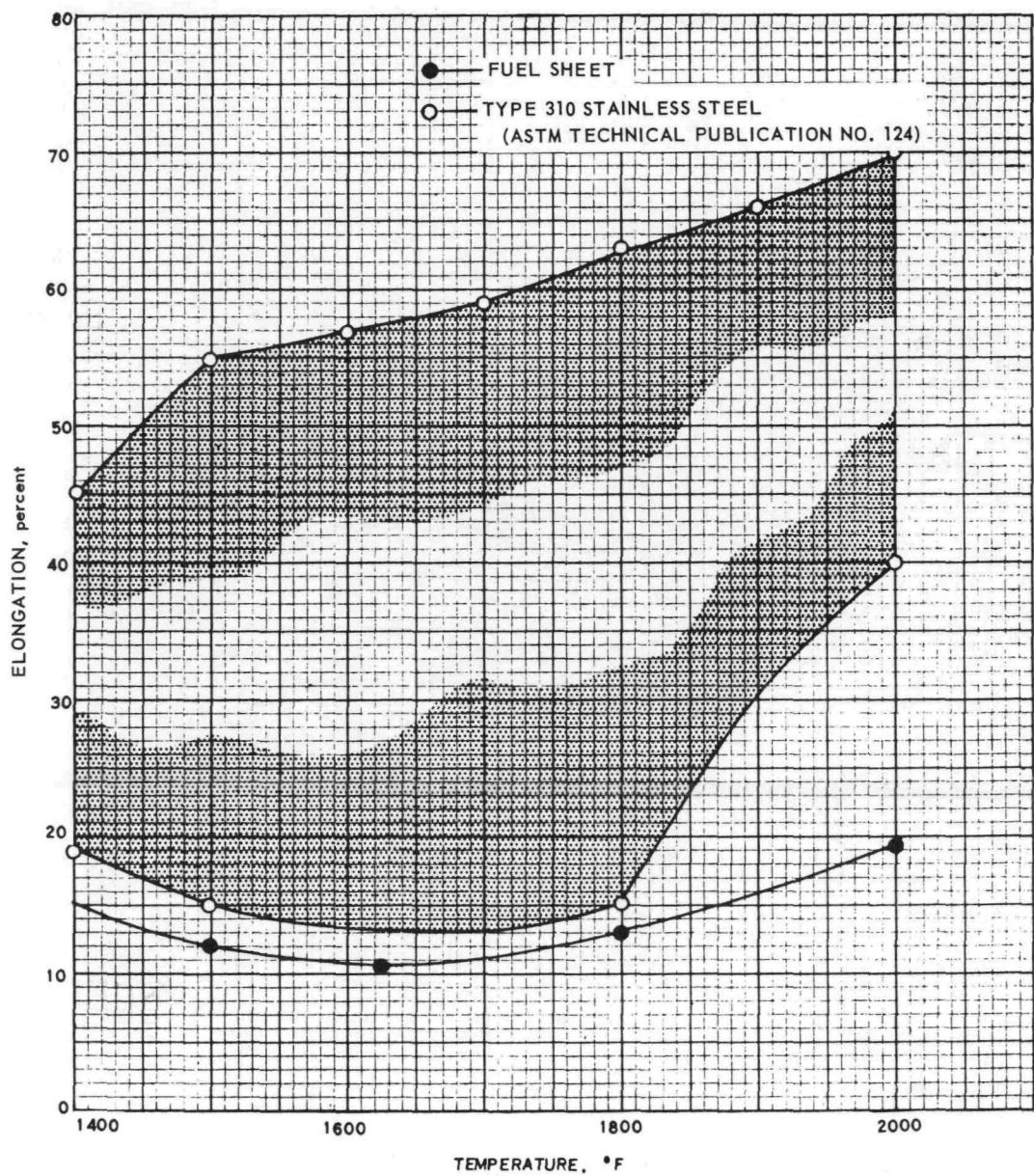
Fig. 2.6 — Ductility R-1 fuel sheet versus commercial Type 310 stainless steel
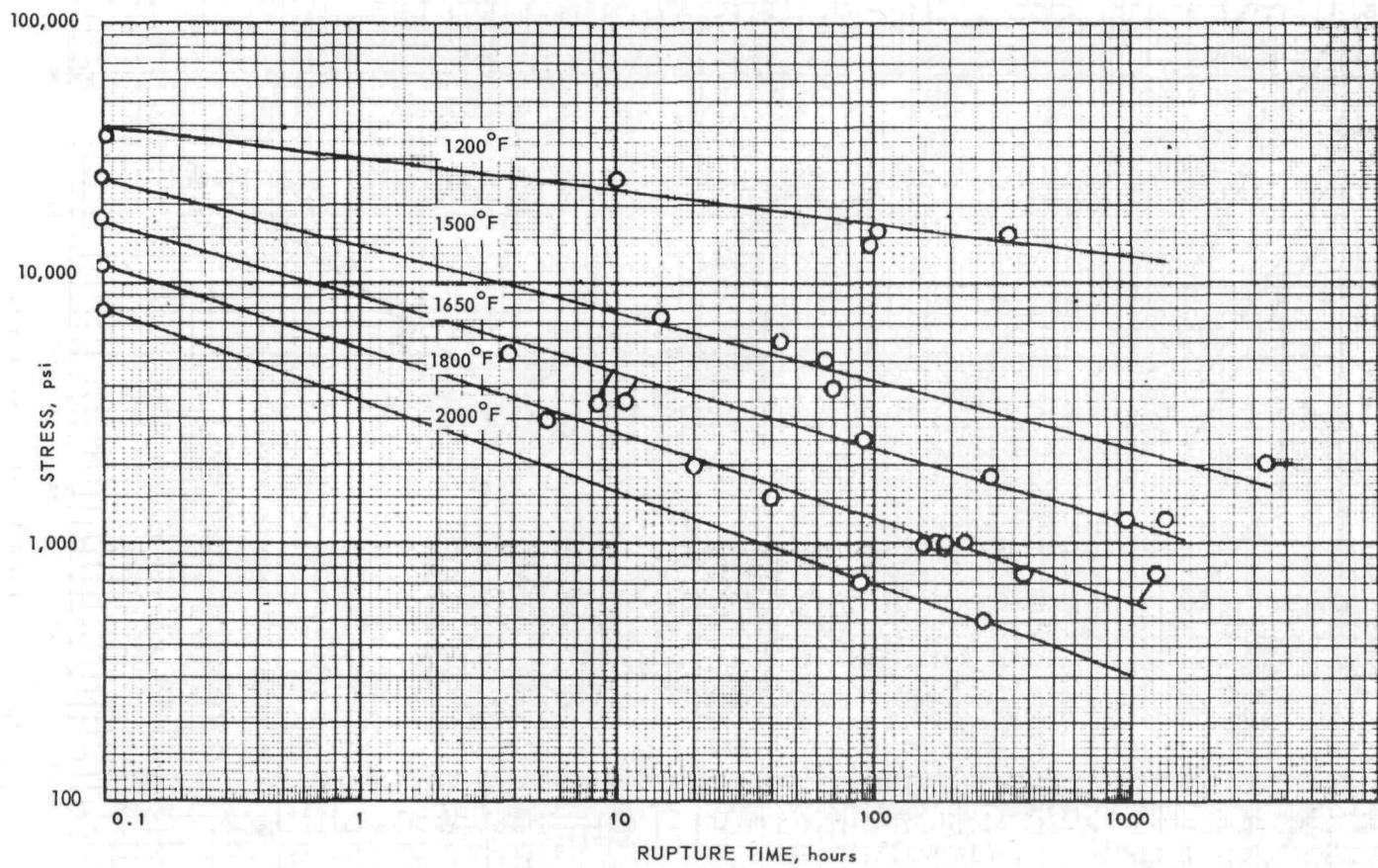
Fig. 2.7 — Stress rupture curves of R-1 fuel sheet, 30 weight percent UO_2 in core
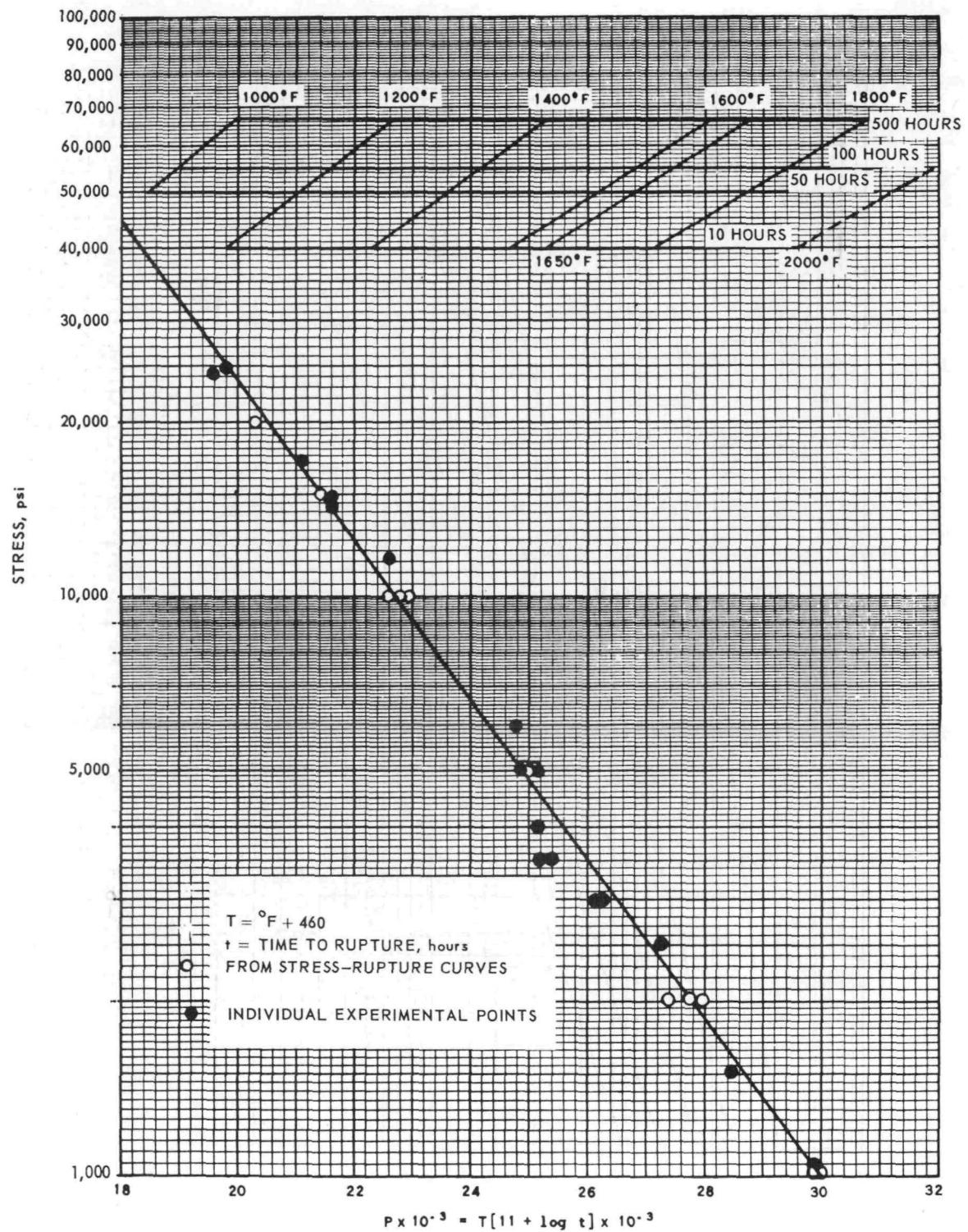
Fig. 2.8 — Master rupture curve of Type 310 stainless steel fuel sheet, 30 weight percent UO_2 in core
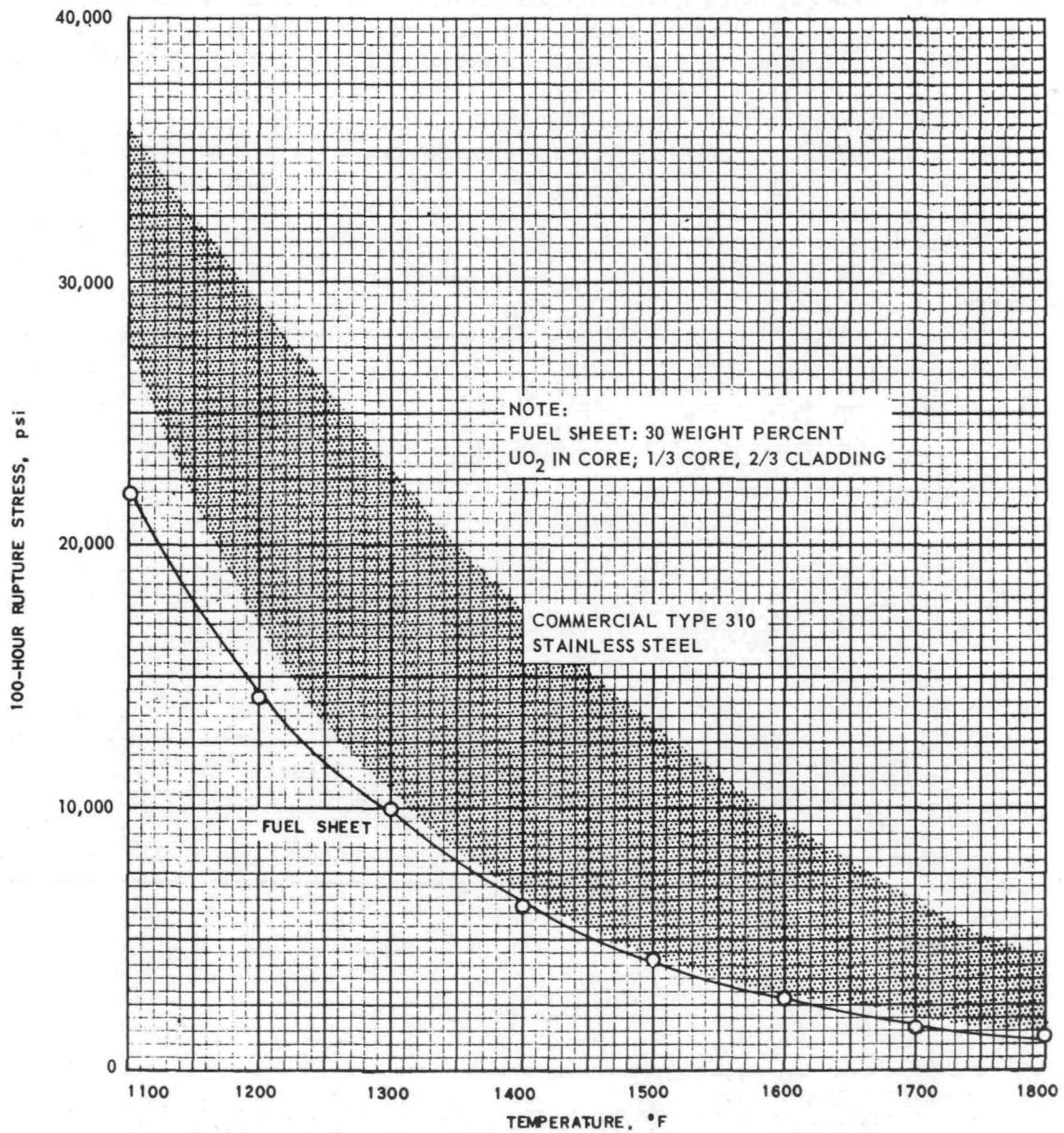
Fig. 2.9 — 100-hour rupture stress of R-1 fuel sheet compared to commercial Type 310 stainless steel

2.4.3.4 Time-Deformation Properties

Figure 2.10 illustrates the degree of deformation which may be expected at a series of temperatures after varying periods of time at a constant stress of 1000 psi. Since the second stage of creep has been found to be almost nonexistent at the temperature and stress of interest, complete time-extension curves are given in lieu of the usual method of reporting the rate of extension noted during the second stage of creep. As shown in the figure, a total extension of 0.28 percent may be expected after a period of 100 hours at 1650°F and 100 psi.

2.4.3.5 Transverse Rupture

The tensile strength of fuel sheet in the transverse direction, i.e., in the plane perpendicular to the core, might be expected to be lower than in the longitudinal direction because of the greater relative area of UO_2 in the plane of rupture. Figure 2.11 represents the transverse tensile strengths of fuel sheet at elevated temperature. Values range from 12,200 psi (± 400 psi) at 1500°F to 5300 psi (± 1400 psi) at 2000°F. In Figure 2.12 the average transverse rupture strength of fuel sheet is compared to the average longitudinal tensile strength. This illustrates the reduction in strength caused by the larger effective loss in load-carrying area in the transverse plane.

2.4.3.6 Fatigue

Fatigue properties were not extensively investigated. However, it was determined that fatigue failure of the fuel sheet investigated would not take place within 1.29×10^8 cycles in reverse bending between the stress limits +7400 psi to -7400 psi at room temperature.

2.5 BRAZED JOINTS

Data presented here were obtained by testing brazed-butt T-joints on a sheet of reactor grade Type 310 stainless steel. In all cases, the braze was No. 62. The braze was applied as a slurry of powder mixed with volatile liquid binder. The brazing cycle was carried out at 2150°F in an atmosphere of dry hydrogen with a dew point of -40°F or better.[4,6]

2.5.1 TENSILE STRENGTH AND DUCTILITY

Data in Figure 2.13 represent minimum values for tensile strength and ductility of brazed-butt T-joints on 0.015-inch Type 310 stainless steel sheet. These data represent joint strengths and do not necessarily represent the tensile strength of braze alloy No. 62 itself. Above 1200°F, rupture generally occurred in the base metal rather than in the braze. The ductility of brazed joints increases with temperature. At room temperature, elongation at rupture is somewhat above 1 percent, although the exact value was not determined. At 1800°F, the elongation at rupture increases to the order of 14 percent.

2.5.2 TENSILE STRENGTH VERSUS JOINT CLEARANCE

The influence of joint clearance is illustrated in Figure 2.14. At elevated temperatures, joint gaps up to 0.006 inch exert little influence upon the rupture strength of the joints. At room temperature, the joint strength decreases from 90,000 psi to 50,000 psi as the clearance is increased from 0 to 0.0015 inch. Beyond 0.0015 inch, the effect of increased joint clearance becomes less pronounced. Tests conducted on joints subjected to a thermal soak at 1800°F for 15 hours before testing revealed minor changes in physical properties as a result of diffusion. The average tensile strength at room temperature was approximately 10 percent lower than in the as-brazed condition, although still within the scatter-band presented in the figure. Ductility was correspondingly increased after the thermal soak; room temperature ductility being of the order of 1.4 percent after heat treatment, as compared to approximately 1 percent in the as-brazed condition.
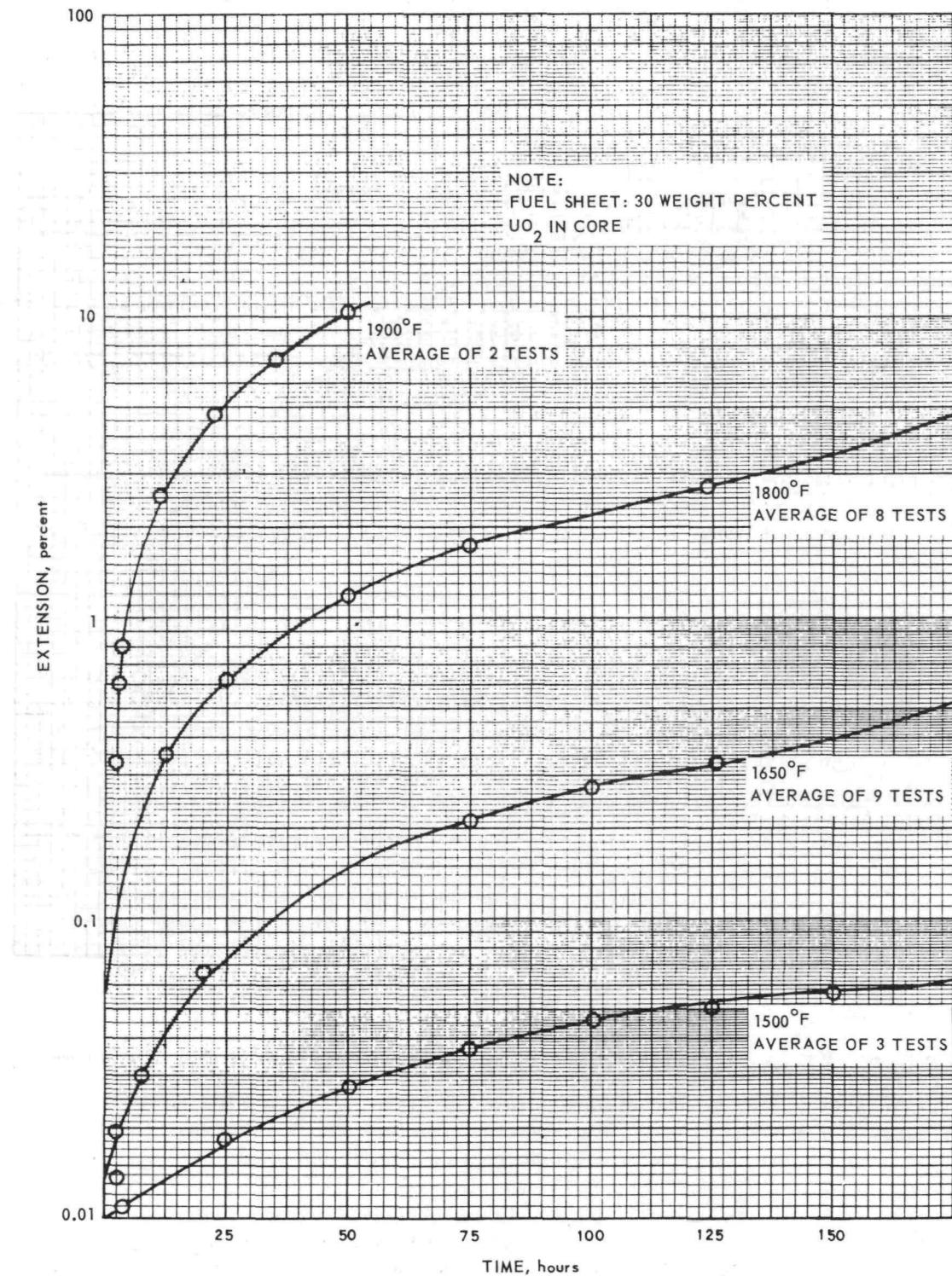
Fig. 2.10—Time-deformation curves of R-1 fuel sheet, 1000-psi stress
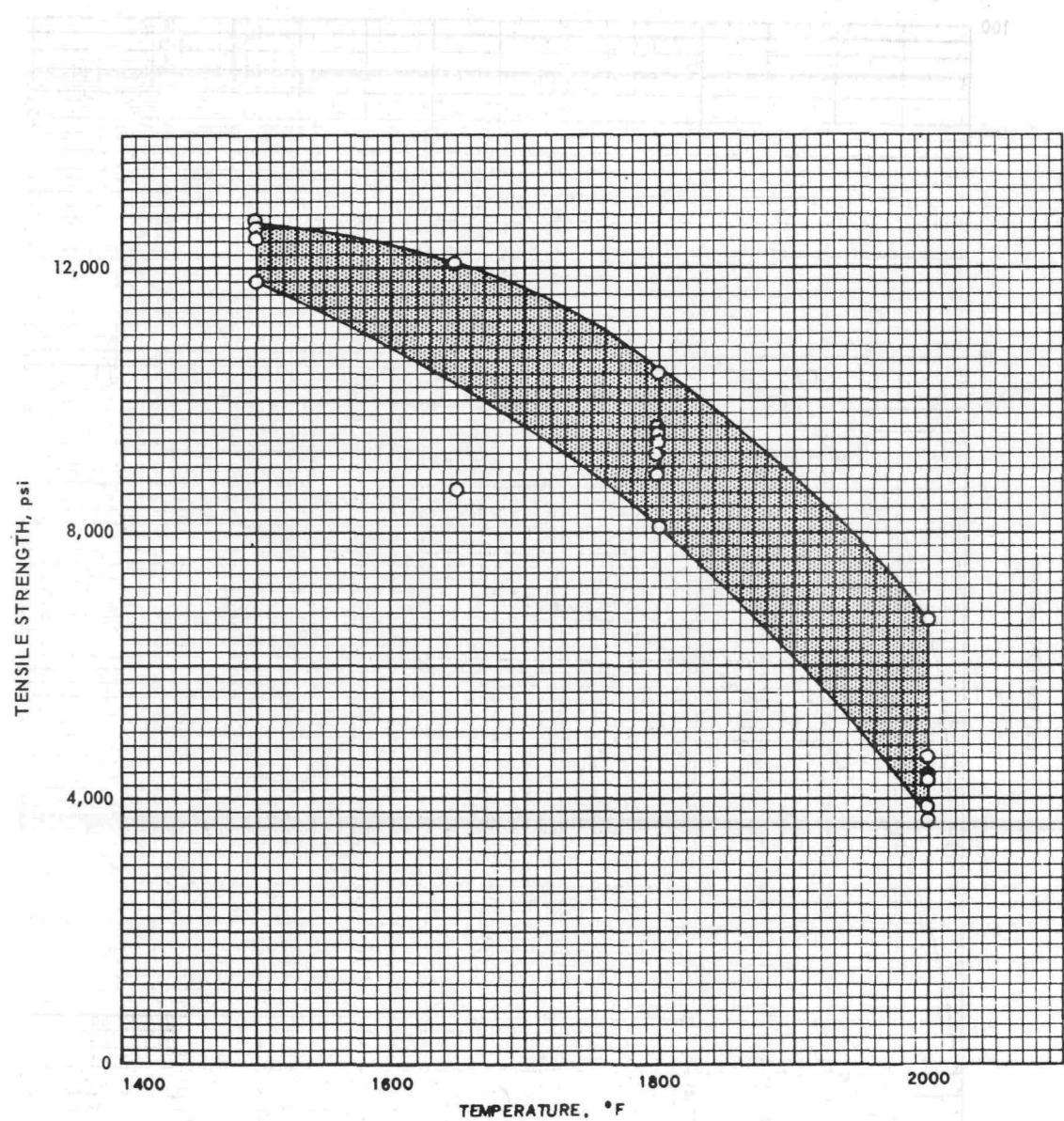
Fig. 2.11 — Transverse tensile strength of fuel sheet with 30 weight percent UO_2 in core
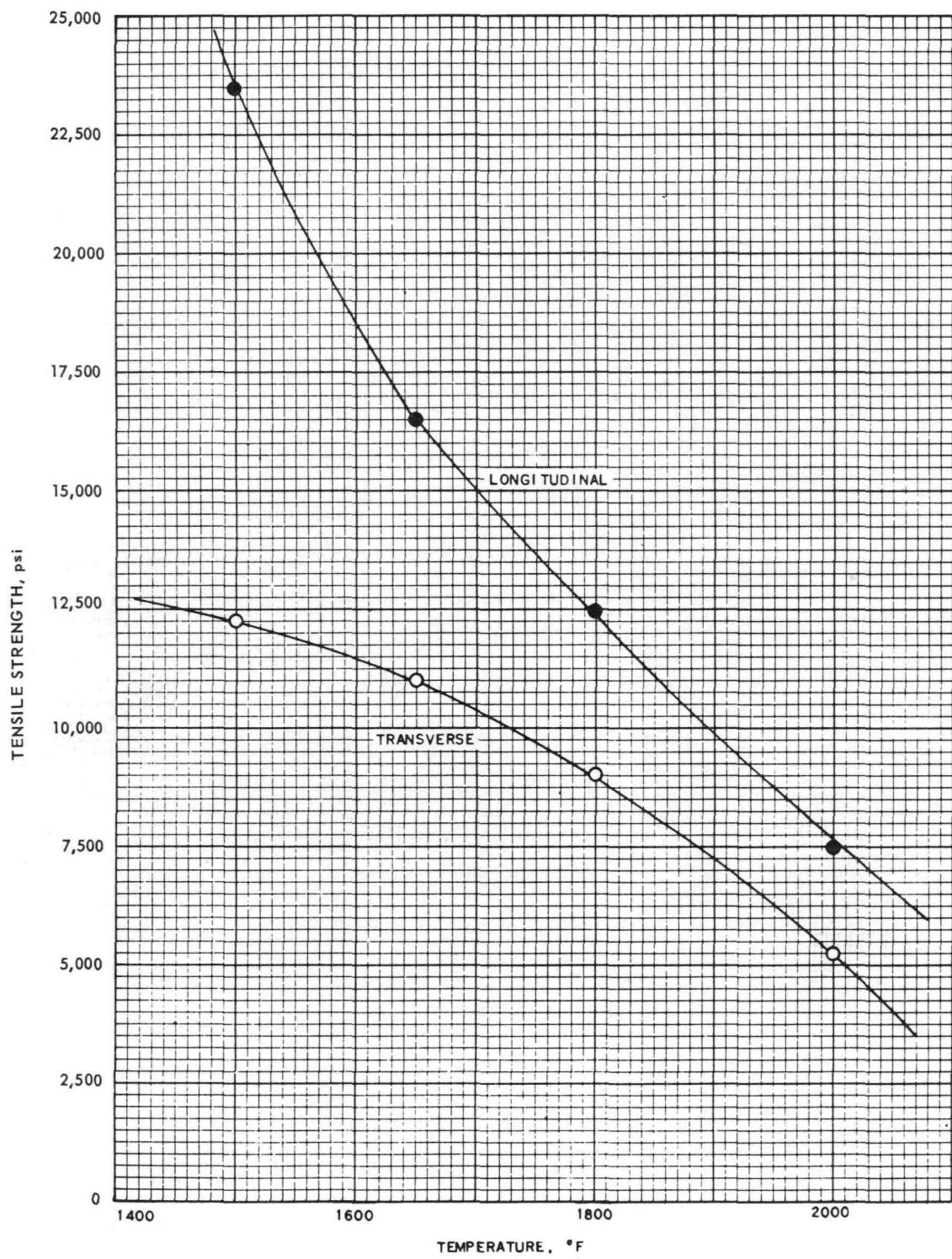
Fig. 2.12—Longitudinal and transverse tensile strength, fuel sheet with 30 weight percent UO_2 in core
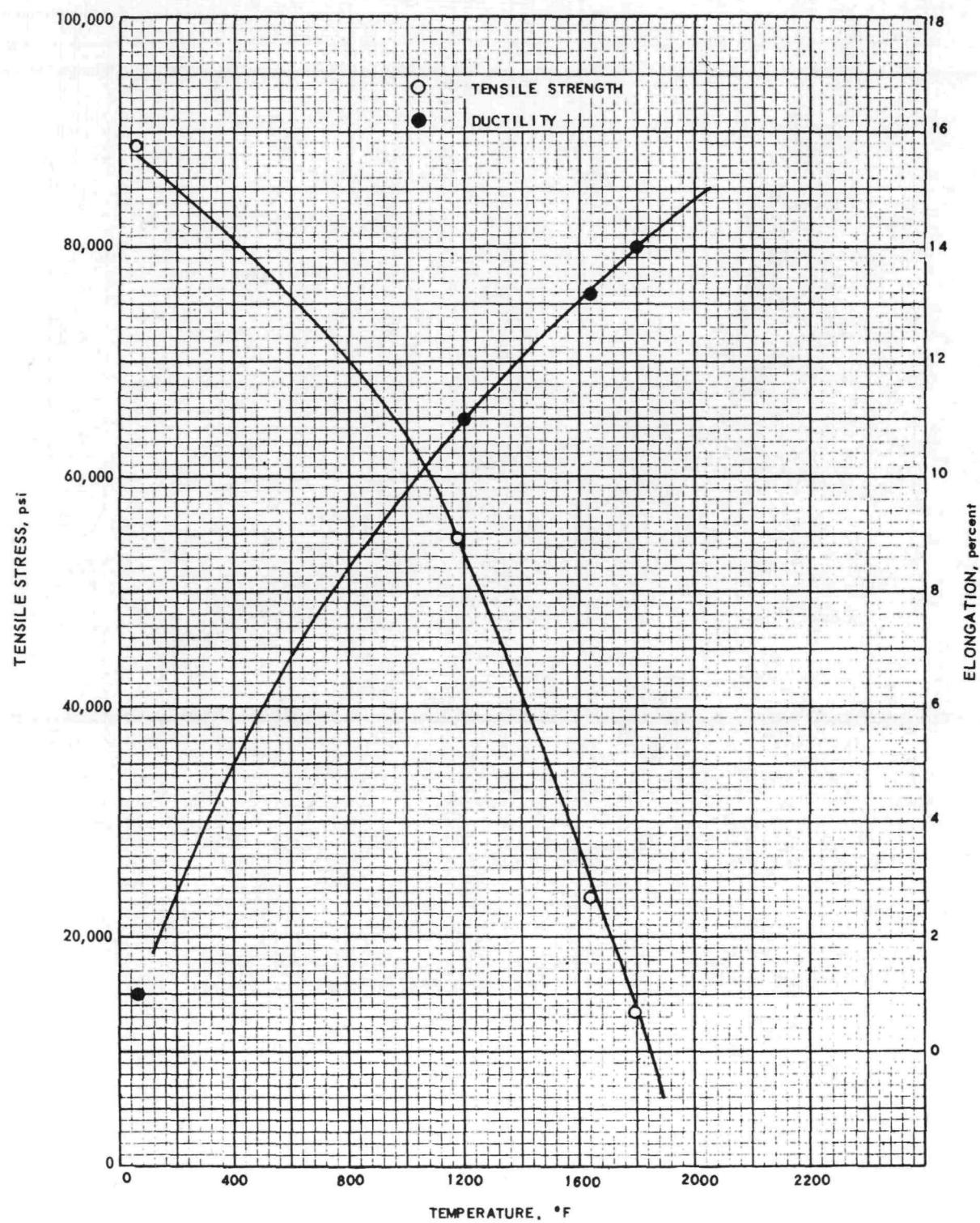
Fig. 2.13 — Tensile properties of No. 62 braze joints
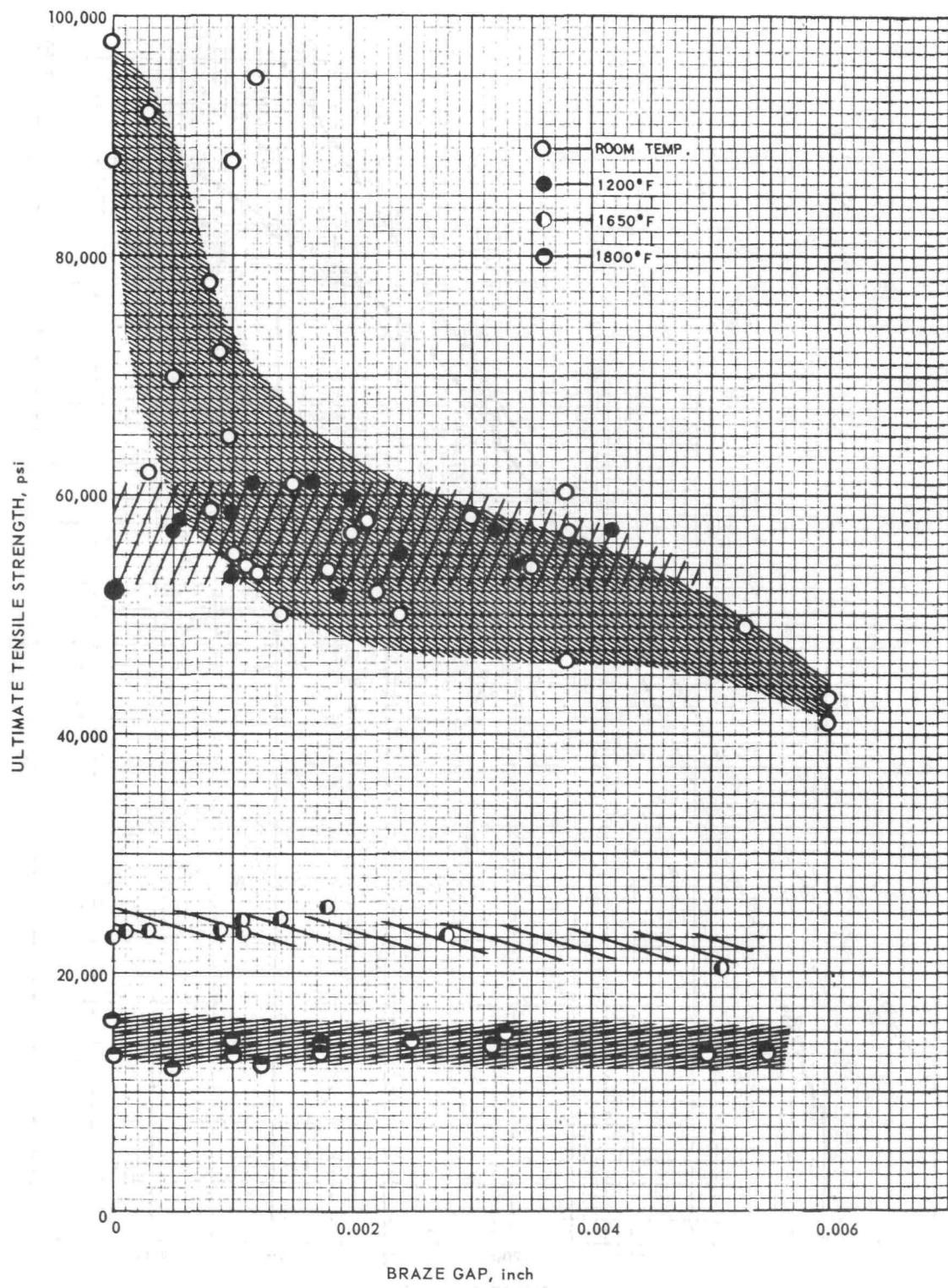
Fig. 2.14 — Tensile strength versus braze joint gap for No. 62 braze on butt-T joints on Type 310 stainless steel sheet
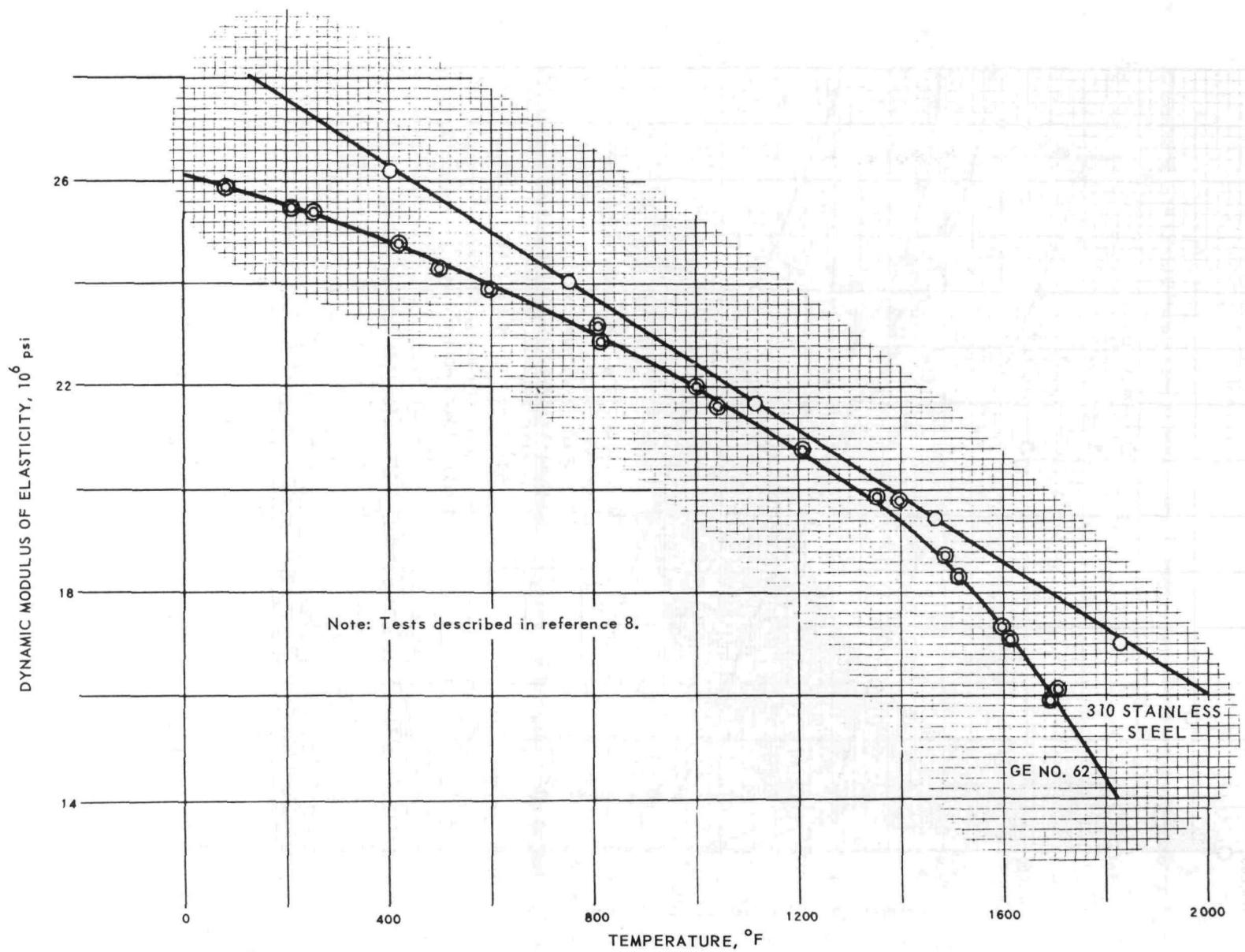
Fig. 2.15 — Dynamic modulus of elasticity for No. 62 braze and Type 310 stainless steel

44
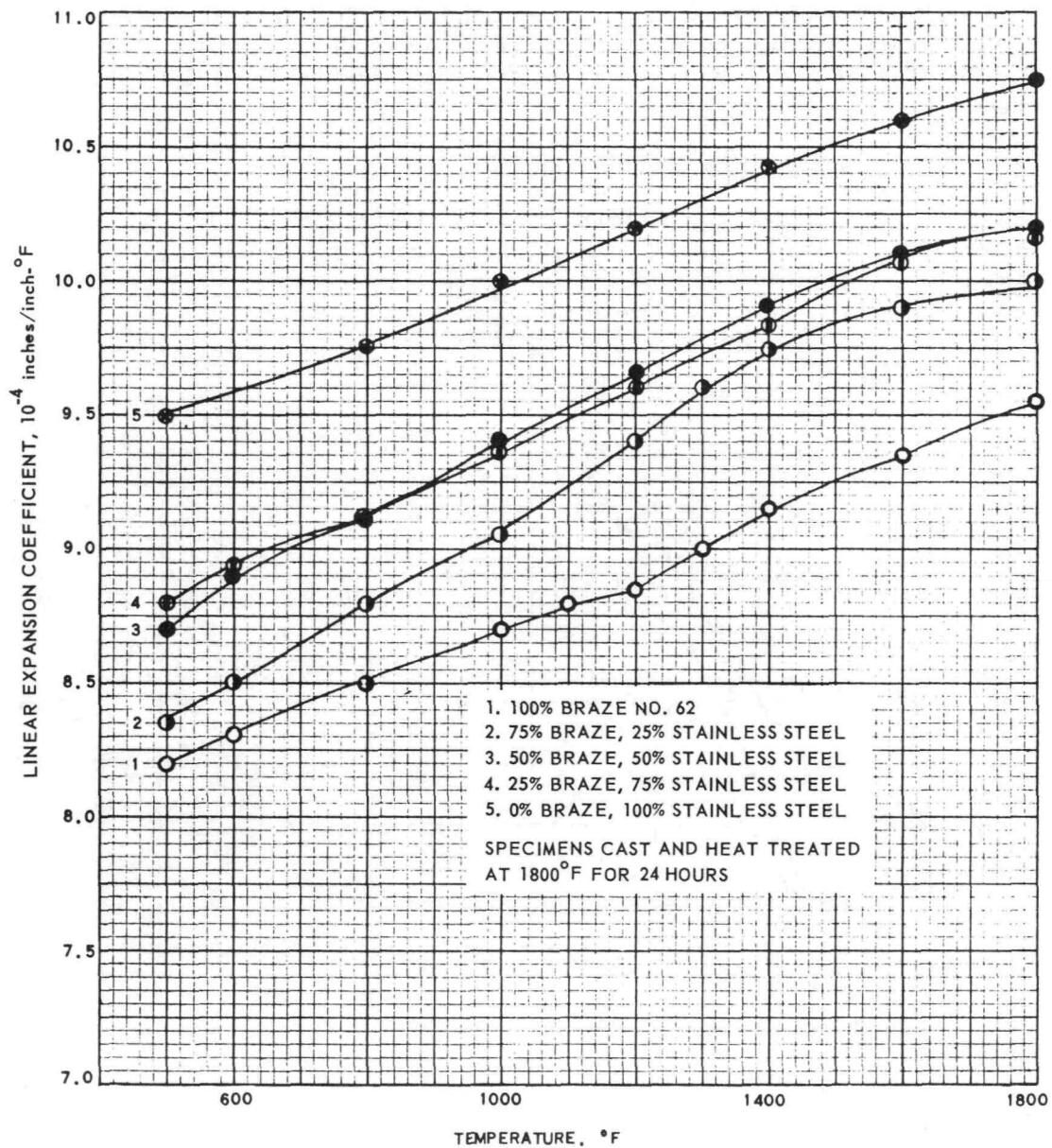
Fig. 2.16 — Mean linear thermal coefficients of expansion

2.5.3 ELASTIC MODULUS OF BRAZE NO. 62

The dynamic modulus of elasticity of No. 62 was determined over a temperature range 75° to 1700°F. Results are given in Figure 2.15 with a comparison of values for Type 310 stainless steel.

The elastic modulus for braze alloy is lower than that of Type 310 stainless steel over the temperature range investigated, although the difference is very slight in the range 1000° to 1400°F. At 1650°F the braze modulus is about 7 percent lower than that of stainless steel.

2.5.4 THERMAL COEFFICIENT OF EXPANSION OF BRAZE ALLOY

Data in Figure 2.16 were obtained from cast bars covering a composition range from 100 percent braze to 100 percent Type 310 stainless steel. The coefficients plotted are mean values between 68°F and indicated temperatures. All specimens were annealed for 24 hours at 1800°F in order to homogenize structure.

2.6 CONCLUSIONS

Tensile strength and ductility of modified Type 310 stainless steel fuel sheet are comparable in value to those of the lower areas of normal scatter bands for commercial Type 310 stainless steel.

Rupture strength of fuel sheet lies on the lower edge of the range of values found to exist for commercial grades of Type 310 stainless steel.

At temperatures above 1650°F, the oxidation resistance of Type 310 stainless steel fuel sheet is adversely affected by applied tensile stress.

The maximum temperature which fuel sheet can be expected to withstand for 100 hours under 1000-psi stress is of the order of 1740°F.

Brazed joint strength is essentially independent of joint gap at elevated temperatures. At low temperatures, maximum strength corresponds to minimum joint clearance.

Braze joint ductility is equivalent to that of the base metal at temperatures above 1200°F.

Thermal expansion of braze No. 62 is approximately 12 percent less than that of 310 stainless steel over the temperature range of 500° to 1800°F.

Modulus of elasticity of No. 62 braze alloy is of the order of magnitude of that for 310 stainless steel.

46

2.7 REFERENCES

1. "Engineering Progress Report No. 1," GE-ANPD, DC 51-9-36, September 1951.
2. "Engineering Progress Report No. 2," GE-ANPD, DC 51-12-25, December 1951.
3. "Engineering Progress Report No. 3," GE-ANPD, DC 52-3-54, March 1952.
4. "Engineering Progress Report No. 4," GE-ANPD, APEX-4, June 1952.
5. "Engineering Progress Report No. 5," GE-ANPD, APEX-5, September 1952.
6. "Engineering Progress Report No. 6," GE-ANPD, APEX-6, December 1952.
7. "Engineering Progress Report No. 7," GE-ANPD, APEX-7, March 1953.
8. "Engineering Progress Report No. 8," GE-ANPD, APEX-8, June 1953.
9. "Engineering Progress Report No. 9," GE-ANPD, APEX-9, September 1953.
10. "Engineering Progress Report No. 10," GE-ANPD, APEX-10, December 1953.
11. Miller, J., "Cyclic Temperature Rupture Tests," General Electric Thompson Laboratory, D. O. 52TL158, June 27, 1952.

3. Ni-Cr FUEL ELEMENTS

A nickel chromium (80Ni - 20Cr) alloy was considered early in the GE-ANPD program as one of several commercially available, workable, high-temperature alloys suitable for fuel element cladding. This alloy was utilized in nearly every principal reactor design including the P-1, the AC series, the HTRE series, the XMA-1, and the advanced folded-flow reactor. With the need for increased reactor temperatures and operational life, which were beyond the capabilities of the Ni-Cr alloy, material programs were accordingly redirected.

The fuel, finely divided, fully enriched U^{235}, as the dioxide, was dispersed in a metallic matrix provided by mixing the oxide with 80Ni - 20Cr powder. Although some fabrication and testing were done on fueled Ni-Cr wire, the principal effort involved fabricating fueled Ni-Cr ribbon, approximately 1.25 inches wide and 0.012 to 0.23 inch thick, which was formed into concentric ring fuel elements. Cladding was approximately 0.004 inch thick, and fuel content varied from 30 to 42 weight percent of the powder metallurgy matrix. Most of the ribbon was cold finished; however, hot finishing was found, near the end of the effort, to be definitely advantageous from the standpoint of fuel distribution and of resistance to deformation and oxidation penetration under stress.

The data[1] plotted in Figure 3.1 illustrate the time-temperature capability of 80Ni - 20Cr concentric-ring fuel elements.

3.1 80Ni-20Cr CLADDING DEVELOPMENT

A program was initiated to determine the effect of additives on stress rupture properties of 80Ni - 20Cr when specimens of this alloy failed at lower-than-expected strength levels during stress rupture tests. Metallographic examination of the test specimens revealed the presence of pits and internal voids, which suggested the detrimental effect of chromium nitrides. Chemical analyses of the specimens confirmed this by indicating that N_2 content had increased from 0.02 to 0.40 percent in 100 hours at 1800°F. The program aimed at determining the effects of the additives included studies of such nitride-forming elements as Al, Zr, Nb, and Ti in addition to rare earths.[2-9] Table 3.1 compares data reported on stress rupture properties of Al-modified and Nb-modified ribbon versus ribbon composed of standard 80Ni - 20Cr. Although the Al-modified alloy exhibited high strength, the elongation was abnormally high. In 100 hours at 2000°F an elongation of 108 percent was observed[10] compared to 41 percent with Nb additive and 20 percent for the base alloy. Table 3.2 indicates the improved resistance to oxide stringer penetration of Ni-Cr with Al and Nb additives. The greater advantage of Al is offset by fabrication difficulty. The formation of an Al_2O_3 film prevented core-to-clad bonding, which resulted in blistered cladding. Forging and rolling of Ti-modified (2.5 wt %) 80Ni - 20Cr indicated the alloy to be hot-short. Alloys containing from 0.25 to 1.5 weight percent Zr were fabricable. A heat of Ni-Cr modified with Nb (1.13 wt %) and Zr (0.59 wt %) possessed superior oxidation resistance. Table 3.3 presents a comparison of properties of this modified

47

Symbol	Fuel Element Design	Test
●	AC-2	Burner rig
○	P 102	Burner rig
▲	P 102	Materials Testing Reactor (MTR)
□	P 103	Burner rig
◇	P 103	Engineering Test Reactor (ETR)
■	P 103 (hot finished)	Burner rig
◆	P 103 (hot finished)	Engineering Test Reactor (ETR)

Numerals represent exit dynamic head in psi

FUEL RIBBON AT 500 PSI
0.002 INCH OXIDE PENETRATION

FUEL RIBBON AT 1000 PSI
0.002 INCH OXIDE PENETRATION

Fig. 3.1 — Time-temperature capability of 80Ni — 20Cr concentric-ring
fuel elements

49

TABLE 3.1

COMPARISON OF STRESS-RUPTURE PROPERTIES OF
STANDARD 80Ni - 20Cr ALLOY RIBBON WITH THOSE
OF ALUMINUM- AND NIOBIUM-MODIFIED STOCK

Temperature: 2000°F

| Material | Rupture Stress, psi | |
	Rupture In 10 hr	Rupture In 100 hr
Standard 80Ni - 20Cr[a]	2900	1300
Nb-modified 80Ni - 20Cr	2700	2100
Al-modified 80Ni - 20Cr	3400	2800

[a]Data from Driver-Harris Company

TABLE 3.2

STRESS-OXIDATION RESULTS ON MODIFIED 80Ni - 20Cr CLADDING
STOCK AND ON FUEL RIBBON AFTER 100 HOURS AT 2000°F
UNDER 500-psi STRESS

Material	Maximum Oxide Penetration, in.	Total Elongation, %
Al-modified cladding	0.00057-0.00079	1 - 2
Nb-modified cladding	0.00063-0.0013	1 - 2
Fuel ribbon clad with Nb-modified cladding	0.00068-0.0010	2 - 5
Fuel ribbon clad with standard 80Ni - 20Cr alloy	0.0011-0.0026	3 - 6

TABLE 3.3

MAXIMUM OXIDE STRINGER PENETRATION OF FUEL RIBBON CLAD
WITH SPECIAL CLAD STOCK COMPARED TO RIBBON CLAD
WITH STANDARD 80Ni - 20Cr CLADDING STOCK

| Temperature, °F | Stress, psi | Time, hr | Maximum Stringer Penetration 10^{-3} Inches[a] | |
			Nb-Zr-Modified Ni-Cr[b]	Standard Ni-Cr
1800	1000	100	0.68[a] (0.52-1.09)[c]	1.47[a] (1.0-1.8)[c]
1850	1000	100	2.09 (0.77-4.40)	3.07 (1.25-5.+)
2000	500	100	0.86 (0.68-1.01)	1.68 (1.1-2.62)

[a]Measurements are the average maximum penetrations based on at least three separate tests at each condition.
[b]Ni-Cr modified with 1.13Nb - 0.6Zr (wt %).
[c]Extremes of penetration.

composition versus unmodified Ni-Cr. A Ni-Cr alloy containing 1 weight percent Y was found to be inferior to Nb-modified Ni-Cr. A material specification, GE-B50T2026, was prepared for commercial vendors to supply a "modified" 80Ni - 20Cr alloy containing 0.9 to 1.2 weight percent Nb. This Nb-modified 80Ni - 20Cr alloy was used for all fuel element data reported herein unless otherwise noted.

Additional studies were performed on the effect of silicon in increasing oxidation resistance. Recommendations were made[11] that (1) a vacuum-melted, instead of an air-melted, Nb-modified Ni-Cr composition containing silicon in a definite range of 1.0 to 1.2 weight percent (instead of a 1.5 maximum as given in GE-B50T2026) be substituted to achieve optimum oxidation resistance and (2) carbon level be reduced to 0.03 weight percent, maximum, to diminish the formation of chromium carbides. Because of an increased operating temperature and life requirements beyond the capabilities of Ni-Cr, these recommendations did not receive extensive application.[1, 2]

3.2 PROCESS DEVELOPMENT

3.2.1 RIBBON-TYPE FUEL ELEMENTS [2]

A flow chart of process steps[12] for producing concentric ring fuel elements is shown in Figure 3.2. A pictorial presentation of the steps is shown in Figure 3.3. Briefly, the process steps involved the following. The UO_2 powder was presintered in H_2 at 2200°F for 1 hour to assure conversion of U_3O_8 to UO_2 and to prevent oxidation of molybdenum crucibles and contamination of the UO_2 with MoO_2 during sintering. Sintering was done in hydrogen at 3092°F and in a molybdenum crucible to agglomerate fine particles and to obtain, after screening, a -325 screen particle size. Nickel and chromium powders were sieved through a 200 mesh screen prior to blending and passed through a 100 mesh screen after blending. Blending of nickel chromium powder with fuel was done in a 45-degree blender. Specified weights of blended nickel chromium powders were leveled into suitable tool steel dies and pressed under controlled pressure (19.3 tsi) to make the frames. Cores containing specified weights of fuel blend were compacted in dies at 24 tsi. After the cores were compacted, they were placed on perforated Inconel X sheets, and the frames slipped in place over them. As shown in Figure 3.4, the darker core contains fuel, while the frame is 80Ni - 20Cr powder. A close fit between core and frame compacts was achieved during sintering in hydrogen (-70°F dewpoint) at 2200°F since the unfueled frame shrank more than the core. The assembled core and frame was referred to as a billet.

The sintered assemblies were placed between sheets of cladding and tack welded between the frame and the cladding. The initial metallurgical bond between cladding and core was established by hot pressing. The billets were kept under pressure of 2400 psi at 2100°F ± 20°F for 8 minutes in a hydrogen atmosphere. Then, the edges of the billets were heliarc welded to provide protection against oxygen diffusing through the frame during hot-rolling. The billet, approximately 0.300 inch thick, was reduced to ribbon by hot- and cold-rolling in a direction parallel with its longest axis. Hot-rolling was done at a temperature of 2050° to 2080°F. The temperature of the billet during rolling was extremely critical in that it affected the compaction and spread of the core. Further, if too low a temperature were used, blistering of the clad occurred. Since surface condition of the rollers was critical, the rolls were replaced often. Hot-rolled ribbon was descaled by immersing in molten NaOH at 930°F ± 70°F for 20 minutes. Then, the ribbon was rinsed in water, in hot muriatic acid, and in water again. Final thickness of ribbon was obtained by cold-rolling and later by warm-rolling. Because surface quality was established at this point, extreme cleanliness had to be maintained. Warm-rolling, at 1500° to 1900°F, improved fuel element physical properties.
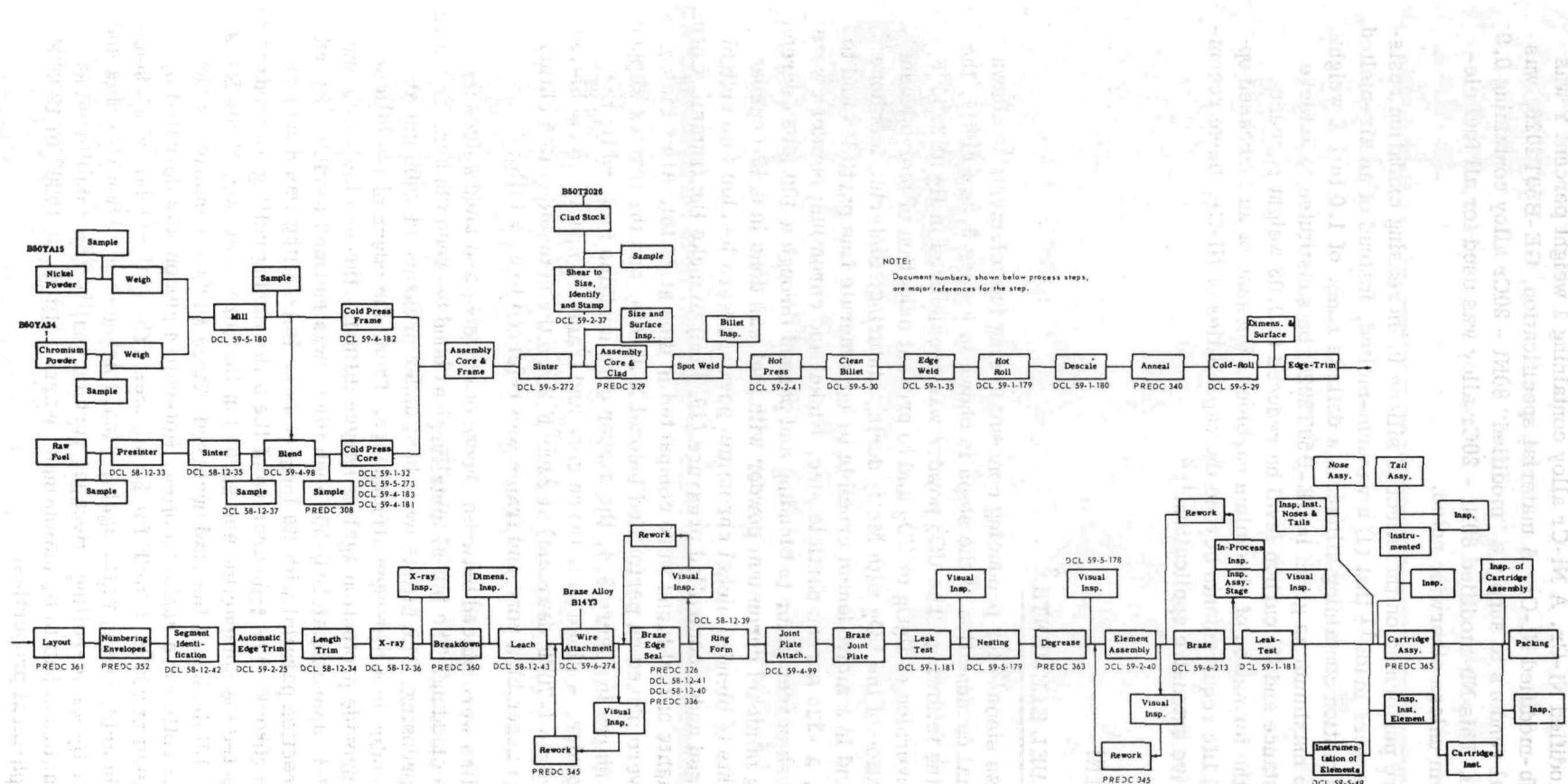
Fig. 3.2—Process flow chart for fabrication of concentric-ring fuel elements
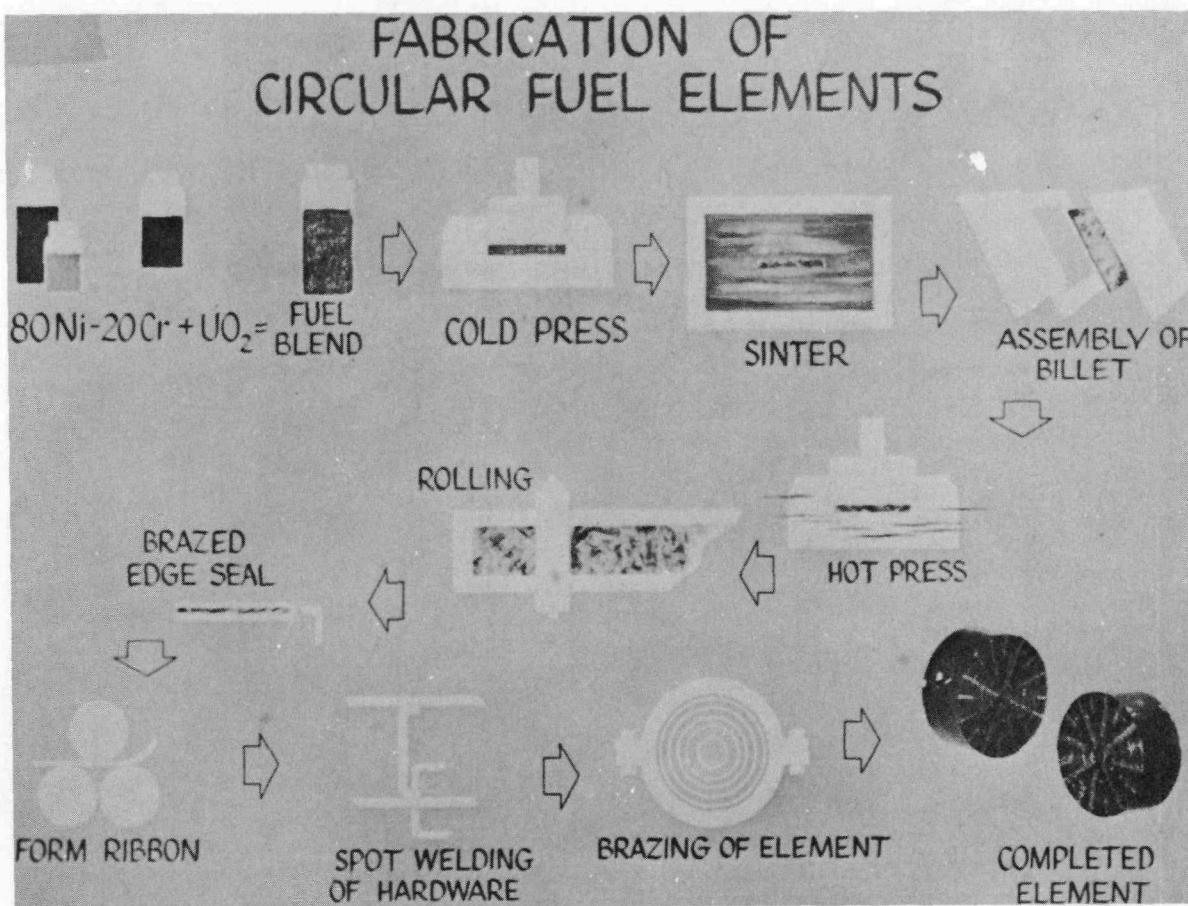
Fig. 3.3 — Fabrication steps in producing concentric-ring fuel elements
(Dwg. 4098099-400)

Designs required that 0.010 to 0.035 inch of dead stock remain on fuel ribbon edges to prevent core oxidation. In early production, radiographs were taken to locate the edge of the core, and hand shears were used to remove the required amount of dead stock. Later, an X-ray device was developed at the General Electric General Engineering Laboratory which sighted through the ribbon, sensed the edge of the core, and positioned a nibbling tool steel die so that, as the ribbon was fed through the machine, the dead edge was trimmed away to leave the required protection at the edge. The ribbon was then sheared to the proper segment length. The cut ends of segments were leached in HNO_3 to remove smeared uranium dioxide from the exposed core so that edge-seal wire (Ni-Cr) could be tack welded to each segment end. Brazing was used to permanently attach the wire and seal the edge of the segment. Braze alloy G-E No. 81 was mixed as a slurry with methyl cellulose, acetone, and water. This mixture was applied through a hypodermic needle to the joint of the edge-seal wire and segment. The segments were brazed at 2160° to 2190^OF for 35 minutes in a hydrogen atmosphere of -40^OF or better.

Fuel element design was a series of concentric rings. Circular rings were formed either by rolling or die forming. The ability of a segment to withstand cracking in the core during ring forming was dependent upon the thickness and fuel percentage of the core and the diameter to which the ring was to be formed. With the exception of the innermost ring, segments were formed into circles through the use of manual three-roll formers. In early designs, where the thickness of the segments allowed it, rings were formed to finished
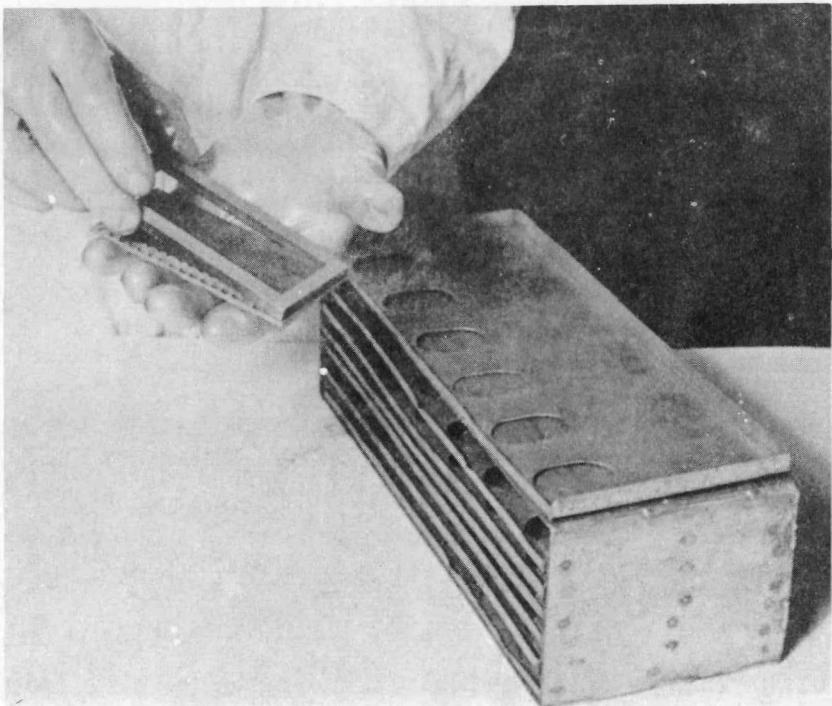
Fig. 3.4 — Placing compacted frame around core prior to sintering
80Ni — 20Cr powder (Neg. C-20727)

diameter without intermediate anneals; however, in the production of later elements of greater thicknesses, the ring was partially formed and annealed several times.

3.2.1.1 HTRE No. 1 and HTRE No. 2 Fuel Elements

Rings were assembled concentrically starting with the smallest diameter. The assembly proceeded as follows:

1. A joint strap was tack welded in place to close the ring.
2. Channels were tack welded to the ring near the leading edge.
3. Spacers were tack welded to the ring near the trailing edge.

As the next ring was attached, the channels were also tack welded to it; the spacers at the trailing edge were welded to one ring only. After tack welding all of the rings comprising the stage, tabs (or feet) for cartridge assembly were attached to the outer ring. A braze alloy (section 3.3) made as a slurry of methyl cellulose, acetone, and water was applied to each channel, joint strap, foot, and spacer (one ring only). Powdered alumina in water was brushed on each spacer (opposite the braze end) to prevent bonding the rings through the spacers.

The stages were brazed, leading edge down, for 15 minutes in hydrogen (-40°F dewpoint) muffle furnaces at 2150°F. Approved stages were assembled into cartridges. Stages were located from the OD with split half-round fixtures and held in place while feet were spot welded to longitudinal rails. The inlet (nose) assembly and tail assembly were also spot welded in place utilizing an appropriate fixture. A completed stage and cartridge are shown in Figure 3.5.

3.2.1.2 HTRE No. 3 Fuel Elements

The HTRE No. 3 design evolved from the experience gained with the HTRE No. 1. Ring thickness ranged from 0.021 to 0.027 inch. Two types of stages were designed; these dif-
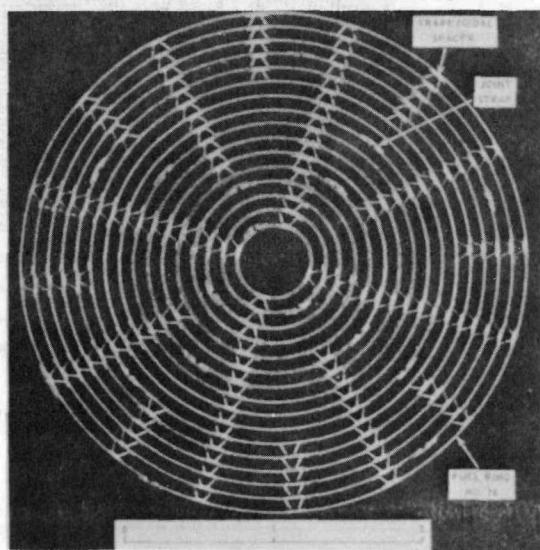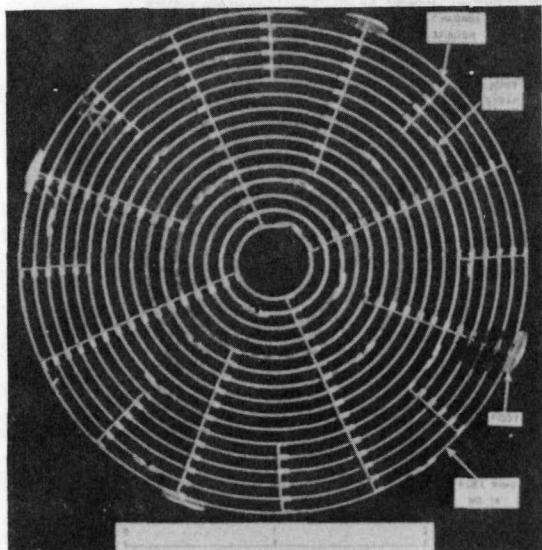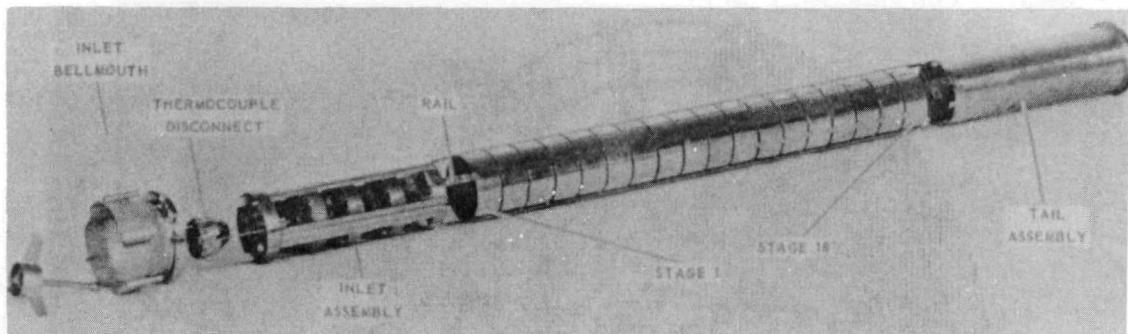
Fig. 3.5 — Completed stage and fuel cartridge

fered only in ring thicknesses and spacing. Both types were 1.5 inches in length, approximately 3 inches in diameter, and contained twelve rings. Sixteen leading-edge combs were used to support the rings rather than the channels and spacers of the earlier design. It had been found that if sufficient support were provided at the leading edge of the stage the rear spacers were not required, and, as a result, in stages for HTRE No. 3 they were eliminated. The HTRE No. 3 cartridge was made up of 19 stages assembled in line and held together by four rails. The major combs of each stage extended beyond the outer ring for insertion into a slot in the rail. In addition, a tab was brazed to the outer ring and comb for providing additional support by welding to the rail. A completed stage and cartridge are shown in Figures 3.6 and 3.7.

3.2.1.3 ETR-Type Cartridges

The P103 design was developed as a result of experience gained during testing of the P102 (HTRE No. 3) type of design. To provide better airflow characteristics, leading edges of the rings and combs were rounded, and the stage length was increased to 3 inches. With the increased width of the fuel ribbon, the number of stages was reduced to nine. Assembly of the cartridge was accomplished by welding the outer rings (which were unfueled) together to form a continuous tube. Further improvement was obtained by a large center hole to accommodate a center moderator rod. To improve the strength of the fuel sheet, all ma-
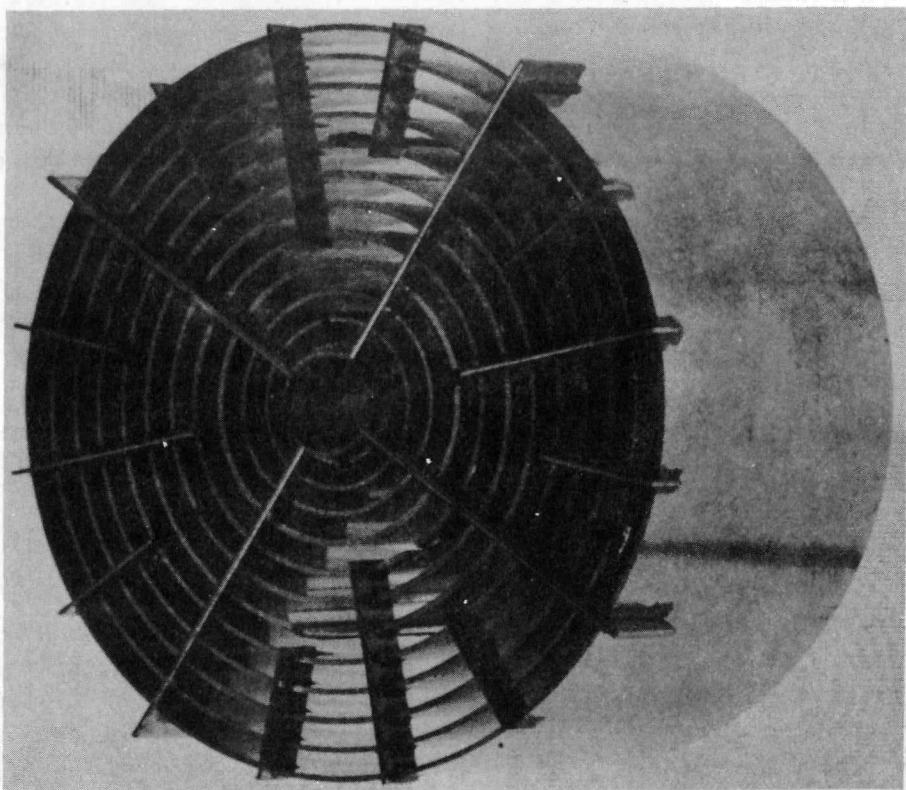
Fig. 3.6 — Completed fuel stage for P102 design (Neg. C-21237)
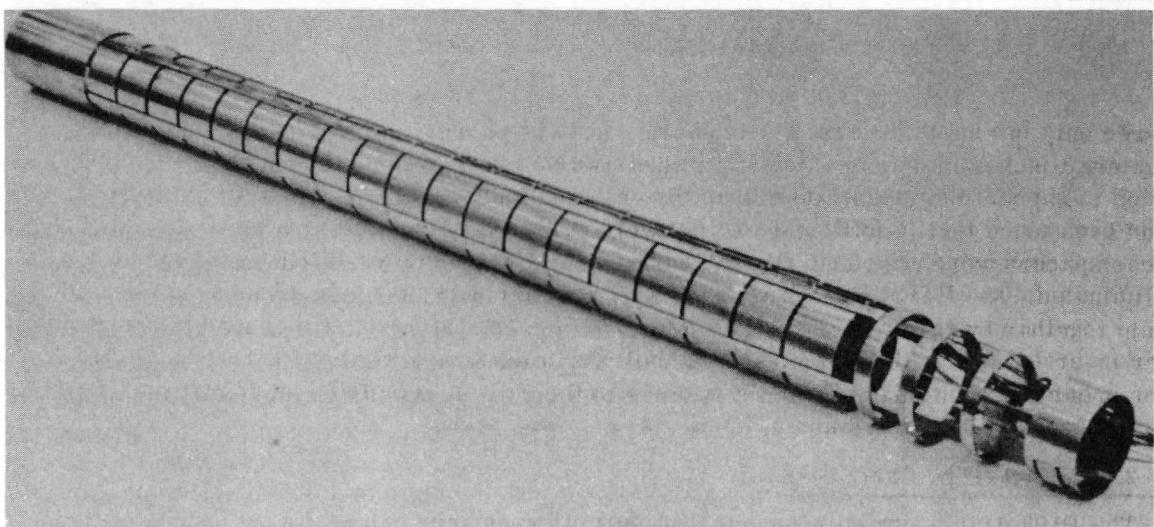
Fig. 3.7 — Completed fuel cartridge (Neg. C-20397)

terial was warm finished and roll formed at elevated temperatures. A completed stage and cartridge are shown in Figures **3.8** and **3.9**.

3.2.2 ALTERNATE CONFIGURATIONS[2, 3]

In addition to the ribbon-type fuel elements, discussed in section **3.2.1**, three other configurations were fabricated: (1) wire-type, (2) corrugated, and (3) tube-type fuel elements.
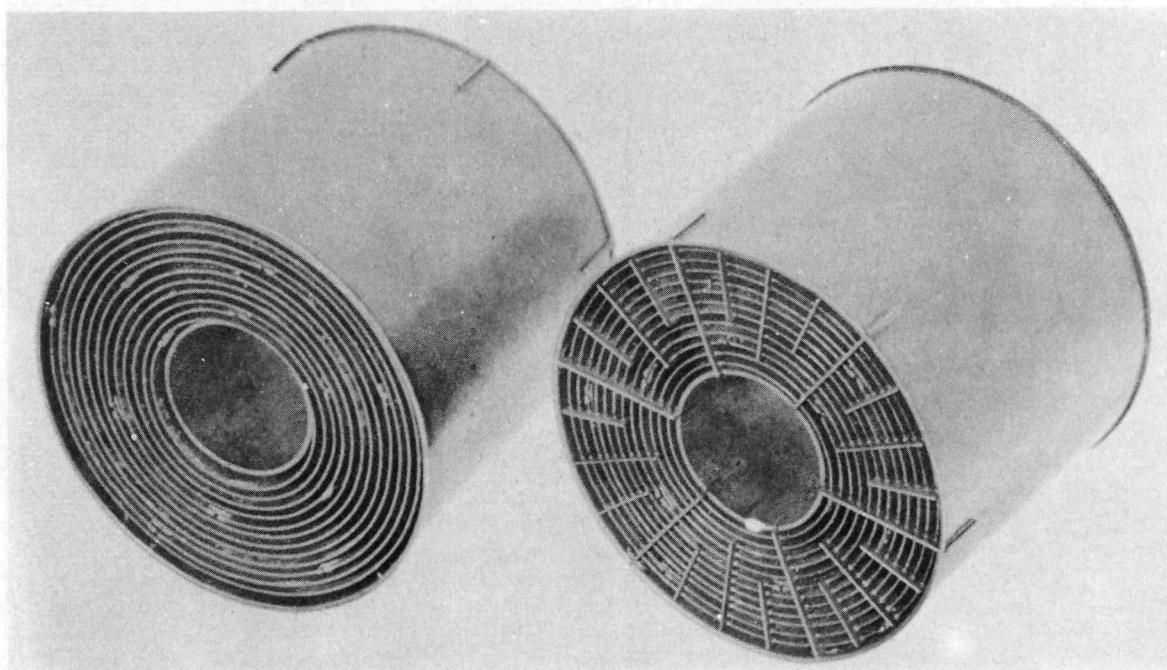
Fig. 3.8 – XMA-1A fuel element (Neg. C-22689)

3.2.2.1 Wire-Type Fuel Elements

During the period in which production techniques for the fabrication of ribbon-type fuel elements were being developed, some attention was paid to development of wire-type fuel elements. Initial design requirements specified 0.020-inch-diameter wire with a cladding thickness of 0.004 inch. As in ribbon-type elements, the wire consisted of Ni-Cr-UO_2 powders pressed, sintered, and enclosed in Ni-Cr alloy. Considerable development was required in order to produce wire which could be drawn to this fine diameter. Work progressed both at GE-ANPD, and on a subcontract basis, at Sylvania Electric Products (now Sylvania-Corning). The process described herein was employed at GE-ANPD. It was determined that success was dependent upon fuel particle size (40-70 microns), sintered density of the core (85% minimum of theoretical, preferable) and proper selection of die angles for drawing the wire.

The fabrication technique was similar in basic technology to that of ribbon fabrication described above. Fueled cores containing 30 weight percent UO_2 were pressed as cylindrical pellets, 5/8 inch in diameter by 1-1/2 inches long, and sintered in dry hydrogen at 2200°F. Two of these pellets were fitted into a hollow cylindrical (0.625-in. ID by 1.15-in. OD) Ni-Cr sleeve, and encapsulation was completed by welding Ni-Cr plugs in the ends of the cylinder. These assemblies were hot rolled to approximately a 1/4-inch diameter, hot swaged, centerless ground, and cold drawn in steps of approximately a 10 percent reduction in diameter per pass. In this manner several thousand feet of 0.020-inch wire were

INSTRUMENTATION LEADS

INSULATION

FUEL ELEMENT

CENTER MODERATOR ROD

ROD AND FUEL ATTACHMENT FINGERS
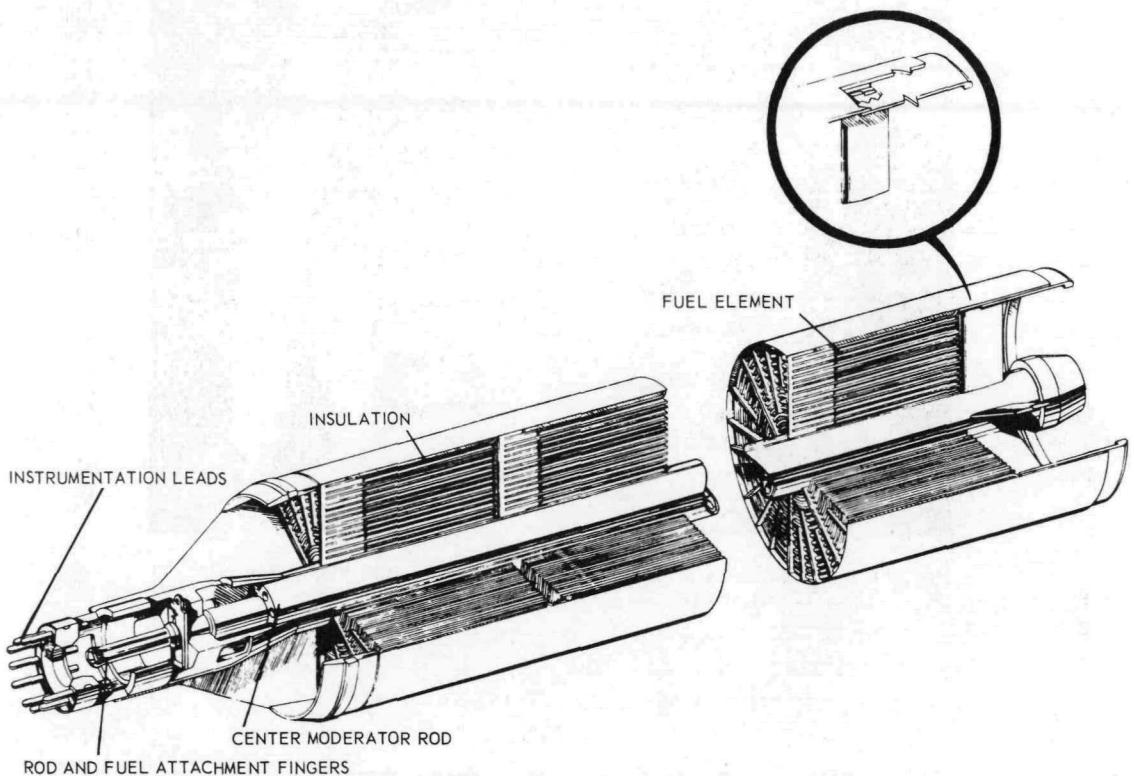
Fig. 3.9 – XMA-1A fuel cartridge (Neg. DI-37)

produced. The Sylvania process, which was also ultimately successful in producing wire, differed from the GE-ANPD process in three principal respects:

1. A nickel plate was applied to the inner wall of the cladding capsule.
2. Core compacts were etched in hot nitric acid prior to insertion in capsules.
3. Hot reduction was performed by swaging rather than by rolling.

A later design specified cored lenticular-shaped wire, 0.020 inch on the minor axis and approximately 0.100 inch on the major axis. For this fabrication, assemblies were made in a normal manner, and the wire-drawing operation halted when the wire reached 0.100 inch diameter. The lenticular shape was formed by using special rolls with grooves. This wire, shown in Figure 3.10, was subsequently formed into fueled stages by wrapping successive layers of wire helices. The fueled stage is shown in Figure 3.11.

Controlling the clad thickness to 0.004 inch was difficult in each of the above designs. It was felt that with additional development effort and the procurement of special forming tools, adequate control of this characteristic could be obtained. Joining of cored wire was attempted without significant success. Considerable development remains to be done before success can be achieved repetitively on wire-bed-type elements.

3.2.2.2 Corrugated-Type Fuel Elements

Both corrugated concentric-ring elements and corrugated plate elements have been evaluated on a component basis. These can be seen in Figures 3.12 and 3.12. Both configurations employed standard fuel ribbon made as previously described for concentric-ring elements. Corrugation of the plate elements was accomplished during hot forming the fuel ribbon. A single-stage punch and die was used to form the corrugations one at a time. The
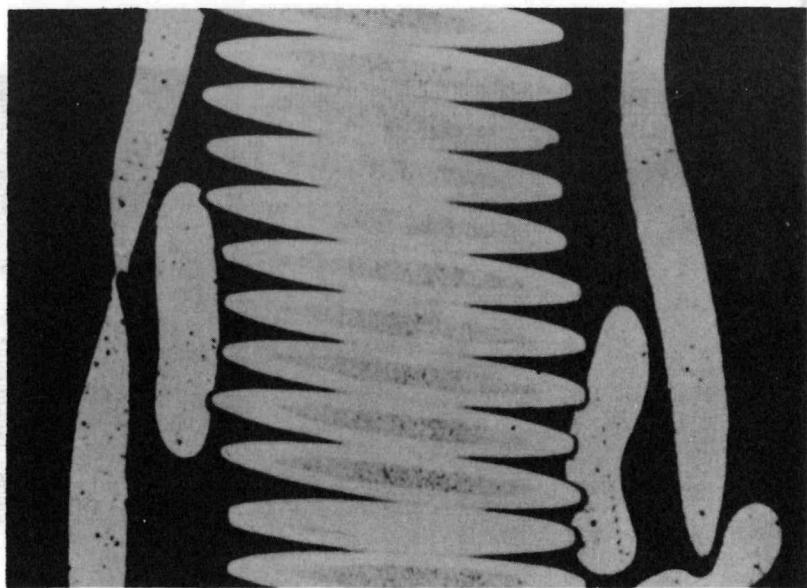
Fig. 3.10 — Cross sections through shaped fuel wire with major axis
of 0.161-inch and minor axis of 0.021-inch
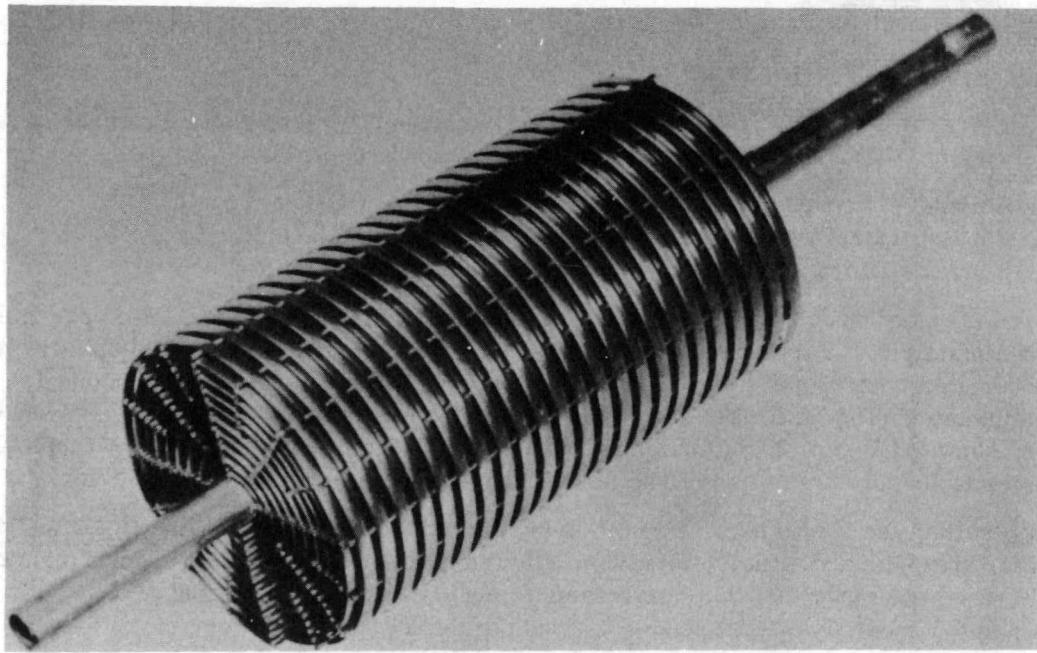
Fig. 3.11 — Fueled stage utilizing lenticular-shaped wire
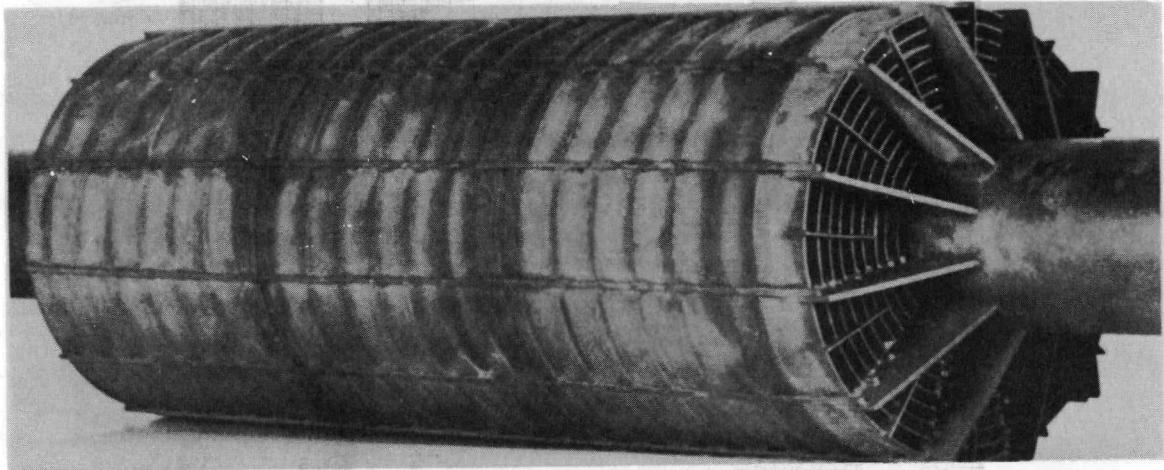
Fig. 3.12 – Corrugated concentric-ring fuel element after 100 hours at 1900°F and a 4.5-psi dynamic head (Neg. C-22280)
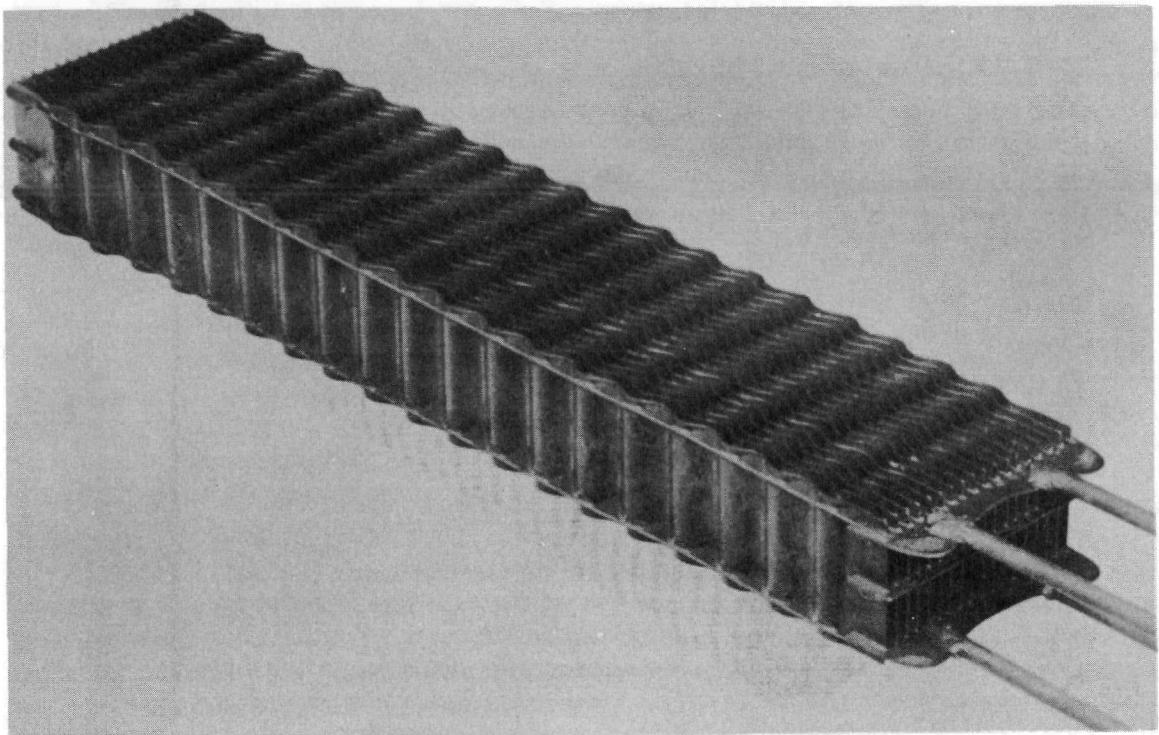
Fig. 3.13 – Corrugated-plate fuel element after 100 hours at 1850°F and 9-psi dynamic head (Neg. C-04739)

work was heated to about 1800°F, and special efforts were made to prevent the temperature from dropping below 1400°F either during transfer from furnace to die or during deformation. Several passes were used for each corrugation. Following corrugation, construction of the element was completed by using assembly and joining techniques patterned after those employed on concentric-ring elements. Corrugated concentric rings were prepared in three different ways: (1) cold forming of rings in rubber dies, (2) hot-roll forming of rings, and (3) cold-explosive forming of rings. The only process that was successful in forming fueled rings was hot-roll forming. However, explosive forming at elevated temperatures was regarded as a promising approach for producing a large number of rings, although this process was never investigated extensively.

In the hot-roll forming operation, the fueled ring was chucked into the headstock of a lathe and rotated while an oxy-acetylene flame was applied to the area to be corrugated. The rapid turning of the cylinder resulted in a very uniform circumferential temperature distribution. The temperature was held constant by the regulation of the oxy-acetylene flame which was controlled by an optical temperature sensor focused on the ring itself. When the desired temperature was reached, the cylinder wall was corrugated by manual feeding of a contoured external roller toward the cylinder and against a mated internal roller, which formed a single corrugation. The rollers were then indexed to the right to form the next corrugation. The rolling operation is shown in Figure 3.14. Forming temperature ranged from 1800° to 1100°F (aim 1400°F minimum) depending on time of roller contact. Standard assembly and joining techniques were employed in preparing stages and cartridges for test.

3.2.2.3 Tube-Type Fuel Element

Both the Martin Company and Nuclear Metals, Inc., attempted to manufacture small-diameter Ni-Cr fueled tubes with a 0.230-inch outside diameter and a 0.190-inch inside diameter. The tubes were 30 inches long, had a clad thickness of 0.004 inch, and a core fuel loading of 40 percent. The work at Nuclear Metals, Inc., involved fabricating fueled tubes by hot extrusion techniques. The work was discontinued when an early exploratory effort was unsuccessful. It was felt, however, that this process was potentially capable of producing satisfactory tubes if adequate development time were available.

The Martin Company employed cold drawing and cold swaging with intermediate diffusion anneals. In this process, thin walled, cylindrical powder metallurgy bushings, approximately 1/2 inch long, 0.275 inch OD, were cold pressed. The bushings had a 0.235-inch ID and were composed of an 80Ni - 20Cr matrix which contained 40 percent UO_2. These were placed, in the green state, on a Ni-Cr tube, which served as the inner clad. Unfueled bushings were placed at either end. A "sacrificial" outer clad, a stainless steel tube, was placed over the bushings. With a magnesia-coated mild steel mandrel in place within the inner tube, the composite was drawn through a die to 25 percent reduction in wall thickness. The assembly was then presintered in hydrogen at 1175°F for one-half hour. After presintering, the outer clad was stripped off; the core and inner clad assembly placed on a hardened tool steel mandrel; and the assembly cold swaged. The inner mandrel was then removed, and the assembly diffusion annealed at 2150°F in hydrogen. Alternate swaging and diffusion annealing were employed until the desired core densities were achieved. After cleaning, the outer clad was positioned over the core assembly, and sizing was accomplished by a series of cold draws. Between the draws and after the final draw, the assembly was diffusion annealed at approximately 2150°F in hydrogen.

In tubes made by the Martin process, bonding of the core to outer clad was difficult to obtain. However, GE-ANPD found that an autoclave treatment for 4 hours at 10,000 psi and 2100°F produced virtually 100 percent bonding. The junctions between bushings were essentially unbonded and remained so even after autoclaving.
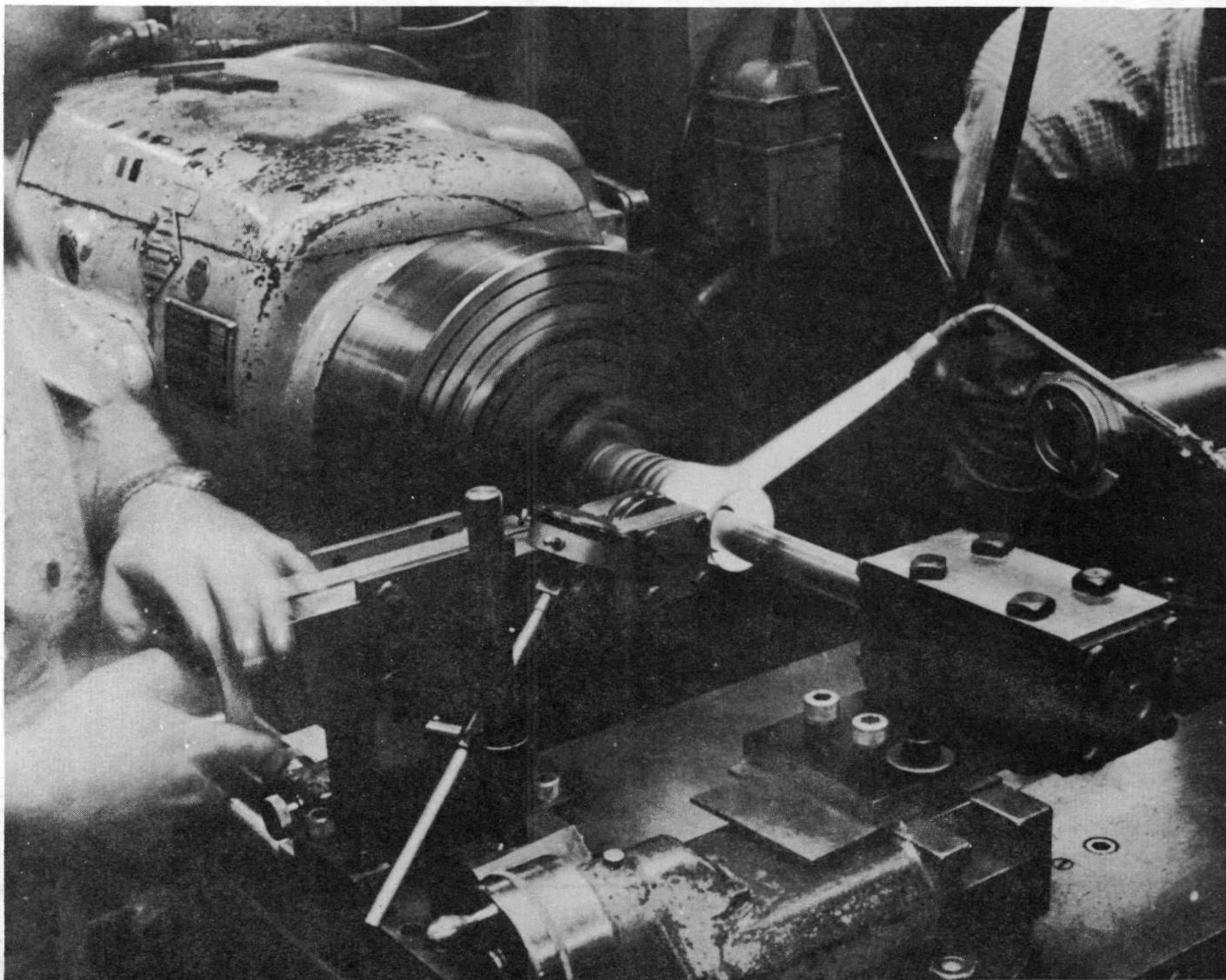
Fig. 3.14 — Hot roll forming of corrugated cylinders (Neg. C-21283)

3.3 BRAZE ALLOY DEVELOPMENT

3. 3. 1 BRAZE ALLOYS[4, 5]

Brazing was used in two critical operations of Ni-Cr fuel element assembly. The more critical was the edge sealing of segments. The second was joining of concentric rings and spacer hardware to form stages of the fuel element cartridge. As for selection of cladding alloys, the requisite of low thermal neutron cross section was also imposed on a useful braze alloy. No commercially available alloy was suitable in the first years of the GE-ANPD program. The silver-base and copper-base alloys had poor strength and oxidation resistance at 1650°F and above. Other systems such as Ni-Cr-B, Ni-Si-B, Ni-Mn, and Ag-Mn, all of which possessed good physical properties, had prohibitively high cross section, and required very close control of joint clearance and of the brazing temperature cycle.

A slight decrease in the silicon content of the base alloy G-E No. 62, discussed in section 2. 3, with small additives of iron resulted in a decrease in as-cast hardness with no significant change in melting point. A material with the following composition was determined to have sufficient ductility without sacrifice of the desirable physical properties of G-E No. 62 alloy.

1. 9. 5 to 10. 0 weight percent Si
2. 3. 5 to 3. 6 weight percent Fe
3. 19. 0 to 20. 0 weight percent Cr
4. Balance Ni

The new composition was termed G-E No. 81 alloy and was used almost exclusively in all GE-ANPD work with nickel chromium.

3. 3. 2 PROPERTIES OF BRAZE ALLOY

Tensile strengths were obtained on butt-brazed joints consisting of a 0. 015-inch-thick Ni-Cr member brazed to a 0. 128-inch-thick Ni-Cr member with contact dimensions at the joint of 0. 015 to 0. 375 inch. Tensile strengths at room temperature, 1200°, 1650°, and 1800°F are given in Figure 3. 15 for the as-brazed condition. Figure 3. 16 gives the tensile strengths at the same temperatures after an anneal for 15 hours at 1800°F. At room temperature, the average strength of the as-brazed joints increased about 50 percent as a result of annealing. At 1200°F and higher, differences in the strength of the as-brazed and the air-annealed joints were negligible.

The ductility of No. 81 braze was determined at room temperature, 1200°, 1650°, and 1800°F using "T-joint" specimens. To one side of the 80Ni - 20Cr sheet tensile specimen, a 1/8-inch-high by 0. 015-inch-thick strip of 80Ni - 20Cr was brazed. These specimens were tested in the as-brazed condition and after a 15-hour anneal at 1800°F in air by straining to produce various amounts of plastic elongation. The amount of elongation was measured and the specimen examined for cracks in the braze fillet. Results of these tests are presented in Figure 3. 17. From these results, it is apparent that the as-brazed and as-annealed ductility is very low (less than 1%) at room temperature. At 1200°F, the as-brazed ductility increased slightly to 1 to 1. 5 percent, whereas the as-annealed ductility increased 3 to 3. 5 percent. At 1650°F and 1800°F, the as-brazed and as-annealed ductilities were the same and were equivalent to that of base metal.
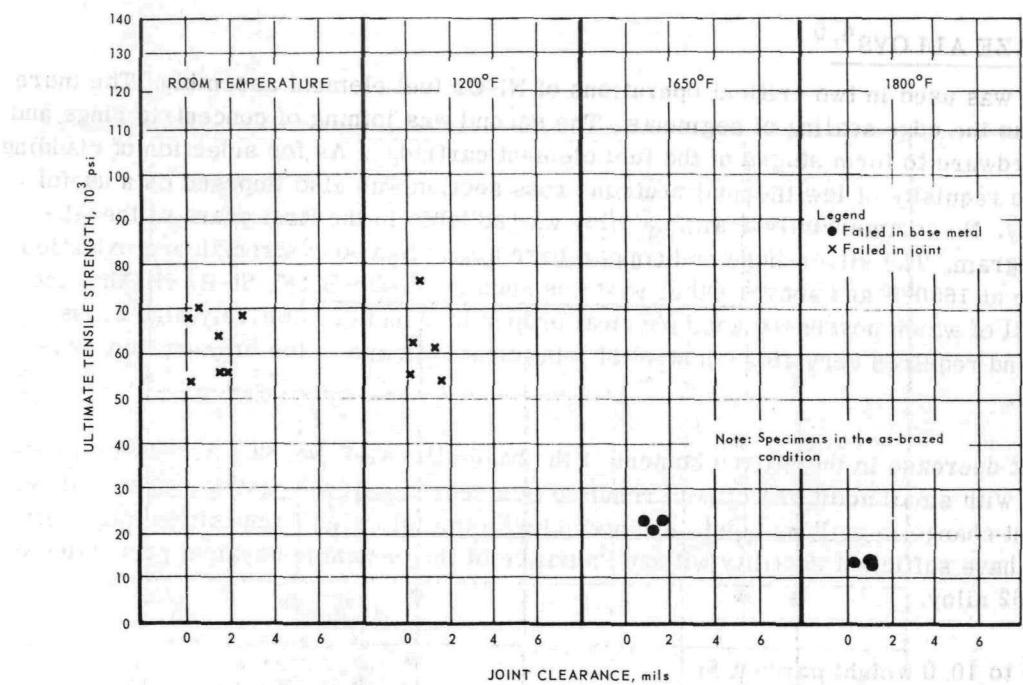
Fig. 3.15 – Ultimate tensile strength of 80Ni – 20Cr joints brazed with
No. 81 specimens (Neg. A-11894)
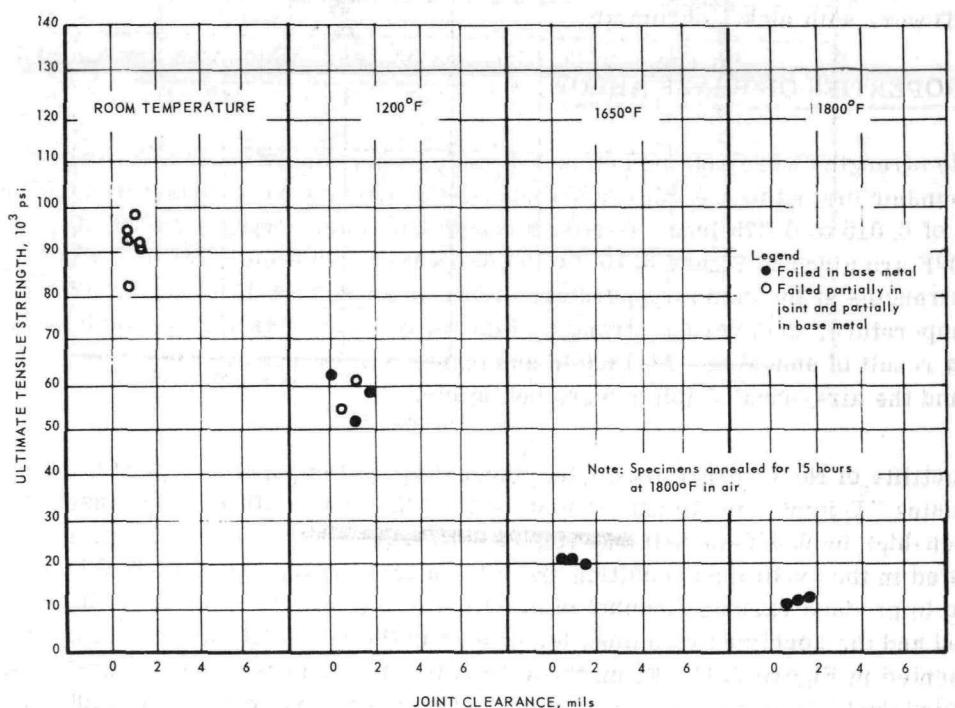
Fig. 3.16 – Ultimate tensile strength of 80Ni – 20Cr joints brazed with
No. 81 (Neg. A-11895)

64
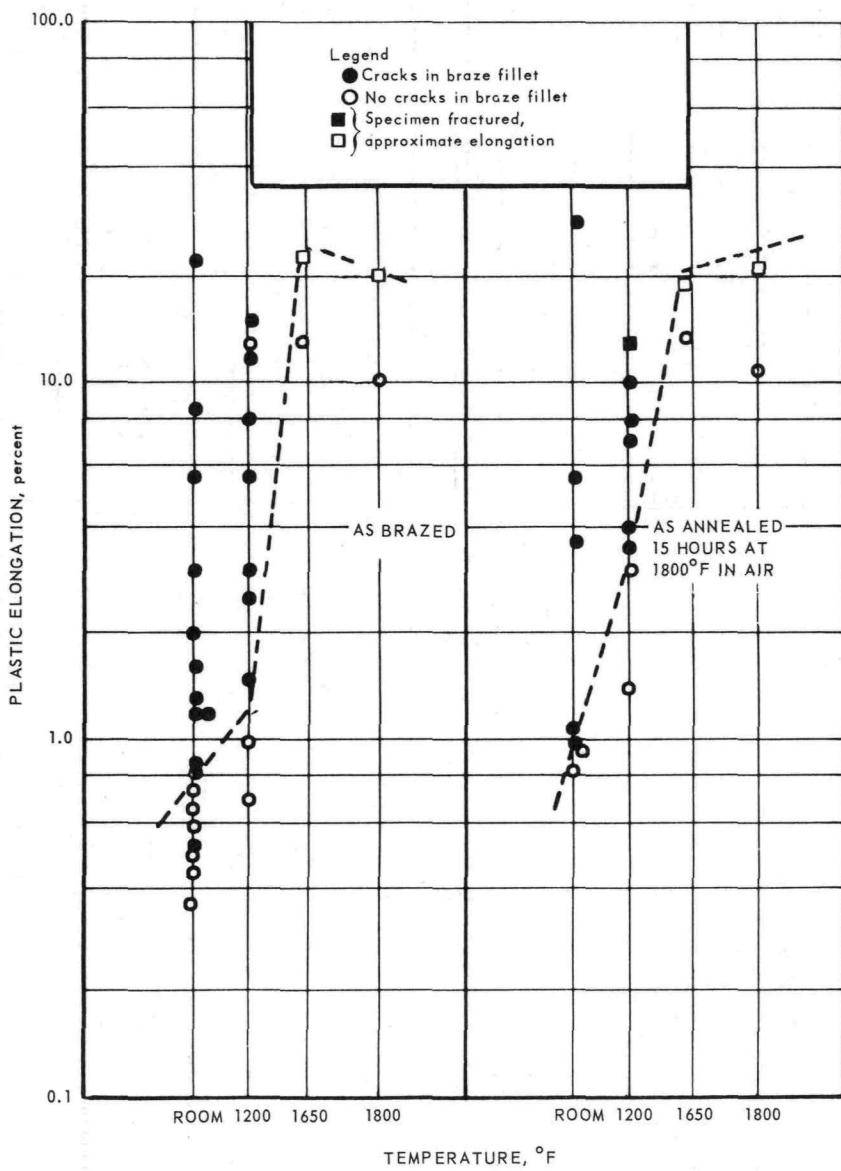
Fig. 3.17 – Ductility of 80Ni – 20Cr T-joints brazed with GE-81 (Neg. A-11896)

3.4 PHYSICAL AND MECHANICAL PROPERTIES

3.4.1 RIBBON-TYPE FUEL ELEMENTS[2, 6, 4]

3.4.1.1 Tensile Properties

Short-time tensile data are presented in Figures 3.18 and 3.19 for temperatures up to 1800°F. Data for both 0.004 and 0.006-inch-clad fuel ribbon and for wrought 80Ni - 20Cr alloy are included for comparison.

Elongation of fuel ribbon during short-time tensile tests was low, as shown in Figure 3.19. No proved theoretical explanation exists for the minimum which occurred at 1500°F.
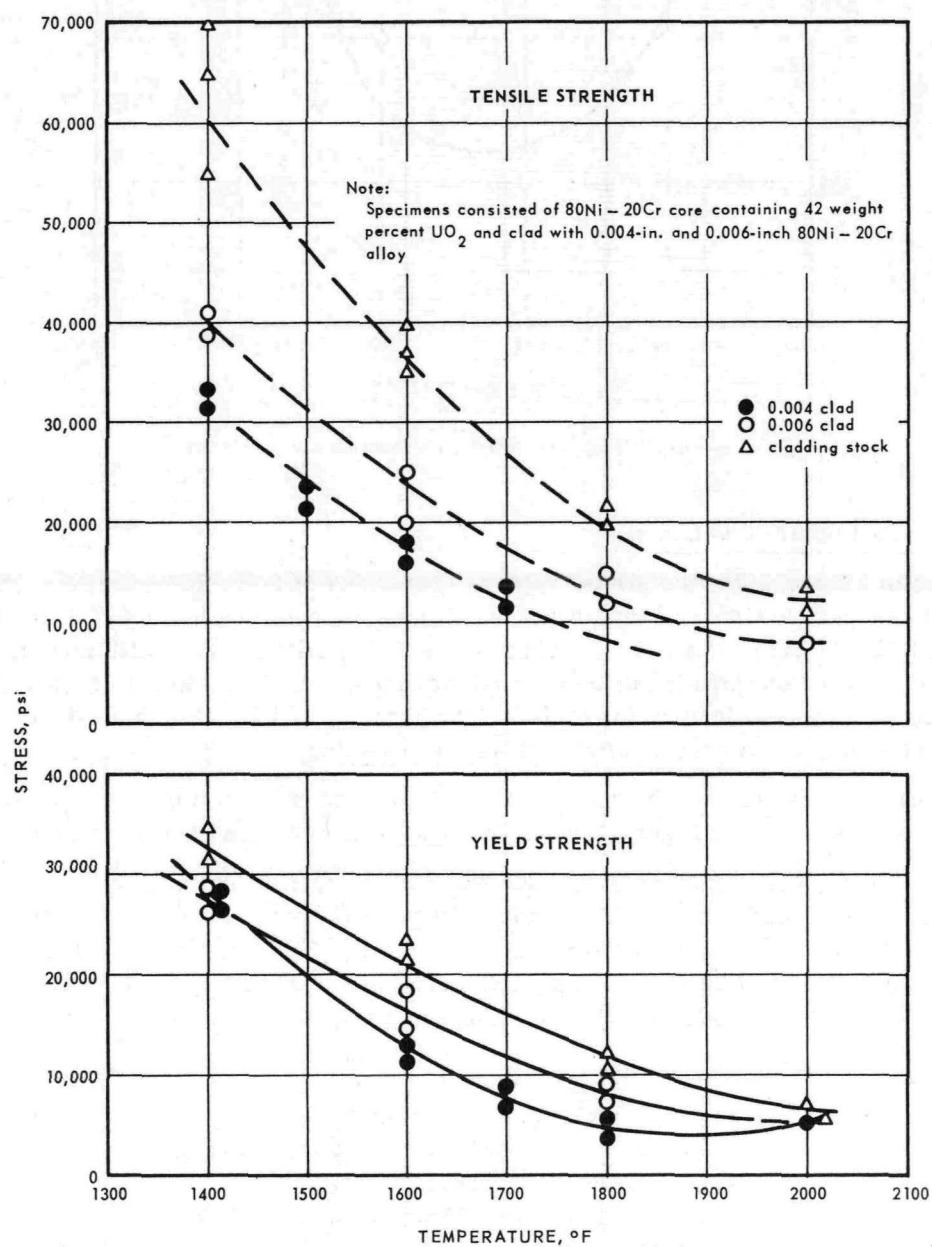
Fig. 3.18 — Tensile strength of fuel ribbon compared with wrought 80Ni — 20Cr cladding alloy

Note:
Specimens consisted of an 80Ni − 20Cr core with 0.004-inch-thick cladding and containing 42 weight percent UO_2. Overall thickness was approximately 0.020 inch.
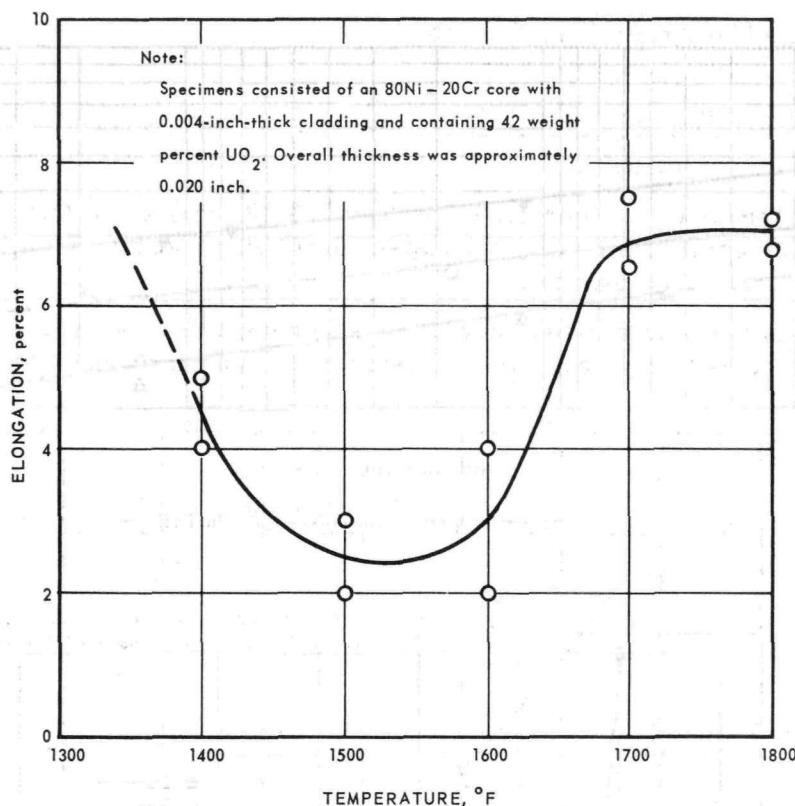
Fig. 3.19 — Ductility of fuel ribbon as a function of temperature

3. 4. 1. 2 Stress Rupture and Creep

As shown in Figure 3. 20, the stress rupture properties of fuel ribbon follow a normal pattern with respect to time and temperature. Though the data are for 0. 012-inch-thick ribbon, with 0. 004 inch clad and 30 weight percent UO_2 in the core, sufficient check points were obtained on thicker ribbon (up to 0. 027 inch) with 0. 004 to 0. 006-inch cladding and higher core fuel loading (up to 42 weight percent) to show that these data are representative in these ranges of thickness and fuel loading.

Design curves have been established for 2 and 5 percent deformation over a 100-hour period. These are shown in Figure 3. 21 together with the 100-hour rupture curve.

Bending (flexure) creep tests were conducted on a few specimens in order to gain some insight into behavior under transverse loads. The specimens were regular ribbon, approximately 1. 5 inches wide by approximately 1. 5 inches long. The ends were sealed with Ni-Cr wire. Results are tabulated in Figure 3. 22 in terms of deflection in 100 hours at the center of a simply supported beam loaded in the center of a 1-inch span.

3. 4. 1. 3 Stress Oxidation

The life of a fuel element is defined somewhat arbitrarily as being that point in time when oxidation has progressed halfway through the protective cladding. Since the cladding thickness was usually 0. 004 inch, the time for 0. 002-inch penetration defined operating life. Oxide penetration in alloys of similar type proceeds not only by uniform attack but frequently by intergranular penetration in the form of oxide stringers. In the case of Ni-Cr fuel ribbon, the depth of penetration of the intergranular attack was a function of stress as well as temperature and time of exposure. Figure 3. 23 represents a typical
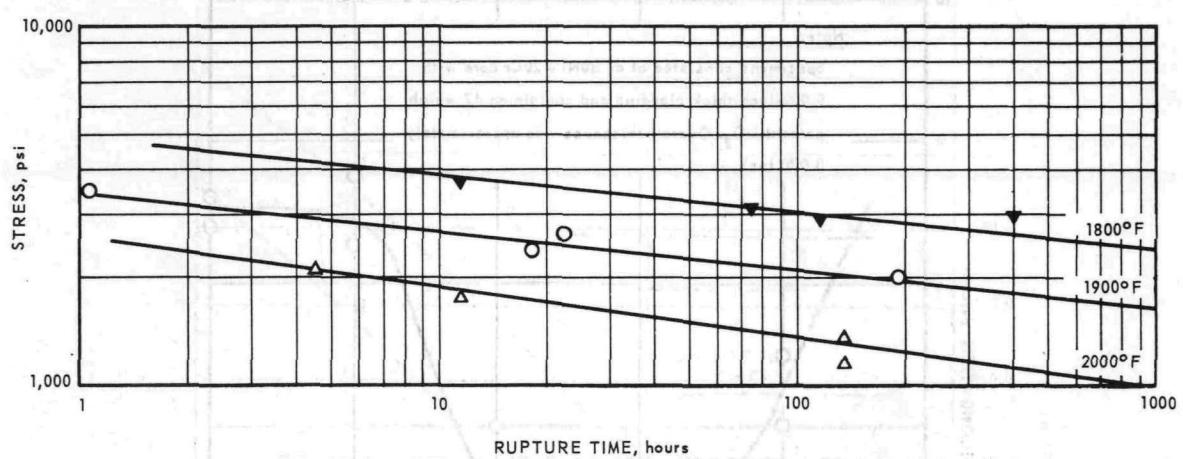
Fig. 3.20—Stress rupture properties for 80Ni—20Cr fuel ribbon
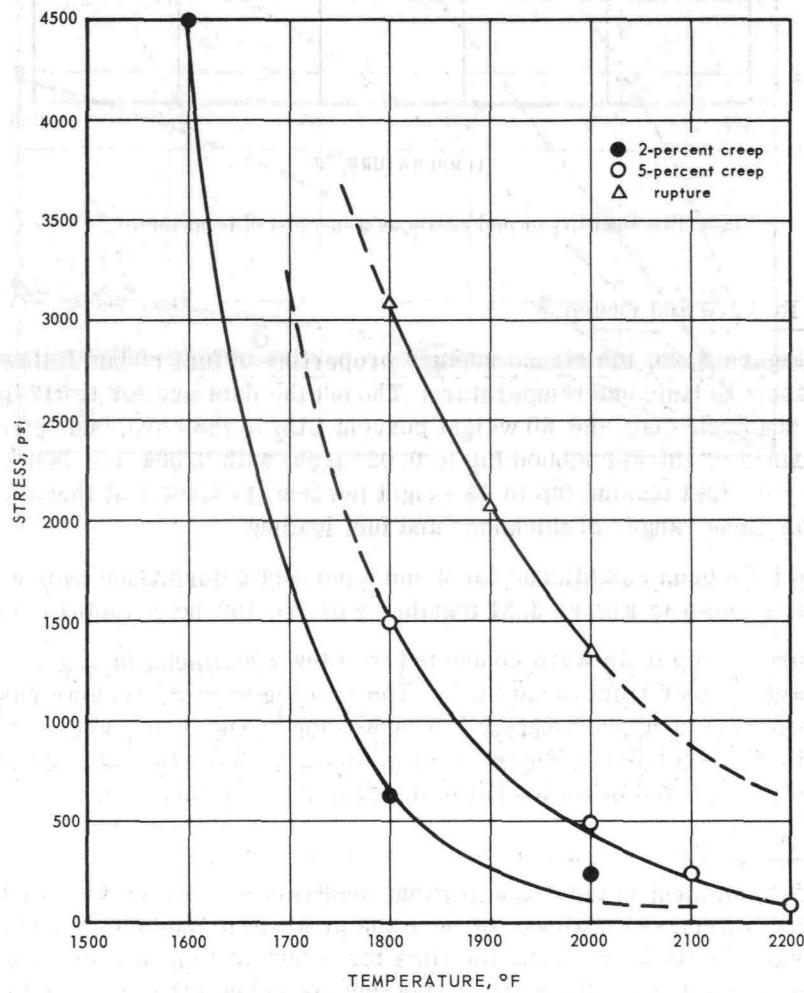
Fig. 3.21— Plot of 2-percent and 5-percent deformation and rupture for
80Ni—20Cr fuel ribbon in a 100-hour period
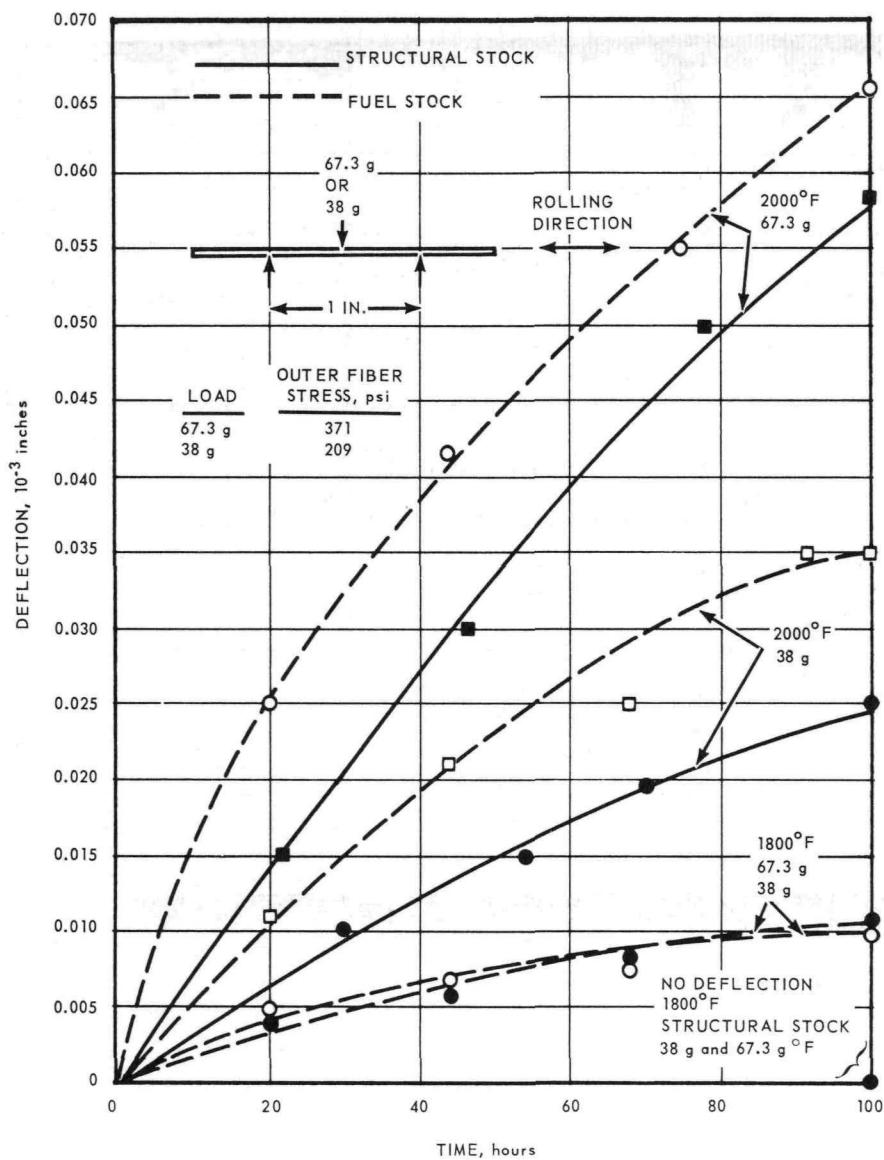
Fig. 3.22—Deflection versus time in bending for both structural stock and fuel
stock at 1800°F and 2000°F

case of what is known as stress oxidation, which occurred during a laboratory stress
oxidation test. The figure shows a cross section through a fuel element which was sub-
jected to the conditions indicated. Also shown in Figure 3.23 is a photomicrograph of a
fuel element which had been subjected to an irradiation test in the MTR. The attack on
both is similar.

By metallographic observation and measurement of oxide stringer depth in a number of
fuel ribbon specimens tested under controlled conditions, the family of isotherms shown
in Figure 3.24 was derived. The data were obtained from metallographic examination of
a series of specimens tested at various stress levels under several conditions of temper-
ature and time. These tests were conducted on 0.012-inch-thick fuel ribbon containing
30 weight percent UO_2 in the core and clad with 0.004 inch of wrought Ni-Cr. Tests were
conducted in standard creep furnaces in an atmosphere of ambient laboratory air. Spot
tests of 0.004-inch-clad ribbon up to 0.027 inch in thickness and containing core fuel
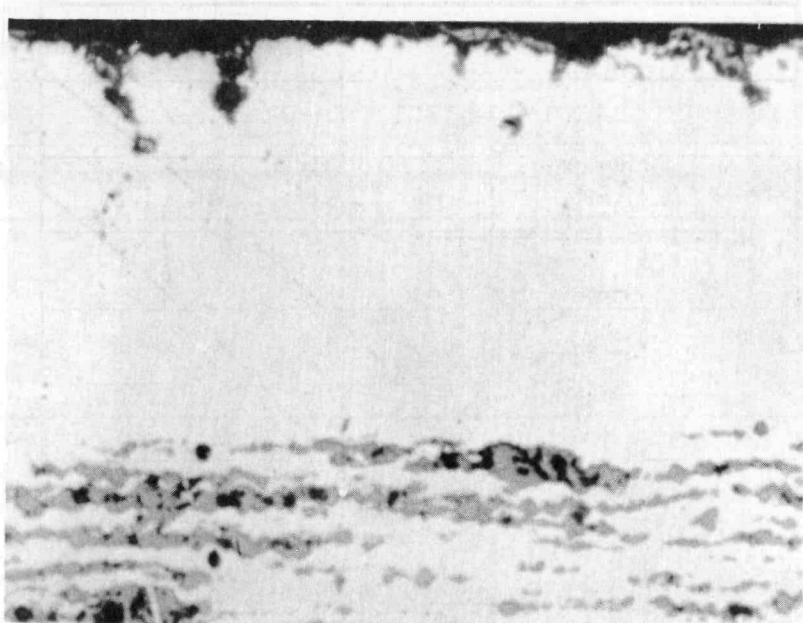
After 100 hours at
600 psi and 2000°F

~0.002-inch intergranular attack after
irradiation at 1×10^3 n/cm^2-sec for
102 hours at 1850°F

Fig. 3.23 – Typical stress oxidation attack

TABLE 3.4

COMPARISON OF OXIDE PENETRATION ON FUEL RIBBON WITH
0.006-INCH CLADDING VERSUS 0.004-INCH CLADDING

Clad Thickness, in.	Temperature, °F	Stress, psi	Time, hr	Oxide Penetration, in.
0.004	1800	1500	50	0.002
0.006	1800	1500	100	0.001
0.004	2000	600	100	0.002
0.006	2000	600	100	0.001

3.3 X
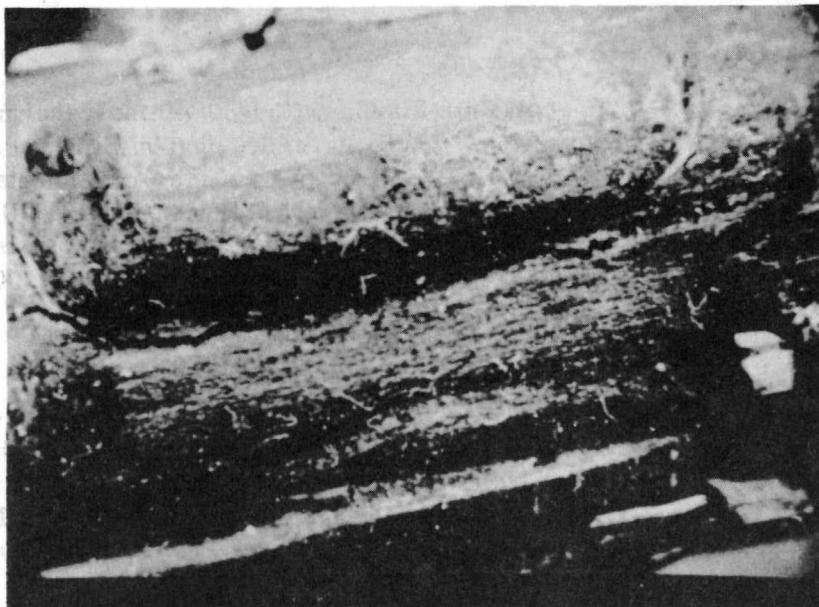
Fig. 3.24 — Crack around tab, welded to Type 310 stainless
steel cladding

loadings up to 42 weight percent UO_2 indicated these data are representative within these
thickness and fuel loading ranges.

The effect of cladding thickness on oxide penetration was evaluated. Data for the 0.006-
inch-clad ribbon is compared in Table 3.4 with 0.004 inch clad data taken from Figure
3.24.

Ribbons tested under thermal cyclic conditions produce about twice the creep elongation
as do ribbons tested isothermally. This is shown in Table 3.5. In the cyclic tests, the
specimens were temperature cycled under load every 2.5 hours from 2000° to 500°F.
Cooling was accomplished by air blasting. Specimen temperature reached 500°F within
2 minutes. Re-heating was begun immediately, and 2000°F was reached within 5 minutes.

TABLE 3.5

ISOTHERMAL VERSUS THERMAL-CYCLIC TESTS

Billet No.	Type Of Test	Temperature, °F	Stress,[a] psi	Time, hr	Elongation, %
9950-A	Thermal cycle test	2000 - 500	1000	100	6.1
9947-A	Thermal cycle test	2000 - 500	1000	100	5.3
9938-A	Thermal cycle test	2000 - 500	1000	120	5.8
9946-A	Isothermal test	2000	1000	100	2.6
9946-B	Isothermal test	2000	1000	100	3.1
9956-A	Isothermal test	2000	1000	100	3.4
8549-A	Thermal cycle test	2000 - 500	1000	100	5.5
8549-B	Thermal cycle test	2000 - 500	1000	100	4.1
8547-A	Isothermal test	2000	1000	100	2.1
8547-B	Isothermal test	2000	1000	100	1.2
8552	Thermal cycle test	2000 - 500	1000	100	3.6
8550-A	Isothermal test	2000	1000	100	1.4

[a]1000 psi based on core (800 psi based on total cross section).

3.4.1.4 Thermal Expansion

The parallel and transverse (to rolling direction) coefficients of linear thermal expansion versus temperature (80°F to indicated temperature) are plotted in Figure 3.25 for both cladding stock and fuel stock. The cladding stock had the same coefficients for both directions. Both cladding and fuel stock were 0.020 inch thick. In the case of the fuel stock, the core contained 42 weight percent UO_2, and the cladding was approximately 0.006 inch thick. Included in Figure 3.25 is a curve for Nb-modified 80Ni - 20Cr bar stock.

3.4.1.5 Hot Finishing versus Cold Finishing

In the course of investigating the effects of various factors on the properties of Ni-Cr fuel ribbon, it was noted that fuel ribbon which was hot finished (~ 1400° to 1800°F) to final thickness possessed superior creep resistance to cold-finished ribbon. A tabulation of the principal data on which this conclusion was based in given in Table 3.6. In each group of specimens, the hot-finished material exhibited less elongation than the cold-finished material.

A summary plot of the stress required to produce 5 percent elongation in 100 hours as a function of test temperature is given in Figure 3.26. In addition to summarizing the data in Table 3.6, this graph is based on data obtained as a result of several exploratory studies designed to evaluate certain other variables, but in which both cold and hot finishing were employed and found to affect the specimens significantly.

With regard to creep rate, time elongation curves for both cold- and hot-finished fuel ribbon are shown in Figure 3.27 for conditions of 2000°F and 1000 psi. Included in this figure is a point obtained for 0.020-inch-thick ribbon in the cold-finished condition containing 42 weight percent UO_2 and 0.006-inch cladding. The slight variations in fuel loading (37% versus 42%), clad thickness (0.004 inch versus 0.005 inch) and over-all thickness (0.020 inch versus 0.022 inch) do not significantly influence the time-elongation curves for either the cold-finished or hot-finished material. There is a significant difference between the cold-finished and the hot-finished fuel ribbon. The cold-finished ribbon enters third-stage creep at approximately 80 hours, whereas the hot-finished ribbon enters third-stage creep in excess of 150 hours. The short-time (25 hours) elongation in the cold-finished ribbon is 11 to 13 percent as compared to 3 to 5 percent for the hot-
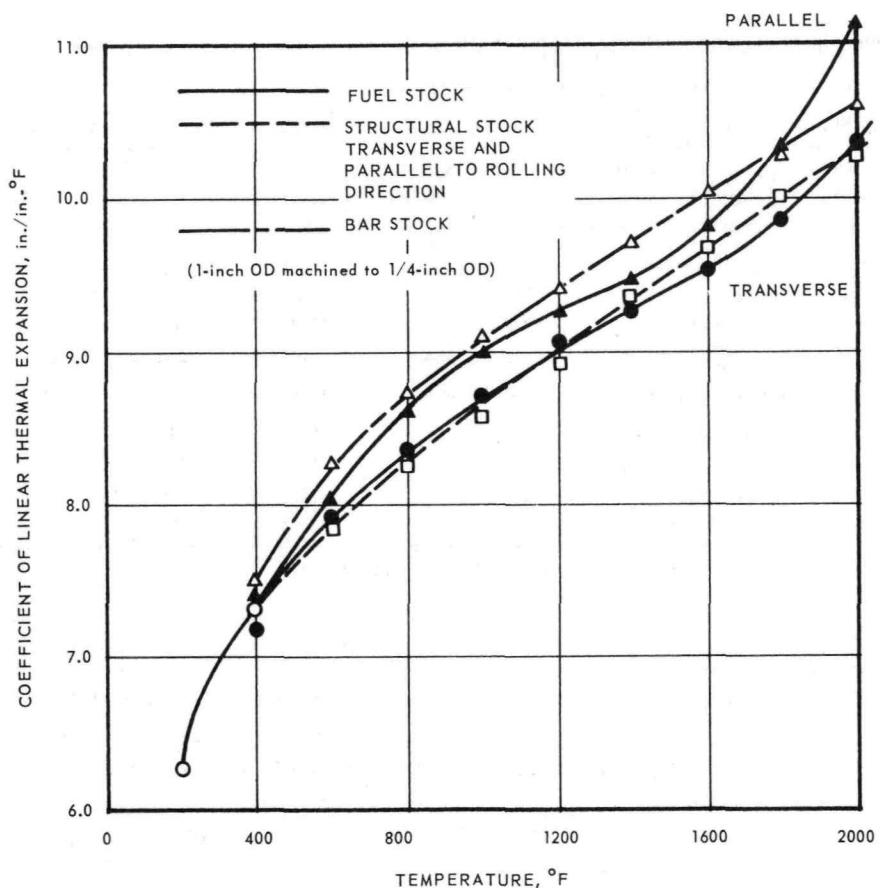
Fig. 3.25 – Coefficient of linear thermal expansion of structural stock and fuel
stock versus temperature, 80°F to indicated temperature

TABLE 3. 6

500-HOUR ISOTHERMAL STRESS-OXIDATION TEST RESULTS
IN Ni-Cr FUEL RIBBON

		Test Results		
Billet No.	Finishing Condition	Temperature, °F	Stress, psi	Elongation, % in 2 inches
11-9268-A	Cold	1850	800	1. 5
11-9272-A	Hot	1850	800	0. 4
11-9269-B	Cold	2000	400	3. 6
11-9273-B	Hot	2000	400	1. 7
11-9449-A	Cold	2000	800	31. 7
11-9449-B	Cold	2000	800	25. 6
11-9431-A	Cold	2000	800	Broke
11-9431-B	Cold	2000	800	17. 1
11-9455-A	Cold	2000	800	31. 0
11-9455-B	Cold	2000	800	35. 9
11-9438-A	Cold	2000	800	11. 1
11-9438-B	Cold	2000	800	8. 8
11-9268-B	Cold	2000	800	17. 0
11-9272-A	Hot	2000	800	3. 8
11-9273-A	Hot	2000	800	4. 7
11-9425-A	Hot	2000	800	3. 9
11-9425-B	Hot	2000	800	6. 4
11-9444-A	Hot	2000	800	3. 1
11-9444-B	Hot	2000	800	2. 3
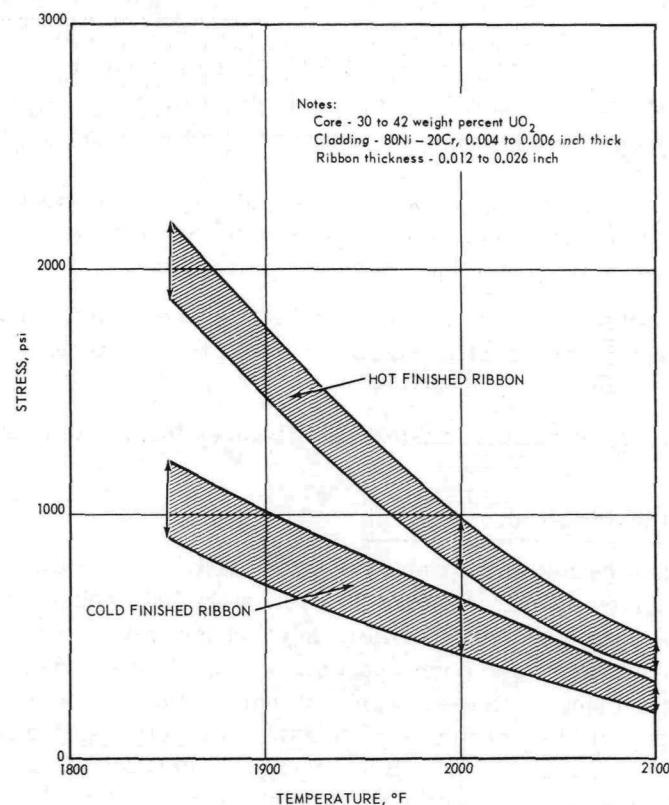
Fig. 3.26 — Stress to produce 5-percent elongation after 100 hours in
80Ni — 20Cr fuel ribbon
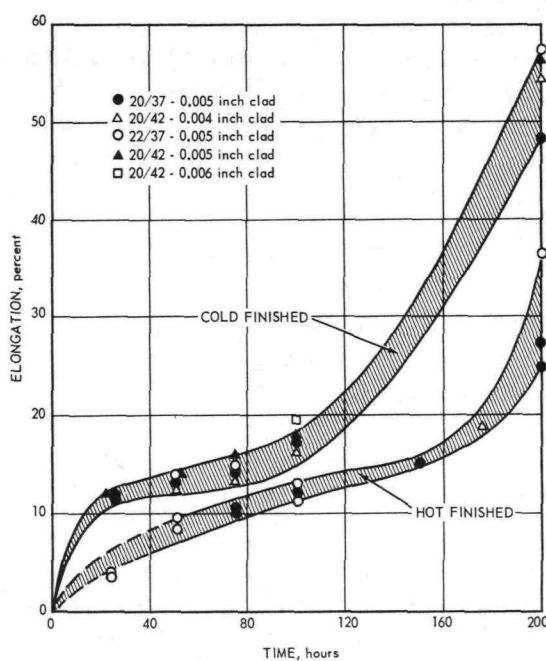
Fig. 3.27 — Elongation versus time for various types of fuel ribbon in both the
hot-finished and cold-finished conditions at 2000°F and 1000 psi

finished ribbon. In addition to the obvious strength margin, this means that the onset of damaging oxide stringer penetration (and resulting embrittlement) is delayed in the hot-finished material. The hot-finished ribbon did not show elongations of 11 to 13 percent until 100 hours. After 200 hours of testing at 2000°F and 1000 psi, both the cold-finished and hot-finished specimens were brittle and completely oxidized.

3. 4. 1. 6 Effect of Sea Water Salts

The effect of concentrated sea water salts on the stability of fuel ribbon was explored. Ring specimens with capped ends were employed. A tube was inserted in and joined to each cap to permit pressurizing with helium gas.

Testing was conducted by applying the salt concentrate to the outside diameter of the rings. The samples were subsequently heated at various temperatures with periodic pressurizing to predetermined stress levels.

The results obtained indicated that blisters and fissures formed in less than 100 hours at 1850°F.

3. 4. 1. 7 Burnup and Fission Product Release

During the time when the minimum required operating life of aircraft nuclear reactors was 100 hours, anticipated operational burnup levels were low enough (less than 2%) that no deleterious effects were expected. Further, in all of the in-pile tests later described involving times up to 500 hours and corresponding burnups to about 6 percent, no superficial or microscopic evidence was ever observed that burnup was contributing to failure either due to pressure from fission gases or contamination effects. Similarly, prior to the development of definite defects through the cladding, no fission fragment release was observed in the MTR or HTRE cores or inserts. This is the best evidence that, if the cladding of these fuel elements remains intact, the fission products are retained.

3. 4. 2 WIRE-TYPE FUEL ELEMENTS [7]

The tensile strength and elongation of 0. 020-inch round Ni-Cr wires containing 30 weight percent UO_2 in a 0. 012-inch core are given in Figure 3.28. Stress rupture data are shown in Figure 3.29. Comparing this data with Figure 3.18 and 3.19 for ribbon illustrates the higher stress properties of the wires versus ribbon. Figure 3.30 compares stress rupture properties of lenticular wire with round wires.

3.5 COMPONENT EVALUATION

Both concentric-ring fuel element configurations and alternate types of fuel elements were evaluated by Burner Rig testing and in-pile testing. In-pile tests were conducted in the Materials Testing Reactor (MTR), the Engineering Test Reactor (ETR), and in the Heat Transfer Reactor Experiments (HTRE).

3. 5. 1 CONCENTRIC-RING FUEL ELEMENT

3. 5. 1. 1 Burner Rig Tests [2, 10, 11]

The evaluation of the structural integrity of the concentric-ring fuel element was one of the major objectives of the initial reactor development program. Because of the unique design and the lack of stress analysis procedures of proven application, it was necessary to obtain verification of the design capability by experimentation. Preferably such testing should be done in facilities similar to the HT-1 hole of the MTR to simulate reactor operating conditions. The complexity and cost of in-pile testing, however, limited such evaluations to the final design development. Further, there was a need to evaluate fuel element
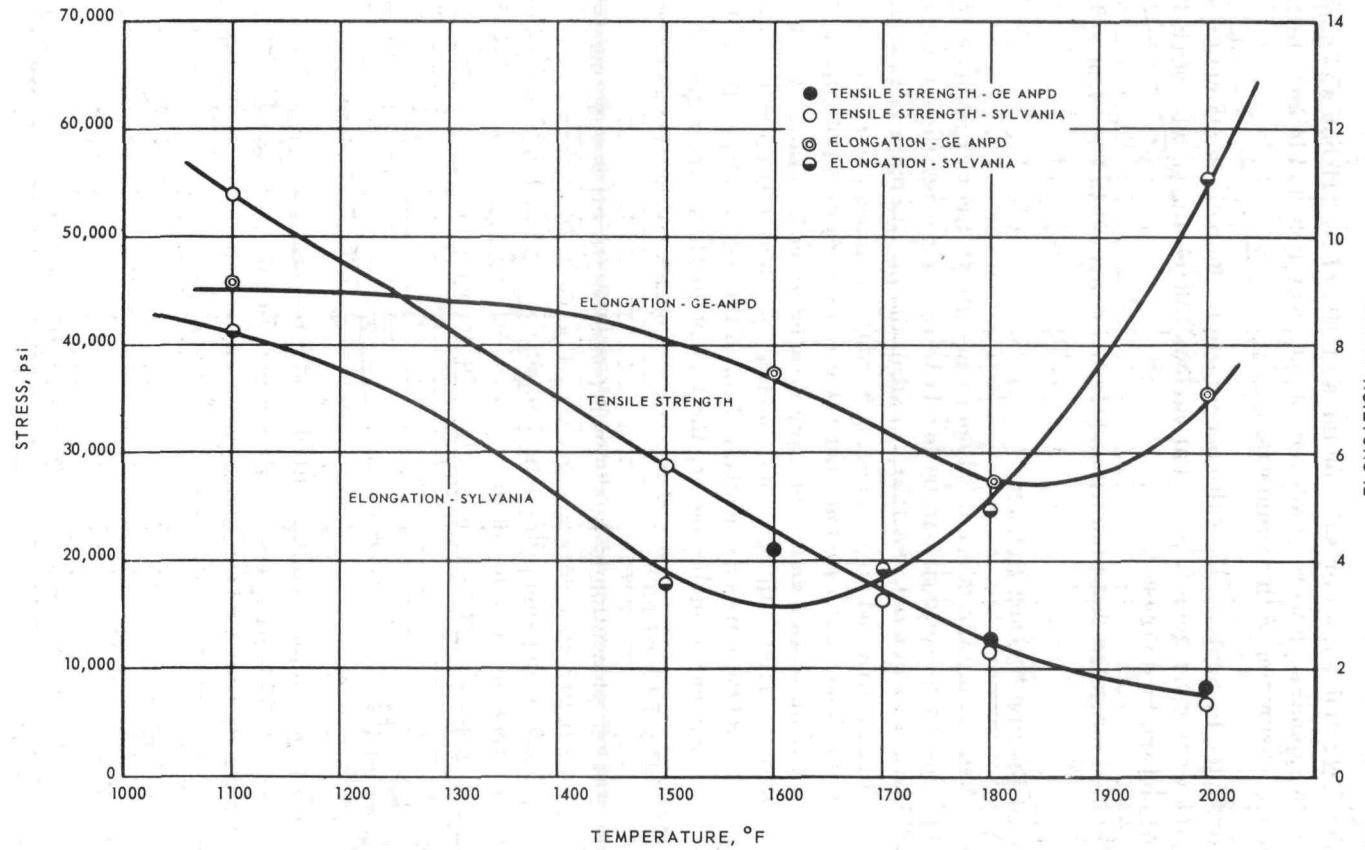
Fig. 3.28 — Elevated temperature tensile properties of 80Ni – 20Cr fuel wire with 30 weight percent UO_2 in core
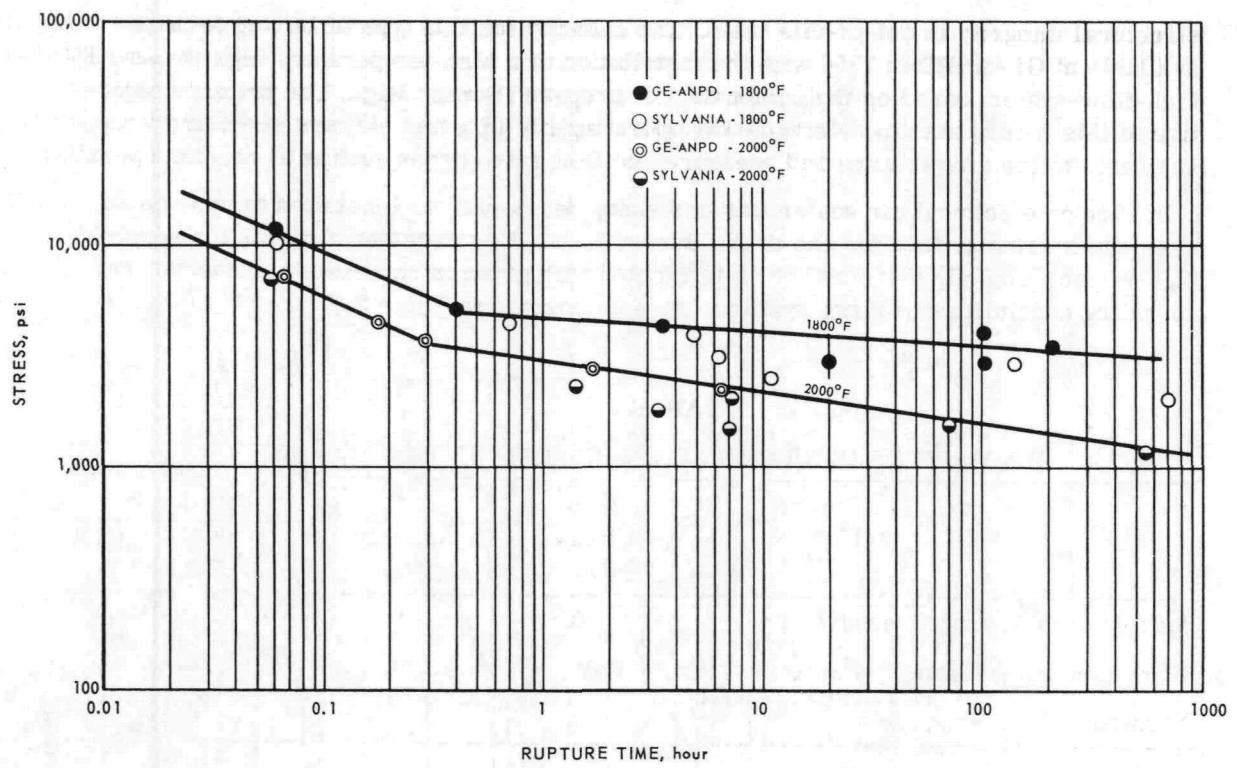
Fig. 3.29 — Stress rupture tests of 0.020-inch-diameter fuel wire
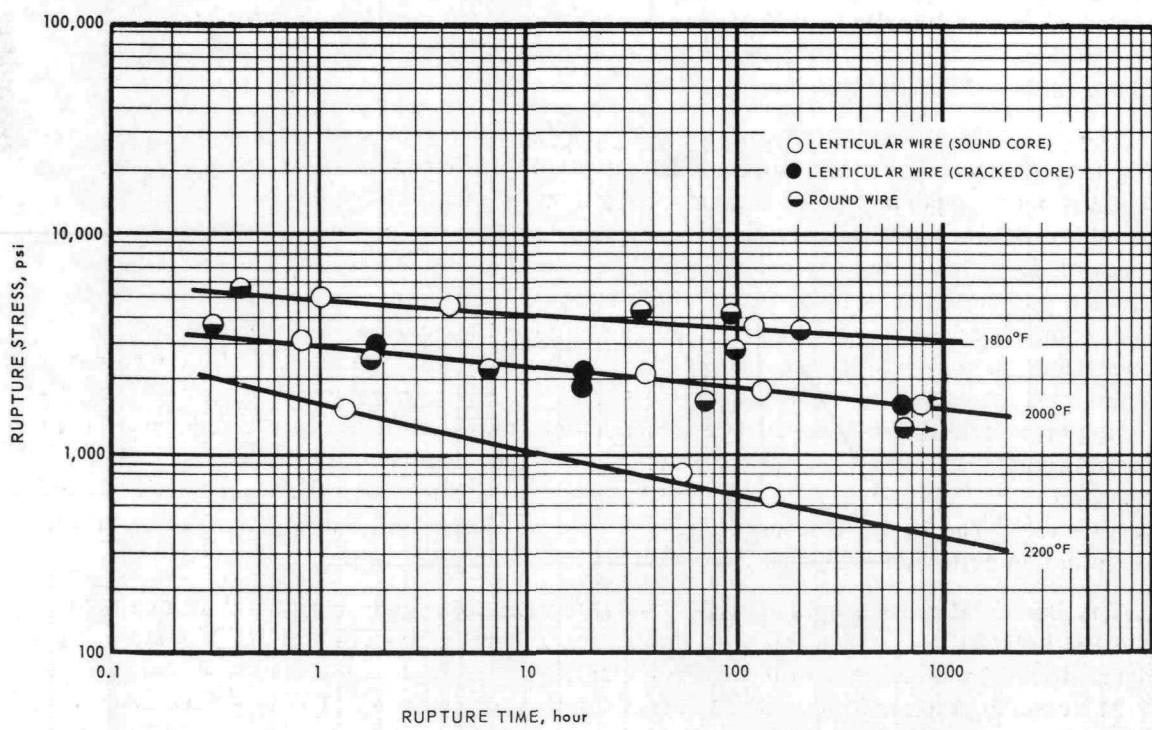
Fig. 3.30 — Fueled wire stress-rupture properties

structural integrity in out-of-pile tests. The capacity for this type of testing became available at GE-ANPD in 1954 with the installation of a high-temperature high-pressure high-flow-system based on the combustion of propane (Burner Rig). The primary objective of this facility was to determine the operating life of a fuel element structure when subjected to the temperature and pressure and flow rate corresponding to reactor operation.

In 1958 an electrical air heater was designed, developed, and installed to provide an alternate heating method for one of the Burner Rigs. This provided a means for supplying high-temperature air that was not contaminated with propane combustion products. The operating capabilities of these systems are summarized in Table 3. 7.

TABLE 3. 7

SUMMARY OF OPERATING CAPABILITIES OF HOT-GAS RIGS

| | Hot-Gas Rig No. 1 | | Hot-Gas Rig No. 2 |
	Propane Fired	Electrically Heated	Propane Fired
Maximum Operating Pressure, psi	70	70	90
Maximum Temperature Obtainable, ^{o}F	2100	2000	2100
Maximum Flow Rate, lb/sec	3. 5	3. 0	4. 0

The extent of the Burner Rig test activity associated with 80Ni - 20Cr fuel element development was fairly extensive. In 1959, for example, there were 57 fuel element specimens of 80Ni - 20Cr tested for a total of 3740 hours. Of these totals, 37 specimens were tested using electrically heated air for a total of 2537 hours. The test activity in terms of fuel element designs was as follows: (1) A-type design - 15 tests, (2) P102 design - 23 tests, and (3) P103 design - 76 tests.

The selection of the test conditions to be imposed on a test specimen during a Burner Rig test was based on a careful study of the conditions anticipated for reactor operations. The two most important test variables were temperature and dynamic head (q). Special consideration was given to see that these parameters were combined to yield test conditions closely simulating nuclear operation. Generally the temperature of the hot-gas stream was adjusted to equal that of the maximum fuel surface temperature of nuclear operation. In addition, the dynamic head was generally made equal to that of nuclear operations in order to impose drag loads closely simulating those of in-pile operation. The static pressure differential across the test specimen was measured to give an indication of sample distortion. Test experience demonstrated that, in the standard 3-stage fuel element test specimens, an increase in pressure differential of 10 percent corresponded to fuel plate distortion that would probably lead to fission product release in an in-pile test. The 10 percent increase in pressure differential, therefore, was the usual termination criterion in Burner Rig tests.

The Burner Rig test which provided final confirmation of the structural adequacy of the P102 (HTRE No. 3) fuel element design for 100-hour operation at 1850°F and 5. 6 psi dynamic head was completed in November 1956. The sample after test is shown in Figure 3. 31 revealing the small amount of ring distortion experienced. The pressure drop increase amounted to less than 5 percent. The effect of dynamic head on the structural stability of the P102 fuel element design is shown in Figure 3. 32. Each element was tested in the Burner Rig for 100 hours at 1850°F. As shown in the figure, very little distortion took place until the dynamic head approached 7. 5 psi.
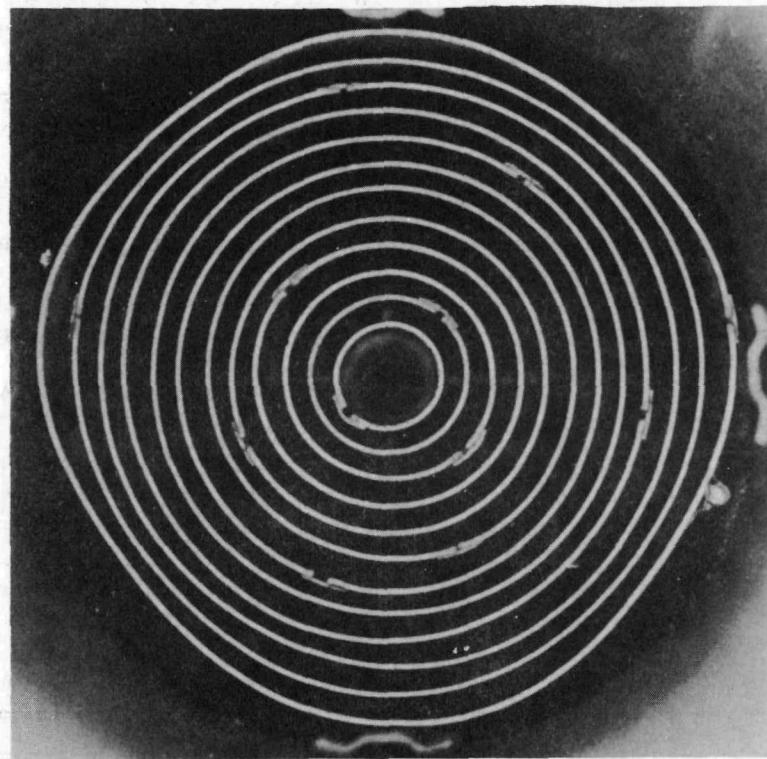
Fig. 3.31 — P102 fuel element after a 100-hour hot-gas rig test at 1800°F
and 5.6 psi dynamic head (Neg. C-03909)
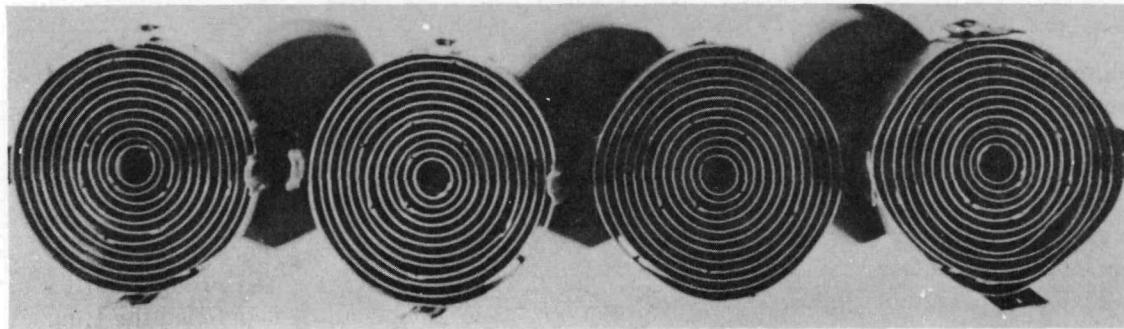
Fig. 3.32 — P102 fuel elements tested for 100 hours at 1850°F and
various dynamic heads (Neg. C-21104)

The P102 fuel stages were tested at temperatures varying from 1850° to 2000°F with
dynamic heads ranging from 2 to 7.5 psi. The more significant test results are tabulated
in Table 3.8. The types of deformation commonly observed in this design were (1) axial
yielding of the front support structure which resulted in dishing and (2) out-of-round
distortion of the rings at the trailing edge of the stage.

The fuel element development program for the XMA-1A power plant was concerned
with fuel stage dimensions quite different from those of the P102 design. Not only was
the stage length changed from 1.5 to 3.0 inches, but the diameter of the element increased
from 2.64 to 3.37 inches. The principal development tests that resulted in establishing

TABLE 3.8

OPERATING CAPABILITIES, Ni-Cr CONCENTRIC RING FUEL ELEMENTS
(All tests on fueled material, 40% UO$_2$)

Design[a]	Test Designation	Temperature °F	Exit Dynamic Head, psi	Time To Cause A 10% Increase In P/q, hr	Equivalent Service
P102 (12-Ring)	A[b]	1850[c]	6	150	Design point, original HTRE No. 3
	TI-1507	1850[c]	7.5	100	Maximum dynamic head for 100-hour operation at 1850°F temperature
	A	1850[c]	2	400	Final operating condition for HTRE No. 3
	TI-1677	1950[c]	2	100	Maximum temperature conditions for HTRE No. 3 operation
	A	1900[c]	5	120	Flight conditions for XMA-1A (compare with P103 12-ring under same conditions)
P103 (9-Ring)	BR No. 16	1900[d]	4	200	XMA-1A flight conditions for the configuration
	BR No. 25	1950[d]	4	98	Over-temperature conditions, XMA-1A flight
	BR No. 27	2000[d]	4	50	Extreme over-temperature conditions, XMA-1A flight
P103 (12-Ring)	BR No. 21	1900[d]	5	96	Best performance at XMA-1A flight conditions, cold-finished material
	BR No. 15	1900[d]	5	180[e]	Flight conditions XMA-1A
	BR No. 29	1900[d]	5	400[f]	Best performance at XMA-1A flight conditions
	BR No. 30	2000[d]	5	105[f]	Extreme over-temperature conditions, XMA-1A flight

[a]Elements made of cold-finished ribbon unless otherwise specified. Ribbon fueled with 40 weight percent UO$_2$.
[b]The values listed are not those of specific tests; they are based on an interpretation of the results of a series of tests.
[c]Combustion of propane.
[d]Electrically heated.
[e]Ribbon was hot finished, rings were cold formed.
[f]Ribbon was hot finished, rings were hot formed.

the operating capabilities for this design are presented in Table 3.8. Hot-finished and hot-formed 80Ni - 20Cr fuel sheet possessed a significant strength advantage over the standard fuel sheet. Based on Burner Rig tests alone, specifically BR No. 21 and BR No. 29, this strength advantage appeared to make possible nearly a four-fold increase in operating life.

The rate at which distortion proceeds as a function of operating temperature was studied. For all the configurations tested, including one using unfueled wrought 80Ni - 20Cr throughout, an increase of 50°F in the operating temperature shortened the time to cause a given increase in $\Delta P/q$ by about 50 percent. This was true for any dynamic head in excess of 4 psi and at temperatures above 1800°F.

Finally, comparison of the distortion experienced in Burner Rig, MTR, and ETR testing of identical fuel element designs operated at the same conditions showed that the in-pile operating capabilities of a particular design was at least equal to those established in Burner Rig tests.

Effects of Staging on Pressure Drop and Heat Transfer

As was indicated previously, in the concentric-ring designs, the fueled stages were separated by approximately a 0.125-inch gap, which allowed cross flow between rings at the end of each stage and for thermal expansion differences. The cross flow was useful in alleviating flow maldistribution caused by a non-uniform distribution of the total pressure at the entrance to the fuel element. The gap also helped equalize the static pressures

within the fuel element so that excessive pressure differences from one ring to another did not build up and cause structural damage.

It was initially recognized that the staging principle of design would result in an increase in pressure loss over a design with smooth, continuous passages. The magnitude of the pressure loss was examined in a series of tests conducted with stages of 1-, 1.5-, 2-, and 6-inch lengths. Each of these stages included the same number of concentric rings and the same sets of fore and aft supporting hardware. Tests were run on six 1-inch stages stacked together, four 1.5-inch stages, three 2-inch stages, and the 6-inch stage. Thus, all these assemblies had the same length and heat transfer surface. Any measured difference in pressure drop would then be attributable to the increased amount of support hardware in the smaller length stages.

Thermal Effect of Thermocouples

Fuel element surface temperatures of all reactor and in-pile experiments were measured with thermocouples. Thermocouple accuracy depends on a number of factors: accuracy of placement of the thermoelectric element junction, control of the thermoelectric element assembly, accuracy of the thermoelectric calibration, tendency to decalibrate, degree of local disturbance of the flow, and heat transfer characteristics caused by the thermoelectric element, proper electrical insulation of the leads, radiation effects, and, of course, the mechanical integrity of the whole measuring system. For the major types of thermocouples that were used for reactor work at GE-ANPD, the thermal effects of the particular geometries and materials used were reduced to a set of correction factors.

Chronologically, the first thermocouple type used for reactor application consisted of attaching the two thermoelectric element wires directly to the surface at the position of desired temperature measurement. This design was designated the bare-wire thermocouple, and correction factors for its use are necessary. The correction factors corrected the temperature indicated by the thermocouple to the temperature that would exist at that location if the thermocouple were not present.

Because of unsatisfactory mechanical durability of the bare-wire-type thermocouple, a different design called the cap-type thermocouple was proposed and used in HTRE No. 3. This design attached the thermoelectric element more firmly to the fuel element, but the thermoelectric junction was not attached to or accurately positioned in relation to the heating surface. Experience showed that the precision of any given thermocouple of this type is subject to considerable question.

The cap-type thermocouples performed quite well mechanically but, because of their limited accuracy, this design was superseded in the development effort by flattened sheath thermocouples. In this design, the thermoelectric junction was firmly attached to the heat generating surface, and a ramp is used ahead of the junction to permit a smooth flow of air over it. The sheath for the thermocouple leads was firmly attached to the fuel element.

This design promised good structural stability and also appeared to have good accuracy. When the performance on test of the flattened sheath design was compared with that of the bare-wire thermocouples, the error had apparently been reduced to a sufficiently low value that it could be neglected for reactor applications.

A disadvantage of the flattened sheath-type thermocouple, as applied to the concentric ring fuel element design, was that the thermoelectric element and leads were subjected to hydrogen and high temperature during the brazing process for the element assembly. A change occurred which affected the basic thermoelectric calibration and consequently a revised calibration curve was used in the temperature recording process.

3.5.1.2 In-Pile Tests [12]

Materials Testing Reactor (MTR)

The initial Ni-Cr tests in the MTR were performed on individual sections of fuel ribbon to determine fission fragment retention, oxidation resistance, and structural integrity. The results of these tests were used in the design of Ni-Cr multistage elements for the GE-ANP-1 series of tests, which are summarized in Table 3.9.

The results of these tests indicated that the A-2 design has the potential for satisfactory operation at 1850°F and a dynamic head of about 1 psi for a period of 500 hours. The P102 design, on the other hand, appeared capable of at least 100 hours operation at 1850°F and a dynamic head of over 5 psi.

Engineering Test Reactor (ETR)

An in-pile testing program utilizing the ETR 6 x 6 facility was established in 1958 to support the fuel element design for the XMA-1A reactor. Though the planned program was never completed because the XMA-1A was cancelled and the Ni-Cr evaluation program was suspended, seven P103 fuel cartridges were tested. These are summarized in Table 3.10.

The purpose of the tests was to demonstrate the ability of the cartridge to operate satisfactorily for 100 hours at the conditions required for D103A performance:

1. Cartridge Total Power, megawatts   0.88
2. Inlet Air Temperature, $^\circ$F   692
3. Bulk Outlet Air Temperature, $^\circ$F   1600
4. Weight Flow, lb/sec   3.45
5. Inlet Pressure, psia   151

The test specimens were full size metallic cartridges of either 9 or 17 stages depending on whether 1.5-inch-long or 3-inch-long stages were being tested. All stages had an unfueled outer ring and an unfueled inner ring to which six major ribs were brazed. Six intermediate and twelve minor ribs were used as spacers. The first three stages had nine (0.025 inch thick) and the last six stages had twelve (0.022 inch thick) rings brazed to the combs. Stage assemblies were connected to form the cartridge by circumferentially welding together the outer rings. All element combs and rings had rounded leading edges.

As shown in Table 3.10, Test 66F4 met the objective of 100-hour life, and Test 66F55 demonstrated a substantial increase in life capability caused by the introduction of the hot-finishing method of ring fabrication. In any case, based on these data and Burner Rig test information on P103 design fuel elements, it is felt that later ETR fuel cartridges could have been operated for 300 to 400 hours or more at design conditions.

In general, most of the tests were terminated because of fission product release which, in turn, was believed associated with ring deformation and localized increase in temperature. Ring deformation, in turn, was directly related to the non-uniform ETR 6 x 6 hole flux pattern. Boron shimming reduced, but did not eliminate, the resulting power scallops.

Heat Transfer Reactor Experiments (HTRE)

The HTRE program of testing represented the operational climax of the three major reactor efforts of GE-ANPD. As previously indicated, all three reactors employed Ni-Cr elements. Consequently, the results of the HTRE tests are particularly valuable in assessing the performance of Ni-Cr fuel elements. Further details of the HTRE No. 1, No. 2, and No. 3 operation are given in APEX-904, APEX-905, and APEX-906, respectively.

HTRE No. 1 - Three series of tests were performed during HTRE No. 1 operation: (1) IET No. 3, (2) IET No. 4, and (3) IET No. 6 (IET Nos. 1, 2, and 5 were zero power

TABLE 3.9
MTR-HT-1 Ni-Cr FUEL ELEMENT EXPERIMENTS

Test Designation[a]	Date	Design Type[b]	Indicated Maximum Plate Temperature, °F	Reference Indicated Temperature, °F[c]	Exit Air Temperature, °F	Exit Dynamic Head, psi	Time On Test, hr	Comments and Results
1F	5/25/54	Concentric-Ring (2 stage)	--	1700	860 - 930	0.09 - 0.26[d]	100	Operation successful - No distortion or fission product release
1G	5/4/58	Concentric-Ring (2 stage)	--	1700	800 - 880	0.35 - 0.48[d]	100	Thermocouple failure - No distortion or fission product release
1H	6/20/54	Concentric-Ring (2 stage)	--	1700	188 - 973	0.2 - 0.64[d]	60	Thermocouple failure - No distortion or fission product release
1J	7/15/54	Concentric-Ring (6 stage)	--	1700	790	0.73	70	Thermocouple failure - No distortion or fission product release
1L	9/2/54	Concentric-Ring (6 stage)	--	1750	740	0.92	200	Operation successful - No distortion or fission product release
1M	11/22/54	Concentric-Ring (6 stage)	1800	--	1150 - 1230	1.08 - 1.20	118	Operation successful - No distortion or fission product release
1N	1/13/55	Concentric-Ring (6 stage)	--	1850	1330	0.89	80	Operation successful - No distortion or fission product release
10	12/30/54	Concentric-Ring (6 stage)	--	1680	1170	1.21	320	Operation successful - No distortion or fission product release
1P	3/26/55	Concentric-Ring (6 stage)	--	1000	--	1.24	322	Yoke failure - No ribbon distortion or fission product release
1R	2/3/55	Concentric-Ring (6 stage)	--	1850	1357	~1	238	Operation successful - No distortion or fission product release
1S	3/7/55	Concentric-Ring (6 stage)	--	1850	1380	~1	200	Operation successful - No distortion or fission product release
1T	12/6/55	A-2[e] (6 stage)	1850	1820	1220 - 1330	1.07 - 1.32	500	Operation successful - No distortion or fission product release
1U	2/8/56	A-2[e] (6 stage)	2005	1992	1200 - 1318	1.26 - 1.32	57	Fission product release (37 hours at maximum indicated plate temperature)
1V	3/5/56	A-2[e] (6 stage)	1920	1920	1390 - 1410	1.17 - 1.37	69	Fission product release - Blister - Air blockage caused by foreign particles lodged between rings (66 hours at maximum indicated plate temperature)
1W	3/15/56	A-2[e] (6 stage)	1850	1830	1320 - 1328	2.76 - 2.96	61	No fission product release - Termination caused by a 10% increase in pressure drop (47 hours at maximum indicated plate temperature)
1X	5/21/57	A-2[e] (6 stage)	1855	1850	1155 - 1350	2.9 - 3.03	33	No fission product release - Termination due to 12% increase in pressure drop. (12 hours at maximum indicated plate temperature)
1Y	7/23/56	A-2[e] (6 stage)	--	1900	1372 - 1380	1.20 - 1.26	42	Fission product release - Blisters
1Z	7/5/56	A-2[e] (6 stage)	1840	1815	1285 - 1330	2.92 - 3.05	75	Thermocouple failure - Some distortion but no fission product release
1A1	9/5/56	A-2[e] (6 stage)	1796	1850	1010	4.5 - 4.6	17	Thermocouple failure - No fission product release (12 hours at maximum indicated plate temperature)
1E1	1/29/57	A-2[e] (6 stage)	1660	1800	1270 - 1305	4.1 - 4.3	22	Thermocouple failure (7 hours at maximum indicated plate temperature)
1F1	2/19/57	A-2[e] (6 stage)	1800	1800	1360	4.7 - 4.8	2.6	No fission product release or distortion - Termination due to increase in pressure drop caused by broken static pressure probe
1B1	11/7/56	P102 (3 stage)	1920	1920	1140 - 1150	4.0 - 5.0	37	Thermocouple failure - No fission product release
1C1	11/27/56	P102 (6 stage)	1860	2100	1250	5.3 - 6.4	27	Fission product release (16 hours at maximum indicated plate temperature)

TABLE 3.9 (Cont'd)

MTR-HT-1 Ni-Cr FUEL ELEMENT EXPERIMENTS

Test Designation[a]	Date	Design Type[b]	Indicated Maximum Plate Temperature, °F	Reference Indicated Temperature, °F[c]	Exit Air Temperature, °F	Exit Dynamic Head, psi	Time On Test, hr	Comments and Results
1D1	12/19/56	P102 (6 stage)	1850	1900	1190 - 1200	5.55 - 5.63	169	No fission product release - serious distortion and oxidation (125 hours at maximum indicated plate temperature)
1G1	6/24/57	P102 (7 stage)	1850	2050	1490	4.0 - 4.2	27	Fission product release - heavy general oxidation in certain locations
1J1	7/15/57	A-2 (6 stage)	1810	1795	1255 - 1350	4.6 - 4.8	278	No fission product release - some distortion and oxidation penetration (252 hours at maximum indicated plate temperature)
1K1	8/5/57	A-2 (6 stage)	1810	1805	1267 - 1370	4.6 - 4.8	181	Serious distortion and oxidation penetration
1N1	1/20/58	P102 (6 stage)	1855	1850	1350 - 1385	3.7	110	Termination due to excessive temperature in MTR shield-slight distortion and oxidation (103 hours at maximum indicated plate temperature)
1P1	12/1/58	A-2 (6 stage)	1908	1900	1400 - 1430	4.6 - 4.7	78	Slight distortion - termination caused by end of cycle (57 hours at maximum indicated plate temperature)
1W1	8/18/58	P102 (6 stage)	1890	--	Varied	Varied	78	Sample contained known defects - Termination caused by inability to reach test conditions - No worsening of defects
1T1	12/22/58	P102 (7 stage)	1860	1850[f]	1240 - 1410	0.4 - 1.4	264	Fission product release occurred 10 hours after completion of 100-hour endurance run at 1850°F - Slight distortion (100 hours at maximum indicated temperature)
1B2	5/10/59	P102 (6 stage)	~1850	--	--	~5	125	Sample contained known defects - No appreciable fission product release - Slight distortion (100 hours at maximum indicated plate temperature)
1F14	7/27/59	P103 4-stage (3-stage length)	1950	--	--	~5	118	Test employed experimental thermocouples and indicated temperatures were questionable - No failure (88 hours at maximum indicated temperature)

[a]All material in these tests was cold finished.

[b]The number of rings per stage varied between tests.

[c]During most of the tests it was not possible to hold the indicated temperatures exactly constant over the full life of the test. Therefore, a reference indicated temperature was established by roughly integrating the time-temperature record to arrive at a value which would be representative of the particular test. In some special cases involving failure of thermocouples, it was necessary to make other adjustments in order to arrive at the reference indicated temperature.

[d]Inlet dynamic head.

[e]Similar to A-1 design.

[f]Flux wire and gamma scan data and post-test evaluations indicated that a peak temperature in excess of 2000°F existed during endurance run.

operations, or shielding tests). A comparison of parameters of these tests is given in Table 3.11.

HTRE No. 2 - The HTRE No. 2 reactor was essentially the same as HTRE No. 1, with the reactor modified to include a large test hole in the center of the active core. The purpose of the HTRE No. 2 program was testing of new materials proposed for use in building future GE-ANPD power plants. Nine inserts were tested. Ni-Cr fuel elements were involved in a few of these, but only in a subsidiary role. Their performance was more than adequate.

The significant point is that five Ni-Cr fuel elements from the original parent core of the HTRE No. 2 were selected from the original loading to be included in the second loading. These accumulated more than 1000 hours operation at test condition temperatures ranging from 1200° to 1750°F.

TABLE 3.10

ETR-66 Ni-Cr FUEL ELEMENT EXPERIMENTS

Test Designation[a]	Date	Design Type[b]	Indicated Maximum Plate Temperature, °F	Average Exit Air Temperature, °F	Maximum Exit Air Temperature, °F	Exit Dynamic Head, psi	Time On Test, hr	Comments and Results
66F5	4/30/59	P103 17 stage (1.5-inch stage length)	1850	1223	1260	4.0	100	No distortion or other damage noted - Indications that dynamic head value is too high due to orifice calibration error - Did not reach design conditions
66F7	5/24/59	P103 17 stage (1.5-inch stage length)	1910	1475	1600	3.76	100	Serious distortion due to airflow blockage caused by foreign material (stainless steel foil) between rings - Did not reach design conditions - Same orifice calibration error
66F6	6/13/59	P103 9 stage (3-inch stage length)	1800 - 1900	1602	1640	3.61	95	Operated at design conditions for 63 hours - Fission product release - Blisters and gross distortion - Same orifice calibration error
66F4	8/21/59	P103 9 stage (3-inch stage length)	1800 - 1900	1600	1670	3.61	120	Operated at design conditions for 116 hours - Fission product release - Extensive ring distortion - Same orifice calibration error
66F22	12/9/59	P103 9 stage (3-inch stage length)	2000 - 2200	1700	1800	3.8	20.2	Similar to 66F4 - Fission product release - Distortion and hot spots developed - Burn-through occurred on stage 7
66F23	12/26/59	P103 9 stage (3-inch stage length)	1900	1600	1670	4.25	89	Similar to 66F6 - Fission product release - Some distortion
66F55	3/4/60	P103 9 stage (3-inch stage length)	1900	1603	1800	4.6	202.5	Hot finished material used - Operated at approximately design conditions for over 200 hours with no fission product release - Less distortion than in previous tests

[a]All material in these tests was cold finished, unless otherwise specified.

TABLE 3.11

COMPARISON OF ENDURANCE TESTING

	IET No. 3	IET No. 4	IET No. 6
Days operated above 200 kw	18.0	35.0	38.0
Total hours of operation above 200 kw	40.2	187.78	257.61
Total energy release to system, mwh	349.08	2064.98	3092.20
Total energy release to air, mwh	317.0	1876.0	2811.0
Maximum power, mw	16.9	18.4	20.2
Total number of transfers	3.0	0	40.0
Total hours at 100% nuclear power	6.02	0	105.82[a] 38.95[b]
Initial k_{ex}	3.52	4.16	3.45

[a]Reactor exit air temperature = 1280°F.
[b]Reactor exit air temperature = 1380°F.

HTRE No. 3 - The HTRE No. 3 employed the first GE-ANPD power plant design that approached flight-type arrangement. The power plant simulated flight-type geometry and structure, including a forward shield plug and air inlet ducts. It incorporated the first solid-moderator-type reactor used in GE-ANPD power plants.

The second phase of the HTRE No. 3 program began early in 1960 with the objective of accomplishing 100 hours of endurance running at the design condition. By February 7, 1960, the power plant successfully fulfilled this objective by accumulating 127 hours at the design condition.

3.5.2 ALTERNATE CONFIGURATIONS

3.5.2.1 Burner Rig Tests [9, 10, 11]

A considerable number of tests were performed on a variety of fuel element configurations. Most of these configurations were adaptable to one of the three reactor concepts discussed in section 3.5.1.2. The configurations and the reactor designs to which they relate are as follows:

Configuration	Related Design
Corrugated Concentric Ring	Cellular
Corrugated Radial Vane	Cellular
Shaped Wire	Cellular
Wire Screen	Folded-flow
Parallel Curved Plate	Polygon
Corrugated Plate	Polygon
Tubular	--
Twisted Ribbon	--

Corrugated Concentric Ring - Three tests were conducted, as shown in Table 3.12, and were successful in demonstrating the structural integrity of this design, shown in Figure 3.33.

Corrugated Radial Vane - Only one test was made; however, the results were extremely encouraging and indicated that this design had the ability to operate under high dynamic heads. The specimen consisted of 30 corrugated radial vanes assembled into a 3.3-inch diameter cylindrical array about a 1.4-inch diameter center moderator rod. The vanes had a developed length of 11.75 inches and a width of 1.2 inches. The radius of the vane was 0.8-inch, and the corrugations were 0.116-inch amplitude with a pitch of 0.6 inch. The vanes were spaced by longitudinal wires brazed to the crests of each corrugation of the two adjacent vanes so that four wires, two on each side, were joined to each vane. The

TABLE 3.12

BURNER RIG TESTS ON CORRUGATED CONCENTRIC-RING DESIGN

Specimen No.	Material	Test Temperature, $^{\circ}$F	Exit Dynamic Head, psi	Time, hr	Results
CCR-1	Wrought 80Ni - 20Cr alloy	1900	4.5	100	Slight misalignment in outer ring of Stage 3
CCRD-2	Fuel ribbon (0.004-in. clad)	1900	5.5	72	Minor distortion
CCRD-3	Fuel ribbon (0.004-in. clad)	1900	4.5	229	Minor distortion - cracks in fuel ribbon
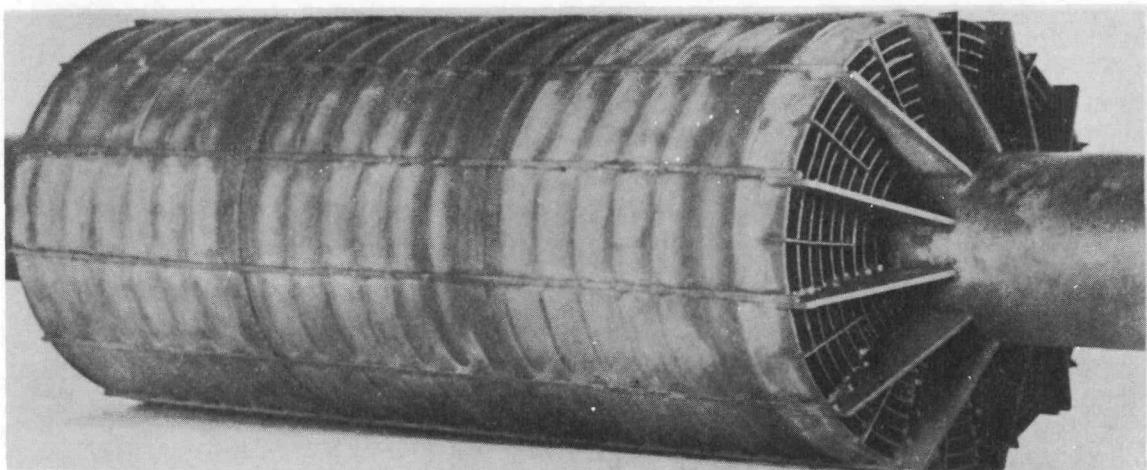
Fig. 3.33 – Corrugated concentric-ring fuel element, CCRD-3, after 100 hours at
1900°F and 4.5-psi dynamic head (Neg. C-22280)

specimen was tested at 1900°F and 6-psi exit dynamic head for 130 hours. The specimen, shown in Figure 3.34, after test was in excellent condition.

Shaped Wire - Two tests were conducted and clearly demonstrated the unstable structural characteristics of this design, which stemmed from inability to maintain wire spacing to aerodynamic drag forces. The two tests were made on a 7-cell array. Each cell was 7.3 inches long with four layers of 28 turns each. The two tests were run for periods of 7 and 14 hours at a maximum temperature of 1900°F and a dynamic head of 6 psi. A typical configuration appears in Figure 3.35.

Wire Screen - Three tests have been made of this configuration. The first specimen was assembled from 20 pieces of Ni-Cr wire screen brazed together to form a 3- by 4- by 1-inch matrix. The wire screen was commercially available, 0.025-inch wire with a 0.025-inch spacing between wires. The element was tested for 100 hours at 1700°F with an airflow of 1.0 pounds per second. The element after test exhibited only minor dishing.

The second wire matrix was similar in construction except that it was positioned obliquely with respect to the flow. The element was tested for 100 hours at 1850°F and a 5-psi pressure drop across the element. The specimen after test exhibited only very slight dishing.

The third sample was fabricated by brazing individual Ni-Cr wires rather than screens into a compact 3- by 4- by 0.6-inch element. The element was tested for 33 hours at 1850°F and 67 hours at 2000°F and 10 hours at 2100°F. The pressure drop across the element was approximately 1 psi, and no visible damage or deflection to the specimen resulted. The element after test is shown in Figure 3.36.

Parallel-Curved Plate - The test specimens used consisted of 0.025-inch-thick plates of wrought 80Ni - 20Cr alloy, 30 inches long and 1 inch wide. The plates had a radius of curvature of 1.3 inches to furnish rigidity. The coolant passed through the plates along their length. A typical specimen is shown in Figure 3.37.

Two unsuccessful tests were conducted. The first test was terminated in the first hour of operation at an air temperature of 1850°F and an exit dynamic head of 6 psi because of complete destruction of the fuel element caused by induced vibration. The second test specimen was modified by brazing the trailing edges of the fuel ribbons in an attempt to eliminate the vibrations that destroyed the first specimen. This test was terminated after only 15 minutes of operation because of a sharp increase in the pressure drop across the element. Examination of the test specimen revealed gross distortion of the ribbons.
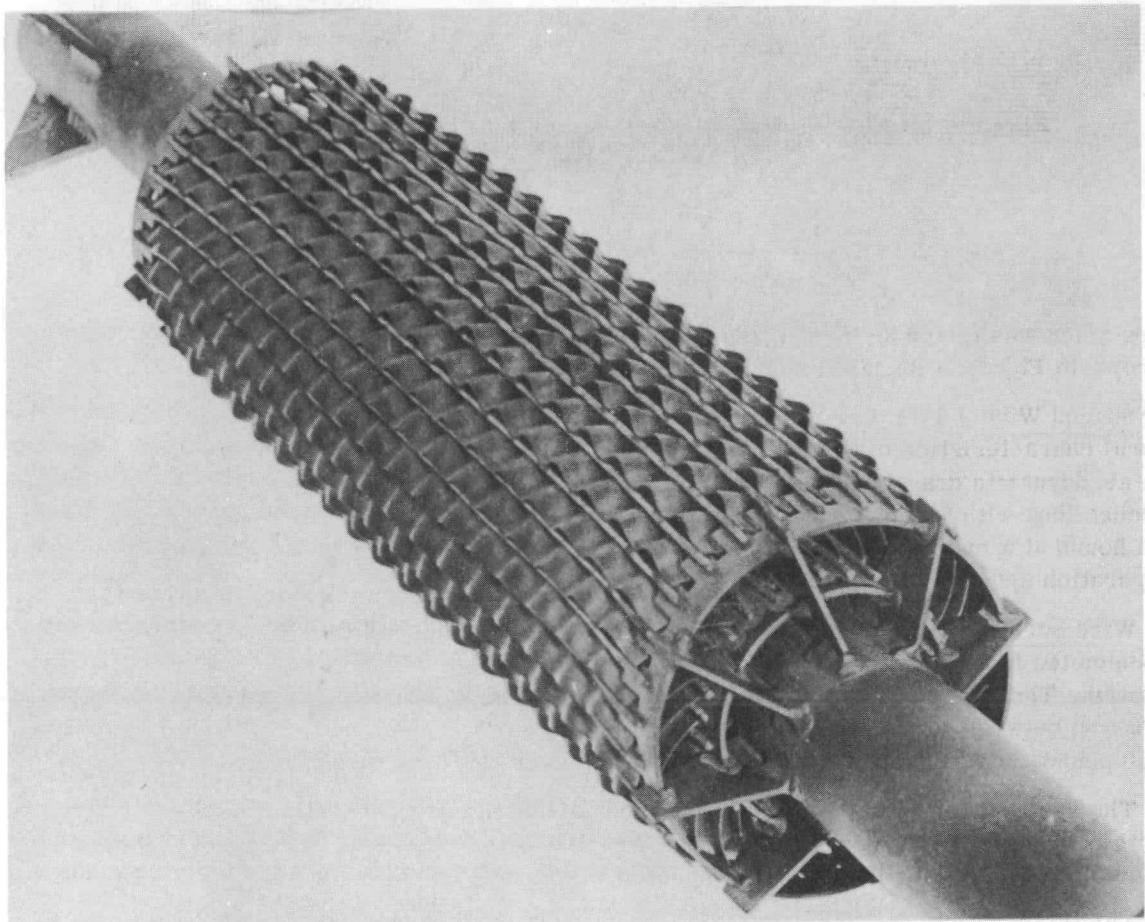
Fig. 3.34 — Radial vane fuel element after 130-hour burner rig test at 1900°F
and 6-psi dynamic head (Neg. C-21600)
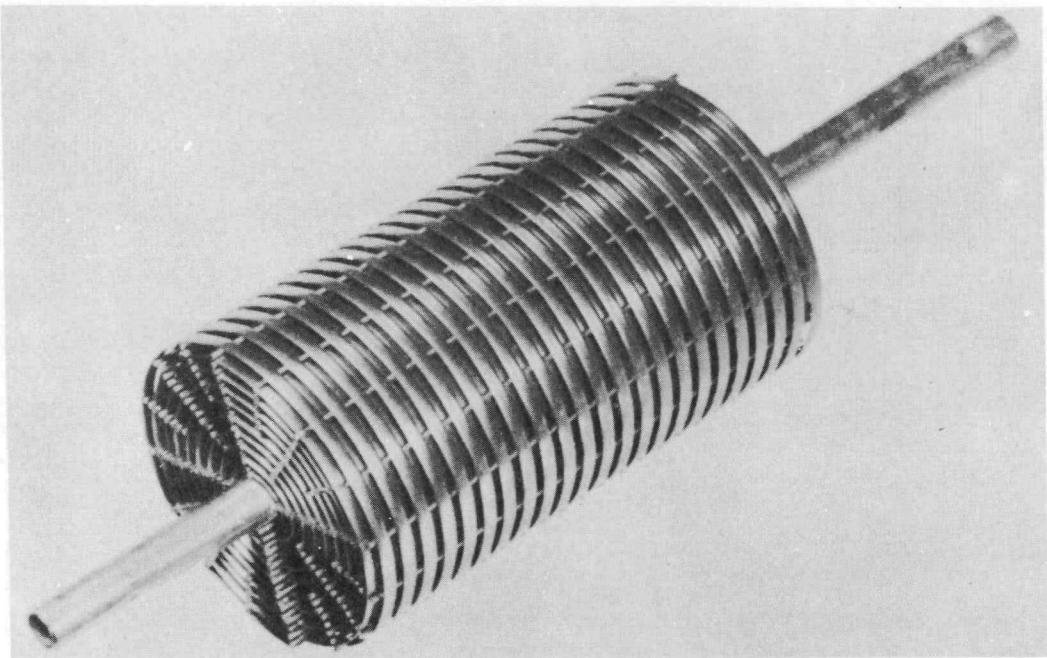
Fig. 3.35 – Fueled stage utilizing lenticular-shaped wire

Corrugated Plate - This design received the most intensive development of the many alternate designs considered. The structural development program progressed from a fuel element design, which had insufficient resistance to vibration, to a structurally reliable design, shown in Figure 3.38, capable of operation at high temperatures and dynamic heads for long periods of time.

Tubular - A single test of a tubular fuel element was made. The specimen consisted of 108 tubes 24 inches long, 0.230 inch OD by 0.190 inch ID, made of wrought 80Ni - 20Cr alloy in a three-layer hexagonal array around a hexagonal, center moderator bar. The test was terminated after 10 hours at 2000°F and a dynamic head of 6 psi because of failure of the brazed joints between tubes at the leading edge of the specimen.

Twisted Ribbon - A 6-inch-long twisted ribbon fuel element was tested for 49 hours at 1850°F and 7.2-psi dynamic head. The damage to the element in this test included breakage of the brazed joints between the ribbons and overlapping and contact of adjacent ribbons so that the pressure drop across the element increased by 10 percent.

3.5.2.2 In-Pile Tests [12, 13]

Wire Screens - Four Ni-Cr wire screen fuel elements were tested in the ANP-3 hole of the MTR. The elements consisted of 18 layers of 0.035-inch diameter wires placed on 0.060-inch centers. The over-all dimensions of the brazed assemblies were 0.61 by 0.61 by 0.60 inch. One sample had the ends sealed by brazing, while the other three had welded ends. The first three samples tested contained 30 weight percent UO_2 in the core and 0.004-inch cladding. The fourth sample had 60 weight percent UO_2 in the core and 0.006-inch cladding.

The first sample was scheduled to be tested at 1850°F with 7.5 scfm of air but did not reach those conditions because of failure of the specimen thermocouples. The second
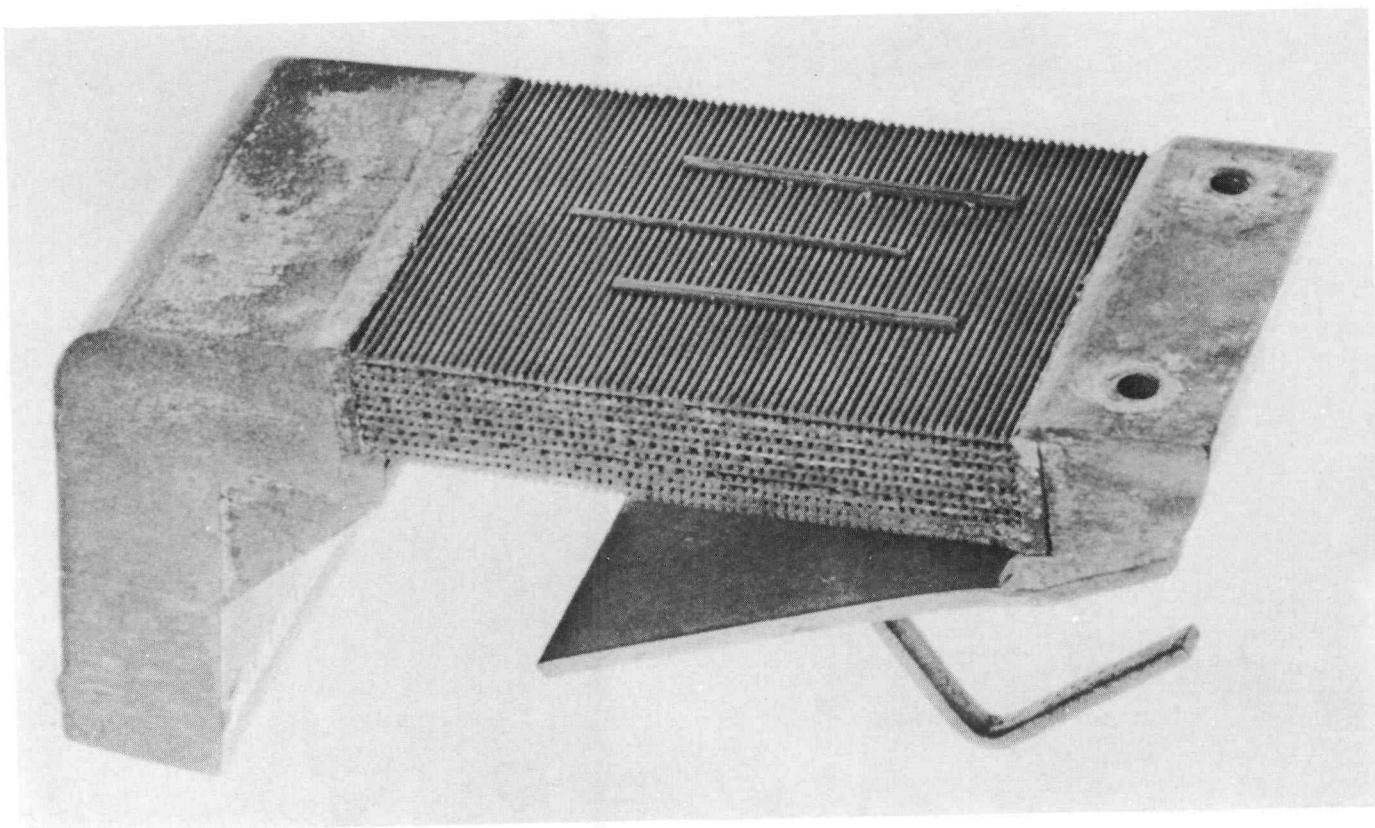
Fig. 3.36 – Wire screen assembly after 33 hours at 1850°F, 67 hours at
2000°F, and 10 hours at 2100°F (Neg. C-23118)
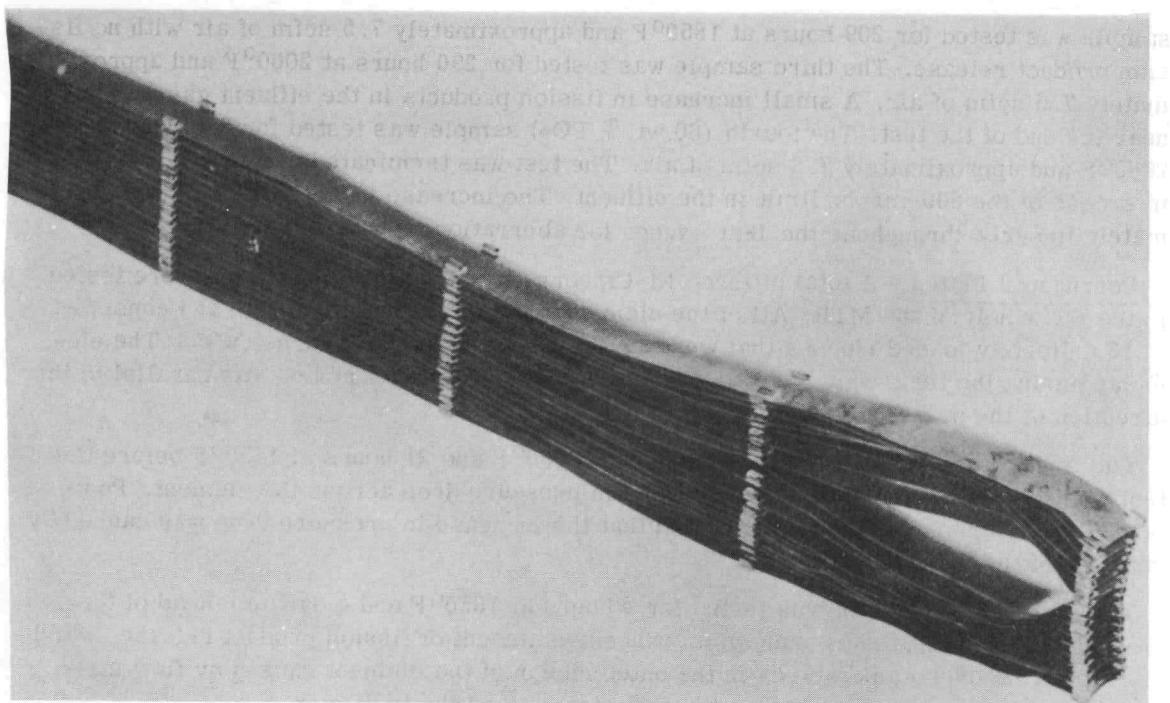
Fig. 3.37 — Parallel-curved plate fuel element after test (Neg. C-04428)
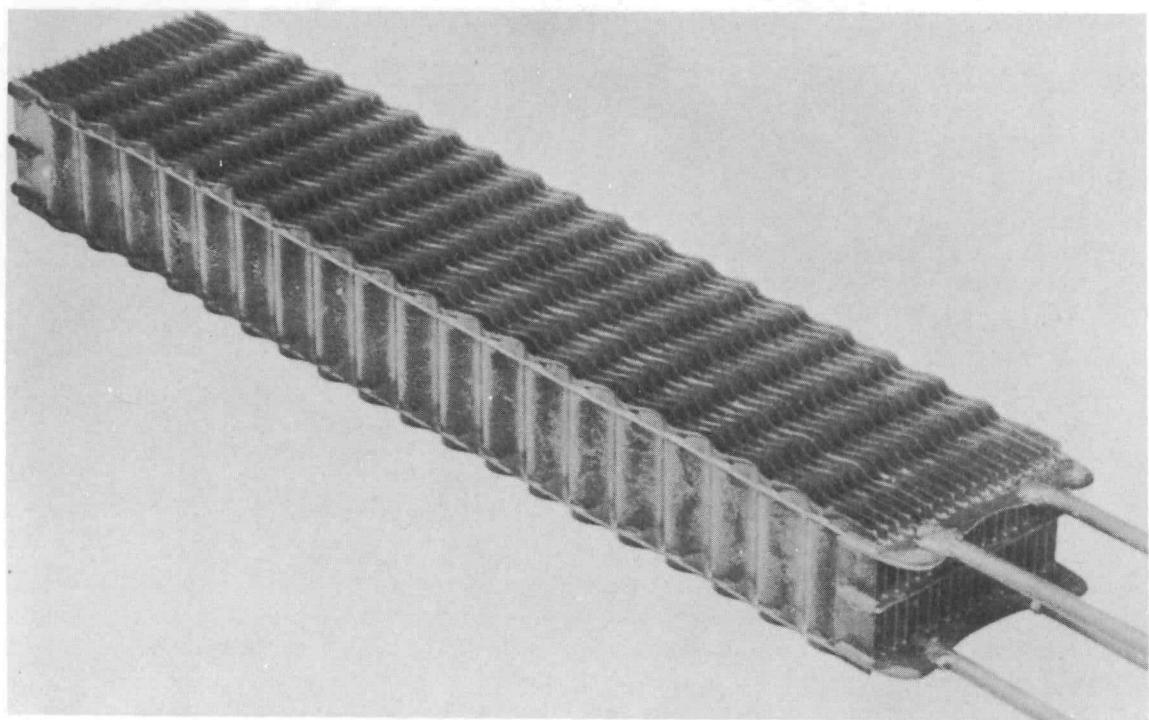
Fig. 3.38 — Corrugated plate fuel element after 100 hours at 1850°F and 9-psi
dynamic head (Neg. C-04739)

sample was tested for 209 hours at 1850°F and approximately 7.5 scfm of air with no fission product release. The third sample was tested for 290 hours at 2000°F and approximately 7.5 scfm of air. A small increase in fission products in the effluent gas was noted near the end of the test. The fourth (60 wt. % UO_2) sample was tested for 370 hours at 2000°F and approximately 7.5 scfm of air. The test was terminated because of activity in excess of the 500-mr/hr limit in the effluent. The increase in activity occurred approximately linearly throughout the test except for aberrations during scrams.

Corrugated Plates - A total of three Ni-Cr corrugated-plate fuel elements were tested in the HT-1 hole of the MTR. All of the elements were of a similar design and consisted of 18 uniformly loaded ribbons that were 12.0 inches long and 1.5 inches wide. The element, during the test, was oriented so that the width of the fuel ribbon was parallel to the direction of the peak neutron flux.

The first sample was tested for 24 hours at 1500°F and 21 hours at 1700°F before the test was terminated because of an increase in pressure drop across the element. Posttest examination of the element revealed that the increase in pressure drop was caused by buckling of the fuel ribbons.

The second fuel element was tested for 9 hours at 1850°F and a dynamic head of 6 psi. The test was terminated because of an excessive amount of fission product release, which resulted from overtemperatures in the outer ribbon of the element caused by flow maldistribution in the channel between the fuel element and the test liner.

The third fuel element was tested for 24 hours at 1500°F and 90 hours at 1800°F. The test was terminated because of an 8 percent increase in pressure drop resulting from the deformation of the outer plate adjacent to the test liner.

3.6 REFERENCES

1. McBride, F. E., "80Ni - 20Cr Recommended Modifications," GE-ANPD, DCL 59-1-18, December 29, 1958.
2. Robertshaw, F. C., "Comprehensive Summary Report on 80 Nickel - 20 Chromium Fuel Elements," GE-ANPD, PREDC-759, October 1960.
3. Lever, R. C., "Fuel Element Fabrication - Wire Type," GE-ANPD, DC 61-11-31, July 1961.
4. Lewis, J. R., "Engineering Properties of Fuel Sheet and Brazed Joints," GE-ANPD, APEX-137, April 30, 1953.
5. Saller, H. A., Stacy, J. T., Klebanow, H. L., "Brazing Nichrome V with GE-81 Alloy," Battelle Memorial Institute, BMI-947, August 27, 1954.
6. Muehlenkamp, G. T., "Co-Modified 80Ni - 20Cr Structural Stock and 0.006-inch Clad Fuel Stock, Properties," GE-ANPD, DC 59-2-23, January 29, 1959.
7. Lewis, J. R., "Shaped Wire Fuel Element Development," GE-ANPD, APEX-281, June 1956.
8. Muehlenkamp, G. T., "Effect of Cladding Thickness on Fuel Element Properties," GE-ANPD, DC 59-3-242, March 1959.
9. Butterfield, A. J., "Summary of Burner Rig Tests from January 1, 1956 Up to September 1, 1959," GE-ANPD, DCL 59-9-229, September 1959.
10. Ryan, P. T., "D103-A1 Burner Rig Testing Summary Report on Tests BR 1-8 and 16," GE-ANPD, DC 59-5-83, May 7, 1959.
11. Ryan, P. T., "Burner Rig Testing Summary Report, Tests BR 15 - 31," GE-ANPD, DC 60-3-202, March 24, 1960.
12. Focke, A. E., "Summary of MTR Tests in HT-1 Facility," GE-ANPD, XDC 59-8-206, September 8, 1959.
13. Schoenberger, M. T., "Irradiation Testing Summary - GE-ANPD, 1953 - 1961," GE-ANPD, DC 61-7-20, July 17, 1961.

4. Nb-UO₂ CORE CLAD WITH Fe-Cr-Al

In order to obtain a fuel element capable of operating at temperatures as high as 2300°F, effort was expended on clad niobium fuel elements. Success could not be attained primarily because of core-clad interfacial products, which formed at elevated temperatures by inter-diffusion between core and cladding materials.

4.1 COMPOSITION

A cross section of a hot-pressed billet is shown in Figure 4.1. Ribbon made from such billets had a total thickness of about 0.020 inch; the core was 0.012 inch and the cladding on each side was approximately 0.004 inch. Ribbon width was 1.5 inches and fuel loading was 30 weight percent. Niobium was used as the metallic phase in the core because of its favorable nuclear properties, high-temperature strength, and ease of fabrication. The composition of the ferrous-base cladding alloy used to protect the core from oxidation and to retain fission products is shown in Table 4.1. Also tabulated is the nominal composition of niobium powder used in core fabrication.

TABLE 4.1

COMPOSITION OF FERROUS-BASE CLADDING ALLOY

Elements	Cladding	Niobium Powder
Fe	balance	0.01
Cr	23.35	–
Al	5.17	–
Nb	–	balance
C	0.02	0.02
O	–	0.18
W	–	0.04
Ti	–	0.2
Si	0.10	0.001
S	0.01	–
P	0.007	–
Mn	0.10	–

The cladding was basically stainless steel with 5 percent aluminum added for increased oxidation resistance.[1-4] The aluminum level of 5 percent was chosen as the compromise yielding optimum oxidation resistance and workability. The aluminum in the cladding material and the oxygen impurity in the niobium powder were the critical constituents of the brittle interfacial material.
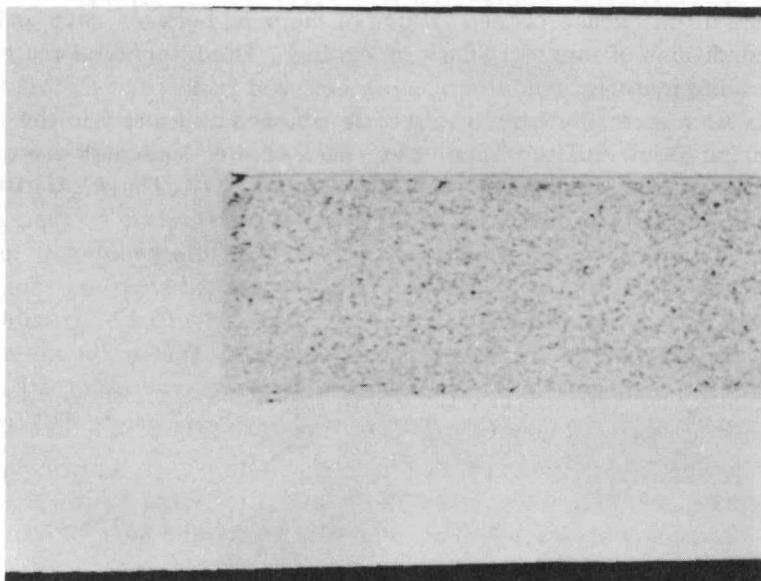
Fig. 4.1 – Cross section through a hot-pressed billet
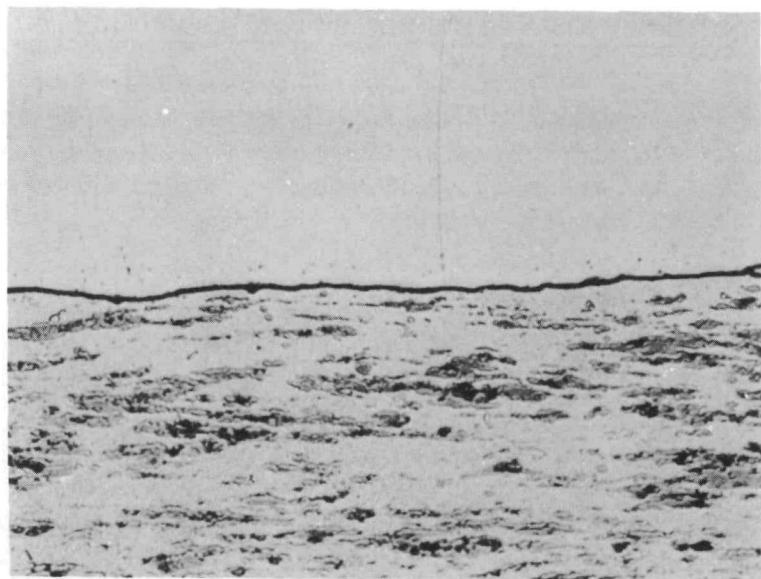
Fig. 4.2 – Cross section through fuel stock after 100 hours at 2200°F

4.2   INTERFACIAL FORMATIONS

When a segment of ribbon was exposed to temperatures in the neighborhood of 2200°F and allowed to remain for a period of about 100 hours, an interfacial zone between core and clad became evident. This zone appeared as a dark horizontal line as shown in Figure 4.2. The existence of this phase caused failure of the bond between core and cladding, particularly under conditions of thermal shock or cycling. The interfacial material proved so effective that cladding material could be readily stripped from core material in finished ribbon. When this was done, the brittle substrate adhered uniformly to the core, which provided a specimen for X-ray diffraction studies. Such studies indicated a major phase of niobium and two minor phases, one of UO_2 and the other, Al_2O_3. The Al_2O_3 lines were attributed to the dark substrate that remained on the core surface after stripping. Similar X-ray diffraction studies of internal cladding surfaces confirmed this hypothesis as a depletion of aluminum. The thickness of the Al_2O_3 substrates in examined samples ranged from less than 0.001 to 0.010 inch. Two of the important variables affecting substrate thickness were time at temperature and the amount of oxygen originally present in the niobium powder raw material. For an original oxygen level of about 0.05 percent, the substrate, in metallographic examination, appeared as a very thin, light line. The Al_2O_3 originated from aluminum in the cladding and oxygen in the niobium.

4.3   THERMAL CYCLING

The appreciable difference in thermal coefficients of expansion of materials in the composite fuel element contributed to poor resistance to thermal shock. The thermal expansion coefficient of the cladding material[1] was approximately twice that of core material, e.g., 4.2 x 10^{-6} inch/inch-^{O}F versus 8 x 10^{-6} inch/inch-^{O}F. A standard test adopted for evaluating thermal shock resistance consisted of a 2200° to 500°F temperature cycle while the ribbon was under a 1000-psi load. The ribbon was held for 2-1/2 hours at 2200°F then cooled to 500°F with an air blast. It was then reheated to 2200°F, and the cycle repeated. As expected, with the Al_2O_3 substrate present to any extent, failure invariably occurred by rupture of the clad-core bond with subsequent oxidation of core material. Oxidation of the core usually extended radially from the point of failure at a rate of about 0.010 inch per hour.

4.4   DEOXIDIZERS

To prevent the rupture and subsequent oxidation described above, carbon and aluminum powders were mixed with the niobium powder raw material during blending operations. The intention was that these elements would act as scavengers for oxygen during subsequent sintering. Shown in Figure 4.3 is the metallographic cross section of a ribbon to which a stoichiometric amount of carbon necessary to combine with available oxygen was added to the core material. The section was taken after the material was exposed to 2200°F for a 200-hour period. It is apparent the Al_2O_3 interface material was reduced substantially by this addition. A similar effect can be noted in Figure 4.4 where aluminum was used as the scavenger. However, in both cases, an additional occurrence was also apparent. An appreciable amount of second interfacial material formed, as evidenced by a horizontal light, banded area. This second material, formed because of the absence of the Al_2O_3 barrier, was also very brittle with a Knoop hardness of 426 (Rc 42), which indicated a compound. The material was extracted from the ribbon and examined by X-ray diffrac-

Fig. 4.3 – Cross section through fuel stock – carbon deoxidized and cycled 208 hours between 2250°F and 500°F
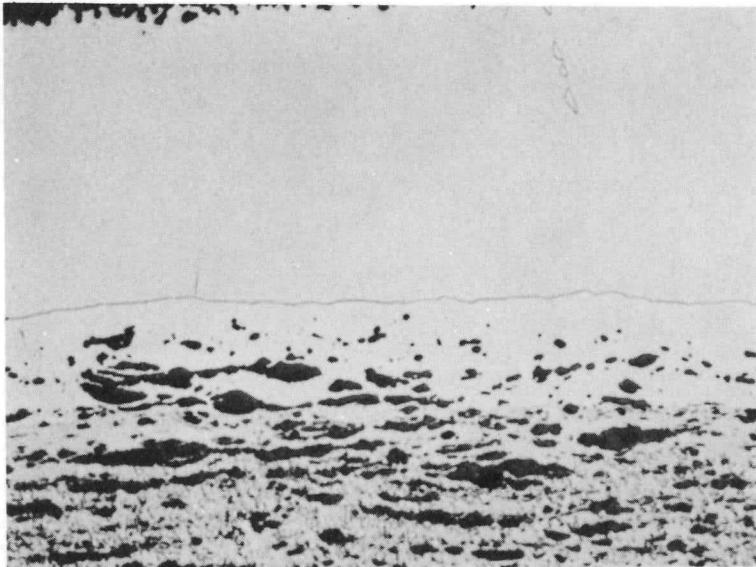
Fig. 4.4 – Cross section through fuel stock – aluminum deoxidized and cycled 100 hours between 2250°F and 500°F

tion. The structure was isomorphous with $NbFe_2$ producing a powder diffraction pattern closely related to the high-temperature form of $TaCr_2$, $TiFe_2$, or $TaFe_2$. The diffraction pattern suggested a possible composition of $Nb(75Fe - 25Cr)_2$. In as-fabricated ribbon, the thickness of the new phase was not measurable; but, after 50 hours at $2200^\circ F$, thicknesses in the order of 1.5 mils were observed.

On the one hand, with any appreciable amount of Al_2O_3 present, failure in thermal cycling almost invariably occurred. On the other hand, if the oxygen content was reduced and the second intermetallic permitted to form, failure was less frequent. However, it was not possible to fabricate a reproducible product.

4.5 CORE REACTION

Aside from poor resistance to thermal shock due to compound formation, an additional effect, not apparent metallographically, occurred when the strong deoxidizers were added. Experiments showed that, with removal of the Al_2O_3 layer, aluminum was free to diffuse into the core and react with UO_2, which produced elemental uranium. The uranium, in turn, diffused through cladding at high temperature and caused high surface activity and release of fission products.

4.6 CONCLUSION

Because of the lack of promise shown in fabricating and testing Fe-Cr-Al clad fuel elements with $Nb-UO_2$ cores, investigation of this system was discontinued in order to study other systems showing greater promise.

98

4.7 REFERENCES

1. McBride, F. E., "Fe-Cr-Al Alloy Properties Thermal Expansion and Oxidation Rate Data," GE-ANPD, XDC 59-4-113, March 20, 1959.
2. "Engineering Progress Report No. 20," GE-ANPD, APEX-20, July 1956.
3. "Engineering Progress Report No. 21," GE-ANPD, APEX-21, October 1956.
4. "Engineering Progress Report No. 24," GE-ANPD, APEX-24, July 1957.
5. "Engineering Progress Report No. 22," GE-ANPD, APEX-22, January 1957.

5. Fe-Cr-Y CLAD FUEL ELEMENTS WITH Cr-Ti-UO$_2$ CORES

During December 1957 an oxidation-resistant alloy of 69Fe - 30Cr - 1Y gave indications of meeting the current GE-ANPD requirements for a fuel element service life of 100 hours at a temperature of 2100°F. A core material having good strength and compatibility with uranium dioxide fuel also became available. This was an alloy of chromium with 1 weight percent titanium.

A major program was undertaken in early 1958 to develop methods of producing the proposed Fe-Cr-Y with Cr-Ti-UO$_2$ fuel ribbon in quantity and high quality, to make fuel cartridges, and to test the resultant material and fabricated elements for 100 hours at 2100°F.

With the change in requirement to 1000 hours at 2300°F, it was found that the then-accepted composition of the Fe-Cr-Y cladding alloy was not capable of protecting the fuel element under these conditions. An alloy development program was conducted which resulted in the achievement of oxidation resistant cladding. Modifications of the Fe-Cr-Y alloy were capable of withstanding 1000 hours at 2300°F. Stronger chromium alloys were also available for selection as core matrix material.

5.1 CLAD ALLOY DEVELOPMENT - Fe-Cr-Y

Fe-Cr-Y cladding alloy had a nominal composition of 69Fe - 30Cr - 1Y. The alloy was essentially a Type 446 stainless steel with 1 weight percent yttrium added. The yttrium addition improved oxidation resistance and maintained a fine, grain-size crystal structure in the metal when heated above 2400°F. Coarse grains developed in Type 446 stainless steel near 1650°F.

The 69Fe - 30Cr - 1Y alloy was frequently referred to by one or more code identifications. Usual designations were:

1. MR-100 alloy.
2. Iron-Chromium-Radex alloy.
3. Iron-Chromium-M55 alloy.
4. M-55 alloy.
5. B50Y (after G-E specification B50YA1-S1).

Modifications of the clad alloy from the nominal composition were investigated. These modifications are discussed in section 5.5.1.

Processing of Fe-Cr-Y presented three major problem areas. First, yttrium recovery was generally erratic in melting, second, cleanliness or freedom from oxide inclusions was necessary and, third, initial hot working of the ingot required trial and error effort to bring the process under control.

5.1.1 MELTING

Melting in the processing of Fe-Cr-Y was sometimes believed to contribute to oxidation resistance through deoxidation practice using yttrium salting, but the product was unreliable from the cleanliness viewpoint. For most applications, the salted product would be satisfactory, but fuel element processing procedures resulted in blisters developing in association with dirt stringers as shown in Figure 5.1. A superior carbon-carbon deoxidation practice was developed that permitted especially clean alloys to be melted.

BLISTER DEFINITELY ASSOCIATED WITH LIGHT STRINGERS OF OXIDE INCLUSIONS

Note: Cladding was made primarily with yttrium salting melting procedure
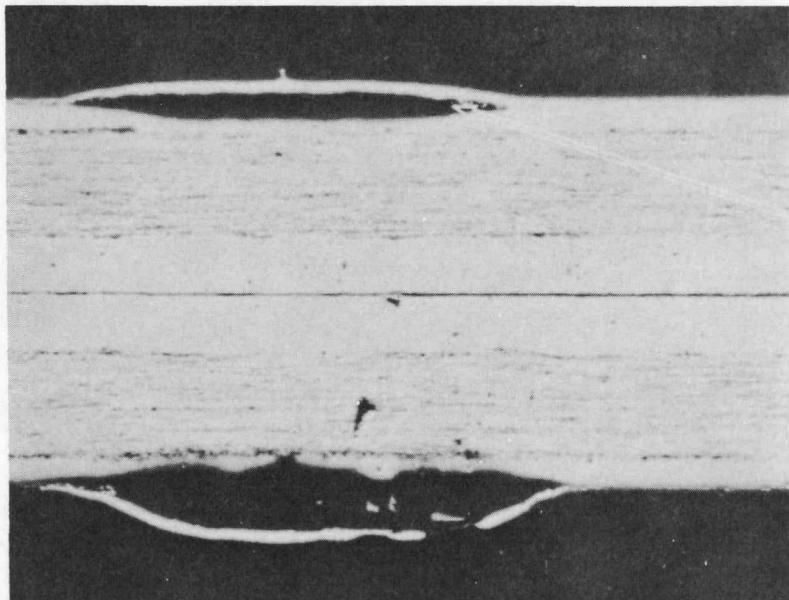
(Neg. 10968)   SN 3969   Unetched, 50 X

Fig. 5.1 — Blisters in Fe-Cr-Y cladding over Cr-Ti-UO$_2$ core

Highly purified starting materials were desired for fuel element purposes, and a number of chromium sources were surveyed. Large heats were made with:

1. Lunex Corporation - magnesium-purified chromium.
2. Electrolytic flake chromium.
3. Purified Grade A flake chromium.
4. Low carbon ferrochromium.
5. Vacuum grade chromium metal.

No significant influence on oxidation resistance was observed. Each chromium source yielded clean melts with carbon deoxidation practice. Low carbon ferrochromium and vacuum grade chromium metal introduced slight traces of other elements.

5.1.1.1 Yttrium Salting Deoxidation

Yttrium salting in melting consisted of melting the iron and chromium while slowly adding yttrium as the reaction stopped. All operations were completed in good vacuum, of less than 5 microns.[1] Good 2300°F oxidation resistance obtained with heat A-3-2 (Table 5.1) apparently stimulated the strong preference. However, comparison was based on a 34 percent chromium heat against 30 percent chromium steels. Among 30

TABLE 5.1

PROCESSING DATA ON VARIOUS Fe-Cr-Y ALLOY CLADDING HEATS

Vendor	Heat Designation	Weight Melted, lb	Type Of Cr	Type Of Iron	Ames Yttrium Added, %	Deoxidant Added, %	Holding Time,[a] minutes	Pressure, microns	Pouring Temperature,[b] °F	Ingot Size, in.	Number Of Ingots	Mold Material	Hot Top	Mold Preheat	Total Time Molten, minutes	Vendor	Ingot Conditioning	Hot Roll Temperature, °F	Intermediate Conditioning	Final Thickness, in.
Battelle Memorial Institute	9-6	100	Electrolytic	101A	1.7	none	3	20-200 100	± 25 2900	-	1 slab	cast iron	none	none	9	BMI	none	2000	grind belt abrased	0.060
Battelle Memorial Institute	8-4	100	Electrolytic	101A	1.7	none	14	40-25 25	2850	-	1 slab 1 ingot	cast iron	none	none	42	BMI	none	2000	grind, grit blast	0.060
Battelle Memorial Institute	B-11	100	LUNEX	101A	1.4	none	22	7-10 9	± 50 2900	-	2 ingots	cast iron	none	none	94	BMI	none	2000	grit blast	0.040
Battelle Memorial Institute	8-10	100	Electrolytic	101A	1.5	none	11	65-5200 5200	± 60 2900	-	1 slab 2 ingots	cast iron	none	none	20	BMI	none	2000	grind, grit blast	0.060
GE-MPD	UO$_{54}$	1000	Grade A	101A	1.3	0.025C	105	10	2860	6 x 6 tapered	4 ingots	cast iron	asbestos	warm	208	2 GE-ANPD 2 Allvac Corporation	-	-	-	-
GE-MPD	UO$_{53}$	1000	LUNEX	101A	-	none	51	< -1	2900	6 x 6 tapered	4 ingots	cast iron	asbestos	warm	211	BMI	none	2000	grit blast	0.060
Allvac Corporation	847	600	Low Carbon Ferrochrome	Electrolytic	-	0.05C	10	< 2	2950	6 x 6	3 ingots	cast iron	pouring dish	warm	45	Allvac Corporation	ground	2200	grind, hand spot	0.060
Allvac Corporation	846	600	Low Carbon Ferrochrome	Electrolytic	-	0.05C	23	< 2	3000	6 x 6	3 ingots	cast iron	pouring dish	warm	85	Allvac Corporation	ground	2200	grind, hand spot	0.060
Allvac Corporation	843	600	Vacuum grade	Electrolytic	1.5	0.3C	35	5	2850	6 x 6	3 ingots	cast iron	yes	none	185	Allvac Corporation	none	2200	ground	0.057
Allvac Corporation	NC-4	500	-	-	-	-	-	-	-	6 x 6	3 ingots	cast iron	-	-	-	-	-	-	-	0.060
GE-ANPD	FCR-34	12	Grade A-Flake	101A	1.3	0.5A1	1	20-50	150°F above melt	2 x 4	1 ingot	graphite	no	none	31	GE-ANPD	none	2200	grind	0.060
GE-ANPD	FCR-46	12	Grade A-Flake	101A	1.3	none	1	20-50	150°F above melt	2 x 4	1 ingot	graphite	no	none	31	GE-ANPD	none	-	grind	0.060
GE-ANPD	A-3-4	40	LUNEX	101A	1.3	none	3	< 20	150°F above melt	4 x 4 tapered	1 ingot	cast iron	JM 3000	none	33	GE-ANPD	machined	2200	machine and grind	0.056
GE-ANPD	A-3-3	40	LUNEX	101A	1.3	none	3	< 20	150°F above melt	4 x 4 tapered	1 ingot	cast iron	JM 3000	none	33	GE-ANPD	machined	2200	machine and grind	0.056
GE-ANPD	A-3-2	40	LUNEX	101A	1.3	none	3	< 20	150°F above melt	4 x 4 tapered	1 ingot	cast iron	JM 3000	none	43	GE-ANPD	machined	2200	machine and grind	0.056

[a] After yttrium addition.
[b] In all cases, vacuum induction melting in MgO crucibles was employe

TABLE 5.2

MR-100 ALLOY COMMERCIALLY MELTED

Heat	Weight Melted, lb	Vendor	Analysis, wt %			Disposition
			C	Y	Cr	
U-053	1,000	GE-MPD	0.024	0.74	29.86	Cladding
310726	1,000	Allvac[a]	-	0.21	-	Scrapped
310889	600	Allvac	-	-	-	Re-melt 687 and 689
NC No. 1	500	Allvac	-	0.87	29.00	Cladding
NC No. 3	500	Allvac	-	0.39	-	Experimental processing
NC No. 2	500	Allvac	0.027	0.57	29.14	Cladding
NC No. 4	500	Allvac	0.011	0.75	29.80	Cladding
687	200	Allvac	0.031	1.06	-	Tubing (TC sheathing
688	600	Allvac	0.016	1.07	-	Cladding
689	400	Allvac	0.016	1.53	-	Scrapped
U-054	1,000	GE-MPD	0.019	0.97	29.38	Cladding
847	600	Allvac	0.030	0.94	29.81	Cladding
846	600	Allvac	0.021	1.10	29.03	Cladding
843	600	Allvac	0.021	1.12	29.06	Cladding
844	600	Allvac	-	0.26	-	Scrapped - low Y
845	600	Allvac	-	0.28	-	Scrapped - low Y

[a]Allvac Metals Company.

percent chromium steels, Heat U-053 (Table 5.2) made with the same chromium and the same melting practice appeared to be above average for 30 percent chromium alloys. However, the good heat, A-3-2, carried a carbon content of 0.081 weight percent which was not acceptable.

5.1.1.2 Carbon Deoxidation

Carbon deoxidation of vacuum-melted Fe-Cr-Y alloy was developed as a necessity and as a practical procedure applicable to available commercial equipment. Contributing factors which necessitated the procedure included: (1) yttrium deoxidation left undesirable yttrium oxide inclusions in the melt; (2) aluminum deoxidation proved erratic and melted with high aluminum residuals yielding an alloy that could not be readily brazed; (3) hydrogen deoxidation was available in only one facility, Metallurgical Products Department (MPD), General Electric Company, Detroit. Hydrogen deoxidation had never been used on commercial melts.

Calculations indicated that desired carbon values could be approximated by adding a slight excess of carbon to the melt and subsequently lowering carbon by either a crucible reaction or added metallic oxides. In contrast to the opinion that carbon deoxidation would foam in a good vacuum and that the metal would overflow the crucible, a carbon boil was never observed to be violent. In fact, less reaction was observed than with yttrium additions.

All commercial-plant-melted heats of Fe-Cr-Y (MR-100 alloy) are listed in Table 5.2. Processing details for most of the heats are given in Table 5.1, and chemistry in Table 5.3.

TABLE 5.3

CHEMISTRY OF VARIOUS Fe-Cr-Y CLAD ALLOY CLADDING HEATS

												Chemical Analysis, wt %										
														Values Determined Spectrographically								
Heat	Cr	Y, X-ray	Y, wet	O_2	H_2	N_2	Al	C	Si	S	P	Mn	Ni	W	Co	Ta	B	Cu	Li	Mf	Ca
9-6	30.51	-	0.95	0.0132	0.0003	0.0006	0.1	0.016	0.065	0.006	0.014	<0.1	<0.1	-[b]	<0.1	0.1	<0.002	0.05	-[b]	-[b]	-[b]
8-4	29.21	-	1.05	-	-	-	-	0.01	200[a]	0.016	<0.01	<10[a]	250[a]	<100[a]	<100[a]	<100[a]	<1[a]	<50[a]	<1[a]	<100[a]	<100[a]
8-11	33.5	-	0.71	-	-	-	0.006	0.027	0.006	-	-	<0.001	0.02	-	0.002	<0.05	<0.0005	<0.0001	-	<0.05	<0.005
8-9	29.20	-	1.04	0.0095	0.0003	0.001	0.58	0.038	<0.1	0.005	0.01	<0.1	<0.1	-[b]	<0.01	-[b]	<0.002	<0.05	-[b]	-[b]	-[b]
8-10	29.47	-	0.97	0.0069	0.0005	0.0013	0.35	0.038	<0.1	0.005	0.008	<0.1	<0.1	-[b]	<0.01	-[b]	<0.002	<0.05	-[b]	-	-
A-2	26.67	-	0.69	0.0002	0.0001	0.0008	2.85	0.03	0.02	0.003	0.005	0.1	0.1	-[b]	0.1	0.1	0.002	-	-[b]	-[b]	0.05
UO53	29.86	-	0.74	-	-	0.012	-	0.024	100[a]	0.002	0.012	10[a]	100[a]	<100[a]	<10[a]	<100[a]	<1[a]	<1[a]	<3[a]	-	-
UO54	29.39	-	0.97	0.007	0.0017	0.001	<0.1	0.019	0.01	0.005	0.005	0.001	<0.1	-[b]	<0.1	-[b]	<0.001	<0.1	-[b]	-	-
843	29.81	0.94	0.65	0.0793	0.0055	0.0035	<0.1	0.03	0.1	0.006	0.005	<0.1	<0.1	<0.1	<0.1	<0.1	<0.001	<0.1	-[b]	-[b]	-[b]
846	29.03	1.10	0.81	0.0131	0.0012	0.0009	<0.1	0.021	0.20	0.006	0.012	<0.1	<0.1	<0.15	<0.1	<0.1	<0.001	<0.1	-[b]	-[b]	-[b]
847	29.06	1.12	0.87	0.0461	0.0014	0.0040	<0.1	0.021	0.19	0.006	0.010	<0.1	<0.1	<0.15	<0.1	<0.1	<0.001	<0.1	-[b]	-[b]	-[b]
NC-4	29.80	-	0.66	0.008	0.0005	0.0008	<0.1	0.011	0.25	0.002	0.006	<0.1	<0.1	-[b]	<0.01	<0.1	<0.002	<0.05	-[b]	-[b]	-[b]
FCR-34	28.4	-	1.04	-	-	-	-	0.027	0.005	0.029	-	-	-	-	-	-	-	-	-	-	-
FCR-46	34.2	-	0.95	-	-	-	-	-	-	-	-	-	-	-	-	-	-	-	-	-	-
A-3-2	33.96	0.83	0.66	0.0039	0.0001	0.0009	0.002	0.081	0.005	0.004	0.004	0.001	0.02	0.003	0.001	0.012	<0.001	0.003	<0.0002	<0.005	0.005
A-3-3	34.81	0.94	0.70	0.0023	0.0003	0.0003	0.001	0.025	0.0005	0.002	0.004	0.001	0.02	0.0005	0.001	0.014	<0.001	0.002	<0.0002	<0.005	0.005
A-3-4	29.14	0.70	0.09	0.006	0.0006	0.0006	0.006	0.025	<0.01	0.004	-[b]	0.003	0.04	0.2	0.006	<0.05	<0.0005	0.0006	-[b]	<0.05	<0.0005

[a] Parts per million.
[b] No data.

103

Heat U-053 was the first large heat made. Chromium powder, which contained a magnesium residual, was furnished by Lunex Corporation and was briquetted for the heat. Only 1 weight percent yttrium was added to the melt with 0.75 weight percent Y recovered. Also, the holding time of 211 minutes for the molten metal was unique. The ingots were processed by Battelle Memorial Institute with fair recovery of material. Allvac Metals Company melted Heat 310726. Upon yttrium addition, 310726 boiled strongly, and was subsequently rejected when large cracks showed on hot-roll breakdown of the ingot. Two steps were taken immediately to remedy the lack of melting control. First, Battelle was requested to produce cladding for GE-ANPD. Results are given in Table 5.4. Second, GE-ANPD initiated laboratory development of carbon deoxidation. Twenty-two laboratory heats were produced with values developed as given in Table 5.5. Heat E-4 in this Table was a remelt trial in preparation for 310889 noted in Table 5.2.

TABLE 5.4

BATTELLE-PRODUCED Fe-Cr-Y HEATS. MR-100 ALLOY

Heat[a]	Analysis, wt %				End Use	Remarks
	C	Y	Cr	Al		
8-1A	0.008	0.10	30.01	0.10	Re-melt as 8-9	$CrO-Al_2O_3$ slag LUNEX Cr
8-2	0.012	0.40	30.12	0.10	Re-melt as 8-9	As above
8-3	–	0.05	–	–	Re-melt as 8-9	As above
8-4-A	0.010	1.10	29.12	0.10	Cladding at GE-ANPD	Electrolytic Cr poor quality
8-5	0.014	0.05	29.75	–	Scrapped	No Y
8-6	0.044	0.02	31.03	–	Re-melt	High C and no Y
8-7	0.049	1.12	29.47	0.53	Some used	High C and Al
8-8	0.038	1.04	29.20	0.58	Scrap	Poor quality
8-9	0.049	1.01	28.99	0.58	Some used	High C and Al poor quality
8-10-B	0.033	1.03	29.47	0.35	Some used	Poor quality
9-4	0.027	1.20	31.78	0.10	Some used	Poor quality
9-5	0.016	1.12	31.28	0.10	Some used	Poor quality
9-6	0.011	1.00	30.23	0.12	Cladding	Good heat
9-7	–	1.08	–	–	Scrapped	Poor quality

[a]All heats 100 pounds nominal.

The laboratory melt program detailed in Table 5.5 established the following:

1. Carbon deoxidation was effective.
2. Impure high oxygen chromiums could be readily deoxidized.
3. With 0.025C to 0.050C, as in Heats E-16 and E-10, 100 percent Y recovery was effected.
4. Low carbon residuals, 0.010 to 0.016 percent, could be directly achieved, as in Heats E-19 and E-21.
5. Overcarburized melts could be oxide-decarburized to the desired carbon as in Heats E-23 and E-24. This is an added control.
6. A very low carbon, 0.0047 weight percent C, could be precalculated as in Heat E-24.

A crucible reaction, MgO plus C yields CO plus vaporized Mg, could be expected to reduce carbon in a vacuum furnace. Heat E-16, Table 5.5, demonstrated the crucible reaction. With 0.04 weight percent carbon added to the melt, the observations, listed in Table 5.6, were made at 566 microns tank pressure.

TABLE 5.5

GE-ANPD MELTS

| Heat[a] | Analysis, wt % | | | Ingot Mold | Remarks |
	C	Y	O		
1	0.022	-	0.104	Iron	Fe wash melt only
2	0.044	-	0.083	Iron	Fe wash melt only
	0.038	-	0.081	Graphite	-
E-1	0.027	-	0.022	Iron	High purity Grade A Cr and Fe only (no Y)
	0.033	-	0.021	Graphite	-
E-2	0.027	0.87	0.0081	Iron	As above, but 18 grams C per 40 pound heat. This is first carbon deoxidized heat.
E-3	0.115	0.45	0.0076	Iron	As above, but 36 grams C added and 0.1Be
	0.137	0.74	0.0108	Graphite	-
E-4	0.014	0.74	0.0054	Iron	Re-melt NC No. 1 and NC No. 2 with 0.5Y added (double melt trial).
	0.014	0.68	0.0033	Graphite	-
E-5	0.030	0.77	-	Iron	Electrolytic Cr flake - held 2 hours after Y addition
E-9	0.044	1.24	0.0062	Iron	As above but 0.2C added
E-10	0.14	0.93	0.0027	Iron	High purity Grade A Cr
E-11	0.15	0.96	0.0015	Iron	Plus 36 grams C (see E-2)
E-12	0.012/0.014	0.82	0.0051	Iron	High purity Cr - 0.04C and 1Y - poor vacuum
E-13	0.030/0.034	1.00	0.0019	Iron	As above, but good vacuum
E-14	0.036	-	0.0058	Iron	As E-13, but no Y added
E-15	0.016	0.86	0.0031	Iron	High purity Cr - 0.04C + 1Y good vacuum but tank opened once
E-16	0.028	0.99	0.0032	Iron	High purity Cr - 0.04C + 1Y
E-17	0.038	1.00	0.0017	Iron	High purity Cr - 0.04C + 1Y
E-18	0.024/0.030	1.01	0.0029	Iron	High purity Cr - 0.03C + 1Y
E-19	0.010	1.01	0.0016	Iron	Electrolytic Cr flake - 0.2C + 1Y
E-21	0.016	1.01	0.0026	Iron	Electrolytic Cr flake - 0.2C + 1Y
E-22	-	1.01	0.0016	Iron	Repeat E-21
E-23	-	0.93	0.0037	Iron	-
	0.027	-	-	Iron	Dip sample - 0.2C added
	0.013	-	-	Iron	Dip sample - after FeO addition[b]
E-24	0.0047	0.91	0.0045	Iron	Dip sample - 0.2C added and FeO (analytical grade) added

[a]All heats experimental, 40 pounds.
[b]FeO made by oxidizing sheet iron.

TABLE 5.6

CRUCIBLE REACTION FOR CARBON REDUCTION

Dip Sample	C, wt %	O_2, wt %	Remarks
1	0.042	0.0032	Melted, C added
2	0.038	0.0042	Hold 17 minutes
3	0.040/0.034	0.0085	Hold 12 more minutes
4	0.028/0.030	0.0072	Hold 12 more minutes, pour

Heats E-17 and E-18 confirmed E-16 results, but led to E-23 and E-24 as more positive approaches to carbon control. Subsequently, most of the melts shown on Table 5.2 were produced with fairly high yields.

5.1.1.3 Hydrogen Deoxidation

The problem of diffusion voids in Fe-Cr-Y clad Cr-Ti-UO$_2$ core fuel ribbon was associated with oxidation of carbon. Subsequently, Heats E-23 and E-24, described in the preceding section, were attempted with the objective of achieving very low carbon.

Hydrogen deoxidation of Fe-Cr-Y prior to the yttrium addition to the melt would be a preferred procedure. The General Electric Research Laboratory has hydrogen equipment in a laboratory melting unit, and a full installation is available at the GE-MPD at Detroit.

Two laboratory heats were completed at the General Electric Research Laboratory after first melting an electrolytic iron wash in a new MgO crucible. Details are shown in Table 5.7.

TABLE 5.7

HYDROGEN DEOXIDATION

Element	Desired Nominal	Heat 437-30[a]		Heat 438-30[a]	
		Added	Chemical Analysis	Added	Chemical Analysis
Fe	69.0	69.0	-	69.0	-
Cr	30.0	31.0	-	30.0	-
Y	1.0	1.2	0.9	1.2	0.9
O	0.004 max	-	0.0002	-	0.001
N	0.0004	-	0.0005	-	0.0004
H	0.0000	-	0.12 ppm[b]	-	0.24 ppm[b]
C	0.002 max	-	0.003	-	0.006

[a]Heat 437-30 was a straight hydrogen deoxidized melt whereas 438-30 was a combined carbon-hydrogen melt. From the cleanliness viewpoint, the hydrogen-processed heats were exceptional. However, oxidation resistance was never determined.

[b]1 ppm = 0.0001 percent.

5.1.2 STRIP PROCESSING

The small melts listed in Table 5.5 were used to gain some knowledge of the proper fabricating factors for strip production. Conclusions were verified in observations on Allvac processed heats identified in Table 5.1.

Basically, ingot reduction by hot-rolling should be at 2200°F on an unground or machined surface. It was established beyond any doubt that grinding of the ingot initiated grinding cracks which opened up in hot working. Preferred procedure was to hot roll 5-inch square ingots to 1-1/4 inches by 5-1/2-inch-wide bar. Bars were cut to short lengths and 1/8 inch was ground from each surface. The grinding was the first conditioning. Bars were hot rolled to about 0.100-inch-thick strip and grit blasted. The 0.100-inch-thick strip was belt sanded on both sides and cold rolled to finish gauge, 0.035 inch to 0.065 inch.

5.1.3 EXTRUSION PROCESSING

Early in the Fe-Cr-Y program, laboratory processing trials had shown 30 weight percent Cr content Fe-Cr-Y to be more easily processed than 35 weight percent Cr.[2]

Work in 1960 showed, however, that 35 weight percent Cr plus 1.50 weight percent Y alloys could be melted in vacuum using MgO or ZrO_2 crucibles and extruded from 3-11/16-inch-diameter machined billets to 3/4-inch-diameter rod. A low melting glass lubricant was used at 1800°F heating temperature on the 24-to-1 area-reduction extrusions. The extrusion pressure normally fell between 400 and 600 tons.

5.2 FABRICATION PROCESS

The fissile material utilized was uranium dioxide. In use, the UO_2 was fired at 2300°F in dry hydrogen to reduce it to stoichiometric proportions, i.e., $UO_{2.0}$ and not UO_{2+}. The dioxide was stable with respect to reacting with the Fe, Cr, Ti, and Y content of the Fe-Cr-Y with Cr-Ti-UO_2 fuel element.

Although UO_2 was an accepted high-temperature fissile fuel source, several other uranium compounds were also investigated. Battelle Memorial Institute calculated the free energy and oxygen equilibrium of UO_2, Cr_2O_3, and TiO.[3] Results established that UO_2 would be stable in chromium and in the presence of titanium, and that oxygen solubility in chromium decreased from 0.008 weight percent O_2 at 2200°F to 0.0017 weight percent O_2 at 2600°F. The addition of 1 to 2 weight percent Ti to the chromium, as in the Cr-Ti-UO_2 fuel element matrix, was favorable. It was concluded that 1 weight percent Ti could probably be tolerated whereas 5 weight percent Ti might reduce excess UO_2. Among fuel proposals were substitution of UN or UC for UO_2 since both the nitride and carbide have higher density and better thermal conductivity than UO_2.

Battelle reported that the first attempts to utilize UN with chromium and Fe-Cr-Y clad were unsuccessful.[5] Results of a trial with UN in chromium-titanium matrix disclosed good fabricability and properties in the finished sheet. Stability, as evaluated metallographically, appeared satisfactory.[5] The uranium carbide was not evaluated for stability in a chromium matrix.

Several high-melting-point sulfides of uranium are known. Hydrogen and hydrogen sulphide were passed over hot uranium metal powder, and the product fired in hydrogen at 2900°F. Uranium sulphide melts at 3600°F, U_2S_3 melts at slightly lower temperatures, and US_2 melts at 2900°F. Both U_2S_3 and US_2 were believed present in various lots of the sulphide. After 16 hours at 2300°F with Fe - Cr - 5Al - Y cladding, the core did not show reaction, but some diffusion of uranium to the surface was noted.[6]

5.3 FUEL ALLOY - Cr-Ti-UO$_2$

The initial major problems in fuel ribbon fabrication were core-edge cracking during hot rolling and the inability to fabricate ribbon containing over 25 weight percent UO$_2$. Five different chromium powders,[7] with compositions as given in Table 5. 8, were used in fabrication of cores but did not show any marked difference with respect to core-edge cracking. Hot pressing temperatures for fuel billet assembly, hot-rolling conditions (temperature, percent reductions, and roll speed), and wide side frames were critical and ultimately permitted satisfactory core-edge quality in fuel ribbon with up to 3-inch core widths.[8,9]

TABLE 5.8

ANALYSIS OF CHROMIUM POWDERS

| | | Impurities, parts per million | | | | |
| | | \multicolumn{2}{c}{O$_2$} | \multicolumn{2}{c}{N$_2$} | H$_2$ | C | S | Mg | Li |
Name	Source	Vacuum Fusion	HCl Insoluble	Vacuum Fusion	Kjerdahl					
Horizons	Horizons, Inc.	482	860	29	120	20	60	180	50	1
Lx4	Lunex Corp.	1960	480	50	30	2	150	210	100	5000
Lx5	Lunex Corp.	710	400	30	30	50	130	190	50	2500
Strontium	AMR Subsection	720	1300	87	33	14	270	100	10	1
Electrolytic	Electromet	5720	-	49	-	120	550	520	-	-

Production of ribbon of between 0. 025-inch and 0. 040-inch thicknesses resulted in core-edge thicking (dog-boning) during rolling with a resultant excessive thinning of the clad over the core-edge area. Figure 5. 2 shows a cross section with thinned cladding, and Figure 5. 3 illustrates a full cladding rupture.[10] This dog-boning was irregular along the core edge resulting in undulation of the clad thickness. Tapering, undercutting, or the introduction of a concavity in the core edge improved this condition.

The main points in the fabrication of the fuel elements are briefly discussed in the following sections.

5. 3. 1 FUEL RIBBON

5. 3. 1. 1 Frame Preparation

The following powdered metals were sieved to the indicated mesh prior to pressing into frames:

chromium	- 140 mesh
iron	- 200 mesh
yttrium hydride	- 325 mesh

The blended powders were pressed into 8000-gram batches of 69Fe - 30Cr - 1Y for 4 hours in a jar mill. The frame was then fabricated by pressing at 22. 7 tons per square inch in a cold-die cavity. The frame was sintered in a H$_2$ atmosphere (dewpoint -25°F, or less) at 2300°F for 2 hours and cleaned with a Cratex* wheel.

5. 3. 1. 2 Core Preparation

The as-received Cr powder was annealed for 3 hours at 1800°F in a H$_2$ atmosphere, ball milled for 1 hour, and sieved to obtain a -140 mesh. This powder was then blended

*Cratex Manufacturing Company, Burlingame, California
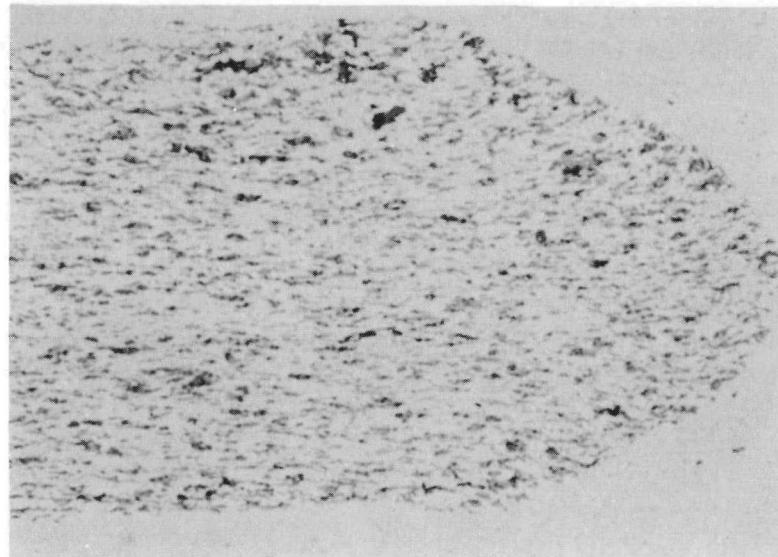
(Neg. 15407) Billet – 41-217-01 Unetched, 75 X

Fig. 5.2 – Cladding thinning caused by core edge thickening in rolling
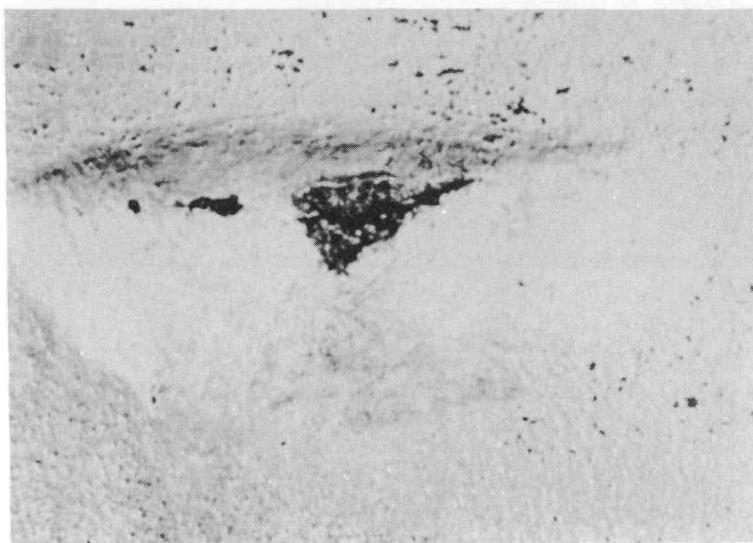
BLISTERS OCCURRED IN AREAS
— WITH LESS THAN 0.001-INCH
CLADDING OVER CORE EDGE

(Neg. 15390) Billet – 41-207-01 Unetched, 10 X

Fig. 5.3 – Top view of core-frame interface blister developed in 24 hours of cyclic testing – between 2100°F and 500°F

with -325 mesh titanium hydride and -325 mesh UO_2, which had been annealed for 2 hours at 2300° F in H_2. Blending time was for 2 hours. The powder was cold pressed at 36 tons per square inch and vacuum sintered by heating for 1 hour at 930° F in a vacuum chamber and then heating to 1100° F. The billet was transferred into a high-temperature furnace zone and heated from 1100° to 2000° F in 50 minutes. At this point, hydrogen was introduced at 20 cubic feet per hour, and the temperature was raised to 2550° F and held for 50 minutes. The furnace was cooled to 2000° F and evacuated for 30 minutes.

5.3.1.3 Cladding Preparation

Cladding strips were cleaned in a trichloroethylene degreaser, put in an alkaline soak, rinsed, dipped in HCl, rinsed again, and electrolytically polished in a chromic acid solution.

5.3.1.4 Fuel Billet Assembly

The frame was spot welded to the bottom cladding with the core in place. The top plate was welded into place. All edges were welded in an argon atmosphere in a dry box.

5.3.1.5 Hot-Pressing Fuel Billets

Billet surfaces were coated with an Al_2O_3 slurry, and molybdenum spacers were inserted in billet stacks. These stacks were then heated to 2200° F in an argon atmosphere (later H_2 was used) with a light load. At 2200° F, an 18,000-pound load was applied and held for 15 minutes. The billets were wire brushed after they cooled.

5.3.1.6 Hot Rolling

The billets were hot rolled at 2350° to 2400° F after a 20- to 30-minute heating period. The first pass reduced the billet by 40 percent. The billet was re-heated for 10 minutes and reduced 38 percent on the second roll pass. Again, the material was re-heated for 10 minutes, reduced 34 percent on the third roll pass, re-heated for 10 minutes, and reduced from 29 to 11 percent for the final hot roll thickness of 0.042 inch.

5.3.1.7 Warm Rolling

Stock, 0.042 inch thick, was warm rolled by heating to 1900° F and reduced 25 percent on the first roll pass to 0.032 inch; re-heated and reduced by no more than 28 percent to finish gauge. If more than a 28-percent reduction was required, an additional re-heat was used to obtain final gauge.

5.3.1.8 X-Ray Inspection

An X-ray inspection was used to examine density variations, cracked edges, and lengthwise camber.

5.3.1.9 Final Conditioning

The final preparation procedures for fabricating fuel ribbon included a degreasing in trichloroethylene, an alkaline soak, an HCl acid dip, and an electrolytic polish in a chromic acid solution.

5.3.2 RING FABRICATION

5.3.2.1 Trimming

A cleaned fuel ribbon, after X-raying, was laid out next to the X-ray film, and good segments marked off.[11] Each segment would yield a fuel ring. Marks were established that permitted trimming the excess side material away without penetrating to the cores. Sides of the fuel ribbon, as rolled, corresponded to leading or trailing edges of the finished ring.

Marked segments were sheared an extra inch in length. With the use of the marks, a dead edge trimming was completed so that a dead edge of 0.040 inch to 0.060 inch was on each segment. A cut-off machine trimmed 0.5 inch from each end to avoid any shearing cracks.

5.3.2.2 End Sealing

Welded End Seals

Clean segments were mounted in plastic protection laminate, and the ends polished to expose the metal. A combination electrolytic etch and nitric acid leach, repeated a number of times, was used to recess the core at the ends of the segment.[12] The plastic prevented heavy cladding attack in the process. The plastic was warmed in water and removed.

The cleaned and dried segment with a recessed core at each end received an Fe-Cr-Y alloy insert in each recess, and the insert was filed flush with the segment end. A heliarc weld was used to seal the insert and cladding at each end.

A three-stage Burner Rig specimen fabricated by segment end welding completed 100 hours of testing at 2000^OF.[8] The first MTR reactor test cartridge, GE-ANPD 1U1, was completed on May 22, 1958. Although the Burner Rig test was quite successful, post-irradiation examination of the MTR cartridge disclosed that a blistering or swelling had developed in association with each end seal, Figure 5.4. Close examination also showed some oxidation of UO_2 to U_3O_8 beneath the welded-in insert piece.

End-seal weld technique was improved[13] with the resulting structure shown in Figures 5.5 and 5.6. A six-stage MTR cartridge completed 100 hours at 2070^OF and failed in 2.25 additional hours at approximately 100^OF higher.[10] Post examination[14] did not reveal any identified end-seal failures.

NOTE: SIMILAR BLISTERING WAS NOT OBSERVED DURING BURNER RIG TESTING. GASEOUS FISSION PRODUCTS MAY HAVE COLLECTED IN THE FREE SPACES, ALTHOUGH OXIDATION PRODUCTS MAY HAVE CAUSED THE BLISTER.
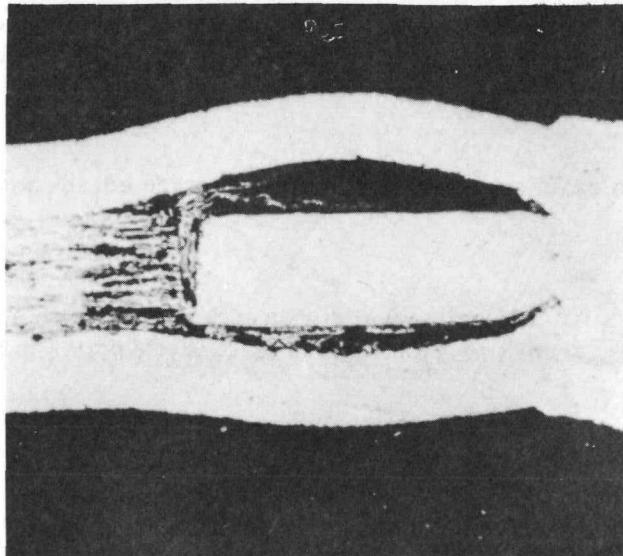
(Neg. R-381) Unetched, 60 X

Fig. 5.4 — End seal blister from weld-sealed segment end

112
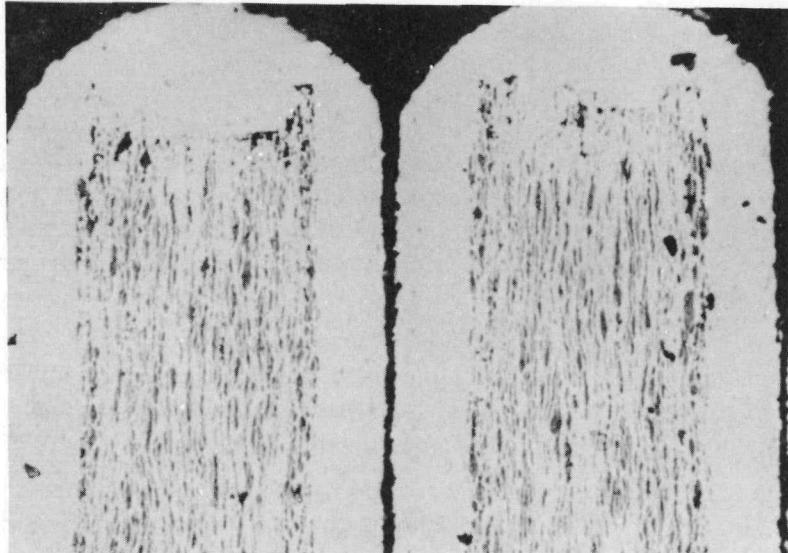
Unetched, 75 X

Fig. 5.5 — Segment end welds thin or lacking in coverage as deter-
mined by X-ray examination. Area has sustained 109.5
hours at 2000°F
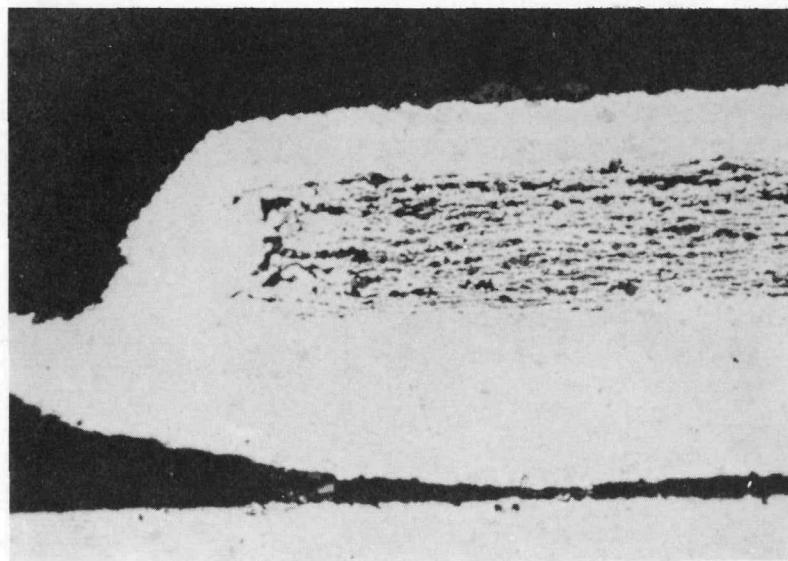
Unetched, 75 X

Fig. 5.6 — A joint plate and edge seal area as in GE-ANPD 1A2
after 100.7 hours 2100° per 500°F cyclic testing

Brazed End Seals

Brazed end seals and joint plates were utilized in construction of GE-ANPD 1Z1, adapting GE-76, 43Pd - 34Ni - 23Cr braze for the work.[15] Post-irradiation of an MTR cartridge containing brazed end seals revealed cracks developed in the braze and indicated that braze alloy penetration was excessive.[16]

5.3.3 Fuel Element Fabrication

Segments containing the welded end seal were heated to a range of 1800° to 1900^oF and roll-formed to a circle. The open ring was completed by tack-welding a joint plate into position. GE-76 braze was put into place and brazed at 2340^oF in hydrogen (-40^oF dewpoint).

Rings and comb hardware were assembled by resistance welding. GE-76 braze alloy (0.010-inch diameter) was tack welded in place and the entire assembly brazed. The use of wire braze permitted control of the amount of braze and minimized the braze attack problem.

5.4 DISPERSION HARDENING

A significant advance in fuel ribbon and elevated-temperature structural materials resulting from the Fe-Cr-Y with Cr-Ti-UO_2 fuel element program was the exploration of dispersion hardening. Following the discontinuance of the major effort, the achievement of reliable 2300^oF-oxidation resistance by Fe-Cr-Y composition modification was an important development. Although this was a specific achievement, the dispersion hardening activity is applicable to many situations of general interest.

The basic procedure in dispersion hardening was to introduce finely dispersed oxides throughout a structural metal in order to provide elevated temperature strength. The oxide dispersion was achieved by blending metal powders with oxide particles and processing to a structural material.

5.4.1 DISPERSION-HARDENED STRUCTURAL MATERIALS

Prior to the Fe-Cr-Y with Cr-Ti-UO_2 fuel element program, GE-ANPD had utilized cladding alloys specified for fuel ribbon as material for combs and ribs in the concentric ring design. The initial approach in the Fe-Cr-Y with Cr-Ti-UO_2 effort was to apply the Fe-Cr-Y alloy to the comb and rib components of the fuel cartridge. However, trouble developed because of weakness of the Fe-Cr-Y as a structural material at elevated temperatures.

Based on the fact that the Cr - Ti - 42 weight percent UO_2 cored fuel ribbon was much stronger than the Fe-Cr-Y cladding, the materials relationships thus defined were adapted to the structural material problem. Thus, ribbon was produced with Cr plus 1.5 weight percent Y powders plus 15 weight percent Y_2O_3 in the core and Fe-Cr-Y cladding. Weight percent of 1.5Y added to the core matrix chromium provided required oxidation resistance whereas Cr plus 1 weight percent Ti in the fuel ribbon proper had poor oxidation resistance.[64]

Only 5.9 percent elongation was noted in 500 hours at 2100^oF with 1000-psi load on the dispersion-hardened ribbon.[17] Actual comb-rib operating temperature in a fuel cartridge operating at 2100^oF-fuel-ribbon temperature has been estimated at 1700^oF. Resistance to oxidation at 1700^oF after 100 hours exposure is shown for the dispersion-hardened ribbon in Figure 5.7. No cartridge failures were attributed to comb weakness after introduction of the dispersion-hardened structural material.
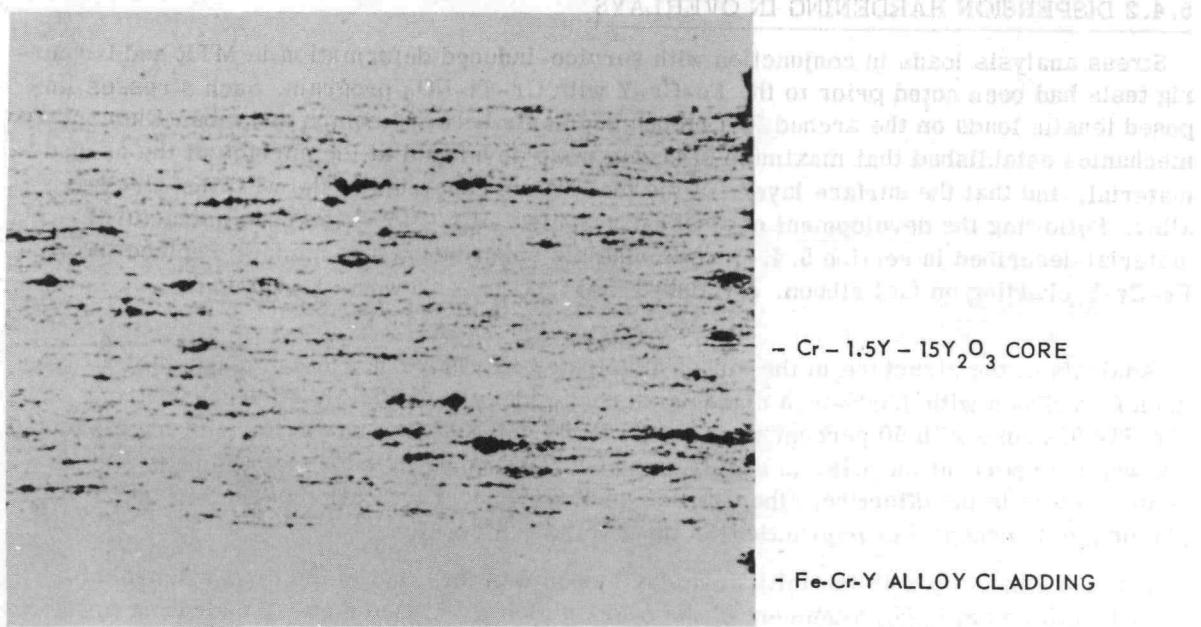
(Neg. 14438)   Unetched, 125 X

Fig. 5.7 — Oxide-dispersion strengthened structural material developed
for combs and ribs after 100 hours of testing at 1700°F.
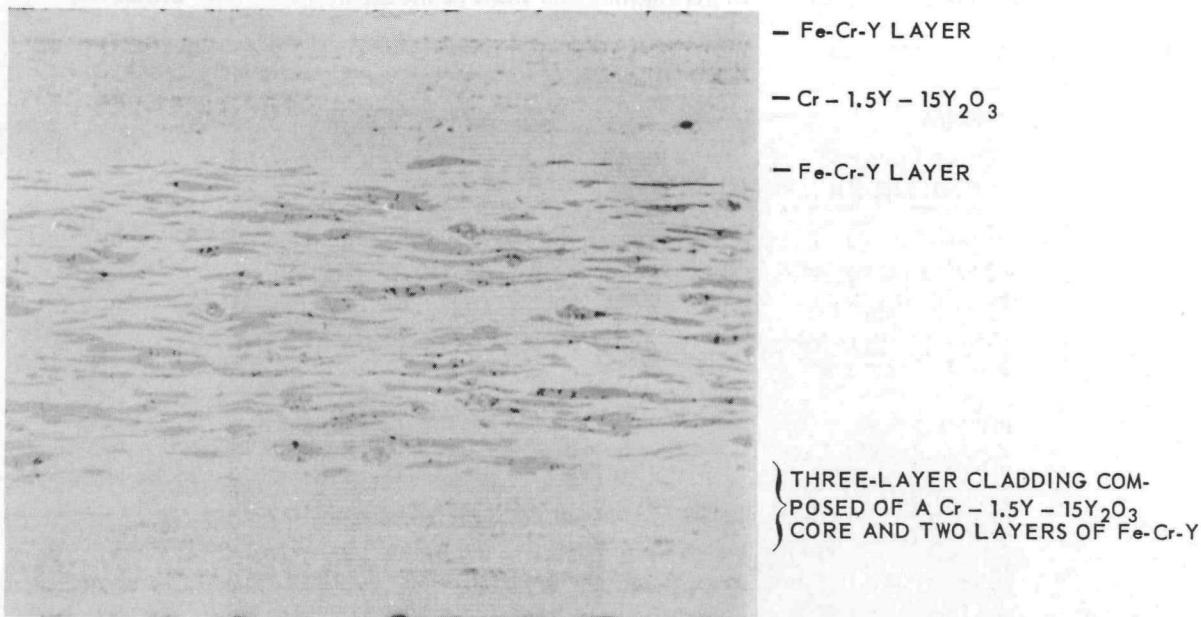
(Neg. 12813)   Unetched, 100 X

Fig. 5.8 — Dispersion-hardened structural material used as cladding
over $Cr - 1Ti - 42UO_2$ fueled core.

5.4.2 DISPERSION HARDENING IN OVERLAYS

Stress analysis loads in conjunction with service-induced deformation in MTR and burner-rig tests had been noted prior to the Fe-Cr-Y with Cr-Ti-UO_2 program. Such stresses imposed tensile loads on the arched fuel ribbon segments between combs and ribs. Elementary mechanics established that maximum stresses were developed at the surface of the arched material, and that the surface layers of the fuel ribbon consisted of the weak Fe-Cr-Y alloy. Following the development of the Fe-Cr-Y clad - Cr - 1Y - 15 (Y_2O_3) structural material described in section 5.4.1, an immediate substitution was made to replace the Fe-Cr-Y cladding on fuel ribbon. A finished fuel ribbon is shown in Figure 5.8.

Analysis of the structure in the ribbon illustrated in Figure 5.8 established that 0.020-inch fuel ribbon with 0.005-inch cladding on each side was originally 50 percent strong Cr-Ti-UO_2 core with 50 percent weak Fe-Cr-Y cladding. After modifying with the clad as shown, a 60 percent increase in strong, oxide-strengthened material was gained. All this material was in the effective, fiber-stress surface zone. Fabrication of the ribbon as in the original concept was impractical in the Figure 5.8 version.

A major difficulty with the initial overlay ribbon was the need in the dispersion-clad structure for very exact alignment of the overlay with the fueled core. Fabricating problems were overcome by introducing combined overlay and fueled core production in a single powder-metallurgy pressing and sintering.[17] An unclad powder composite is shown in Figure 5.9.

An overlay-strengthened fuel ribbon processed with co-pressed core-overlay-frame is shown in Figure 5.10 after processing. Systematic investigations were completed in fabricating dispersion-strengthened fuel ribbon.[10,17] Among other variables, the type of hard, dispersed constituents introduced to strengthen the matrix metal was studied. Materials
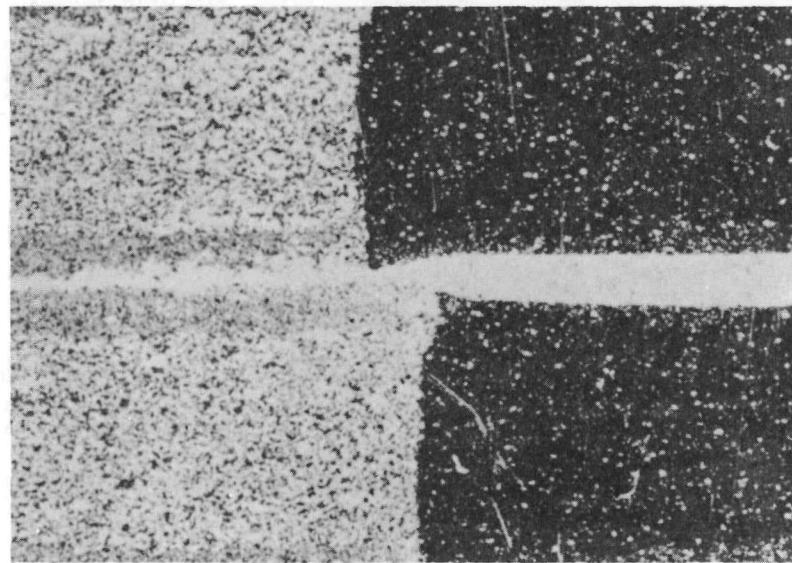
(Neg. 13708)   Unetched, 10 X

Fig. 5.9 — Overlay of Cr — 15Y_2O_3 over Cr — 1Ti — 42UO_2 core both
co-pressed and sintered with 69Fe — 1Y — 30Cr frame

Unetched, 250 X

Fig. 5.10 – Cross section through typical fuel ribbon with
Cr – 1Ti – 42UO$_2$ core; overlay or sub-cladding of
Cr – 1Y – 15Y$_2$O$_3$ adjacent core and outer cladding
of clear Fe-Cr-Y alloy
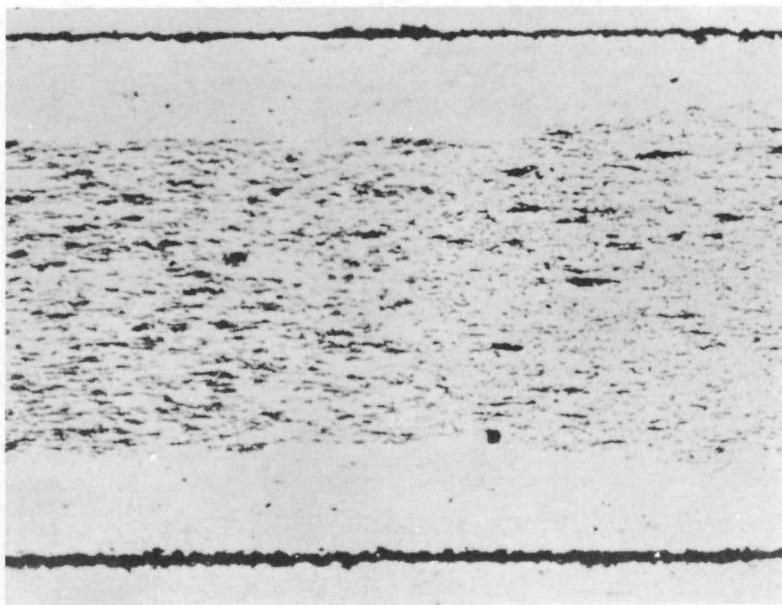
(Neg. 15203)   Ribbon 41-903-05   125 X

Fig. 5.11 – Usual 42 weight percent UO$_2$ restrained to a thinner
core carrying 62 weight percent UO$_2$ with a propor-
tionate increase of protective cladding achieved as
an overlay of Cr – 1Y – 10Y$_2$O$_3$ and Fe-Cr-Y outer
cladding

surveyed included: Cr_2O_3, TiO_2, Al_2O_3, BeO, Y_2O_3, ZrO_2, and TiC, $Cr_{27}C_3$, and TiN.[15,17,18] The carbides tended to dissolve into the chromium matrix. Each added oxide exhibited desirable characteristics, except TiO_2, which tended to partially agglomerate.

A major advance was made when the overlay concept was applied in conjunction with total oxide loads. For example, straight Fe-Cr-Y with Cr-Ti-UO_2 fuel ribbon was limited to 42 percent UO_2 in the core. More UO_2 caused the core to break up in rolling. By varying the Y_2O_3 of the overlay layer, 60 weight percent UO_2 was used satisfactorily and processed as shown for fuel ribbon 41-171-5 in Table 5.9.

Another variation was to condense the usual 42 weight percent UO_2 into a thinner core of 60 weight percent UO_2 in order to increase the effective cladding layer of overlay plus Fe-Cr-Y cladding as shown in Figure 5.11.

TABLE 5.9

FABRICABILITY WITH 60 WEIGHT PERCENT UO_2 IN CORE

Blend	UO_2 In Core, wt %	Y_2O_3 In Overlay, wt %	Fabricability In Rolling
41-171-01	60	None - Cladding Only	Poor
41-171-03	60	Cr - 1Y Overlay,[a] No oxide added	Poor
41-171-05	60	Cr - 1Y - $5Y_2O_3$	Excellent
41-171-07	60	Cr - 1Y - $10Y_2O_3$	Good
41-171-09	60	Cr - 1Y - $15Y_2O_3$	Poor
41-171-11	60	Cr - 1Y - $20Y_2O_3$	Poor

[a]Matrix metal for overlay or subcladding is chromium plus 1 weight percent yttrium metal added for oxidation resistance. Subcladding or overlay is considered part of the protective cladding of the fuel ribbon.

Another important development was obtained in dog-bone correction on fuel ribbon greater than 0.025 inch in thickness. Flow characteristics associated with corners of the strong-fueled cores caused penetration of the weak clad during hot rolling. By substituting a frame of Cr - 1Y - $10Y_2O_3$ for the softer Fe-Cr-Y frame, the dog-boned corner intrusion rather than the fueled core was changed to oxidation resistant material. The structure of the improved frame is shown in Figure 5.12.

Generally, the preceding demonstrated that dispersion of fine oxides permitted numerous advantageous fuel ribbon structures to be made. As the total oxide content of fuel ribbon increased, the strength at elevated temperatures increased.[10]

5.4.3 RETARDATION BY DISPERSED OXIDES

The use of Fe-Cr-Y alloys containing about 5 percent aluminum as the cladding over a Cr-Ti-UO_2 core would probably yield a 2500°F fuel element. Use of Fe-Cr-Al-Y alloy was limited because the aluminum would diffuse into the fuel ribbon core and reduce the UO_2 to uranium metal while the aluminum stole the oxygen to form Al_2O_3. Released uranium eventually diffused to the fuel ribbon surface, where it sometimes reformed to UO_2, but destroyed the protective characteristics of the oxides on the surface at 2300° to 2500°F. Even more detrimental, uranium on the surface fissioned with direct release of fission products into the air stream. The preceding was well known prior to the Fe-Cr-Y with Cr-Ti-UO_2 program.[19]

118
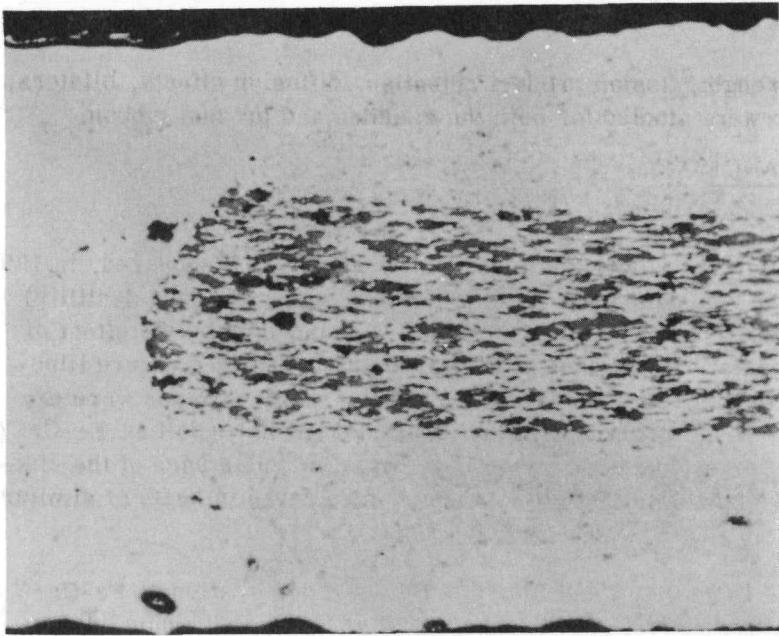
Note: Dog-boning in rolling does not
permit fueled core to intrude
into the cladding.

(Neg. 13893)   Unetched, 100 X

Fig. 5.12 — Weak Fe-Cr-Y frame material has been replaced by
$Cr - 1Y - 10Y_2O_3$

Many attempts to introduce diffusion barriers between two reacting metals in order to stop or suppress diffusion of one or more metals have been reported. The GE-ANPD effort initiated the use of reactive, dispersed oxides which would be preferentially reduced instead of UO_2. For example:

$$4Al \quad + UO_2 \quad \rightarrow 2Al_2O_3 + 3U$$
$$\text{(from Cladding) \quad (Oxide) \quad (Oxide) \quad (Metal)} \tag{1}$$
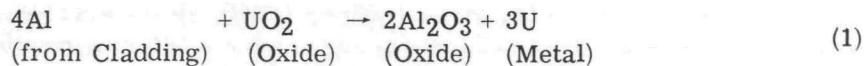
Should the U contact a reducible oxide, then:

$$3U \quad + 2Cr_2O_3 \rightarrow 3UO_2 \quad + 4Cr$$
$$\text{(Metal) \quad (Oxide) \quad (Oxide) \quad (Metal)} \tag{2}$$

or

$$4Al \quad + 2Cr_2O_3 \rightarrow 2Al_2O_3 + 4Cr$$
$$\text{(Metal) \quad (Oxide) \quad (Metal) \quad (Metal)} \tag{3}$$
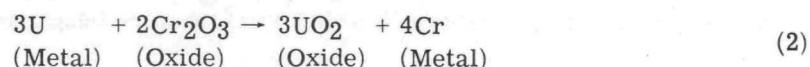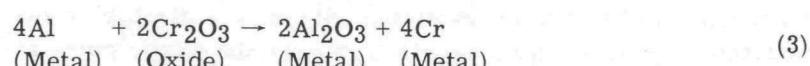
In equation (1), metallic aluminum reduced UO_2 to release metallic uranium while forming Al_2O_3. By introducing Cr_2O_3, which is less stable than UO_2, equations (2) and (3) became operative. Equation (2) established that uranium released immediately reacted with Cr_2O_3 to reform UO_2 with a harmless chromium release. Also, equation (3) shows that aluminum directly reduced the Cr_2O_3 to form Al_2O_3 without reacting with the UO_2. The GE-ANPD innovation was the introduction of the Cr_2O_3 into the system through dispersion of this oxide. Oxides capable of yielding the desired reactions were readily selected from thermodynamic considerations, as well as cross section, availability, and particle-size characteristics.

Oxides evaluated included TiO_2, ZrO_2, NiO, SiO_2, FeO, and Cr_2O_3. Reactions of TiO_2 and ZrO_2 were not detected. NiO was reduced in processing and caused breakup of the fuel ribbon in rolling. FeO, SiO_2, and Cr_2O_3 appeared quite satisfactory.

5.5 PROPERTIES

Oxidation resistance, strength, fission product retention, diffusion effects, blisters, and chromium vaporization were studied for both the cladding and the fuel ribbon.

5.5.1 OXIDATION RESISTANCE

5.5.1.1 Cladding

The addition of 1 weight percent of yttrium to Fe - 25Cr alloy was discovered, in 1958, to impart excellent oxidation resistance and retention of fine grain size (and ductility) after prolonged heating at temperatures up to 2300°F. Eventually data on the effect of chromium and yttrium on oxidation resistance was accumulated. These data are illustrated in Figure 6.4 of section 6 of this report. Alloys of the Fe-Cr-Y types were extensively studied as part of the program to develop fuel ribbon composed of an Fe-Cr-Y cladding over a Cr-Ti-UO_2 core. Although, generally, oxidation resistance of the cladding was good, variation in oxidation behavior was encountered even in heats of similar analysis.

A basic study showed that a parabolic rate law was followed in oxidation of Fe-Cr-Y and similar alloys at 700°C and 1200°C.[20,21] Additions of yttrium, lanthanum, dysprosium, gadolinium, erbium, and 2 to 6 weight percent aluminum resulted in alloys of good oxidation resistance whereas gallium, cerium, and less than 2 weight percent aluminum developed less oxidation-resistant alloys. The study showed yttrium-containing alloys formed internal oxides at 1000°C or higher. Internal oxide was either R_2O_3 or $RCrO_3$, with R being Y, La, Dy, Gd, or Er, depending on temperature. The oxidation of aluminum-containing alloys progressed by aluminum oxidation followed preferentially by chromium.[20]

A survey on oxidation resistance of Fe-Cr-Y alloy at the 30-percent chromium level[22] was conducted at Battelle Memorial Institute (BMI). Heats were secured from BMI and tested as cladding stock and as fuel-element cladding after fabrication. The hot-rolled strip was empirically classified according to quality on the basis illustrated in Figure 5.13. Test results for the alloys are given in Table 5.10. The major conclusion was that aluminum and silicon in combination with yttrium were beneficial to oxidation resistance.

Specimens cold rolled to 0.022-inch strip from 22 heats of 12 pounds each were tested for 100 hours at 2300°, 2400°, 2500°, and 2600°F. Results are given in Table 5.11. With the exception of several low-yttrium alloys or a titanium-containing alloy, the oxidation resistance appeared quite satisfactory over the temperature range of interest.

The Fe-Cr-Y alloys of 25 to 93.5 weight percent chromium were screened for oxidation resistance as arc-cast button melts. Yttrium-free standards or controls, Al, Ti, Ce, Pd, and Ni-Cr alloys were included in the 2300°F, 100-hour tests. Results are given in Table 5.12. Values reported in Table 5.12 represent early work without chemically determined values for Y. However, Y additions appeared to be equal to 5 weight percent Al, and Al plus Y additions were an extremely effective combination in developing oxidation resistance. Besides the fourth element additions to Fe-Cr-Y shown in Table 5.12, change in weight due to oxidation attack was also surveyed for periods of 100 hours at 2300°F for additions of Sc, Th, La, Gd, Ni, Th-Al, and Al without revealing important new information.[23] However, without moderate aluminum additions, Fe-Cr-Y alloys at 30 weight percent Cr level are apparently unsatisfactory for service to 1000 hours at 2300°F. Table 5.13 includes 1000-hour test results with only one heat of 4.67 weight percent aluminum rated good in 0.012-inch gauge after testing.[24]
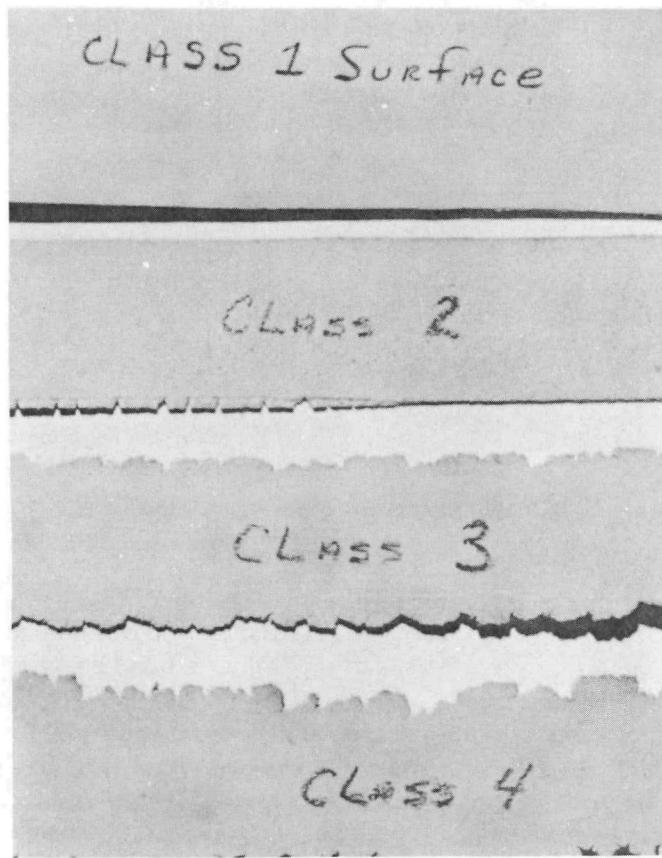
1/2 X

Fig. 5.13 — Workability of Fe-Cr-Y modifications arbitrarily classified as marked (Neg. U36566)

A major aspect of oxidation evaluation was the thickness or gauge of the metal. Figure 5.14 illustrates gauge effect on Heat U-053 at 2300°F with a 0.004-inch strip disintegrating, a 0.006-inch strip beginning to deform at the edges, and the 0.008-inch material appearing to be satisfactory. Failure by oxidation on both fuel elements and Fe-Cr-Y strip followed this pattern. For a time, specimens displayed fairly dark, tenacious oxide that formed a protective coating. Failure was initiated by appearance of a lighter colored oxide, which completely consumed the metallic portion of the specimen and which broke into fragments on contact. Crystallographic studies by the General Electric General Engineering Laboratory (GEL) showed the protective or dark oxide to be Fe_2O_3 plus Cr_2O_3-Fe_2O_3. The nonprotective or distinctive lighter grey oxide was identified as Fe_2O_3 plus $3Cr_2O_3$ - Fe_2O_3. Analytically, the metallic composition was unchanged, but structure and color differed from good, dark oxides to the light grey oxides which were not protective. Although some scatter occurred in points, increasing yttrium correlated with increase in oxidation resistance.

5.5.1.2 Fuel Ribbon

Although LTFCRR-8, a single ring of clad fuel element, completed without failure, 382 hours at 2300°F and 1000 hours at 2050°F in the Low Intensity Test Reactor, the Fe-Cr-Y with Cr-Ti-UO$_2$ fuel ribbon was regarded as marginal in oxidation resistance for 1000 hours at 2300°F.

TABLE 5.10

Fe-Cr-Y MODIFICATIONS TESTED AS CLADDING STOCK AND ON FUEL RIBBON

Heat	Nominal Fe	Cr	Nominal Y	Actual Y	Nominal Composition, wt % Al	Si	Ce	Pd	Be	Stock Class, as in Figure 5.10	Cladding Stock Weight Gains,[a] g/in.^{2}	500-psi Fuel Test[b] Time, hr	Elongation, %
1	69.0	30.0	1.0	-	-	-	-	-	-	2	0.3259	17.5	19.5
2	68.0	30.0	2.0	-	-	-	-	-	-	3	0.0296	-	-
3	68.5	30.0	1.0	0.11	0.5	-	-	-	-	1	0.0514	15.0	4.4
4	68.0	30.0	1.0	0.35	1.0	-	-	-	-	2	0.0550	90.9	13.6
5	67.5	30.0	2.0	1.33	0.5	-	-	-	-	4	0.0695	-	-
6	67.0	30.0	2.0	1.74	1.0	-	-	-	-	4	0.0422	-	-
7	63.5	35.0	1.0	0.05	0.5	1.0	-	-	-	2	0.0270	-	-
8	67.5	30.0	1.0	0.24	0.5	2.0	-	-	-	1	0.0467	18.2	16.5
9	67.0	30.0	1.0	0.38	-	1.0	-	-	-	2	0.0157	36.6	8.1
10	66.0	30.0	2.0	0.71	-	-	1.0	-	-	4	0.0406	-	-
11	68.0	30.0	1.0	0.06	-	-	1.0	-	-	1	0.1885	62.8	35.8
12	67.5	30.0	1.0	0.04	0.5	-	1.0	-	-	1	0.0439	18.0	16.5
13	67.0	30.0	1.0	0.10	-	-	2.0	-	-	1	-	65.6	30.8
14	68.0	30.0	1.0	0.02	-	-	-	1.0	-	1	0.0346	35.6	12.2
15	67.0	30.0	-	-	1.0	-	-	1.0	-	1	-	-	-
16	66.0	30.0	1.0	0.66	1.0	-	-	1.0	-	1	0.0775	40.0	15.6
17	68.9	30.0	1.0	0.04	-	-	-	-	0.1	1	0.0614	20.7	19.6
18	67.9	30.0	2.0	0.38	-	-	-	-	0.1	1	0.0749	20.5	1.0
19	68.4	30.0	1.0	0.07	0.5	-	-	-	0.1	1	0.0608	19.2	26.3
20	67.9	30.0	1.0	0.05	1.0	-	-	-	0.1	1	0.0155	20.0	27.6
21	67.9	30.0	1.0	0.18	-	-	-	1.0	0.1	1	-	35.3	29.6
22	67.9	30.0	1.0	-	-	-	1.0	-	0.1	1	-	-	-
23	67.0	30.0	1.0	0.56	-	-	1.0	1.0	-	1	-	75.5	20.8
24	67.0	30.0	1.0	0.24	-	1.0	-	1.0	-	1	-	-	-
25	66.0	30.0	1.0	0.05	-	2.0	-	1.0	-	1	0.0247	36.6	29.2

[a]After 100 hours at 2300°F.
[b]Cycled from 2300° to 500°F.

TABLE 5.11

OXIDATION RESISTANCE OF VARIOUS IRON-CHROMIUM-YTTRIUM CLADDING ALLOYS AT 2300° TO 2600°F

Heat[c]	Composition, wt % Nominal	Chemical Analysis	2300°F Visual	2300°F Change, wt %	2400°F Visual	2400°F Change, wt %	2500°F Visual	2500°F Change, wt %	2600°F Visual	2600°F Change, wt %
FCR-2	Fe - 35Cr - 1Y	35.6Cr - 0.91Y	-	-	-	+0.19	-	-0.76	-	-2.29
FCR-7	Fe - 35Cr - 1Y	33.7Cr - 0.88Y	-	-	-	-0.42	-	-0.60	-	-2.49
FCR-11	Fe - 25Cr - 1Y	23.7Cr - 0.49Y	-	-	-	-0.34	-	+0.01	-	-
FCR-14	Fe - 35Cr - 3Y	33.9Cr - 2.61Y	G	+1.06	G	+1.18	G	+1.06	G	-1.69
FCR-15	Fe - 35Cr - 1Y	35.1Cr - 0.5Y	F	+2.37	F	-3.85	F	-5.00	F-P	-3.52
FCR-16	Fe - 35Cr - 1Y	36.16Cr - 0.61Y	F	+1.02	F	-3.50	F	-3.00	F	-0.66
FCR-18	Fe - 35Cr - 1Y	34.04Cr - 0.70Y	G	+0.25	G	+0.28	G	-0.50	G-F	-5.20
FCR-19	Fe - 35Cr - 1.5Y	32.3Cr - 1.16Y	G	+0.67	G	+0.22	G	-0.26	G	-1.15
FCR-20	Fe - 35Cr - 2Y	33.0Cr - 1.76Y	G	+0.68	G	+0.20	G	-0.24	G	-1.40
FCR-21	Fe - 35Cr - 1Y	34.9Cr - 0.28Y	F-G	+0.79	F	-2.10	F	-4.66	F	+4.50
FCR-22	Fe - 35Cr - 1Y	34.9Cr - 0.27Y	F-G	+0.79	F	-3.70	F	-3.27	F	+4.10
B-3	Fe - 35Cr - 1Y	33.9Cr - 0.82Y	G	-0.42	G	-0.37	G	-0.13	F	-6.65
B-4	Fe - 25Cr - 1Y	25.4Cr - 0.81Y	G	+0.03	G	-0.43	G	-1.40	G	-1.61
B-5	Fe - 25Cr - 1Al - 1Y	25.2Cr - 0.95Al - 0.59Y	G	+1.75	G	+1.55	F	-1.47	P	+2.09
FCRA-5	Fe - 25Cr - 2Al - 1Y	24.8Cr - 1.89Al - 0.64Y	G	+1.00	G	+1.40	F	+2.00	P	+3.30
FCRA-6	Fe - 25Cr - 3Al - 1Y	25.2Cr - 2.93Al - 0.82Y	G	+0.95	G	+1.17	G	+1.57	G	+2.60
U-053	Fe - 30Cr - 1Y	29.86Cr - 0.74Y	G	-0.41	G	-2.30	P	-5.00	P	-7.42
FCR-30[b]	Fe - 30Cr - 1Y[a]	30.4Cr - 0.61Y	G	+1.78	G	+0.96	F	-1.94	F	+0.60
FCR-32[b]	Fe - 30Cr - 1Y	30.4Cr - 0.71Y	G	+0.40	G	-0.19	F	-4.30	F	-4.23
FCR-33[b]	Fe - 30Cr - 1Y	29.9Cr - 0.28Y	G	+0.55	F	-4.09	P	+4.48	F	-2.73
FCR-34[b]	Fe - 30Cr - 1Y[a]	28.4Cr - 1.0Y	Ex.	+1.05	G	+1.30	F	-1.34	F-G	+0.40
B-11A	Fe - 35Cr - 1Y	-	G	+0.54	G	-0.77	F	-5.92	-	-
B-11B	Fe - 35Cr - 1Y	-	G	+0.51	G	-3.11	F	-8.16	-	-
B-14	Fe - 25Cr - 1Y - 4Al - 0.5Pd	-	G	+0.46	G	-0.60	P	-4.00	-	-

[a]Melt deoxidized by addition of 0.5 weight percent aluminum prior to yttrium addition.

[b]Electrolytic chromium used as starting material. All other heats based on Lunex chromium.

[c]Specimens were 0.022-inch strip as cold rolled. Area is approximately 1 square inch per side. Data shown are average measurements of duplicate specimens.

TABLE 5.12

OXIDATION RESISTANCE AT 2300°F OF YTTRIUM-BEARING ALLOYS[a]

Nominal Composition, wt %	Hardness, R_A As Cast	Hardness, R_A Oxidized	Relative Oxidation Resistance At 100 Hours Visual Rating	Relative Oxidation Resistance At 100 Hours Weight Gain, percent	Relative Oxidation Resistance At 100 Hours Weight Loss, percent
Fe - 35Cr	34	38	Very Poor	2.5	6.0
Fe - 35Cr - 0.5Y	48	47	Good	0.56	1.5
Fe - 35Cr - 1Y	50	51	Good	0.50	1.2
Fe - 35Cr - 1.5Y	54	48	Good	0.61	1.0
Fe - 35Cr - 2Y	59	53	Fair	0.54	0.37
Fe - 35Cr - 3Y	62	56	Fair	0.56	0.07
Fe - 35Cr - 5Y	67	58	Fair	0.72	Nil
Fe - 25Cr, Standard	46	-	Very Poor	29.1	68.8
Fe - 25Cr - 1.5Y	49	36	Good	0.06	0.30
Fe - 35Cr - 1.5Y	59	53	Fair	0.70	0.65
Fe - 48.5Cr - 1.5Y	58	59	Fair	0.40	0.30
Fe - 63.5Cr - 1.5Y	61	63	Good	1.20	Nil
Fe - 73.5Cr - 1.5Y	61	65	Good	0.33	Nil
Fe - 78.5Cr - 1.5Y	65	62	Good	0.42	0.02
Fe - 83.5Cr - 1.5Y	63	62	Good	0.37	0.03
Fe - 88.5Cr - 1.5Y	65	66	Good	0.19	0.14
Fe - 93.5Cr - 1.5Y	58	57	Good	0.36	0.10
Ni - 20Cr, Standard	43	32	Poor	0.23	1.40
Ni - 20Cr - 1.5Y	54	47	Good	0.08	0.02
Ni - 40Cr - 1.5Y	55	49	Good	0.04	0.15
Fe - 25Cr - 5Al, Standard	49	43	Good	7.0	0.2
Fe - 25Cr - 4Al - 1Y	-	-	Excellent	Nil	Nil
Fe - 25Cr - 1Al - 1Y	52	52	Very Good	0.53	Nil
Fe - 25Cr - 1Ti - 1Y	52	49	Poor	1.90	3.20
Fe - 25Cr - 1Ce - 1Y	55	46	Very Good	0.75	Nil
Fe - 25Cr - 0.5Pd - 1Y	47	44	Good	-	0.67

[a]Arc-melted specimens tested in duplicate. Surface area approximately 3/4 square inch.

TABLE 5.13

OXIDATION RESISTANCE OF IRON-CHROMIUM-YTTRIUM-ALUMINUM ALLOYS
AT 2300°F FOR 1000 HOURS

Heat	Chemical Composition, wt %				Sample Thickness, in.	Visual Examination Rating	Metallographic Evaluation	
	Fe	Cr	Y	Al			Surface Oxide, mils	Oxide Stringer, mils
BMI 16-2	70.90	25.38	0.58	3.01	0.012	Fair	0.78	4.10
					0.030	Fair	1.00	4.10
GE-3	71.02	25.11	0.56	3.09	0.012	Poor	0.71	2.20
					0.030	Fair	0.92	6.10
GE-5	72.01	24.50	0.17	3.09	0.012	Poor	0.92	6.70
					0.030	Fair	1.20	9.90
GE-6	71.51	24.72	0.31	3.38	0.012	Fair	0.90	2.04
					0.030	Good	0.90	4.33
GE-7	71.9	24.35	0.72	3.03	0.012	Poor	-	-
GE-12	69.83	24.90	0.35	4.67	0.012	Good	0.98	3.42
					0.030	Good	1.06	7.08
BMI 16-3	66.32	32.83	0.82	-	0.012	Poor	Completely oxidized	
					0.030	Poor	Completely oxidized	
BMI 16-5	66.69	32.65	0.60	-	0.012	Poor	Completely oxidized	
					0.030	Poor	Completely oxidized	

1/2 X

Fig. 5.14 — Influence of thickness of Fe-Cr-Y alloy on oxidation resistance
at 2300°F. Lightest gauge, 0.004 inch completely oxidized
(Neg. U36241B)

Surface attack by propane combustion products was observed in Burner Rig tests of Fe-Cr-Y clad fuel elements. At first unusual surface roughening of Fe-Cr-Y clad fuel had been associated with Burner Rig testing. By September 1, 1958, four Burner Rig cartridge tests had been completed. Three were tested in combustion products and the last in electrically heated air.[15] Smoother, more adherent oxides were noted for the test run with electrically heated air. An XR-27 concentric ring design cartridge was purposely tested to confirm early conclusions on the detrimental effects of combustion products.[17] The test operated 64 hours at 1950°F, 6 psi dynamic load. Four cycles from room temperature to 1950°F were completed. Carbon and nitrogen pickup was significantly high. The attack on fuel ribbon with core oxidation is shown in Figure 5.15. A deteriorated fuel element ring is shown in Figure 5.16.

5.5.2 STRENGTH

5.5.2.1 Cladding

Tensile strength characteristics of Fe-Cr-Y cladding stock is presented in Table 5.14 with two 80Ni - 20Cr compositions for comparison. Although the 80Ni - 20Cr - 1Y alloy showed a high level of strength, other factors such as workability were unfavorable. Stress-rupture properties of the cladding stock at 2300°F are shown in Table 5.15 and in more detail in references 25, 26, and 27.

5.5.2.2 Fuel Ribbon

The fuel ribbon strength objective at the start of this program was a minimum 5-percent creep strength of 1000 psi for 100 hours at 2100°F. Later the requirements became, first, a minimum 5-percent creep strength of 500 psi for 100 hours at 2100°F and, finally, a minimum 5-percent creep strength of 100 psi for 1000 hours at 2300°F.

Two related stress-time-temperature tests were made on the Fe-Cr-Y with Cr-Ti-UO_2 fuel ribbon. A conventional isothermal, single-stress-to-rupture, or creep test was the first type. A harsher, but more appropriate test, was the cyclic stress test. In a thermal-cyclic stress test, an air blast was periodically applied to cool the specimen to 500°F.

Strength properties of Fe-Cr-Y with Cr-Ti-UO_2 fuel elements are presented in reference 28. Comparative data for 80Ni - 20Cr, all Fe-Cr-Y and Fe-Cr-Y with Cr-Ti-UO_2 fuel elements are shown in Figure 6.2 of section 6 of this report.

5.5.3 FISSION-PRODUCT RETENTION

One or more elemental particles are created by each fission of a uranium atom. Generally, the released particles are in an unstable or excited state and decay to a more stable condition in a period of time. The decay mechanisms sometimes include loss of energy through radiation of gamma rays or other undesired phenomena. Because of the inherent chemical characteristics of the elements created as fission products or fragments, they tend to be ingested by living organisms and, therefore, constitute a hazard in some instances.

In general, the fission products born as metals were metallurgically entrapped in the fuel ribbon. However, a number of gaseous elements were fission products, such as Xe^{135}, Xe^{133}, I^{131}, I^{133}, and Kr^{89}. One characteristic of metallic fuel elements was the ability to contain most of the gaseous fission products. Differing fractions of each product element were released through the cladding. Mechanisms of fission-product release included recoil, grain boundary diffusion, surface defect diffusion, and similar phenomena, most of which were temperature dependent. Unless a rupture or defect occurred or was developed by the cladding, no readily measurable releases developed.
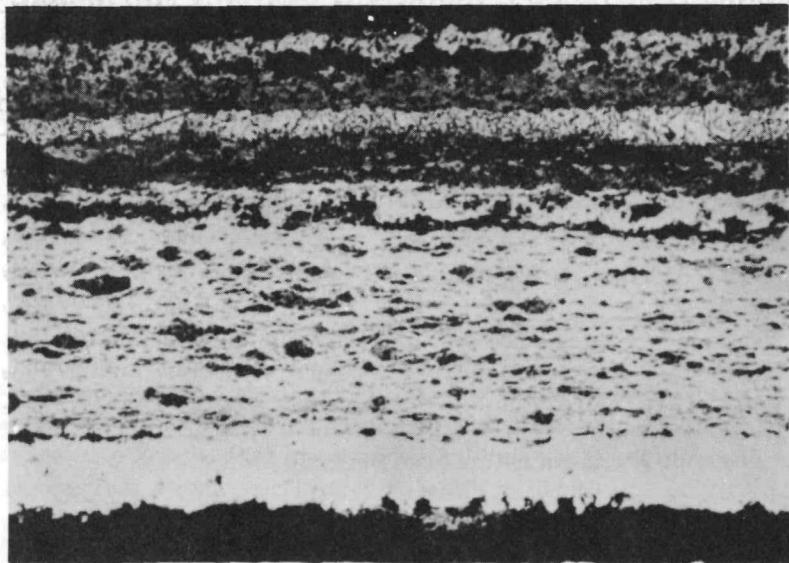
Unetched, 100 X

Fig. 5.15 — Attack by combustion products on fuel ribbon with
accompanying core oxidation
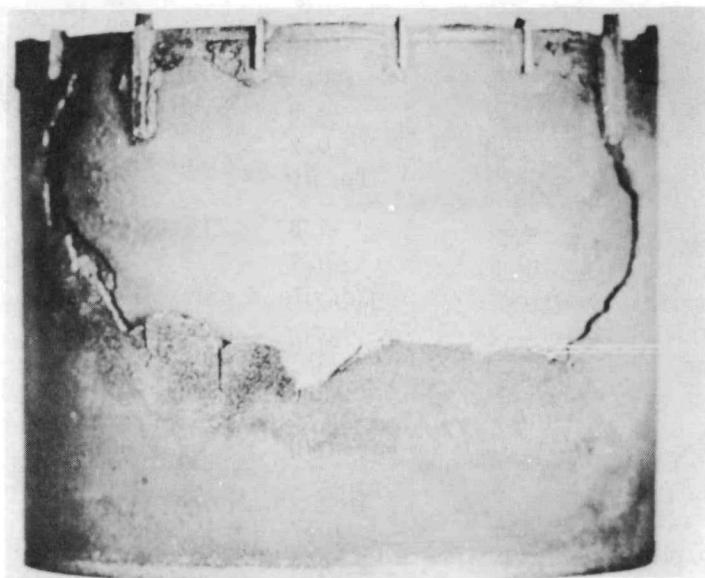
CLADDING DETERIORATION
CAUSED BY CARBON AND NITRO-
GEN ABSORPTION FROM PROPANE
COMBUSTION PRODUCTS

2 X

Fig. 5.16 — Ring from XR-27 design fuel cartridge fabricated from
chromium-base fuel ribbon after 64 hours at 1950°F

TABLE 5.14

TENSILE PROPERTIES OF IRON-CHROMIUM-YTTRIUM AND NICKEL-CHROMIUM-YTTRIUM CLADDING ALLOYS AT ELEVATED TEMPERATURES

Heat[a]	Nominal Composition, wt %	Ultimate Strength And Elongation At Temperature		
		2000°F	2200°F	2300°F
FCR-8	Fe - 25Cr - 1Y	-	2475 psi, 12%	2020 psi, 11%
FCR-11	Fe - 25Cr - 0.5Y	-	2100 psi, 50%	1710 psi, 60±%
FCR-18	Fe - 35Cr - 1Y	3,515 psi, 30%	2410 psi, 30%	2110 psi, 18%
FCR-19	Fe - 35Cr - 1.5Y	4,280 psi, 27%	2750 psi, 24%	2480 psi, 60%
FCR-20	Fe - 35Cr - 2Y	-	2910 psi, 70%	2700 psi, 46%
NC-1	Ni - 20Cr - 1Y	11,740 psi, 28%	7510 psi, 22%	5580 psi, 24%
Standard	80Ni - 20Cr	7,500 psi, -	5930 psi, 50%	4000 psi, 35%
Standard	Fe - 25Cr - 5Al	2,325 psi, 60+%	2230 psi, 60+%	1620 psi, 60+%

[a]Specimens machined from 0.022-inch-thick cold-rolled strip.

TABLE 5.15

STRESS-RUPTURE PROPERTIES OF VARIOUS HEATS OF IRON-CHROMIUM-YTTRIUM ALLOYS AT 2300°F

Heat[a]	Chemical Composition, wt %	Stress, psi	Rupture Time, hr	Elongation, %
B-2	Fe - 29.5Cr - 0.88Y	750	5.8	42
		1000	0.7	39
B-3	Fe - 34.6Cr - 1.1Y	500	100.2	46
		750	2.6	25
		1000	0.2	65
		1600	Tensile	70
B-4	Fe - 25.4Cr - 0.64Y	500	7.6	11
		1000	0.7	39
		1200	Tensile	60
B-5	Fe - 24.8Cr - 0.6Y - 0.9Al	500	3.8	26
		750	0.7	37
		1000	0.1	58
		1200	Tensile	64
U-053	Fe - 29.8Cr - 0.7Y	500	153.4	_b
		750	10.5	25
		1000	0.4	36
		1800	Tensile	75

[a]Cold-rolled strip stock 0.022 inch thick by 1-1/2 inch wide.
[b]No determination.

However, a burst of fission products was easily detected by fission gas monitors. Detection of such a large release terminated tests and was regarded as fuel element failures in reactor operations. Fission-product release was also determined by sampling the air stream after it had passed over a test specimen operated at temperature in a test reactor. The air-stream sample was passed through absorbent charcoal traps, which collected fission products for radiochemical analysis.

Nine fission-product-release experiments were completed on Fe-Cr-Y-clad Cr-Ti-UO_2 cored fuel elements or very similar fuel elements. A number of temperatures and reactor operating times were utilized in the Fe-Cr-Y with Cr-Ti-UO_2 test program. Details are given in Table 5.16. Approximately 1.0×10^{-4} percent of I^{131} was released in LTFCRR-8 and -9 in the 2050° to 2300°F temperature range.[5,29,30] The value of 1.0×10^{-4} percent was considered acceptable. LTFCRR-8 and -9 demonstrated that the fission-product retention did not vary markedly at temperature for long periods of time.

TABLE 5.16

FISSION PRODUCT RELEASE

Test[a]	Time At[b] Temperature, hr	Temperature, $^\circ$F	Neutron Dose, x 10^{19} nvt	Remarks
LTFCRR-1	40.8	2300	0.3	Cladding failure
LTFCRR-2	47.9	2300	-	Probably clad failure
LTFCRR-3	125.0	2300	0.89	Dead edge cracks
LTFCRR-4		Not available		
LTFCRR-5	47.0	680	-	Loaded with depleted fuel, N test
LTFCRR-6	147.0	2200	0.82	Showed Cr vapors, had 4 weight percent Ta in core
LTFCRR-7	56.2	2300	0.178	Defect at edge seal
LTFCRR-8	286.6	2260[c]	3.3	No cracks or blisters
LTFCRR-9	1000.0	2050	7.2	Terminated - no failure

[a]All tests in C-48 hole of LITR.
[b]Before test failed or was terminated.
[c]Also 37 hours at 1800°F, 28.8 hours at 2050°F, and 94.7 hours at 2300°F.

References: 20, 37, 50 through 60.

Supplementing the LTFCRR tests was a series of tests primarily directed toward high-fuel burnups. Test ORR-FCRR-1 operated in 160°F water to 10 percent burnup. A failure developed in post-irradiation, high-temperature, fission-product-release studies, but no damage developed in the original 1167-hour exposure to flux.[31]

5.5.4 DIFFUSION EFFECTS

During exposure to air at high temperatures, Fe-Cr-Y clad lost iron to the Cr-Ti-UO_2 core, which, in turn, lost chromium to the cladding. A photomicrograph of a fuel ribbon prepared to show iron diffusion from the cladding to the core is shown in Figure 5.17.
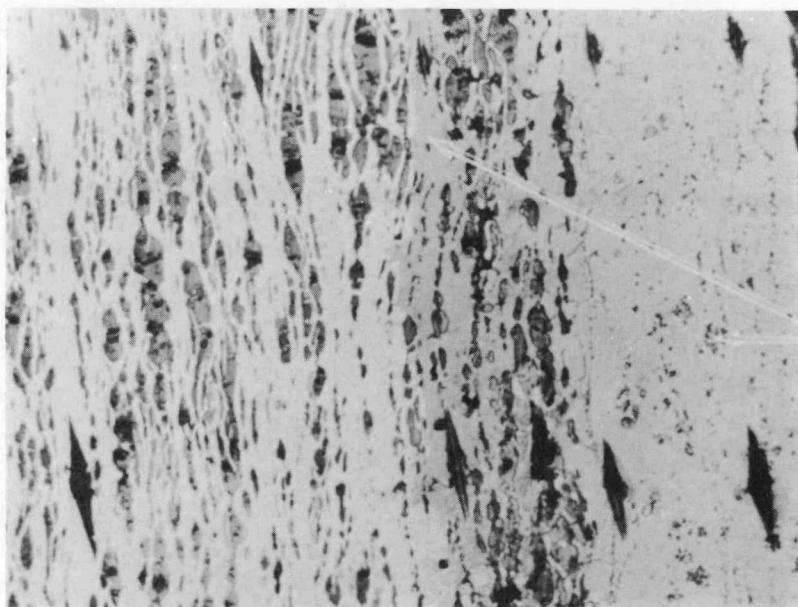
HIGH IRON CONCENTRATIONS ON
BOTH THE Fe-Cr-Y CLADDING AND
IN THE FORMERLY IRON-FREE
Cr-Ti CORE MATRIX

(Neg. 14005)   SN 7805   250 X

Fig. 5.17 – Fe-Cr-Y cladding over Cr – Ti – 40UO$_2$ core after 100 hours
of thermal cycling at 2100°F per 500°F with a 500-psi stress

Yttrium in the cladding also diffused during oxidation.[32] The diffusion of yttrium from Fe - 30Cr - 0. 7Y alloy into pure chromium at 2500°F gave an approximate diffusion constant of 10^{-9} cm^2 per second.[33] Diffusion curves were established by electron probe microanalyzer for a number of fuel ribbons after elevated temperature testing.[34] An examination of fuel ribbon 41-7885 after 266 hours at 2300°F established large movements of iron and chromium as shown in Figure 5. 18.[35]

Initially, the voids that developed in the iron diffusion area shown in Figures 5. 17 and 5. 19 were attributed solely to a well-known diffusion phenomenon. However, a study was initiated to investigate the relationship of these effects and blisters, which developed in testing the early fuel ribbon and were through to be associated with the diffusion voids. The approach used was to analyze the fuel ribbon for gas content. The first analysis of fuel ribbon identified CO, N$_2$, and H$_2$. A later analysis with improved equipment surveyed a large blister on fuel ribbon 41-7889 after 402 hours at 2300°F; it showed CO, A, and H$_2$O.[15] Other ribbon yielded CO plus N$_2$, A, and CO$_2$. Later data revealed N$_2$ was not present in these determinations but the values reported for it should have been attributed to CO.

As a direct consequence of the identification of CO and A in the blisters and diffusion voids, several corrective actions were initiated:

1. Hydrogen-deoxidized or very-low-carbon cladding was sought.
2. Vacuum and hydrogen-atmosphere hot-pressing of sintered cores was substituted for argon atmosphere. This eliminated the only source of argon.

Fuel ribbons were never fabricated with hydrogen-deoxidized cladding, but some decrease in voids was observed with hydrogen-sintered cores. Complete carbon elimination generally minimizes void formation. The thermodynamics of carbon in the presence of chromium and chromium oxide favors carbon monoxide formation at elevated temperatures. Void formation appeared to be enhanced when gases were present.
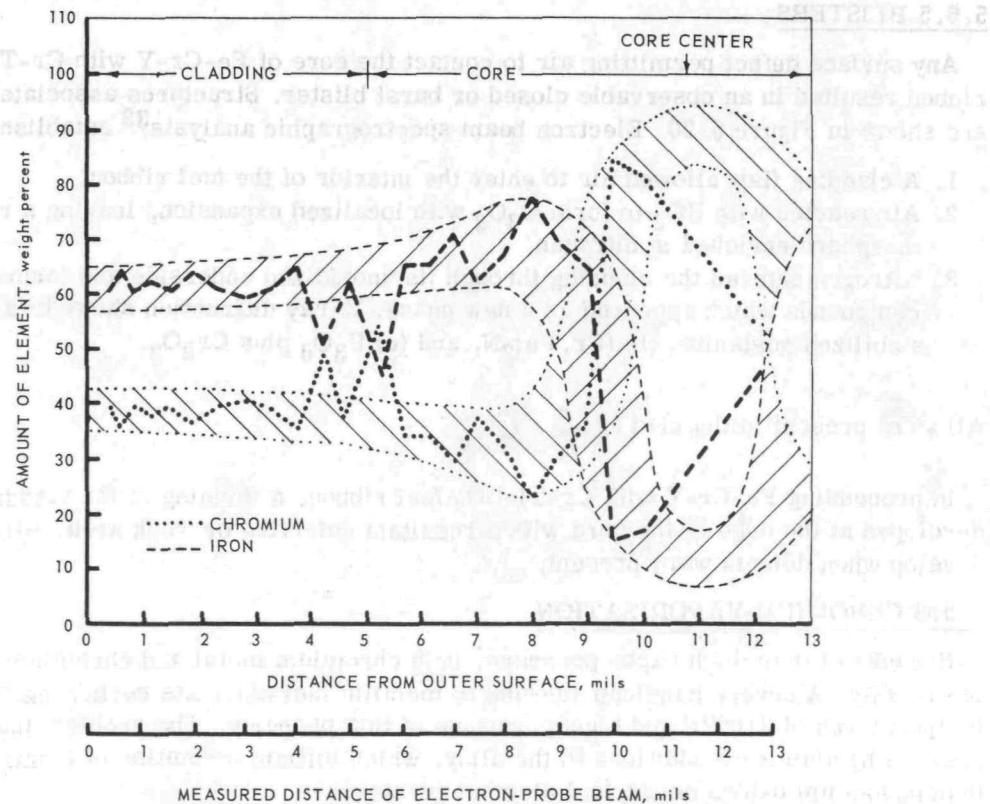
Fig. 5.18 – Diffusion pattern for iron and chromium in Specimen 41-7885
(Neg. A-32212)

(Neg. 10703)   Unetched, 500 X

Fig. 5.19 – Porosity in the core-cladding diffusion zone as observed
in uncracked material near the center of the specimen

5.5.5 BLISTERS

Any surface defect permitting air to contact the core of Fe-Cr-Y with Cr-Ti-UO$_2$ fuel ribbon resulted in an observable closed or burst blister. Structures associated with a blister are shown in Figure 5.20. Electron beam spectrographic analysis[32] established that:

1. A cladding flaw allowed air to enter the interior of the fuel ribbon.
2. Air reacted with UO$_2$ to form U$_3$O$_8$ with localized expansion, leaving a residual atmosphere enriched in nitrogen.
3. Nitrogen entered the cladding through its unoxidized underside and formed Cr(Fe)N compounds which appeared as a new phase. X-ray diffraction showed: (a) Nitrogen-stabilized austenite, (b) (Cr, Fe)$_2$N, and (c) U$_3$O$_8$ plus Cr$_2$O$_3$.

All were present in the clad area.

In processing Fe-Cr-Y with Cr-Ti-UO$_2$ fuel ribbon, a thinning of the cladding sometimes developed at the edge of the core with a resultant defective or weak area. Blisters would develop when defects were present.

5.5.6 CHROMIUM VAPORIZATION

Because of their high vapor pressure, both chromium metal and chromium oxide vaporize readily. A severe handicap accrues to metallic fuel elements containing chromium at temperatures of 2100°F and higher because of this property. The problem may be suppressed by aluminum additions to the alloy, which initiate formation of aluminum rather than chromium oxides on the fuel element surface.

A single ring test piece operated in the MTR top hole for 100 hours at 2000°F plus 8 minutes at 2100°F exhibited chrome oxide crystal deposits on the surface, as shown in Figure 5.21. Zone of metal depletion beneath a crystal is shown on Figure 5.22. Observers estimated temperatures in excess of 2100°F had been attained during the test.[17] In any case, the oxide crystal growth phenomena was immediately emphasized as a significant technical problem. Two induction heated single ring specimens tested in flowing air showed a small number of crystals after 100 hours at 2000°F, and a very large number after 64 hours at 2300°F.[10]

Seven experimental Fe-Cr-Y alloy heats with 30 weight percent and 35 weight percent chromium content were surveyed for crystal growth. Alloy additions included Th, Al, Pd, Si, and Be. In 3 hours at 2175°F, each material, except N1393 with 0.90 weight percent Al, developed crystal growth. Additional heating caused growths to appear on N1393.[36] The compositions surveyed are given in Table 5.17. Micro-emission X-ray results established that a chromium-depleted area developed beneath the crystal growth zone. Chromium oxide evaporation rates measured are shown in Table 5.18.[37]

An 8-stage cartridge, MTR-GE-ANP-1A2, operated at 2070°F for 100 hours and for 2.25 hours at a higher temperature without post-irradiation observation of crystal growths. A 6-stage cartridge tested at lower temperature, MTR-GE-ANP-1Z1, was not observed to develop crystal growths nor was MTR-GE-ANP-1U1.[16,38] Lack of crystal growth on the larger reactor tests was considered to be caused by the action of high-speed airflow. Chromium loss as a function of temperature and time, correlation with observed tests, and calculations on reactor performance were investigated.[39]

The growth of chromium oxide crystals on Fe - 25Cr - Al - Y alloys in 500 hours at 2300°F in flowing air has been shown to be suppressed by sufficient aluminum.[40] Surfaces developed in 128 hours testing are shown in Figure 5.23.
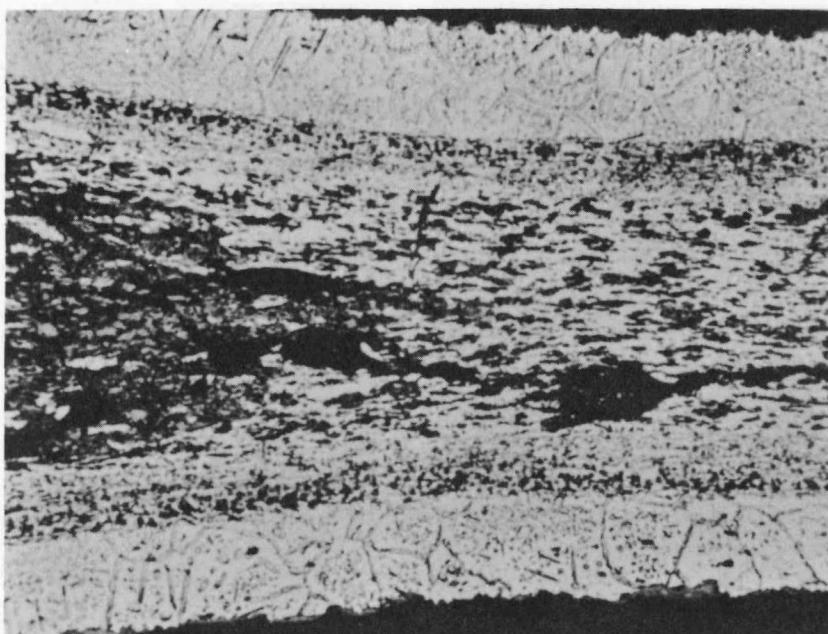
AREA OF SPECIMEN SN8084 NEAR
THE FRACTURE

100 X   N58464

AREA IN SPECIMEN SN8084 DIRECTLY
ADJACENT TO THAT SHOWN ABOVE
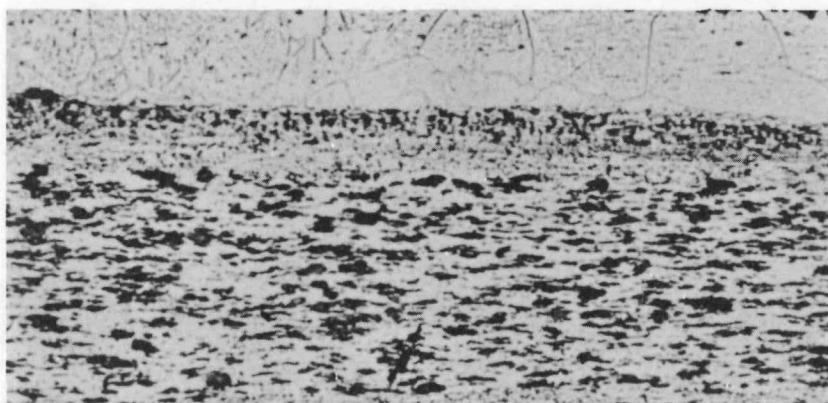
100 X   N58465
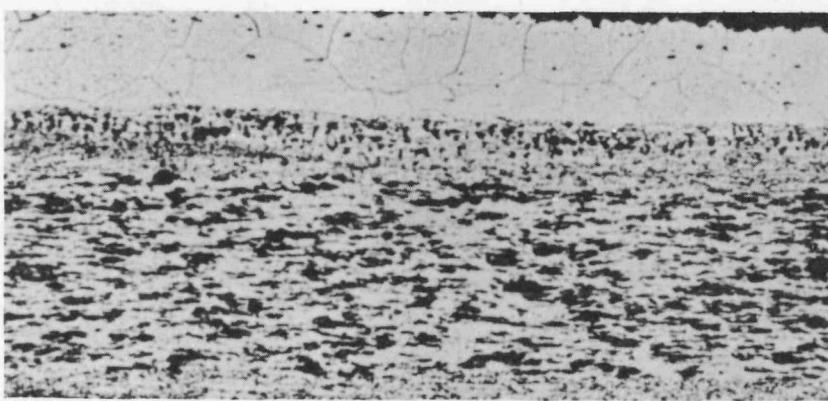
AREA IN SPECIMEN SN8084 DIRECTLY
ADJACENT TO THAT SHOWN ABOVE
AND EXTENDING, AT THE RIGHT, TO
THE UNAFFECTED REGION

100 X   N58466

Fig. 5.20 – Blister structures
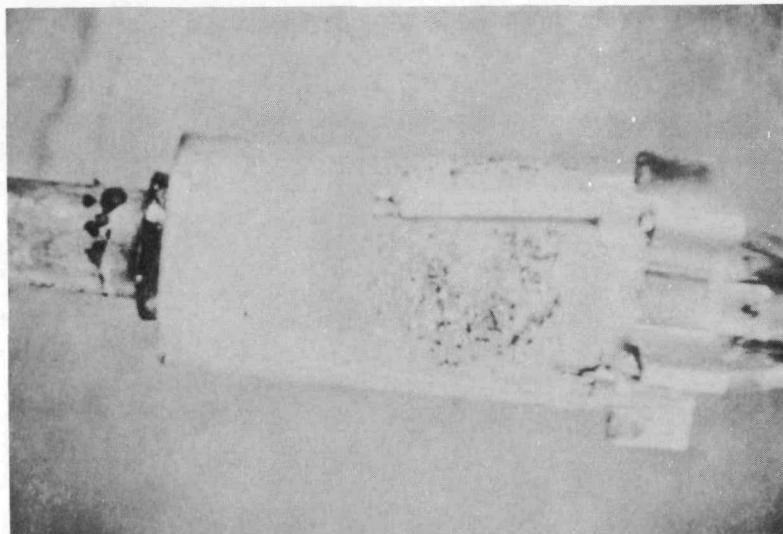
1 X

Fig. 5.21 — Chrome oxide crystal growth on in-pile test in 100 hours
at 2000°F plus 8 minutes at 2100°F (Neg. RML 820)
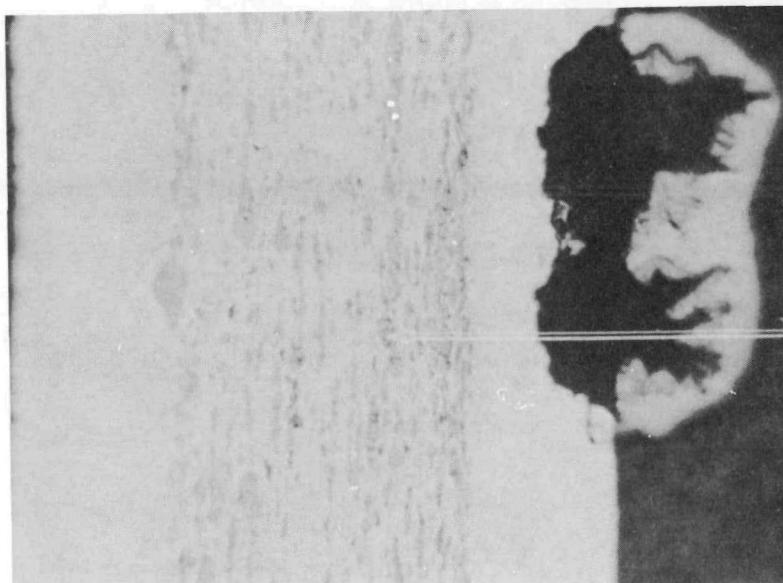
Note: Chromium vaporized and iron
oxidized.

— GROWTH OXIDES

Etched, 150 X

Fig. 5.22 -- Area of removal beneath Cr_2O_3 growth. Chromium vaporized
and iron oxidized. Growth oxides appear grey. (Neg. R-560)

TABLE 5.17

MR-100 ALLOY MODIFICATIONS SURVEYED FOR
CHROMIUM OXIDE SURFACE CRYSTAL GROWTH

Heat	Composition	Cr	Y	Others	Balance
N1389	Nominal	30.0	1.0	0.2 Al	Fe
	Actual	-	0.95	0.17 Al	-
N1390	Nominal	35.0	1.0	0.2 Al	Fe
	Actual	-	0.67	0.19 Al	-
N1384	Nominal	30.0	1.0	0.1 Th	Fe
	Actual	-	0.70	0.11 Th	-
N1393	Nominal	35.0	1.0	0.7 Al	Fe
	Actual	-	0.70	0.90 Al	-
N1370	Nominal	35.0	1.0	2.0 Pd	Fe
	Actual	-	0.71	1.2 Pd	-
N1375	Nominal	35.0	1.0	2.0 Si	Fe
	Actual	-	0.96	2.22 Si	-
N1377	Nominal	30.0	1.0	0.2 Ce	Fe
	Actual	-	0.80	0.13 Ce	-

TABLE 5.18

CHROMIUM OXIDE EVAPORATION

Temperature, $^{\circ}F$	Rate Of Loss, mg/cm^2/hr	Reference
2100	0.009	43
2200	0.068	43
2300	0.062	44
2300	0.040/0.087	45
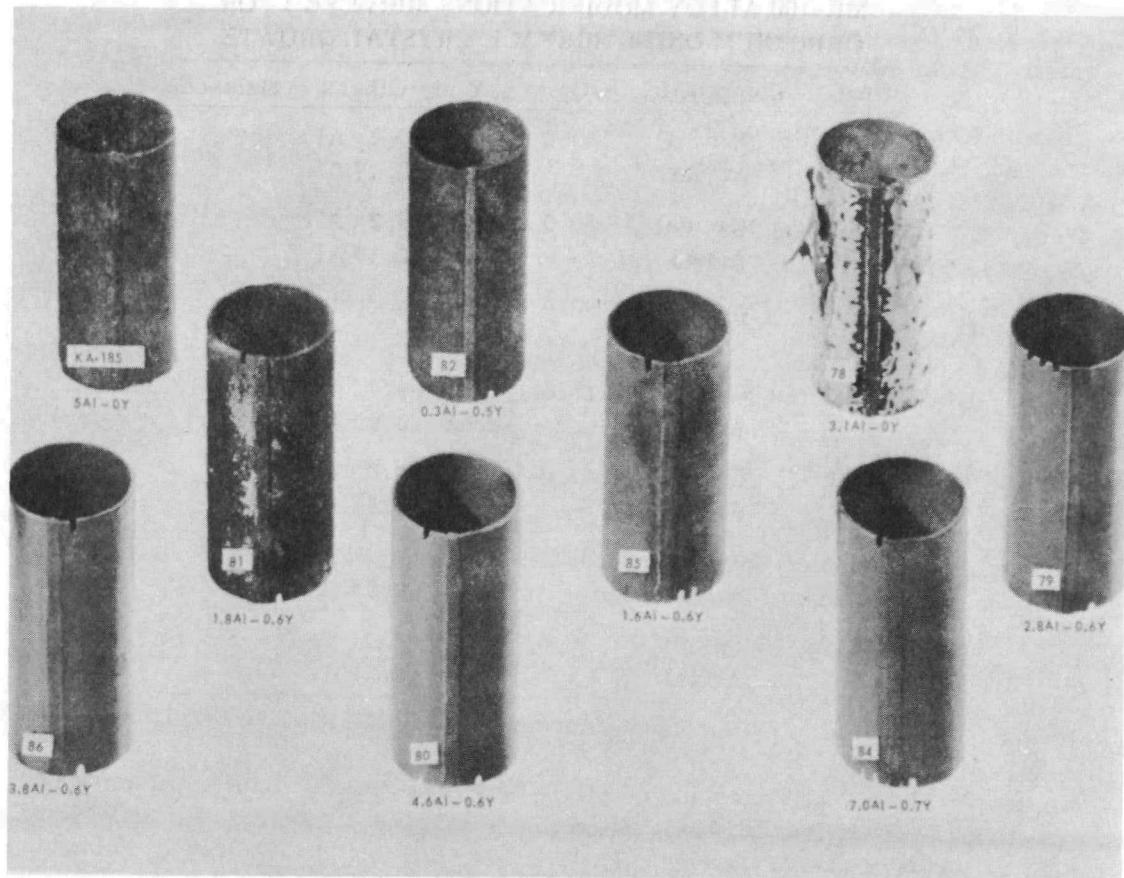
Fig. 5.23 — Specimens of various Fe-Cr-Y-Al alloys 128 hours at 2300°F in flowing air (Neg. U-38546-B)

5.6 REFERENCES

1. Collins, J. F., and Draghic, J., et al., "An Appraisal of Iron-Chromium-Yttrium Alloys for High Temperature Materials," GE-ANPD, DC 61-2-48, December 19, 1960.
2. Collins, J. F., McConnaughey, N., and Walker, F. E., "Evaluation of Iron-Chromium-Yttrium Alloys for Service to 2300°F," GE-ANPD, DC 61-6-29, June 1961.
3. Carlson, R. J., "Progress Relating to ANP Applications, February - April 1958," Battelle Memorial Institute, BMI 1266, 1958.
4. Carlson, R. J., "Progress Relating to ANP Applications, August - October 1959," Battelle Memorial Institute, BMI 1393, 1959.
5. Ward, R., "Primary Metallic Fuel Element Materials Task Force Activity, May to August 1959," GE-ANPD, DC 60-6-107, June 1960.
6. "Applied Materials Research Quarterly Task Report - January through March 1960," GE-ANPD, DC 60-3-12, March 1960.
7. Lewis, J. R., "Fuel Element Materials Development Progress Report for March 1958," GE-ANPD, DC 58-5-138, May 1958.
8. Lewis, J. R., "Fuel Element Materials Development Progress Report for June 1958," GE-ANPD, DC 58-8-62, August 1958.
9. McGurty, J. A., "Applied Metallurgical Research Quarterly Engineering Report, Task 7474, January through March 1958," GE-ANPD, DC 58-4-198, April 1958.
10. "Materials Development Quarterly Task Report," GE-ANPD, DC 59-6-8, June 1959.
11. Yanisch, V., "Assembly Procedures for Advanced Fuel Elements," GE-ANPD, DC 59-6-179, June 1959.
12. Foertmeyer, C. E., "End Leaching of Fuels," GE-ANPD, DCL 58-4-164, April 23, 1958.
13. Yanisch, V., "Welding of Edge Seals Advanced Fuel Elements," GE-ANPD, DC 59-3-241, March 1959.
14. Gelezunas, V. L., and Simmons, C. R., "1A2, Post Irradiation Analysis of MTR-GE-ANPD," GE-ANPD, DC 59-10-39, October 1959.
15. "Materials Development Quarterly Task Report," GE-ANPD, DC 58-9-8, September 1958.
16. Ketron, W. V., "1Z1, Post Irradiation Metallographic Analysis of MTR-GE-ANP," GE-ANPD, DC 59-11-75, November 1959.
17. "Materials Development Quarterly Task Report," GE-ANPD, DC 59-3-8, January through March 1959.
18. "Materials Development Quarterly Task Report," GE-ANPD, DC 58-12-8, October through December 1958.
19. Dietrich, N. T., "Materials Development Compilation of Quarterly Task Reports, January through March," GE-ANPD, DC 58-3-198, March 1958.
20. Felten, E. J., "Progress Report on Corrosion Project at Research Laboratory," GE-ANPD, DCL 58-11-135, November 1958.
21. Felten, E. J., "High Temperature Oxidation of Fe-Cr Base Alloys, with Particular Reference to Fe-Cr-Y Alloys," GE-ANPD, XDC 60-2-153, February 1960.
22. Foster, E. L., Jr., "A Report on Chromium-Iron-Yttrium Alloys," Battelle Memorial Institute, GV 59-32-17, December 30, 1959.
23. McGurty, J. A., "Applied Metallurgical Research Quarterly Engineering Report," GE-ANPD, DC 58-11-81, November 1958.
24. McGurty, J. A., "Applied Metallurgical Research Quarterly Engineering Report No. 13," GE-ANPD, DC 60-1-16, December 1959.
25. Bates, W. J., and Robertshaw, F. C., "An Investigation of the Properties of Various Heats of Fe-Cr-Y Cladding Alloy," GE-ANPD, DC 60-1-204, January 1960.

26. Hammons, G. L., and Robertshaw, F. C., "Milestone I - Job 53289 - Advanced Fuel Element Materials," GE-ANPD, DC 60-1-205, January 1960.

27. Bartocci, R. S., and Robertshaw, F. C., "Advanced Fuel Element Materials, Addendum to Reports DC 60-1-204 and DC 60-1-205," GE-ANPD, DC 60-3-131, March 1960.

28. Lever, R. C., "Rough Draft - Estimated Service Capacity of Fuel Elements," GE-ANPD, PREDC 510, May 6, 1959.

29. Reagan, M. P., "Fission Fragment Sampling Test LTFCRR-1, Appendix I," GE-ANPD, DC 58-9-156, September 1958.

30. Simmons, C. R., "LTFCRR-8 Post Irradiation Photographs," GE-ANPD, DC 59-6-229, June 1959.

31. McGurty, J. A., et al., "Status of Chromium Fuel Element Research Milestone I for Job 54279," GE-ANPD, DC 60-5-163, May 1960.

32. Carlson, R. J., "Progress Relating to ANP Applications, May - July 1959," Battelle Memorial Institute, BMI 1369, 1959.

33. Aitken, E. A., "Diffusion of Yttrium in Chromium," GE-ANPD, DC 58-8-95, August 1958.

34. Robertshaw, F. C., "Meeting on Fuel Element Materials," GE-ANPD, DCL 58-3-113, March 1958.

35. Robertshaw, F. C., "Meeting on Fuel Element Materials," GE-ANPD, DCL 58-5-110, May 1958.

36. "Materials Development Quarterly Task Report," GE-ANPD, DC 59-9-8, September 1959.

37. Tarr, C. O., "Advanced Fuel Ribbon Fabrication - Fabrication Process Development Status Report," GE-ANPD, DC 58-6-216, June 1958.

38. Ketron, W. V., and Lacefield, K., "1U1, Post Irradiation Metallographic Analysis of MTR-GE-ANP," GE-ANPD, DC 60-1-67, December 1959.

39. Baranow, S., "Vaporization of Chromium Effects on XMA-1C Operation," GE-ANPD, DC 59-7-216, July 1959.

40. McGurty, J. A., "Applied Metallurgical Research Quarterly Engineering Report No. 16," GE-ANPD, DC 60-10-70, October 1960.

6. Fe-Cr-Y-UO₂ CORE CLAD WITH Fe-Cr-Y

In December 1957 a demonstration of the improvement of the oxidation resistance of Fe - 30Cr through small yttrium additions indicated this cladding alloy had good potential for fuel element applications. Specific desirable characteristics of the Fe-Cr-Y alloy were retention of fine grain or crystal sizes at temperatures to about 2500°F and ductility at room temperature even after prolonged heating.

6.1 CONFIGURATIONS AND SPECIFICATIONS

Fuel ribbon consisting of an Fe-Cr-Y-UO$_2$ core clad with Fe-Cr-Y alloy was fabricated for application to the concentric-ring design discussed in sections 3. and 5. When this composite was first considered early in 1958, strength requirements included a creep strength equivalent to 5 percent maximum elongation during 100 hours at 2100°F under a 1000-psi stress. Later, design adjustments were made which, first, permitted a creep strength equivalent to 5 percent maximum elongation during 100 hours at 2100°F and 500 psi and, later, 5 percent elongation during 1000 hours at 2300°F and 100 psi.

6.2 FABRICATION

General fabrication procedures for Fe-Cr-Y with Fe-Cr-Y-UO$_2$ fuel ribbon closely followed methods described for Ni-Cr, section 3, and Fe-Cr-Y with Cr-Ti-UO$_2$, section 5.

6.2.1 FUEL RIBBON

A reference process suitable for producing quality Fe-Cr-Y fuel ribbon was prepared and issued.[1,2]

6.2.2 FUEL CARTRIDGE

Utilizing techniques described in section 5, this volume, two cartridges were fabricated into two-stage burner-rig test specimens. However, the cartridges were never tested under simulated ANPD reactor conditions because of other priorities. In these cartridges, all rings over 3/4-inch outside diameter were cold formed. The smaller rings were hot formed.

6.2.3 WIRE-MESH-BED FUEL ELEMENT

A small amount of fueled wire was produced in which an Fe-Cr-Y-UO$_2$ core was employed. Criticality considerations in the proposed reactor caused suspension of the work on the metal-UO$_2$ core matrix in favor of a 100-percent UO$_2$ core. An experimental quantity of wire of the latter type was successfully prepared.

6.3 PROPERTIES

Studies of Fe-Cr-Y with Fe-Cr-Y-UO$_2$ fuel elements were conducted in two phases. First, fuel ribbon with both enriched and depleted UO$_2$ was fabricated as part of the Fe-Cr-Y with Cr-Ti-UO$_2$ fuel element development program reviewed in section 5.[3] During this period in the first quarter of 1958, elevated temperature strength design requirements were established as 5-percent maximum elongation during 100 hours at 2100°F under a 1000-psi stress. Therefore, after determining the fuel ribbon did not meet requirements, studies were terminated except for completing the two burner-rig cartridges mentioned in section 6.2.2. Studies were resumed after the stress requirements were lowered to a creep strength equivalent to 5-percent maximum elongation during 100 hours at 2100°F and 500 psi.

Strength data on Fe-Cr-Y with UO$_2$ appears in Figures 6.1 and 6.2. These tests[4] indicated the superiority of the Fe-Cr-Y with UO$_2$ fuel ribbon over 80Ni - 20Cr fuel ribbon. They also indicated its relatively low strength as compared to Fe-Cr-Y clad Fe-Cr-Y-UO$_2$ fuel ribbon. Elongation in the thermal cyclic test[5] was observed to approximate useable values at 2100°F as shown in Figure 6.1.

The cores of Fe-Cr-Y with UO$_2$ fuel ribbon were markedly superior in oxidation resistance at 2300°F to either 80Ni - 20Cr cored or Cr-Ti cored fuel ribbon, as shown in Figure 6.3. In all of these evaluation there was a general absence of blister formation. The Cr$_2$O$_3$-crystal growth is reviewed in section 5. and did develop on Fe-Cr-Y at 2300°F.[6,7]

A slightly lower thermal neutron growth cross section was calculated for Fe-Cr-Y with Fe-Cr-Y-UO$_2$-cored fuel ribbon than for Fe-Cr-Y with Cr-Ti-UO$_2$ ribbon. Both were approximately 20 percent less than 80Ni - 20Cr ribbon.[6]

The oxidation resistance of the Fe-Cr-Y cladding stock as a function of Cr and Y contents is shown in Figure 6.4. Although a life expectancy of at least 500 hours at 2300°F
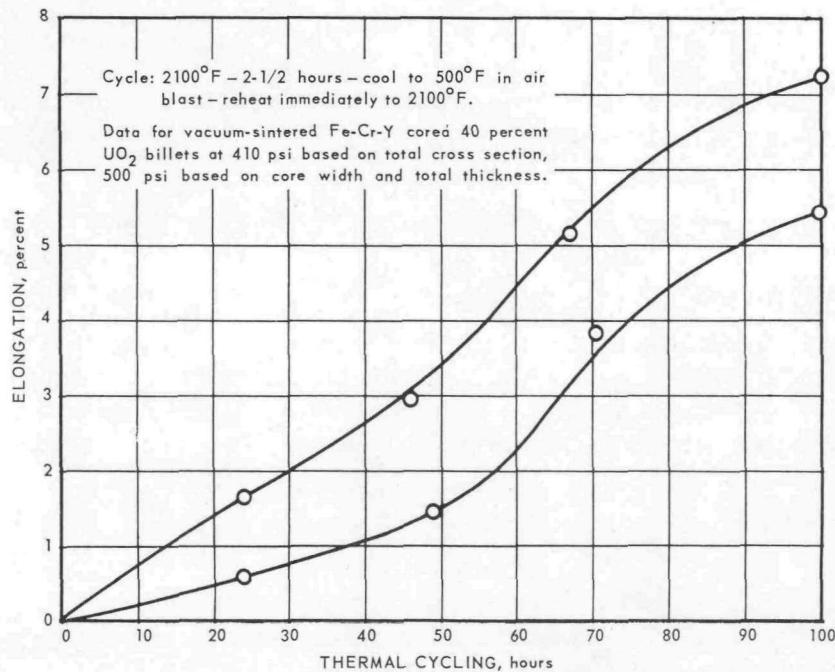
Fig. 6.1 – Thermal cyclic effects on Fe-Cr-Y cored fuel elements

Cycle: 2100°F – 2-1/2 hours – cool to 500°F in air blast – reheat immediately to 2100°F.

Data range for standard Ni-Cr billets at 410 psi based on total cross section, 500 psi based on core width and total thickness.

Same as above with 205 psi based on total cross section, 250 psi based on core width and total thickness.

Best Cr-1Ti cored billets at 825 psi based on total cross section, 1000 psi based on core width and total thickness.

Experimental points for Fe-Cr-Y cored billets at 410 psi based on total cross section, 500 psi based on core width and total thickness.

Fig. 6.2 – Thermal cyclic effects on metallic fuel elements

DIRECTION OF ROLLING
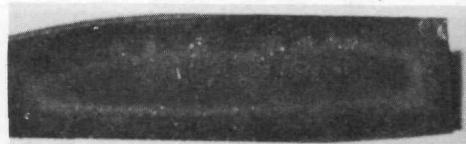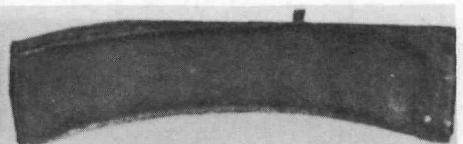
Ni-Cr CORE, 42% UO$_2$ Cr-Ti CORE, 40% UO$_2$ Fe-Cr-Y CORE, 40% UO$_2$

A. SECTIONS CUT FROM FUELED BILLETS
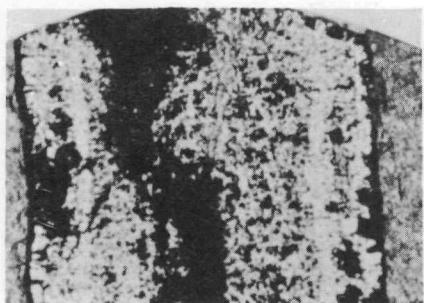
(NEG. 11803)   (NEG. 11804)   (NEG. 11805)

80Ni – 20Cr CORE, 42% UO$_2$ Cr-Ti CORE, 40% UO$_2$ Fe-Cr-Y CORE, 40% UO$_2$
UNETCHED   100X   UNETCHED   100X   UNETCHED   100X
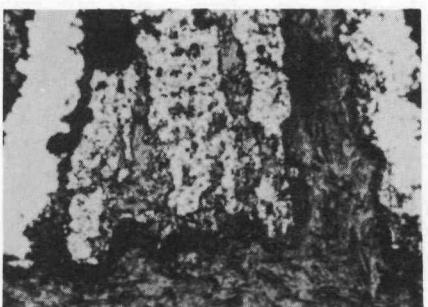
B. PHOTOMICROGRAPH OF CROSS SECTION

TREATMENT: 80 HOURS AT 2300°F IN AIR

Fig. 6.3 — 2300°F oxidation resistance of metallic fuel elements having exposed cores
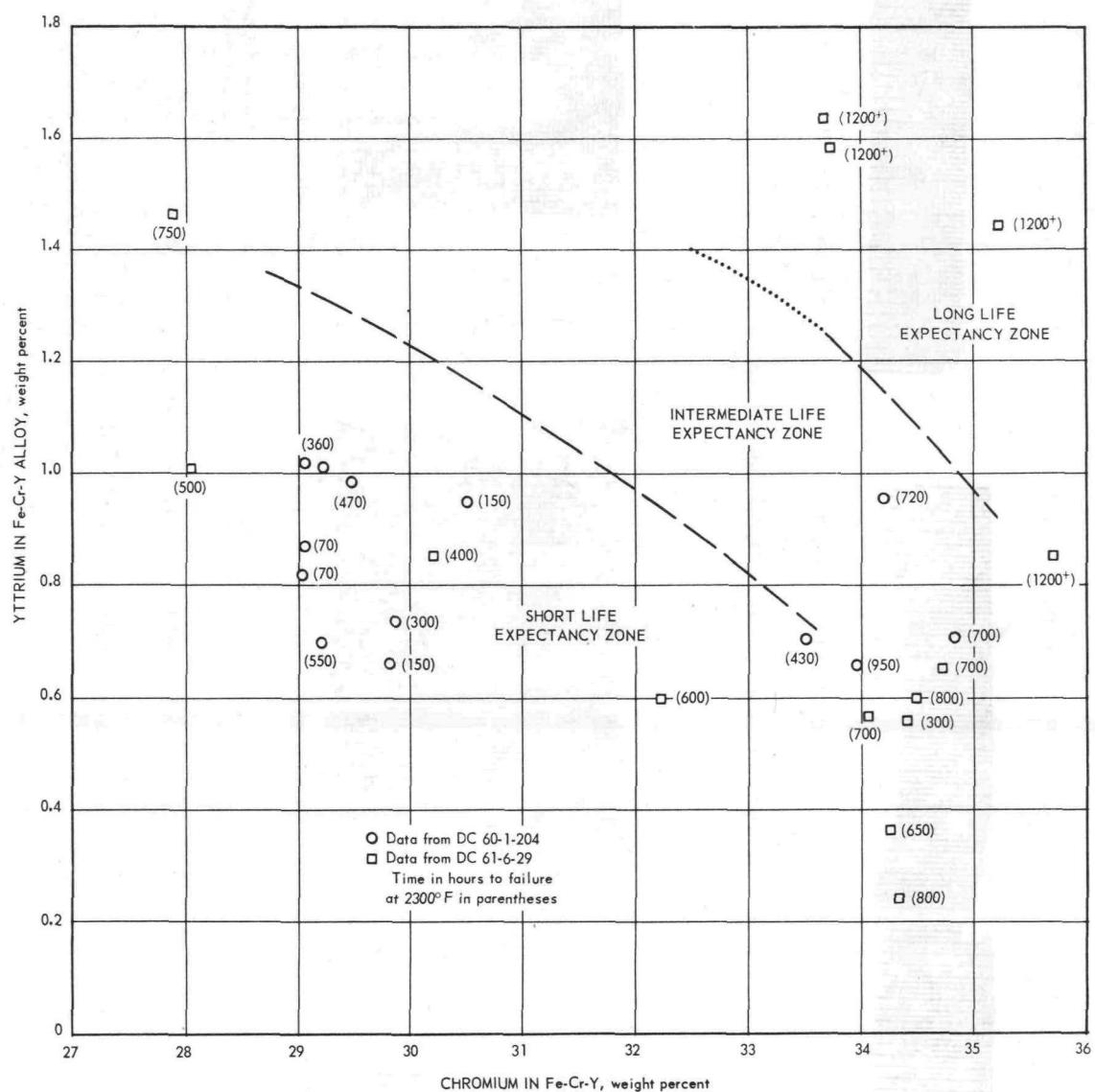
Fig. 6.4 – Life expectancy at 2300°F for Fe-Cr-Y alloy

was anticipated for Fe-Cr-Y-clad Fe-Cr-Y-UO$_2$ fuel ribbon,[7] these data indicated that longer life is possible.

The action of core hardness relative to cladding hardness results in undulations or dog-boning when a strong core such as Cr-Ti-UO$_2$ is rolled to a fuel ribbon in conjunction with Fe-Cr-Y cladding. No edge defects were observed with Fe-Cr-Y-UO$_2$ cores, and the core edges apparently were satisfactory with up to 57 weight percent UO$_2$ dispersed in the core. In addition, 1000 hours at 2300°F did not destroy ductility.[7] Comments pertaining to blister suppressing given in section 5, this volume, appeared applicable to Fe-Cr-Y with Fe-Cr-Y-UO$_2$ fuel ribbon although the problem appeared less troublesome than in Cr-Ti-UO$_2$ fuel ribbon.

Direct fission-product retention of Fe-Cr-Y with Fe-Cr-Y-UO$_2$ fuel ribbon was not measured but was expected to be as satisfactory as for Fe-Cr-Y with Cr-Ti-UO$_2$ fuel ribbon, section 5. Stability of UO$_2$ in Fe-Cr-Y was measured for 1000 hours, and no reaction could be detected.[8]

Work on Fe-Cr-Y with Fe-Cr-Y-UO$_2$ fuel ribbon was ultimately discontinued in favor of Fe-Cr-Y over Cr-Ti-UO$_2$ because of its relatively low strength.

6.4   REFERENCES

1. Antony, K. C., "Reference Process for Fe-Cr-Y Cored Billets," GE-ANPD, DCL 59-8-145, August 1959.
2. Hammons, G. L., and Antony, K. C., "Reference Process for Fe-Cr-Y Cored Billets - Revision 1," GE-ANPD, DC 59-9-192, 1959.
3. "Materials Development Quarterly Task Report, July through September, 1958," GE-ANPD, DC 58-9-8, Table MAT-4322-11-1, 1958.
4. Hammons, G. L., "Special Studies on Advanced Fuel Element Materials-I," GE-ANPD, DC 58-5-111, 1958.
5. Hammons, G. L., "Special Studies on Advanced Fuel Element Materials-II," GE-ANPD, DC 58-8-20, 1958.
6. Hammons, G. L., Robertshaw, F. C., Yario, W. R., "Milestone I - Job 53289 - Advanced Fuel Element Materials," GE-ANPD, DC 60-1-205, 1960.
7. Bartocci, R. S., and Robertshaw, F. C., "Addendum to Reports DC 60-1-204 and DC 60-1-205 on Advanced Fuel Element Materials," GE-ANPD, DC 60-3-131, 1960.

7. Cr-Ti-UO₂ CORE CLAD WITH Cr-Y

Research on chromium alloys for fuel element applications was initiated at GE-ANPD as early as 1950. The inherent oxidation resistance, relatively high melting point, and low thermal neutron cross section of chromium were the bases for the interest in this element. In addition to extensive work carried on at GE-ANPD, subcontracts related to chromium alloy research were placed at various times with Battelle Memorial Institute, General Electric Research Laboratory, Armour Research Foundation, Denver Research Institute, and Nuclear Metals, Inc. In 1959, a subcontract was placed with Clevite Research Division to produce experimental chromium alloy fuel ribbon.

7.1 CHROMIUM-BASE ALLOYS

Two principal discoveries were made during the course of the GE-ANPD program on chromium-base alloys. One of these occurred in 1956 when it was noted that approximately 1 weight percent of yttrium added to chromium significantly improves its oxidation resistance in the 2100° to 2500°F temperature range and also inhibits nitrogen absorption. The second occurred during a portion of the program directed toward the development of higher strength alloys when it was noted that the addition of 1 weight percent of titanium has a strongly positive effect on the 2300°F stress-rupture strength. Figure 7.1 shows the relative strength levels of this and other chromium alloys compared with those of molybdenum, niobium, and 80Ni - 20Cr.

The major portion of the GE-ANPD research on chromium-base alloys is described in considerable detail in references 1 through 5.

7.2 CHROMIUM FUEL RIBBON

The work at Clevite[6,7] involved two approaches to the making of chromium fuel ribbon, viz., (1) the use of wrought clad and frame stock in conjunction with a powder metallurgy core and (2) the use of powder metallurgy techniques for clad, frame, and core. From a fabrication standpoint, only limited success was attained with the process employing wrought cladding and frame. The principal problem was internal cracking of the powder metallurgy core during hot rolling. On the other hand, ribbon produced entirely by powder metallurgy techniques followed by hot rolling was produced with considerably more success.

Although early test results[7] indicated an encouraging level of strength and oxidation resistance, later data[8] demonstrated that the powder metallurgy product, in addition to being impossible to hot form into rings without cracking, had neither the strength nor the oxidation resistance for fuel element applications at temperatures of 2100°F and above.
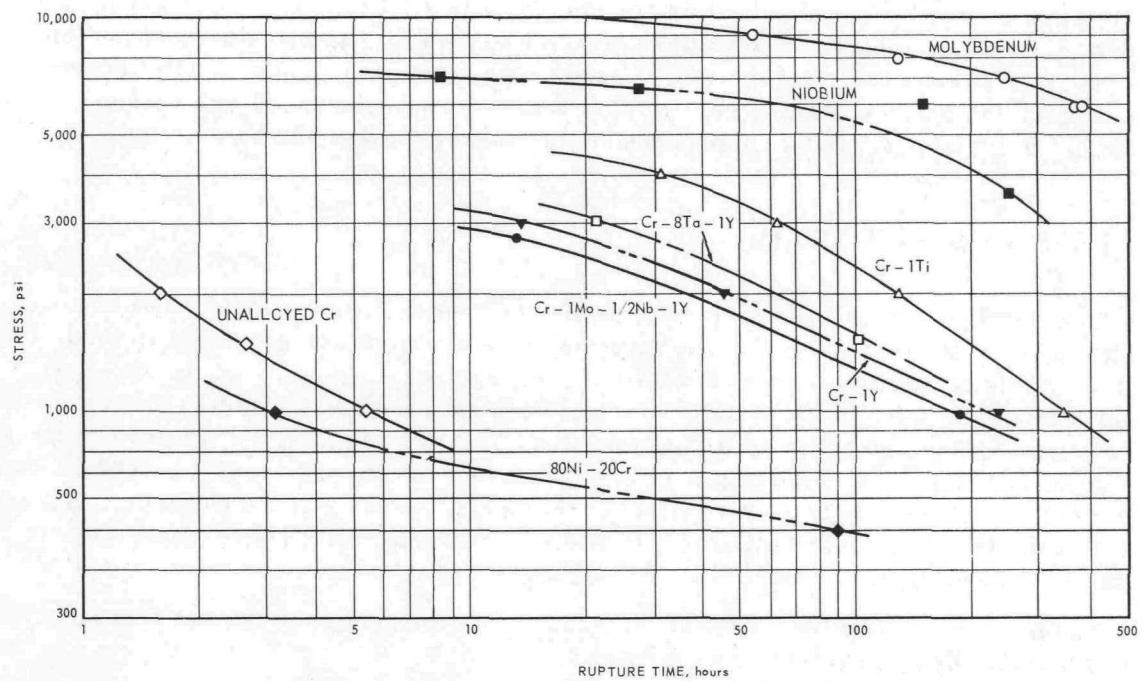
Fig. 7.1 – Applied stress versus rupture life for chromium-base alloys at
2300°F in argon. Molybdenum, niobium and 80Ni – 20Cr tested
under same conditions shown for comparison. Test specimens
were two inches long, button-end type, ground from extruded rod.

7.3 REFERENCES

1. McGurty, J. A., "GE-ANPD Chromium Research," GE-ANPD, January 1959 (Revised April 1961).
2. Fox, J. E., "Chromium-Base Alloy Development," GE-ANPD, APEX-680, April 1962.
3. "Progress Relating to ANP Applications - November 1957 - January 1958," Battelle Memorial Institute, BMI-1255, February 12, 1958.
4. "Progress Relating to ANP Applications - November 1958 - January 1959," Battelle Memorial Institute, BMI-1320, February 12, 1959.
5. "Progress Relating to ANP Applications - February 1959 - April 1959," Battelle Memorial Institute, BMI-1343, May 11, 1959.
6. Toaz, M. W., "Rough Draft - Summary Technical Report, April 10, 1959 through October 6, 1959," GE-ANPD, PREDC-581, October 27, 1959.
7. Toaz, M. W., "Rough Draft Final Technical Report, November 15, 1958 through August 15, 1959," GE-ANPD, PREDC-582, October 2, 1959.
8. McGurty, J. A., Collins, J. F., and Fox, J. E., "Status of Chromium Fuel Element Research - Milestone I for Job 54279," GE-ANPD, DC 60-5-163, May 31, 1960.

8. COATED NIOBIUM

The higher temperatures and performances required of aircraft nuclear reactors caused an ever-increasing interest in the refractory metals: tungsten, molybdenum, tantalum, and niobium. Niobium was emphasized because of its unique combination of favorable properties for nuclear application. This element possesses (1) high melting point, (2) high strength at elevated temperatures, (3) thermal-shock resistance, (4) relatively low density, (5) moderate thermal-neutron cross section, (6) low thermal expansion, (7) nonvolatile oxides, (8) workability, and (9) availability.

Intensive work on niobium fuel element development began with the investigation of protective coatings to satisfy service requirements involving oxidizing atmospheres at temperatures up to 2500°F for periods of 1000 hours. A protective coating was developed that withstood thermal cycling at 2500°F in static air for periods exceeding 1400 hours. However, this coating, based on niobium aluminides, was found to be subject to rapid failure by spalling if held at temperatures for any period of time in the intermediate range of 1200° to 1600°F. Detailed metallurgical studies of the coating system were undertaken and resulted in a shift of emphasis to Nb-Ti-Al alloys not affected at intermediate temperatures.

Alloys with useful levels of oxidation resistance up to 2500°F were identified. In many cases, however, they possessed certain other characteristics that appeared to limit their usefulness for the application intended.

The niobium fuel element development program comprised studies of (1) various coatings for niobium and (2) combinations of materials with niobium to form new alloys for coatings.

8.1 COATING OF NIOBIUM

Materials studied for use in coating niobium included alloys based on aluminum, zinc, silver, and tin.

8.1.1 ALUMINUM COATINGS

Early work performed by Sylvania Nuclear Corning Corporation and others was utilized in studying coating systems based on niobium aluminides. In the most successful of these systems, the coating process consisted of the following: coupons, measuring 1 inch by 0.75 inch by 0.020 inch, of unalloyed Nb were spray coated with -325 mesh Nb powder suspended in a sodium alginate-water solution. The thickness of powder applied was about 0.006 inch. After drying, the specimens were sintered for 1 hour in vacuum at 3600°F and then dipped in a molten bath of Al - 10Cr - 3Si or Al - 10Cr - 3Si - 5Ti at 1950° to 2000°F for 15 seconds. Specimens were than packed in a powder mixture of Al_2O_3 plus 10 weight percent Al for initial diffusion at 1900° to 2000°F for 24 hours in an argon atmosphere.

The oxidation testing of such specimens consisted of placing them in ground aluminum plates and exposing to static air at 2500°F with daily thermal cycling and visual examination.

Protection was based on the formation of NbAl$_3$, which has fair oxidation resistance at 2500°F.[1] During initial periods at 2500°F, protection was provided by the compound NbAl$_3$ at the surface by formation of Al$_2$O$_3$. Aluminum from NbAl$_3$ diffused to the surface to form the ceramic and also inwardly into the underlying niobium.

Consequently, the NbAl$_3$ compound disappeared after approximately 100 to 200 hours. X-ray diffraction of coating layers formed after such times indicated the presence of Al$_2$O$_3$ at the surface and Nb$_2$Al as the underlying layer in the coating.

After 500 to 700 hours, the Nb$_2$Al also disappeared by aluminum depletion and left Nb$_3$Al that, in turn, was eliminated in 800 to 1000 hours by continued aluminum diffusion and internal oxidation. Neither compound, Nb$_2$Al or Nb$_3$Al, was oxidation resistant at high temperatures. The coated niobium was protected by the ceramic oxide formed on the surface. The aluminum-containing compounds acted as reservoirs, continually supplying necessary constituents to surface oxides. When the reservoirs became depleted, failure, due to oxygen diffusion inward, resulted. In such a protected sample, specimen contamination by nitrogen resulted after a time.

X-ray diffraction studies of residues from electrolytic digestion of a tested specimen after the coating was removed identified Nb$_2$N. Nitrogen analyses were performed to determine rate of contamination. Results are given in Table 8.1.

The major part of contamination occurred within the first 23 hours of testing. Comparison of these results with similar data obtained from specimens from which the coating was not removed located the major portion of nitrogen. Contamination resided mainly in the base niobium with little in the coating itself. The nitrogen apparently diffused inward before an impervious oxide was formed at the surface. It also may have entered through cracks which formed during thermal cycling of the specimen. The nitrogen contamination could possibly be lessened by a preoxidation treatment in pure oxygen prior to exposure to atmosphere.

A clear zone free from nitride precipitate formed under the oxide and compound layers. Apparently, the presence of Al in Nb increases the solubility of nitrogen. Therefore, as the Al diffused inward, the nitrogen also diffused inward and became more concentrated in the Nb low in Al. The implication is that the free energy of formation of Nb$_2$N is more negative than that of AlN, otherwise AlN would be in evidence.

TABLE 8.1

NITROGEN ANALYSIS OF Al-Cr-Si
COATED SPECIMENS

Description	Nitrogen, wt %
Nb specimen before testing with coating removed	0.0098, 0.0140
After diffusion with coating removed	0.0160
After 25 hours at 2500°F in air with coating removed	0.0756
After 100 hours at 2500°F in air with coating removed	0.088
After 264 hours at 2500°F in air with coating removed	0.090

The coatings, based on the compounds $NbAl_3$, Nb_2Al, and Nb_3Al, while offering oxidation resistance at 2500° F, were found to be deficient in protection at intermediate temperatures in the range of 1200° to 1600° F.[2] Briefly, the failure occurred as follows. The coating and the surface oxides cracked because of difference in expansion constants when specimens were cooled to room temperature. When the specimens were reheated rapdily to 2500° F, the cracks closed because of the plasticity of the scale and the mobility of aluminum. However, if the specimens were allowed to remain in the vicinity of 1200° to 1600° F, the cracks remained open and the exposed Nb-Al intermetallic compound existing under the surface oxidized. The oxides formed by the high oxide-to-metal compounds in this process caused sufficient volume changes to spall the surface oxides. Such coatings would be useful for high-temperature isothermal applications or under conditions of rapid thermal cycling, but not for intermediate temperature service.

In later work titanium was found to be an effective inhibitor of the spalling phenomenon. However, Nb-Ti-Al coating alloys containing the necessary amount of titanium were found to be unsuitable for coating Nb due to rapid diffusion between the alloys and base niobium. This is best illustrated by Figure 8.1, a plot of changes in structure as a function of time at 2500° F. In only 10 hours, the structure of the coating alloy was changed to a depth of 0.020 inch from the original interface. The structure changed from (Nb-Ti) Al to a two-phase structure which was probably (Nb-Ti) Al and Nb-Ti solid solution having poor oxi-
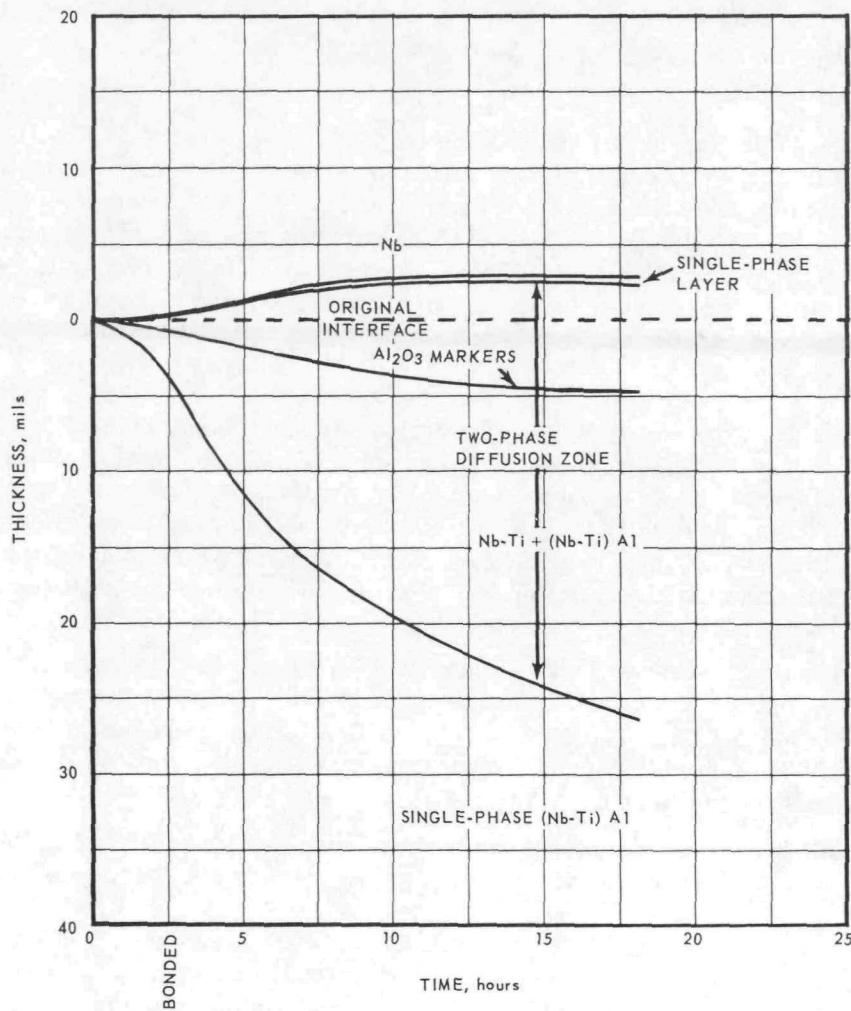
Fig. 8.1 – Diffusion between Nb and Nb-Al-Ti alloy at 2500°F

dation resistance. This change involved only a slight increase in Nb content. The single-phase layer adjacent to the Nb was probably Nb_3Al because Al diffuses into the Nb at a faster rate than does Ti. This was substantiated by electron probe analysis of the diffusion specimens. The Al_2O_3 markers resulted from surface oxides present on the bonding surfaces. The markers moved toward the alloy, demonstrating that the Al and Ti diffused into the Nb faster than Nb diffused in the opposite direction (Kirkendall effect). The microstructure of the diffusion zone after 7 hours at 2500^OF is shown in Figures 8.2 and 8.3.

Oxidation tests of specimens coated with the two complex alloys indicated about a 16-hour life at 2500^OF. The coatings cracked on thermal cycling because of a difference in expansion coefficients and possibly solid-state transformation which occurred on cooling.

8.1.2 ZINC COATINGS

The excellent protection of niobium at temperatures below 1800^OF by coating with zinc was extensively investigated by the Naval Research Laboratory. Experiments were carried out by GE-ANPD to determine ultimate temperature limitations of such coatings. Results are given in Table 8.2.

The highest melting compound in the Nb-Zn system decomposes at about 2050^OF which probably accounts for the ignition of the Zn observed with samples tested at 2100^OF and above. The samples dipped in Zn-Al solution did not ignite at 2300^OF, the highest test temperature. No samples tested lasted 100 hours.

8.1.3 SILVER COATINGS

The General Electric Research Laboratory examined coatings based on Ag-Al, which were of particular interest because of their crack-free nature. A 3-mil coating on Nb of Ag - 20Al (optimum composition) gave a life expectancy of 150 hours under noncyclic conditions at 2300^OF. The cold-bend ductility of these samples was quite good compared with samples coated with aluminum-base solutions. Since copper, like silver, is insoluble in niobium, Cu-Al dips were also tried. It was quickly demonstrated that copper was extremely deleterious to oxidation resistance.

8.1.4 TIN COATINGS

Although Sn and Nb were known to form Nb_3Sn, Sn-Al base dips were examined. It was immediately apparent that a similarity existed between Ag-Al and Sn-Al coatings. Although a ternary diagram of Nb-Al-Sn is not available, observations led to the conclusion that Sn is not soluble in the more readily formed compounds of Nb and Al. Thus, a liquid Sn phase would persist within the coating, providing a buffer to thermal shock. Variations in dip time, temperature, and composition were studied. The best dip composition found was Sn - 10Al - 1Cr - 0.50Ti with a life expectancy of 300 to 350 hours at 2220^OF.

Although only limited success could be obtained with Ag-Al base dips, the combination of Ag, Sn, and Al proved to be the best in the 2200° to 2350^OF range. The best coating solution found was Ag - 22Sn - 15Al - 0.50Ti - 0.50Cr; two samples lasted 1000 hours at 2200^OF and 100 hours at 2300^OF. The reasons for the superiority of Ag-An-Al coating over either Sn or Ag alone were probably as follows:

1. The possibility of free Sn bubbling out of the coating was eliminated with this lower concentration. When bubbling did occur, a highly exothermic reaction with O_2 resulted.

2. In the critical early stages of testing, the ductile phase consisted of Ag-Sn solid solution which has lower melting than pure Ag. Thus, there was less temperature difference between the solidus point of the ductile phase and room temperature with the Ag-Sn combination compared with Ag alone. The lower this temperature difference, the lower the thermal stresses incurred in cycling.

Nb →

SINGLE-PHASE
LAYER

DIFFUSION
ZONE

(Nb, Ti) + (Nb, Ti) Al

(Nb, Ti)
Al ALLOY
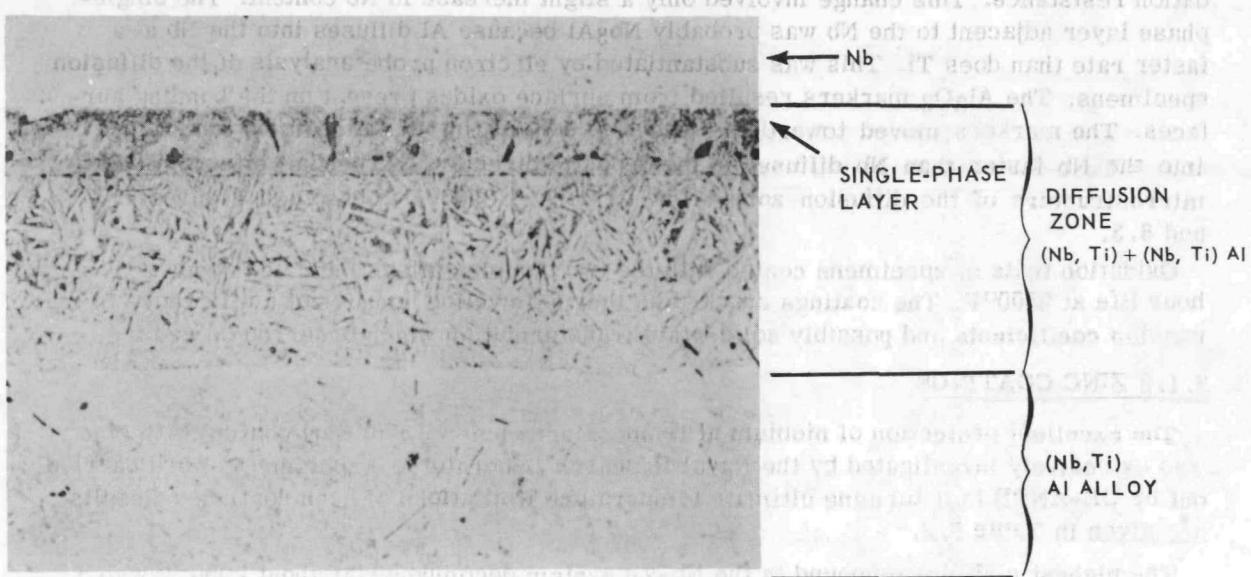
Neg. 20780, Etched HF + HNO₃   75X

Fig. 8.2 — Nb versus Nb-Al-Ti alloy diffusion couple after 7 hours at 2500°F

Nb →

Al₂O₃ MARKERS →
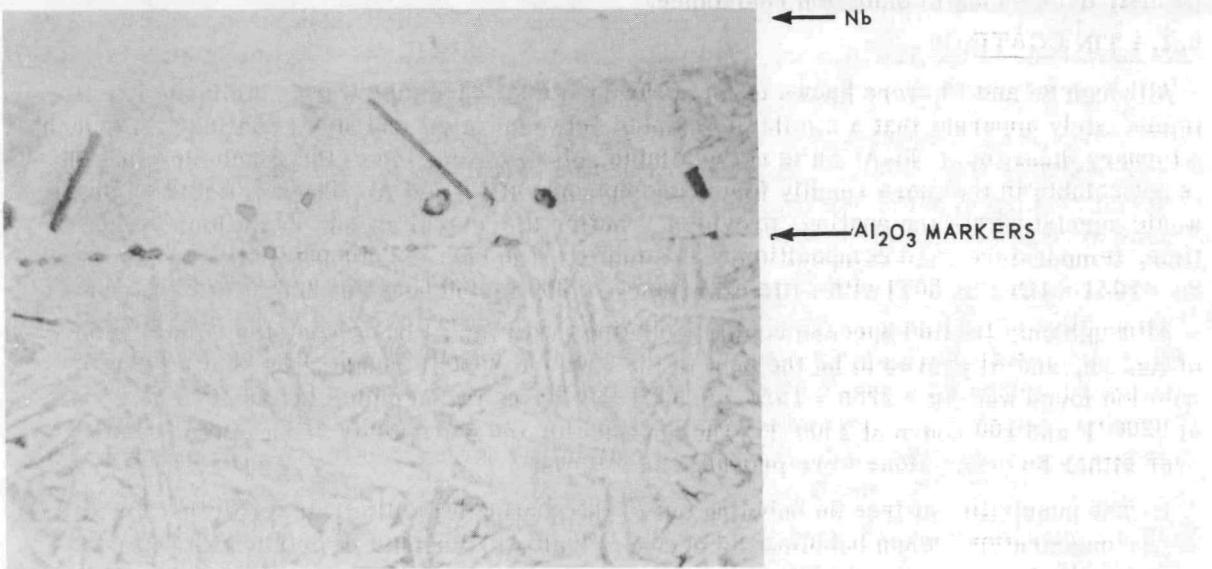
Neg. 20781, Etched HF + HNO₃   150X

Fig. 8.3 — Nb versus Nb-Al-Ti alloy diffusion couple after 7 hours at 2500°F

TABLE 8.2

TEMPERATURE LIMITATIONS OF ZINC COATINGS

Sample Tested	Dip Solution	Test Temperature, ^{O}F	Comments
2	Zn	2300	Ignition - immediate failure
2	Zn	2200	Ignition - immediate failure
1	Zn	2100	Ignition - immediate failure
1	Zn	2000	Gross oxidation in 2.5 hours
1	Zn	1900	Complete oxidation between 24 and 72 hours
2	Zn - 4Al	2300	Both failed in less than 1.5 hours
2	Zn - 4Al	2200	Both failed in less than 1.5 hours
1	Zn - 4Al	2100	Failed in 4 hours
1	Zn - 4Al	2000	Failed between 8 and 24 hours
1	Zn - 4Al	1900	Failed between 24 and 72 hours

8.2   NIOBIUM ALLOY DEVELOPMENT

Work was undertaken in Nb-Al, Nb-Al-Ti, and Nb-Al-Ti-Cr alloys.

8.2.1 NIOBIUM-ALUMINUM ALLOYS

The spalling of Al-base coatings and Nb-Al alloys results from a stress-oxidation phenomena where the stress is caused by the oxide that forms on the surface.[2] Two groups of specimens were tested to 1000 hours at 1300° to $1400^{O}F$. The results are reported in the following paragraphs with a discussion of the effects of composition on spalling.

In order to determine the effects of alloying additives in the spalling behavior of Nb-Al compounds, primarily $NbAl_3$, a group of approximately 50 alloys was prepared at Battelle Memorial Institute. The alloying additions were made so that either the niobium or aluminum were replaced in $NbAl_3$.

A group of 22 complex alloys was produced by arc-melting at GE-ANPD. The alloys were basically Nb-Al-Ti with Si and Cr additions. All alloys were tested in a muffle furnace on aluminum plates for times up to 1000 hours in still air at 1300° to $1400^{O}F$. Specimens were removed from test upon the completion of spalling or fragmentation.

The compositions of the Nb-Al compounds and the test results are given in Table 8.3. The additions which inhibited spalling were Ag, excess Al, Bi, Co, Cu, Si, Sn, and Ti. Silver inhibited spalling when 5 atomic percent was substituted for Nb. The presence of molten Al was noted during testing in that bubbles of Al appeared in the surface of the test specimen. When as much as 10 atomic percent Ag was substituted for the Al, spalling readily occurred. Other additions which resulted in the formation of free aluminum were excess Al, Bi, Cu, Si, and Sn.

The elements which inhibited spalling without the appearance of free aluminum were Ti, Co, Si, and Sn, when substituted for aluminum. Of these, the only ones which would be of value for fuel element applications are Si and Ti. Cobalt has a high cross section and tin is limited because of melting point. The combination of Ti plus Si has been found to provide reasonable stability to $NbAl_3$ at intermediate temperatures.

The results from the series of complex Nb-Al-Ti alloys are given in Table 8.4. Combinations of high Nb and low Al resulted in some spalling or cracking of the specimens. This

TABLE 8.3

EFFECTS OF ALLOYING ADDITIONS ON THE SPALLING OF NbAl$_3$ AT 1300° TO 1400°F

Alloying Element	Compound Formula	Composition, wt %			Time To Spall, hr
		Nb	Al	X	
Ag	Nb$_{20}$Ag$_5$Al$_{75}$	42	45.8	12.2	Al bubbles[a]
Ag	Nb$_{25}$Ag$_{10}$Al$_{65}$	45	34	21	10 - 22
Al	NbAl$_3$	53	47	-	4 - 6
Al	Nb$_2$Al	87	13	-	10 - 22
Al	Eutectic Composition	71	29	-	4 - 6
Al	NbAl$_3$ + 2 wt % Al	51.5	48.5	-	44 - 84
Al	NbAl$_3$ + 4 wt % Al	49.5	50.5	-	Al bubbles[a]
Bi	Nb$_{20}$Bi$_5$Al$_{75}$	37.6	41.2	21.2	Al bubbles[a]
Ce	Nb$_{20}$Ce$_5$Al$_{75}$	40.4	44.3	15.3	6 - 12
Co	Nb$_{25}$Co$_5$Al$_{70}$	51.5	42.0	6.5	10 - 22
Co	Nb$_{25}$Co$_{37.5}$Al$_{37.5}$	41.8	18.4	39.8	_[a]
Cr	Nb$_{25}$Cr$_5$Al$_{70}$	52.0	42.3	5.7	4 - 12
Cr	Nb$_{25}$Cr$_{10}$Al$_{65}$	50.5	38.0	11.5	2 - 6
Cu	Nb$_{20}$Cu$_5$Al$_{75}$	44.1	48.3	7.6	Al bubbles[a]
Er	Nb$_{20}$Er$_5$Al$_{75}$	39.3	43.0	17.7	10 - 22
Fe	Nb$_{25}$Fe$_5$Al$_{70}$	51.6	42.0	6.4	10 - 22
Ga	Nb$_{25}$Ga$_5$Al$_{70}$	51.0	41.5	7.5	4 - 12
Ge	Nb$_{25}$Ge$_5$Al$_{70}$	50.8	41.4	7.8	44 - 84
Hf	Nb$_{20}$Hf$_5$Al$_{75}$	38.8	42.5	18.7	2 - 6
Ir	Nb$_{25}$Ir$_5$Al$_{70}$	45.0	36.6	18.4	2 - 12
Mn	Nb$_{25}$Mn$_{25}$Al$_{70}$	51.7	42.2	6.1	10 - 22
Mo	Nb$_{20}$Mo$_5$Al$_{75}$	42.5	46.5	11.0	4 - 12
Ni	Nb$_{25}$Ni$_5$Al$_{70}$	51.5	42.0	6.5	6 - 12
Os	Nb$_{25}$Os$_5$Al$_{70}$	45.0	36.6	18.4	2 - 6
Pd	Nb$_{25}$Pd$_5$Al$_{70}$	49.0	40.0	11.0	6 - 12
Pt	Nb$_{25}$Pt$_5$Al$_{70}$	44.7	36.4	18.9	2 - 6
Re	Nb$_{25}$Re$_5$Al$_{70}$	45.1	36.7	18.2	2 - 6
Ru	Nb$_{25}$Ru$_5$Al$_{70}$	49.2	40.0	10.8	2 - 6
Ru	Nb$_{25}$Ru$_{37.5}$Al$_{37.5}$	32.4	14.1	53.5	2 - 6
Ru	Nb$_{25}$Ru$_{10}$Al$_{65}$	45.5	34.3	20.2	2 - 6
Sc	Nb$_{20}$Sc$_5$Al$_{75}$	45.0	49.5	5.5	10 - 22
Si	Nb$_{25}$Si$_5$Al$_{70}$	53.3	43.5	3.2	2 - 6
Si	Nb$_{25}$Si$_{10}$Al$_{65}$	53.3	40.2	6.5	_[a]
Si	Nb$_{20}$Si$_5$Al$_{75}$	46.2	50.4	3.4	Al bubbles[a]
Sn	Nb$_{25}$Sn$_5$Al$_{70}$	48.3	39.4	12.3	_[a]
Sn	Nb$_{20}$Sn$_5$Al$_{75}$	41.5	45.3	13.2	Al bubbles[a]
Ta	Nb$_{20}$Ta$_5$Al$_{75}$	39.6	42.2	18.2	4 - 6
Ti	Nb$_{20}$Ti$_5$Al$_{75}$	45	49.2	5.8	22 - 28
Ti	Nb$_{25}$Ti$_5$Al$_{70}$	52	42.5	5.5	22 - 28
Ti	Nb$_{25}$Ti$_{20}$Al$_{55}$	48.8	31.2	20.0	_[a]
Ti	Nb$_{25}$Ti$_{37.5}$Al$_{37.5}$	45.0	20.0	35.0	_[a]
V	Nb$_{20}$V$_5$Al$_{75}$	45.0	49	6.0	2 - 6
W	Nb$_{20}$W$_5$Al$_{75}$	38.6	42.2	19.2	1 - 12
Y	Nb$_{20}$Y$_5$Al$_{75}$	42.8	47.0	10.2	6 - 12
Y	Nb$_{25}$Y$_5$Al$_{70}$	50.0	40.6	9.4	4 - 6
Y	Nb$_{25}$Y$_{10}$Al$_{65}$	47.0	35.0	18.0	6 - 22
Yb	Nb$_{20}$Yb$_5$Al$_{75}$	39.1	42.7	18.2	10 - 22
Yb	Nb$_{25}$Yb$_{10}$Al$_{65}$	40	30	30	2 - 4
Zr	Nb$_{20}$Zr$_5$Al$_{75}$	43.0	46.8	10.4	2 - 6
Zr	Nb$_{25}$Zr$_{20}$Al$_{55}$	41.3	26.4	32.3	10 - 22

[a]Tested 1000 hours with no spalling.

TABLE 8.4

BEHAVIOR OF COMPLEX Nb-Al-Ti ALLOYS
TESTED 1000 HOURS AT 1300°F

Alloy Composition, wt %					
Nb	Ti	Al	Cr	Si	Results
40	40	20	-	-	Spalling - white oxide
38	38	24	-	-	Thick white oxide
30	36	28	-	-	Thin white oxide
34	34	32	-	-	White-gray oxide
39	38	20	3	-	Spalling - yellow oxide
37	36	24	3	-	Yellow oxide
35	34	28	3	-	Yellow oxide
33	32	32	3	-	Tan-gray oxide
37	37	20	6	-	Spalling - tan oxide
35	35	24	6	-	Tan oxide
33	33	28	6	-	Tan-gray oxide
40	40	20	-	0.3	Spalling
38	38	24	-	0.3	Thin adherent white oxide
36	36	28	-	0.3	Thin adherent white oxide
34	34	32	-	0.3	Thin adherent gray oxide
39	38	20	3	0.3	Spalling - yellow oxide
37	36	24	3	0.3	Yellow oxide
35	34	28	3	0 3	Gray oxide
32	33	32	3	0.3	Tan-gray oxide
37	37	20	6	0.3	Spalling
35	35	24	6	0.3	Tan-gray oxide
33	33	28	6	0.3	Tan-gray oxide

cracking was initiated after relatively long times, between 500 and 1000 hours. No specimens were reduced to powder during a 1000-hour test period. The specimens which spalled could possibly contain some Nb_2Al or $NbAl_3$ as a minor phase to account for the spalling.

8.2.2 NIOBIUM-ALUMINUM-TITANIUM ALLOYS

The ternary alloys evolved from a study of the Nb-Al binary alloys in which it was found that $NbAl_3$ was oxidation resistant at high temperatures but deficient at intermediate temperatures of 1100° to 1600°F.[2] The addition of Ti to Nb-Al alloys was found to inhibit the effect. Some compositions exhibited good oxidation resistance to 2500°F. Metallographic and X-ray diffraction analyses indicated that the best alloy was essentially the Ti-Al intermetallic compound (gamma phase) with Nb in solution. The estimated ternary Nb-Al-Ti phase diagram is shown in Figure 8.4.

The primary objective of this work was the evaluation of the oxidation resistance of a number of Nb-Al-Ti and more complex alloys. Alloys were prepared either by inert arc melting or by induction melting under an argon cover. In the arc melting process, 25-gram charges were melted in a water-cooled upper crucible under a partial pressure of one-third atmosphere of helium. The buttons were turned four times and re-melted in order to insure homogeneity. In the induction melting process, 100-gram charges were melted in an alumina crucible under an argon cover. Test specimens were obtained by drawing up the molten alloy in a small diameter quartz tube. The rods, 0.075 inch to 0.20 inch in diameter, contained some porosity but were considered to be suitable for initial evaluation. The materials used in the alloys were of commercial purity unless otherwise noted.
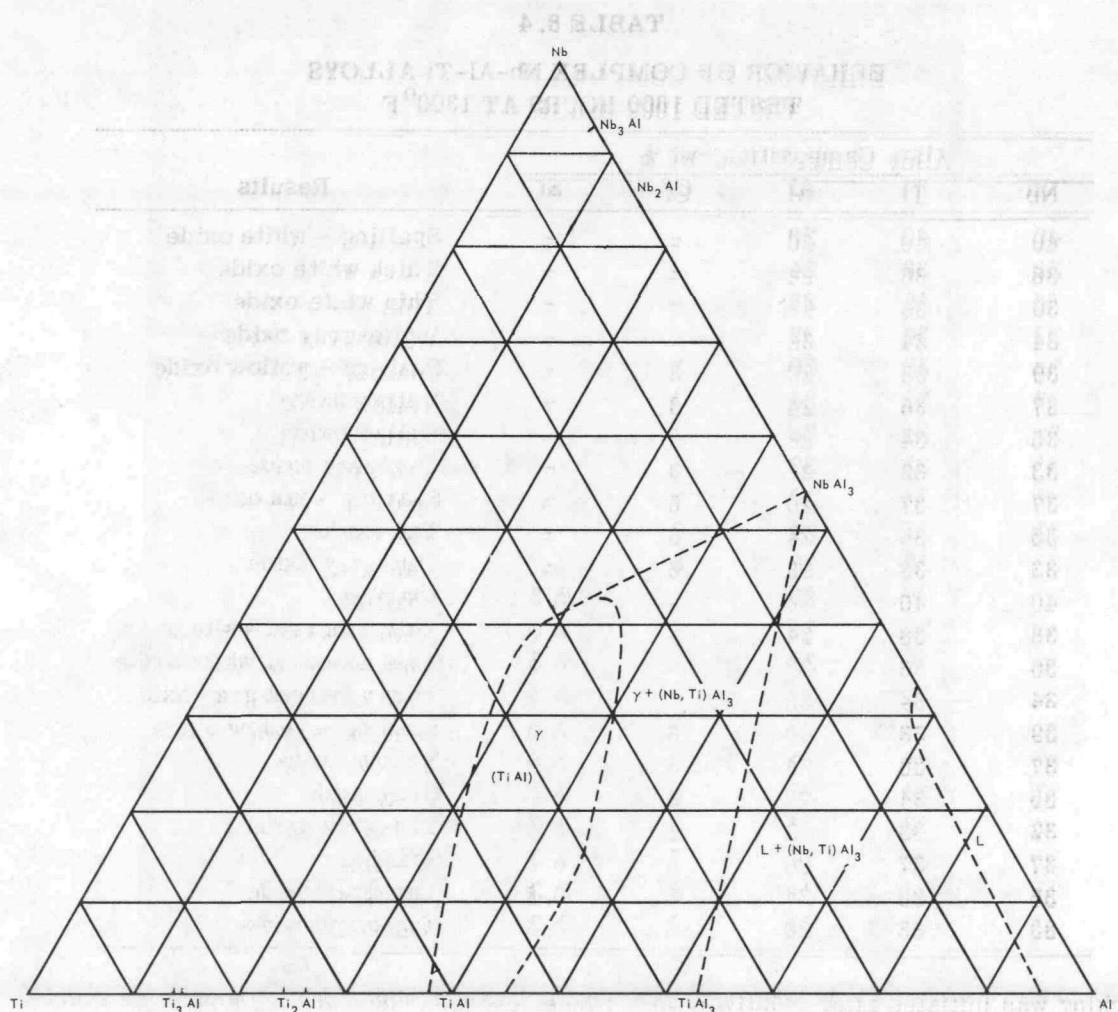
Fig. 8.4 – Nb-Al-Ti ternary phase diagram

Oxidation tests were conducted in a muffle or tube furnace in static air. Most of the tests involving weight-change measurements were intermittent in nature. One continuous weight-gain test was run in a Mettler thermobalance. Tests were conducted at temperatures from 1300° to 2500^OF. The alloy structures were determined by metallography, X-ray diffraction, and electron microprobe analysis.

An initial series of 20 alloys was prepared in the form of arc-melted buttons. Portions of the arc-melted buttons were tested for 100 hours at 2500^OF in air. The results are shown pictorially in Figure 8.5. Alloy No. 8 appeared to be best, based on visual examination. An intermittent oxidation test was carried out for 920 hours at 2500^OF. As indicated in Figure 8.6, the data follows a cubic relationship during the initial portion of the test. The rate equation for 500 hours is $W^3 = kt$, where W = weight gain in mg/cm^2, k is the rate constant and t is the time. After de-scaling the specimen at 500 hours, the rate changed due to flaking of the oxide in cooling. The continuous flaking of the specimen was probably due to the depletion of Al from the surface resulting in a two-phase layer of structure different from the matrix. Figure 8.7 is a photomicrograph of the specimen showing the depleted zone. The adherence of the scale was probably dependent on the thickness of the depleted layer. The layer was two-phase, probably gamma plus beta (Nb-Ti) Al plus Nb solid solution with the possibility of a transformation of the beta

*The composition range of these alloys was 30 to 50Nb, 20 to 40Ti, 20 to 30Al.

160
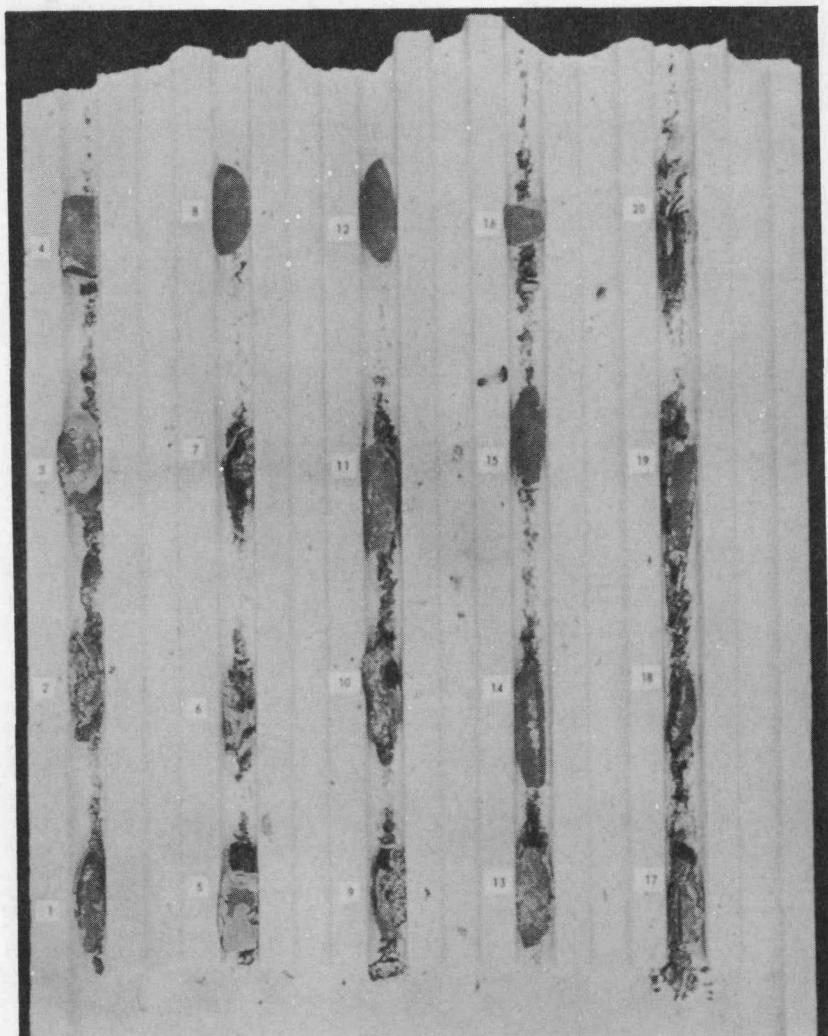
Fig. 8.5 – Nb-Al-Ti alloys tested 100 hours at 2500°F in air (Neg. U-39000)
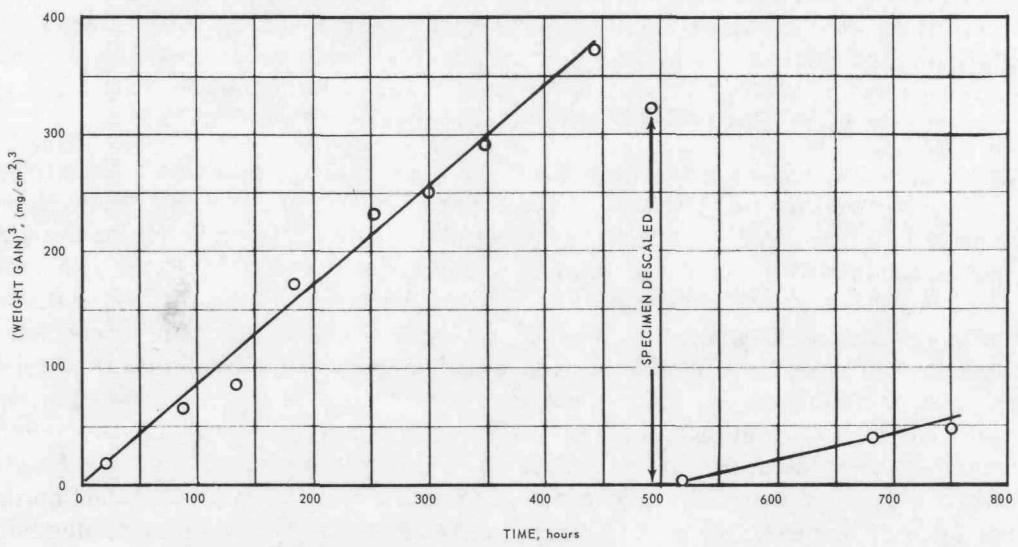
Fig. 8.6 – Weight gain versus time for Nb – 34Ti – 28.3Al alloy tested at
2500°F in air

AI-DEPLETED LAYER
Al_2O_3 PARTICLES CAUSED
BY INTERNAL OXIDATION
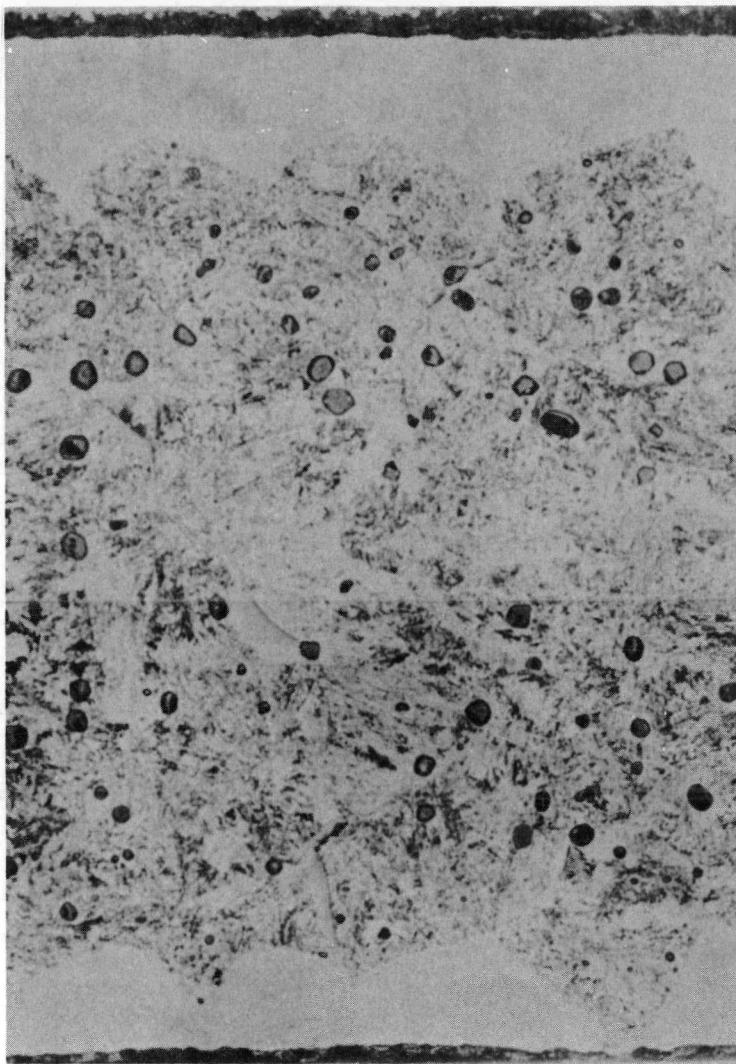
Neg. 20160, Etched $45H_2O$,
20159, 43 Glycerine, $5HNO_3$,
5Hf, 2HCl (vol. %)

75X

Fig. 8.7 — CAT-I alloy tested for 920 hours at 2500°F

occurring in heating and cooling. Stresses, resulting in flaking of the oxides, tended to increase as the thickness of the zone increased. Internal oxidation occurred since Al_2O_3 particles were clearly visible. No inclusions were noted in the depleted zone indicating the solubility of oxygen was higher in this zone than in the center of the specimen. Further proof that internal oxidation occurred was obtained from the measurement of the specimen after testing 500 hours. The total weight gain was 20 milligrams. The metal loss, 0.0006 inch per side, was calculated as 10 milligrams. Therefore, the density of the specimen decreased as in Figure 8.8 due to the formation of the oxide particles internally.

This particular behavior was due to the instability of the intermetallic compound. At 2500^OF, Al depletion of the surface layers occurred. The development of an imperious oxide depended on the diffusion of Al to the surface, requiring Al in the (Nb-Ti)Al compound to dissociate into two phases of (Nb-Ti)Al plus Nb, Ti solid solution. At lower temperatures such as 2300^OF, the Al did not diffuse rapidly enough to form a protective oxide. Apparently Ti, added to Nb-Al alloys, raised the spalling temperature from 1100° to 2300^OF. Most recent efforts were aimed at alloying Nb-Al-Ti to improve the oxidation resistance at 2100° to 2300^OF.

8.2.3 NIOBIUM-ALUMINUM-TITANIUM-CHROMIUM ALLOYS

An initial series of Nb-Al-Ti alloys included the following alloy elements added individually: Cr, Si, Fe, Sn, Co, Ni, Pd, Zr, Mn, Mg, Y, Pb, Mo, Bi, W, Ag, Cl, Ta, Er, Yb, Rh, Ru, Hf, Ir, Re, Pt, B, Zr, V, Cu, and Ce. Evaluation based on the retention of oxide at 2100^OF, 2300^OF, and 2500^OF resulted in the selection of Cr as the most promising alloying element. The effect of 3 weight percent Cr in the oxidation behavior is shown in Figure 8.9. Flaking of the oxide still occurred but some improvement was noted over the ternary alloy. Figure 8.10 shows the effect of 6 weight percent Cr. This
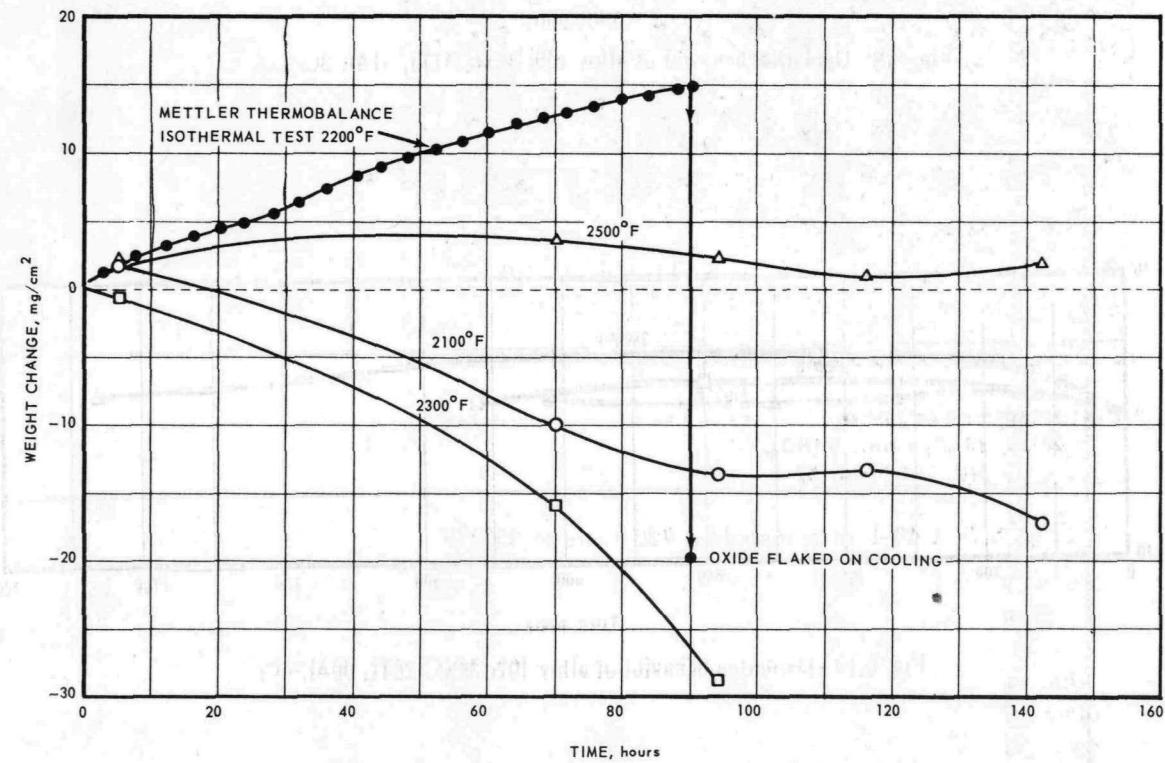
Fig. 8.8 – Oxidation behavior of Nb-Al-Ti alloy 8; 36.7Nb, 33.7Ti, 29.6Al

occurring in heating and cooling. Stresses, resulting in flaking of the oxide, tended to increase as the thickness of the zone increased. Internal oxidation occurred since Al_2O_3 particles were clearly visible. No inclusions were noted in the depleted zone, indicating the solubility of oxygen was higher in this zone than in the center of the specimen. Further proof that internal oxidation occurred was obtained from the measurement of the specimen after testing 600 hours. The total weight gain was 20 milligrams. The nodal area, 0.0006 inch per side, was estimated as 10 milligrams. Therefore, the density of the specimen decreased as in figure 8.9 due to the formation of the oxide particles internally.

This particular behavior was due to the instability of the intermetallic compound Nb_3Al. Adsorption of the oxide layer occurred. The development of the two-phase oxide formation of the destruction of Al_2O_3 in the direction resulting in the formation of two masses of other oxides by an oxidation reaction. At temperatures such as 2100°F, the AlN of the Nb phase oxides conversion rapidly. Apparently, Nb added to Nb-Al alloys raised the melting temperature above 2100°F. Nb-Al-Cr alloys were oxides at elevated times and in temperatures between these conditions as a 1974 to 2500°F.


Fig. 8.9 – Oxidation behavior of alloy 109; 35Nb, 31Ti, 31Al, 3Cr
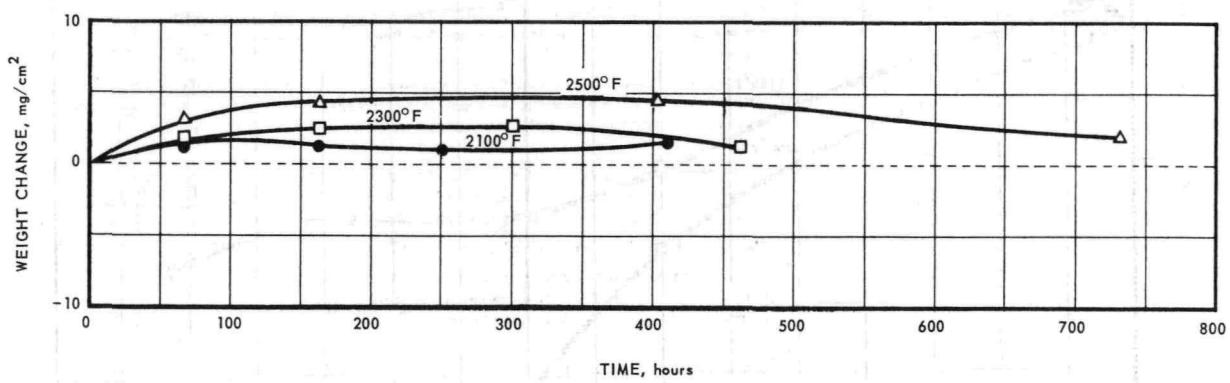

Fig. 8.10 – Oxidation behavior of alloy 107; 36Nb, 28Ti, 30Al, 6Cr

alloy did not flake in approximately 500 hours at all three temperatures. At 2300°F and 2500°F, some loss in weight has occurred due to volatilization of Cr from the specimens.

In an effort to determine the basic mechanism by which Cr improved the oxidation resistance of the Nb-Al-Ti ternary alloys, X-ray diffraction analyses were performed on oxides removed after testing for 4 hours at temperatures from 1600° to 2500°F. Results are given in Table 8.5.

For the ternary alloy at 1600°F and 1800°F, the oxide consisted of a major phase of TiO_2 and a minor phase of gamma-Al_2O_3. At 2000°F and above, traces of an $Nb_2O_5 \cdot Al_2O_3$ phase was found. For the 6 weight percent Cr alloy the $Nb_2O_5 \cdot Al_2O_3$ phase was absent at all temperatures. An unidentified face-centered cubic phase was found in the oxides from the 6 weight percent Cr alloy. The only known cubic oxide of any of the elements that were present was NbO which has a larger lattice parameter, $a = 4.21$ Å, than the unknown phase. The structure did not correspond to any of the metallic phases that were present. It was determined that the initial oxide formed was primarily TiO_2 at all temperatures.

TABLE 8.5

X-RAY DIFFRACTION OF OXIDES FORMED ON
Nb-Al-Ti AND Nb-Al-Ti-Cr ALLOYS

Temperature, °F	Results
Alloy No. 1[a]	
1600	Major phase is TiO_2 and a minor phase of α-Al_2O_3
1800	Major phase is TiO_2 and a minor phase of α-Al_2O_3
2000	This sample consists of a major phase of TiO_2 and a minor phase of α-Al_2O_3 plus a trace phase of $Nb_2O_5 = Al_2O_3$
2100	This sample consists of a major phase of TiO_2 and a minor phase of α-Al_2O_3
2200	This sample consists of a major phase of TiO_2 and a minor phase of α-Al_2O_3
2300	This sample consists of a major phase of TiO_2 and a minor phase of α-Al_2O_3
2400	This sample consists of a major phase of TiO_2 and a minor phase of α-Al_2O_3 plus a trace phase of $Nb_2O_5 = Al_2O_3$
2500	This sample consists of a major phase of TiO_2 and a minor phase of α-Al_2O_3 plus a trace phase of $Nb_2O_5 = Al_2O_3$
Alloy No. 2[b]	
1600	This sample consists of a major phase of TiO_2 (rutile) and a minor phase of α-Al_2O_3 plus an unidentified phase
1800	This sample consists of a major face-centered cubic (FCC) phase with $a = 3.70$A and is an unknown composition plus a minor phase of TiO_2 and a trace phase of α-Al_2O_3
2000	This sample consists of a major phase of TiO_2 and a minor phase of α-Al_2O_3 plus a second minor phase which is FCC with $a = 3.70$A and is unidentified
2100	Major phase is TiO_2 and minor phase is α-Al_2O_3
2200	Major phase is TiO_2 and minor phase is α-Al_2O_3 plus a second minor phase which is FCC, the same as noted above. There is also a trace phase of an unknown phase
2300	Major phase TiO_2 and minor phase α-Al_2O_3 plus an unknown trace phase
2400	Major phase is TiO_2 and minor phase is α-Al_2O_3
2500	Major phase is TiO_2 and the minor phase is α-Al_2O_3 plus a second FCC minor phase the same as noted previously

[a] 0.5-inch diameter discs oxidized for 4 hours at temperature.
Alloy No. 1 flaked on cooling. Nb, 33.7 Ti, 29.6 Al.
[b] Alloy No. 2 did not flake on cooling. Nb, 28 Ti, 30 Al, 6 Cr.

8.3 REFERENCES

1. Lever, R. C., and Wukusick, C. S., "Contribution to the Twelfth Meeting of the High Temperature Fuels Committee of AEC," GE-ANPD, XDC 61-5-45, May 16, 1961.
2. Wukusick, C. S., "Intermediate Temperature Behavior of Cb-Al Alloys,"GE-ANPD, XDC 61-4-54, March 27, 1961.